SYNTHESES OF SELF-SUPPORTED TUBULAR ZEOLITE A MEMBRANES

A THESIS SUBMITTED TO
THE GRADUATE SCHOOL OF NATURAL AND APPLIED SCIENCES
OF
MIDDLE EAST TECHNICAL UNIVERSITY

BY

CANAN GÜCÜYENER

IN PARTIAL FULFILLMENT OF THE REQUIREMENTS
FOR
THE DEGREE OF MASTER OF SCIENCE
IN
CHEMICAL ENGINEERING

SEPTEMBER 2008

Approval of the thesis:

"SYNTHESES OF SELF-SUPPORTED TUBULAR ZEOLITE A MEMBRANES"

submitted by **CANAN GÜCÜYENER** in partial fulfillment of the requirements for the degree of **Master of Science in Chemical Engineering Department, Middle East Technical University** by,

Prof. Dr. Canan Özgen _____
Dean, Graduate School of **Natural and Applied Sciences**

Prof. Dr. Gürkan Karakaş _____
Head of Department, **Chemical Engineering**

Assoc. Prof. Dr. Halil Kalıpçılar _____
Supervisor, **Chemical Engineering Dept., METU**

Prof. Dr. Ali Çulfaz _____
Co-Supervisor, **Chemical Engineering Dept., METU**

Examining Committee Members:

Prof. Dr. Hayrettin Yücel _____
Chemical Engineering Dept., METU

Assoc. Prof. Dr. Halil Kalıpçılar _____
Chemical Engineering Dept., METU

Prof. Dr. Ali Çulfaz _____
Chemical Engineering Dept., METU

Asst. Prof. Dr. Meltem Doğan _____
Chemical Engineering Dept., Gazi Üniversitesi

Prof. Dr. Deniz Üner _____
Chemical Engineering Dept., METU

Date: **02.09.2008**

I hereby declare that all information in this document has been obtained and presented in accordance with academic rules and ethical conduct. I also declare that, as required by these rules and conduct, I have fully cited and referenced all material and results that are not original to this work.

Name, Last name : Canan Gücüyener

Signature :

ABSTRACT

SYNTHESES OF SELF-SUPPORTED TUBULAR ZEOLITE A MEMBRANES

Gücüyener, Canan

M.Sc., Department of Chemical Engineering

Supervisor: Assoc. Prof. Dr. Halil Kalıpçılar

Co-supervisor: Prof. Dr. Ali Çulfaz

September 2008, 160 pages

Zeolites are microporous hydrated aluminosilicate crystals containing alkali and/or alkali earth metal cations in their frameworks. Due to their molecular size pores, they can separate molecules according to their size and shape. Zeolites are mostly used in ion exchange, adsorption processes and catalytic applications. The hydrophilic/hydrophobic character of zeolites also makes them favorable materials for adsorption based separations.

Recently the potential of zeolite/ceramic composite membranes have been shown in the separation of liquid and gas mixtures. Self-supported zeolite membranes with asymmetric structure can be an alternative to the composite zeolite membranes. Because asymmetric structure may eliminate the problems originated from the differences in thermal expansion coefficients of zeolites and ceramics.

In this study tubular zeolite A membranes were prepared on binderless zeolite A

supports. The supports were perepared by hydrothermal conversion of amorphous aluminosilicate tubes into zeolite A. The amorphous aluminosilicate powder, which was obtained by filtering the homogenous hydrogel with a composition of $2.5Na_2O:1Al_2O_3:1.7SiO_2:150H_2O$, was mixed with an organic binder (HEC-Hydroxyethyl Cellulose) and water to obtain the paste. The paste was then extruded through a home-made extruder into bars and tubes. These extrudates were dried at room temperature for 24 hours, calcined at 600°C for 2 hours to remove organic binder and finally synthesized at 80°C for 72 hours in hydrothermal conditions to convert amorphous aluminosilicate to zeolite. The effect of composition of the synthesis solution on the crystallinity and morphology of zeolite A tubes and bars were investigated. The crystallization field of zeolite A bars has been established and shown on a ternary phase diagram. Tubes were mechanically stable, typically had a crystallinity over 90% and a macroporosity of 35%. The tubes were composed of highly intergrown crystals of zeolite A. The average particle size was 3.5 μm.

The asymmetric membranes were synthesized by growing zeolite A films on binderless zeolite A supports with a geometry of disk, bar and tube. Continuous zeolite A films can only be obtained when the supports were saturated with water prior to synthesis. The film thicknesses were approximately 5 μm on disks and approximately 10 μm on tubes. A method was proposed to prepare self-supported tubular zeolite A membranes in this study.

Keywords: Zeolite A, Binderless Zeolite A Tube, Zeolite A membrane, Self Supported Membrane, Pervaporation

ÖZ

KENDİNDEN DESTEKLİ TÜP ZEOLİT A MEMBRANLARININ SENTEZLENMESİ

Gücüyener, Canan
Yüksek Lisans, Kimya Mühendisliği Bölümü
Danışman: Doç. Dr. Halil Kalıpçılar
Eş Danışman: Prof. Dr. Ali Çulfaz

Eylül 2008, 160 sayfa

Zeolitler, yapı iskeletlerinde alkali ve/veya toprak alkali katyonlar içeren mikro gözenekli sulu aluminosilikat kristalleridir. Molekül boyutundaki gözenekleri sayesinde, molekülleri boyut ve şekillerine göre ayırabilirler. Zeolitler genellikle iyon değiş tokuşu, adsorpsiyon ve kataliz uygulamalarında kullanılırlar. Su sever/su sevmez karakteriyle zeolitler, adsorpsiyon bazlı ayırımlar için uygun malzemelerdir.

Son zamanlarda zeolit/seramik kompozit membranların sıvı ve gaz karışımlarının ayırımındaki potansiyeli gösterilmiştir. Kendinden destekli ve asimetrik yapıdaki zeolit membranlar kompozit membranlara bir alternatif olabilir. Çünkü asimetrik yapı zeolit ve seramiğin ısıl genleşme katsayılarındaki farklılıklar nedeniyle ortaya çıkabilecek sorunları ortadan kaldırabilir.

Bu çalışmada tüp zeolit A membranlar bağlayıcısız zeolit A destekler üzerinde hazırlanmıştır. Destekler amorf alüminosilikat tüplerin hidrotermal olarak zeolit A

dönüşümü ile elde edilmiştir. $2.5Na_2O:1Al_2O_3:1.7SiO_2:150H_2O$ kompozisyonuna sahip homojen hidrojelin filtrasyonu ile elde edilen amorf yapıdaki alümino silikat tozu organik bir bağlayıcı (HEC-Hidroksi etil selüloz) ile karıştırılarak bir hamur elde edilmiştir. Hamur daha sonra el yapımı bir ekstrüder ile şekillendirilerek çubuk ve tüpler elde edilmiştir. Ekstrüzyon ürünleri oda sıcaklığında 24 saat kurutulmuş, ardından 600°C'de 2 saat kalsine edilerek organik bağlayıcı yakılmış ve son olarak da 80°C'de 72 saatte hidrothermal koşullarda aluminosilikat zeolit'e dönüştürülmüştür. Sentez çözeltisinin zeolit A tüp ve çubukların kristallenmelerine ve morfolojilerine olan etkileri incelenmiştir. Zeolit A çubukların kristalleşme bölgesi belirlenmiş ve üçlü faz diyagramında gösterilmiştir. Tüpler mekanik olarak dayanıklı, % 90'nın üzerinde kristalliniteye ve %35 makrogözenekliliğe sahiptir. Tüpler tamamen iç içe girmiş zeolit A kristallerinden oluşmuştur. Ortalama tanecik boyu 3.5 μm'dir.

Disk, çubuk ve tüp şeklinde bağlayıcısız zeolit A destekler üzerinde zeolit A filmler büyütülerek asimterik membranlar sentezlenmiştir. Sürekli zeolit A filmler ancak destekler sentez öncesinde su ile doyurulduğunda elde edilebilmiştir. Disk üzerindeki film kalınlığı yaklaşık 5 μm, tüp üzerindeki film kalınlığı ise yaklaşık 10 μm'dir. Bu çalışmada kendinden destekli zeolit A membranlar hazırlamak için bir yöntem önerilmiştir.

Anahtar Kelimeler: Zeolit A, Bağlayıcısız Zeolit A Tüpü, Zeolit A Membran, Kendinden Destekli Membran, Pervoparasyon

to the spirit of my grandpa,
Mustafa Gücüyener
and my sister,
Çavlan Gücüyener

ACKNOWLEDGEMENTS

I am deeply grateful to my supervisor Assoc. Prof. Dr. Halil Kalıpçılar and my co-supervisor Prof. Dr. Ali Çulfaz for their constructive criticism, valuable advice and guidance throughout this study.

I am also thankful to Prof. Dr. Deniz Üner, for her advice, precious criticism and kindness.

I would like to thank both the Central Laboratory and the Machine Shop technicians of the Chemical Engineering for their help during the study.

I want to thank my dear friend and my lab mate Belma Soydaş for her continuous guidance and the friendship we had, which made sometimes easier to hold on. I am also greatful to Ayşenur Özcan, for her thesis and her helps as a whole, which provided a basis for this thesis.

I would also like to show my appreciation to my friends Canan Yeniova, Güzide Aydın, Damla Eroğlu, Filiz Cengiz and Osman Karslıoğlu for being there for me everytime I have needed.

I want to thank Mert Kılınç for the problems he caused and for the love he brought during the writing period of the thesis.

I am greatly indebted to my sister, Çavlan Gücüyener, for her patience and support, care and encouragement when I asked for. I also want to thank my parents, Berrin Büyükkapancı and Vedat Gücüyener, for their support for my dream of becoming a researcher.

TABLE OF CONTENTS

ABSTRACT……. iv
ÖZ……... vi
DEDICATION……... viii
ACKNOWLEDGMENTS…….. ix
TABLE OF CONTENTS……... x
LIST OF TABLES……... xii
LIST OF FIGURES…… xiv
CHAPTERS
1. INTRODUCTION…… 1
2. LITERATURE SURVEY……. 4
3. EXPERIMENTAL…… 16
3.1. Materials for Synthesis of Zeolite A Macrobodies…….. 16
3.2. Preparation of Alumino Silicate Hydrogel…….. 16
3.3. Synthesis of Zeolite A Bars and Tubes from Amorphous Alumino Silicate Extrudates……...…… 18
3.4. Parameters Investigated in the Crystallization of Tubes…..……... 22
3.4.1. Effect of gel washing……...……. 22
3.4.2. Effect of synthesis liquid……...……..... 23
3.4.3. Effect of synthesis liquid to solid extrudate weight ratio……..… 24
3.5. Characterization of the Macrobodies……...……. 24
3.5.1. Phase identification and determination of crystallinity by XRD…….. 24
3.5.2. Determination of morphology by SEM……. 26
3.5.3. Determination of weight loss by TGA……...……... 26
3.5.4. Characterization of pore structure by mercury porosimetry and nitrogen adsorption……. 26

3.5.5. Elemental analysis by EDX and ICP……..…….. 27
3.6. Synthesis of Membrane Layer on Tubes and Disks……...…….. 27
3.7. Construction of Pervaporation Set-Up……...…. 28
4. RESULTS AND DISCUSSION……...…... 32
4.1. Characterization of Binderless Zeolite 4A Bars, Tubes and Disks..... 32
4.2. Simplifying The Synthesis Procedure by Changing Washing Procedure... 39
4.3. Simplifying the synthesis procedure by using synthetic liquid solutions... 46
4.4. Crystallization field of zeolite A macrobodies……..…… 50
4.5. The course of crystallization……..... 54
4.6. Synthesis of Self-Supported Zeolite 4A Disk and Tube Membranes…… 62
5. CONCLUSIONS……...……. 75
RECOMMENDATIONS……..…..... 76
REFERENCES……....…….…….. 77
APPENDICES
A. SAMPLE CALCULATION FOR A BATCH COMPOSITION..... 83
B. SYNTHESIS CONDITIONS OF THE BINDERLESS MACROBODIES AND THEIR CHARACTERIZATION RESULTS BASED ON XRD AND SEM..... 87
C. XRD FIGURES OF THE MACROBODIES..... 92
D. SEM IMAGES..... 114
E. CALCULATION OF THE SOLID COMPOSITION FROM THE ICP RESULTS..... 147
F. TERNARY DIAGRAM DATA OF THE LIQUID AND THE OVERALL COMPOSITION..... 150
G. SAMPLE CALCULATION OF THE OVERALL COMPOSITION IN THE REACTIVE MEDIUM..... 155
H. MEMBRANE SYNTHESIS CONDITIONS AND CHARACTERIZATION RESULTS BASED ON XRD AND SEM..... 157
I. EDX ANALYSIS..... 159

LIST OF TABLES

TABLES

Table 2.1. Examples from the literature for zeolite membranes synthesized by different conditions……... 13

Table 3.1. Washing methods……. 23

Table 4.1. Average weight and dimensions of the green, calcined and synthesized macrobodies……... 35

Table 4.2. Crystallinity values of the tubes synthesized by using differing washing methods. The syntheses of tubes were performed in the original liquid solution at 80°C for 72 h…….. 41

Table 4.3. Summary of the results obtained for the zeolite A tubes prepared by washing method 1 and 2. 46

Table 4.4. Tubes used for the synthesis of the reactive solutions prepared to imitate the original liquid solution……...…… 47

Table 4.5. The percent crystallinities of the tubes synthesized using different reactive solutions, in comparison to the original liquid…… 49

Table A.1. Composition of raw materials used in the synthesis experiments..... 83

Table A.2. Formula weight of raw materials..... 83

Table A.3. Molecular weights of reactants..... 84

Table B.1. Experimental conditions for the prepared samples and their characterization based on XRD and SEM..... 88

Table E.1. ICP analysis of the solid composition for the batch CG6 and CG16..... 147

Table E.2. Solid Composition for batch CG6 determined according to the ICP analysis..... 149

Table F.1. Ternary diagram data of liquid and overall compositions..... 151

Table F.2. Ternary diagram data for the overall compositions results from different solid extrudate to reactive liquid composition, $4.8Na_2O:Al_2O_3:0.07SiO_2:400H_2O$..... 153

Table F.3. Ternary diagram data for the overall compositions results from different solid extrudate to reactive liquid composition, $2.33Na_2O:SiO_2:330H_2O$... 154
Table G.1. ICP analysis of the solid composition for the batch CG6 and CG16..... 155
Table H.1. Membrane synthesis conditions and characterization results based on XRD and SEM..... 157
Table I.1. EDX analysis of the bars prepared for the crystallinity curve..... 159
Table I.2. EDX analysis of the bars prepared for the determination of the effect of the solid extrudate to reactive solution ratio..... 160

LIST OF FIGURES

FIGURES

Figure 2.1. Framework structure of zeolite A [4]…….. 5
Figure 2.2. Schematic drawing of a general pervaporation process…… 14
Figure 3.1. Preparation of (a) the sodium silicate solution, (b) the sodium aluminate solution and (c) the hydrogel……. 17
Figure 3.2. Synthesis procedure of zeolite A tubes and bars…… 19
Figure 3.3. (a) Schematic presentation of stainless steel ram extruder, which can be used to extrudate bars with central spacer stick and tubes without central spacer stick filler (b) Schmetic representation of the extrusion process…… 20
Figure 3.4. Schematic presentations of the four washing methods……. 22
Figure 3.5. XRD pattern of commercial zeolite A powder. The peaks marked with asterisk (*) were used for crystallinity calculation……... 25
Figure 3.6. Schematical drawing of the pervaporation set-up..... 30
Figure 3.7. Feed tank and placement of the membrane in the tank..... 31
Figure 4.1. XRD patterns of (a) Green tube/CG21 – dried at room temperature for 24h, (b) Calcined tube/CG32 – calcined at 600°C for 2 h, (c) Synthesized tube/CG16F – hydrothermally converted into zeolite A at 80°C for 72 h (d) Reference/TZ4A – the XRD pattern of the commericial zeolite 4A powder……..... 33
Figure 4.2. Photographs of a zeolite A tube (a), bar (b), disk (c) and zeolite A powder (d)……... 34
Figure 4.3. TGA analysis of the green (CG16G), calcined (CG16C) and synthesized (CG16F) tubes……..……..…….. 36
Figure 4.4. Schematic representation of the differentiation of the cross section parts for a tube from where the SEM images taken……..…...…….. 37
Figure 4.5. SEM pictures taken from (a) outer (b) middle (c) inner sides of the cross section of the CG16F…….……...……... 38

Figure 4.6. XRD patterns of the synthesized tubes according to the varying washing method in comparison to commercial zeolite 4A powder (a) first method (CG6A) (b) second method (CG16F) (c) third method (CG14F1) (d) fourth method (CG15F) (e) commercial zeolite 4A powder. The syntheses of tubes were performed in the original liquid solution at 80°C for 72 h..... 40
Figure 4.7. SEM images taken from the middle cross section of the zeolite A tubes that are prepared by (a) Method 1 (AÖ129H) (b) Method 2 (CG13F1). The synthesis was carried out in the liquid solution with a molar composition of $4.8Na_2O:Al_2O_3:0.07SiO_2:400H_2O$ at 80°C for 72 h..... 43
Figure 4.8. Pore size distrubition by mercury porosimetry of the synthesized tubes using washing Methods 1 (AÖ35T) and 2 (CG13F1)..... 44
Figure 4.9. BET isotherms of the zeolite A tubes prepared using Method 1 (AÖ120) and Method 2 (CG13F1)...…...… …… 44
Figure 4.10. TGA results obtained for the synthesized zeolite A tubes using different washing methods. Sample codes AÖ60H for Method 1 and CG16F for Method 2…….……...……..……... 45
Figure 4.11. XRD patterns of the synthesized tubes using the imitated solution (a) Solutions A, (b) B, (c) C, (d) D, (e) E, (f) F. The oxide formulas of solutions are given in Table 4.4..... 49
Figure 4.12. Ternary phase diagram based on the liquid solution composition in the autoclave for the synthesis of binderless macrobodies at 80°C. The H_2O content of the liquid compositions are greater than 97 mole %. Bounded Areas [1]: Projection of N-A-S-H system for the hydrogels synthesized at 100°C. H_2O content of the gel is 90-98 mole %. The affirmations represent the zeolite A, X, Y, B (P) and hydroxy sodalite (HS). Corners: N represents the Na_2O, A represents the Al_2O_3, S represents the SiO_2..... 51
Figure 4.13. Ternary phase diagram based on the overall composition in the autoclave for the synthesis of binderless macrobodies at 80°C. The H_2O content of the overall compositions are greater than 96 mole %. Bounded Areas [1]: Projection of N-A-S-H system for the hydrogels synthesized at 100°C. H_2O content of the gel is 90-98 mole %. The affirmations represent the zeolite A, X, Y, B (P) and hydroxy sodalite (HS). Corners: N represents the Na_2O, A represents the Al_2O_3, S represents the SiO_2..... 53
Figure 4.14. Ternary phase diagram based on the overall composition determined by changing the solid extrudate to liquid composition ratio in the autoclave for the synthesis of binderless macrobodies at 80°C for 72 h. The H_2O content of the overall compositions are greater than 92 mole %. Bounded Areas [1]: Projection of N-A-S-H system for the hydrogels synthesized at 100°C. H_2O content of the gel is 90-98 mole %. The affirmations represent the zeolite A, X, Y, B (P) and hydroxy sodalite (HS). Corners: N represents the Na_2O, A represents the Al_2O_3, S represents the SiO_2..... 54

Figure 4.15. Crystallization curve of binderless bars and powder……..…….. 56
Figure 4.16. Change of crystallization by time according to the SEM pictures of the binderless zeolite bars (a) 4 h (b)5.5 h (c) 6.5 h..... 58
Figure 4.17. Change of crystallization by time according to the SEM pictures of the binderless zeolite bars (a) 7 h (b) 8 h (c) 9 h..... 59
Figure 4.18. Change of crystallization by time according to the SEM pictures of the binderless zeolite bars (a) 12 h (b) 48 h (c) 72 h..... 60
Figure 4.19. Molar % change of the Na_2O, SiO_2 and Al_2O_3 during synthesis with time..... 61
Figure 4.20. Change of crystallization of bars according to the cross section for 9 h of synthesis……...……... 62
Figure 4.21. XRD patterns of (a) the disk shaped zeolite A support (sample code: CG25D5) and (b) the membrane after synthesis of the thin zeolite A layer (sample code: CGM5; synthesized in solution with a composition of $49Na_2O:1Al_2O_3:5SiO_2:980H_2O$ at 80°C for 8h)……... 64
Figure 4.22. SEM pictures of the disk shaped supports (a) cross-section (sample code: CG25D5) and (b) surface (sample code: CG20D6)…… 66
Figure 4.23. SEM pictures of the zeolite A films formed on disk shaped supports (a) cross-section (sample code: CGM5) and (b) surface (sample code: CGM7). The molar composition of synthesis solution and synthesis conditions for CGM5 is $4.8Na_2O:Al_2O_3:0.07SiO_2:400H_2O$ and 80°C for 72 h. The molar composition of synthesis solution and synthesis conditions for CGM7 is $2Na_2O:1Al_2O_3:2SiO_2:120H_2O$ and 100°C for 4 h……. 67
Figure 4.24. SEM pictures of tubular zeolite A membrane prepared on dry-support sample code:CGM8), (a) outer cross section (b) magnified view of the outer cross section (c) inner cross section (d) crystals seen over the inner cross section. The molar composition of synthesis solution and synthesis conditions for CGM8 is $2Na_2O:1Al_2O_3:2SiO_2:120H_2O$ and 100°C for 4 h…….. 69
Figure 4.25. SEM pictures of CGM8, taken from (a) inner surface (b) amorphous particle on the inner surface. The molar composition of synthesis solution and synthesis conditions for CGM8 is $2Na_2O:1Al_2O_3:2SiO_2:120H_2O$ and 100°C for 4 h……. 70
Figure 4.26. The surface SEM images of a tubular zeolite A membrane prepared on wet-support (sample code: CGM26). (a) outer surface, (b) closer view of the outer surface given in (a). The molar composition of synthesis solution and synthesis conditions is $2Na_2O:1Al_2O_3:2SiO_2:120H_2O$ and 100°C for 4 h…… 72

Figure 4.27. The cross-sectional SEM images of a tubular zeolite A membrane prepared on wet-support (sample code: CGM26). (a) inner cross section (b) closer view of the inner cross section given in (a), (b) inner cross section (c) closer view of the inner cross section given in (b). The molar composition of synthesis solution and synthesis conditions is $2Na_2O:1Al_2O_3:2SiO_2:120H_2O$ and 100°C for 4 h……. 73
Figure 4.28. The cross-sectional SEM images of a tubular zeolite A membrane prepared on wet-support (sample code: CGM30). (a) inner cross section (b) closer view of the inner cross section given in (a). The molar composition of synthesis solution and synthesis conditions is $2Na_2O:1Al_2O_3:2SiO_2:120H_2O$ and 100°C for 4 h……. 74
Figure C.1. XRD pattern of (a) CG6A (XRD5972), (b) CG6B (XRD5975) and (c) CG6C (XRD 5976)..... 92
Figure C.2. XRD pattern of (a) CG6D (XRD 5974), (b) CG6E (XRD 5973), (c) CG6F (XRD 5978) and (d) CG6G (XRD 5977)..... 93
Figure C.3. XRD pattern of (a) CG6H (XRD 5974), (b) CG13F1 (XRD 6225), (c) CG13L1 (XRD 6226) and (d) CG13F2 (XRD 6246)..... 94
Figure C.4. XRD pattern of (a) CG13L2 (XRD 6248), (b) CG14F1 (XRD 6223), (c) CG14L1 (XRD 6224) and (d) CG14F2 (XRD 6228)..... 95
Figure C.5. XRD pattern of (a) CG14L2 (XRD 6241), (b) CG15F (XRD 6287), (c) CG15L (XRD 6286) and (d) CG16F (XRD 6235)..... 96
Figure C.6. XRD pattern of (a) CG16L (XRD 6237), (b) CG17F (XRD 6346), (c) CG17L (XRD 6344) and (d) CG18F (XRD 6345)..... 97
Figure C.7. XRD pattern of (a) CG18L (XRD 6347), (b) CG25D1 (XRD 6442), (c) CG25D1-b (XRD 6444) and (d) CG25D3 (XRD 6451)..... 98
Figure C.8. XRD pattern of (a) CG25D3-b (XRD 6452), (b) CG25D4 (XRD 6453), (c) CG25D4-b (XRD 6454) and (d) CG25D5 (XRD 6445)..... 99
Figure C.9. XRD pattern of (a) CG25D5-b (XRD 6446), (b) CG20D1 (XRD 6397), (c) CG20D21-b (XRD 6398) and (d) CGM1 (XRD 6383)..... 100
Figure C.10. XRD pattern of (a) CGM1-b (XRD 6377), (b) CGM2 (XRD 6386), (c) CGM2-b (XRD 6378) and (d) CGM3 (XRD 6385)..... 101
Figure C.11. XRD pattern of (a) CGM3-b (XRD 6380), (b) CGM4 (XRD 6384), (c) CGM4-b (XRD 6379) and (d) CGM5 (XRD 6479)..... 102
Figure C.12. XRD pattern of (a) CGM6 (XRD 6478), (b) CGM7 (XRD 6480), (c) CGM7-b (XRD 6481) and (d) CGM9 (XRD 6479)..... 103

Figure C.13. XRD pattern of (a) CGM10 (XRD 6508), (b) CG27A1 (XRD 6511), (c) CG27B1 (XRD 6512) and (d) CG27B2 (XRD 6510)..... 104
Figure C.14. XRD pattern of (a) CG27C1 (XRD 6529), (b) CG27C2 (XRD 6526), (c) CG27G1 (XRD 6527) and (d) CG27C3 (XRD 6524)..... 105
Figure C.15. XRD pattern of (a) CG27C4 (XRD 6535), (b) CG27D2 (XRD 6537), (c) CGM29G2 (XRD 6538) and (d) CG27H2 (XRD 6536)..... 106
Figure C.16. XRD pattern of (a) CG31C5 (XRD 6558), (b) CG31D3 (XRD 6560), (c) CG31E1 (XRD 6559) and (d) CG33M1 (XRD 6639)..... 107
Figure C.17. XRD pattern of (a) CG33N1 (XRD 6640), (b) CG31K1 (XRD 6563), (c) CG31I1 (XRD 6564) and (d) CG33J1 (XRD 6567)..... 108
Figure C.18. XRD pattern of (a) CG33L1 (XRD 6568), (b) CG34P1 (XRD 6676), (c) CG34P2 (XRD 6677) and (d) CG34P3 (XRD 6669)..... 109
Figure C.19. XRD pattern of (a) CG34P4 (XRD 6666), (b) CG34P5 (XRD 6678), (c) CG34P6 (XRD 6708) and (d) CG34P7 (XRD 6709)..... 110
Figure C.20. XRD pattern of (a) CG34P8 (XRD 6710), (b) CG34P9 (XRD 6737), (c) CG34P10 (XRD 6738) and (d) CG34P11 (XRD 6739)..... 111
Figure C.21. XRD pattern of (a) CG34P12 (XRD 6740), (b) CG34P13 (XRD 6830), (c) CG34P14 (XRD 6765) and (d) CG34P15 (XRD 6766)..... 112
Figure C.22. XRD pattern of (a) CG34P16 (XRD 6767), (b) CG34P17 (XRD 6768)..... 113
Figure D.1. SEM image of (a) CG6A inner cross section (X1000) and (b) CG6A inner cross section (X500)..... 114
Figure D.2. SEM image of (a) CG6A middle cross section (X 1000), (b) CG6A middle cross section (X 500) and (c) CG6C outer cross section (X 500)..... 115
Figure D.3. SEM image of (a)CG6A outer cross section (X 1000), (b) CG14F1 inner cross section (X 1000) and (c) CG614F1 inner cross section (X 1500)..... 116
Figure D.4. SEM image of (a) CG14F1 middle cross section (X 51000), (b) CG14F1 middle cross section (X 1500) and (c) CG14F1 outer c..ross section (X 500)..... 117
Figure D.5. SEM image of (a) CG14F1 outer cross section (X 1000), (b) CG14F1 inner surface (X 1500) and (c) CG14F1 outer surface – tilted 60° (X 1500)..... 118

Figure D.6. SEM image of (a) CG15F inner cross section (X 1500), (b) CG15F inner cross section (X 1000) and (c) CG15F middle cross section (X 1000)..... 119
Figure D.7. SEM image of (a) CG15F middle cross section (X 1000), (b) CG15F outer cross section (X 1500) and (c) CG15F outer cross section (X 2000)..... 120
Figure D.8. SEM image of (a) CG15F inner surface (X 1500), (b) CG15F outer surface – tilted 60° (X 1500) and (c) CG16F inner cross section (X 1000)..... 121
Figure D.9. SEM image of (a) CG16F inner cross section (X 1500), (b) CG16F middle cross section (X 1500) and (c) CG16F middle cross section (X 1000)..... 122
Figure D.10. SEM image of (a) CG16F outer cross section (X 1000), (b) CG16F outer cross section (X 1500) and (c) CG16F inner surface (X 1500)..... 123
Figure D.11. SEM image of (a) CG16F outer surface – tilted 60° (X 1000), (b) CG6C inner cross section (X 1000) and (c) CG6C middle cross section (X 1000)... 124
Figure D.12. SEM image of (a) CG6C middle cross section (X 5000), (b) CG6C outer cross section (X 1500) and (c) CG31E1 inner cross section (X 1500)..... 125
Figure D.13. SEM image of (a) CG31E1 middle cross section (X 1500), (b) CG31E1 outer cross section (X 1500) and (c) CG31E1 inner surface (X 1500)..... 126
Figure D.14. SEM image of (a) CG33M1 inner cross section (X 1500), (b) CG33M1 middle cross section (X 1500) and (c) CG33M1 outer cross section (X 1500)..... 127
Figure D.15. SEM image of (a) CG33M1 inner surface (X 1500), (b) CG29D1 inner cross section (X 1500) and (c) CG29D1 middle cross section (X 1500)..... 128
Figure D.16. SEM image of (a) CG29D1 outer surface (X 1500), (b) CG29D1 inner surface (X 1500) and (c) CG31I1 inner cross section (X 1500)..... 129
Figure D.17. SEM image of (a) CG31I1 middle cross section (X 1500), (b) CG31I1 outer cross section (X 1500) and (c) CG31I1 inner surface (X 1500)..... 130
Figure D.18. SEM image of (a) CG31J1 inner cross section (X 1500), (b) CG31J1 middle cross section (X 1500) and (c) CG31J1 outer surface (X 1500)..... 131
Figure D.19. SEM image of (a) CG31J1 inner surface (X 1500), (b) CG33L1 inner cross section (X 1500) and (c) CG33L1 middle cross section (X 1500)..... 132
Figure D.20. SEM image of (a) CG33L1 outer cross section (X 1500), (b) CG33L1 inner surface (X 1500) and (c) CG33K1 inner cross section (X 1500)..... 133

Figure D.21. SEM image of (a) CG33K1 middle cross section (X 1500), (b) CG33K1 outer cross section (X 1500) and (c) CG33K1 inner surface (X 1500)..... 134
Figure D.22. SEM image of (a) CG42L-4h middle cross section (X 10000), (b) CG42L-5.5h outer cross section (X 3100) and (c) CG42L-6.5h middle cross section (X 3100)..... 135
Figure D.23. SEM image of (a) CG42L-7h middle cross section (X 3000), (b) CG42L-8h outer cross section (X 5000) and (c) CG42L-9h middle cross section (X 3000)..... 136
Figure D.24. SEM image of (a) CG42L-12h middle cross section (X 3000), (b) CG42L-48h outer cross section (X 5000) and (c) CG42L-72h middle cross section (X 3000)..... 137
Figure D.25. SEM image of (a) CG40L - 1/3.5 middle cross section (X 20000), (b) CG40L-1/7 middle cross section (X 20000) and (c) CG40L-1/14 middle cross section (X 20000)..... 138
Figure D.26. SEM image of (a) CG40L - 1/28 middle cross section (X 20000), (b) CG40L-1/49 middle cross section (X 20000) and (c) CG40L-1/105 middle cross section (X 20000)..... 139
Figure D.27. SEM image of (a) CGM30 outer surface (X 4000), (b) CGM30 outer surface (X 2000) and (c) CGM30 inner cross section (X 1500)..... 140
Figure D.28. SEM image of (a) CGM30 outer surface (X 4000), (b) CGM30 outer surface (X 6000) and (c) CGM33 outer surface (X 1000)..... 141
Figure D.29. SEM image of (a) CGM33 inner cross section (X 500), (b) CGM33 inner cross section (X 3000) and (c) CGM33 outer cross section (X 500)..... 142
Figure D.30. SEM image of (a) CGM33 outer cross section (X 3000), (b) CGM33 outer surface (X 1000) and (c) CGM33 outer surface (X 5000)..... 143
Figure D.31. SEM image of (a) CGM28 outer surface (X 1500), (b) CGM28 outer surface (X 6000) and (c) CGM28 inner cross section (X 5000)..... 144
Figure D.32. SEM image of (a) CGM28 outer surface (X 3000), (b) CGM28 outer cross section (X 1000) and (c) CGM28 outer cross section (X 5000)..... 145
Figure D.33. SEM image of (a) CGM26 inner cross section (X 3000), (b) CGM26 inner cross section (X 1000) and (c) CGM26 outer cross section (X 3000)..... 146

CHAPTER 1

INTRODUCTION

Zeolites are microporous hydrated aluminosilicate crystals containing alkali and or alkali earth metal cations in their frameworks [1]. The surface properties and the size of micropores, which ranges between 0.3 and 1 nm, vary depending on the type of zeolite. Zeolites can separate molecules with respect to their size and shape by molecular sieving, and with respect to their polarity by preferential adsorption. Therefore zeolites have great potential in adsorption processes [2], and in membrane applications [3-5]. For instance zeolite A, which is a well-known zeolite that has pores with a diameter of 0.42 nm and hydrophilic character, strongly adsorbs water over small non-polar hydrocarbons. Hence it is a particularly appropriate material to make membranes for the removal of water from aqueous solutions by pervaporation.

Zeolite membranes are mostly composite materials which are composed of a thin and compact zeolite layer on a thick and macroporous support. Thin zeolite layer accomplishes separation while the macroporous support mainly provides mechanical strength to the membrane [6]. Different types of support materials and geometries were used in the literature [7-9]. The support is chosen considering the resistance of the support to the flux, adhesion of the zeolite film to the support, leaching of support into the synthesis solution and the differences between the thermal expansion coefficients of the support and the zeolite film [10-13]. Leaching of the support may locally change the chemical composition of the synthesis solution around the support so that undesired phases may form [14]. The diffrence between the thermal expansion coefficients between the support and the zeolite layer may also cause formation of microcracks during the thermal treatment to remove water and organic template from

the zeolite pores. The microcracks may drastically decrease the performance of the membrance in separation processes. These problems can be overcome by forming assymetric membranes; both the separating layer and the support originates from the same material.

Nevertheless zeolites are typically synthesized as powder [1, 6] and then shaped into beads either by granulation or by extrusion [15-20]. The procedures to prepare zeolite beads are well-established because zeolites are often employed in adsorption beds and in catalytic reactors and in these systems low pressure drop is desired for cost-efficient operations. Recently honeycomb and sponge-like monoliths of zeolites were also prepared for use in adsorption processes [17, 18].

In the preparation of zeolite macrobodies like beads or monoliths, clays are mostly used as binder [1, 7, 17]. However, the inorganic binder decreases the purity of the zeolite bead and the accesibility to the zeolite pores by partially covering the surface of zeolite crystals [19]. This problem can be overcome by preparing binderless zeolite macrobodies. Hydrothermal conversion of kaolinite type clays into zeolite beads [1], conversion of the amorphous alumina silicate gel particles formed in a shaping oil into zeolite spheres [12-14] are the techniques used for the preparation of the binderless zeolite bodies. However, these techniques are rather difficult and the prepared bodies are usually smaller than a few centimeters.

In this study, synthesis of asymmetric and self-supported zeolite A tubular membranes were aimed. This kind of a membrane consist of a thin and compact zeolite A layer on a thick and macroporous zeolite A support. Thus, the synthesis of the binderless zeolite A macrobodies as support is the first step to synthesize the thin zeolite A layer over it.

The binderless zeolite A tubes and bars were firstly synthesized by following the procedures developed by Ural [20] and Özcan [17]. Their procedures were then modified to produce binderless zeolite A tubes by a more efficient and simple synthesis procedure. The tubes were characterized by X-ray Diffraction (XRD) to determine the crystallinity, Scanning Electron Microscopy (SEM) to determine the macrostructure and

the crystal morphology, Mercury Intrusion Porosimetry and N_2 adsorption to determine the pore size distribution and the BET surface area.

The effect of synthesis solution on the crystallinity of zeolite A tubes was also examined and the crystallization field of zeolite A tubes was established. The course of conversion of amorphous tubes to zeolite A tubes was also investigated by XRD and SEM.

The zeolite A tubes were then subjected to a second hydrothermal treatment to coat the tube surface with a compact zeolite A layer, which is expected to act as the separating membrane layer. The synthesis of membrane layer was accomplished by using three different mixtures, such as $2Na_2O:Al_2O_3:2SiO_2:120H_2O$ [8], $2Na_2O:Al_2O_3:2SiO_2:150H_2O$ [5] and $49Na_2O:Al_2O_3:5SiO_2:980H_2O$ [21]. Membrane morphology was determined by Scanning Electron Microscopy. The membranes prepared in this study were one of the few self-supported zeolite A membranes with reasonable mechanical strength reported in the literature.

The objective of this study was therefore, to synthesize self-supported and asymmetric zeolite A tubular membranes. A significant part of the study was devoted to the synthesis of binderless zeolite A tubes to be used as support. In addition, crystallization conditions of the binderless macrobodies as well as the thin membrane layer were studied.

CHAPTER 2

LITERATURE SURVEY

2.1. Description of Zeolites and Zeolite A

Zeolites are three-dimensional, microporous crystals consisting of aluminum, silicon, and oxygen in their regular framework. Zeolites are resistant to many chemicals and high temperatures [1]. Zeolite A, Beta, Y, mordenite and ZSM-5 are some of the industrially important synthetic zeolites [26].

The silicon and aluminum atoms are tetrahedrally coordinated with each other through shared oxygen atoms. The charge difference between the silicon (+4) and aluminum (+3) atoms causes negatively charged framework which is balanced by a cation of alkaline or alkaline earth metals. These cations, which are located in the pores of zeolite, are mobile and can be exchanged by other cations. The Si/Al ratio of the zeolite framework changes between one and infinity depending on the type of zeolite. Zeolite A with a Si/Al ratio of one has the highest Al content among all zeolites; on the other hand, silicalite-1 is a pure silica zeolite with a Si/Al ratio of infinity [1].

The pore size of zeolites varies between 0.3 and 1 nm, which are similar to the kinetic diameter of many molecules so that zeolites exhibit size and shape selectivity. Therefore they are also called as molecular sieves. Zeolite X with a pore size of 0.72 nm is an example for zeolites with large pores and zeolite A with a pore size of 0.42 nm is a small-pore zeolite [1]. The pore size of zeolite A is smaller than the kinetic diameter of n-butane (0.48 nm) and larger than that of hydrogen (0.29 nm), therefore zeolite A is expected to be effective in the separation of H_2 from H_2/n-butane mixtures.

Zeolite A has a pseudo unit cell formula of $Na_2O.Al_2O_3.2SiO_2.4.5H_2O$. It forms by combination of secondary building units (SBU) of double four ring (D4R) and β-cage (truncated octahedron) as shown in Figure 1. This combination creates a large cavity called α-cage. For Na-form of zeolite A, the α- and β-cages have pore openings of 0.42 nm and 0.22 nm, respectively [1].

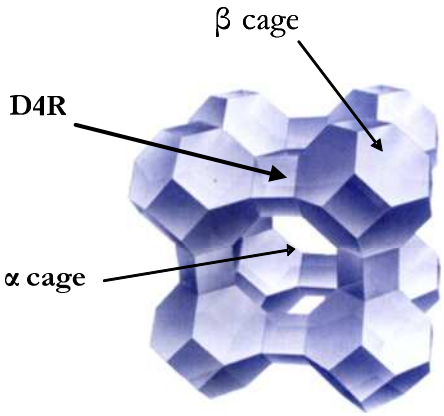

Figure 2.1. Framework structure of zeolite A [27]

Zeolite A has high affinity for water and polar molecules, and has high ion exchange capacity [1]. The type of cation within the structure determines the pore size of the zeolite A, for instance, 3A, 4A and 5A represent potassium, sodium and calcium forms, respectively. The K- and Ca-forms of zeolite A have pore sizes of nearly 0.3 nm and 0.5 nm, respectively [1].

2.2. Zeolite Macrobodies

Zeolites are typically synthesized as fine powder. However for some applications, like adsorption and catalysis, the synthesized powder is usually formed into spheres [16] bodies [28], monoliths [10, 15, 17, 21]. The need for the macrobodies for these applications is due to high pressure drop caused by the powder form which also leads to high energy consumption. As oppose to, the zeolite macrostructures are likely to cause lower pressure drop. The macrobodies are expected to have higher purity, moderate mechanical strength with maximum mechanical attrition resistance and minimum diffusion resistance [1, 29].

Macrobodies are generally prepared by mixing a binder, usually clays, with the zeolite powder and shaping the mixture into beads or pellets by granulation or extrusion [1, 20, 29]. Recently, inorganic binders were also used to prepare zeolite monoliths by Li et al. [30]. The monoliths were made using zeolite 5A powder, bentonite as inorganic binder and hydroxyl ethyl cellulose (HEC) as organic plasticizer. They aimed to determine the minimum bentonite content necessary to obtain a crack-free and self-standing monolith. Monoliths with desired mechanical properties were obtained from pastes with a composition of 25 wt% bentonite and 75 wt% zeolite 5A.

A binder provides mechanical stability to zeolite macrostructure, yet it decreases the efficiency of the adsorbent and catalysis mainly because of its dilution [10] and pore blocking [10, 15, 21] effects. As the binder content of the zeolite macrobody increases the purity and consequently adsorption capacity of the macrobody decreases, which can only be compensated by increasing the amount of macrobodies in the adsorber and the volume of the adsorption bed. This can be viewed as the dilution of zeolite by binding material. Secondly, the binder may cover the zeolite crystal partially or totally so that accessibility to some of the zeolite pores can be obstructed. This can be viewed as the pore blocking effect of binder. The decrease in capacity can again only be counterbalanced by increasing the amount of macrobodies in the adsorber and the volume of the adsorption bed. Thus, significant effort have been devoted to prepare

zeolite macrobodies with lower amount of binder or no binder at all, while maintaining the firm structure [1, 15-18, 21, 22, 28, 30-36].

There are several studies in the literature for the preparation of the binderless zeolite macrobodies. In 1960s, the binderless zeolite beads were synthesized by hydrothermal conversion of performed amorphous gel particles with a diameter of several millimeters. However, this method was intricate and involved many delicate steps such as shaping of gel particles in shaping oil [16-18]. Recently, zeolite microspheres were prepared by hydrothermal synthesis of zeolite particles in organic ion exchange resins. The resin was then burned out to obtain binderless zeolite microspheres [19, 20]. However larger zeolite structures with high surface area/volume ratio are desired for adsorption beds and catalytic reactors, and also for membrane applications.

The first attempts involved conversion of a clay macrobody to a zeolite macrobody. Breck [1] reports the conversion of kaolin into zeolite A, X and Y macrobodies. The kaolin is firstly calcined to obtain metakaolin and then converted hydrothermally to zeolite A in aqueous NaOH solution. For synthesis of zeolite X and Y, the synthesis solution also contained SiO_2 and Al_2O_3 precursors. However, this method depends on the composition and crystallinity of kaolin, and often required adjustment of SiO_2/ Al_2O_3 ratio of kaolin.

Recently Shimuzu et al. [32] prepared MFI tubes from quartz tubes with a length of 16.5 mm, outer diameter of 10 mm and inner diameter of 8 mm. The authors named this technique as dynamic bulk-material dissolution method. A quartz tube was converted to a MFI tube at 200°C in a PTFE autoclave containing a mixture of tetrapropylammoniumoxide (TPAOH), HF acid and approximately 50 mg of MFI seed crystals. Meanwhile the autoclave rotated horizontally at 10 rpm. Highly crystalline MFI tubes were obtained when the synthesis period was 61 days.

Jung et al. [35, 36] prepared TS-1 tubes from a precursor cogel, which is prepared by sol-gel process. Tetraethyl orthosilicate (TEOS) was firstly hydrolyzed in water in the presence of HCl at room temperature where H_2O/TEOS molar ratio was kept 4. On

the other hand titanium butoxide was dissolved in isopropyl alcohol, and the resultant solution was added to the silica solution dropwise. The mixture obtained was converted into a gel by the addition of 20% TPAOH at room temperature. The gel was then dried and pelletized into tubes with 16-mm outer diameter, 8-mm inner diameter and 5-mm long. The tube was put in an autoclave with proper amount of template solution (TPAOH or TPABr) and synthesized at 443K with varying synthesis times between 40 and 90 h. Binderless TS-1 monoliths were obtained when ratio of weight of 20% TPAOH to the weight of amorphous tube was 0.4 and the synthesis period was 90 hours.

Ural and Çulfaz [24] prepared binderless zeolite A and zeolite X discs with 20 mm outer diameter and 1 mm thickness, from amorphous aluminosilicate powder. The amorphous powder was obtained by filtrating a sodium aluminosilicate hydrogel. The wet cake was washed with distilled water to decrease the pH of the cake. It was then dried to obtain an amorphous aluminosilicate powder. The powder was shaped into disks by pressing. The disks obtained are firstly calcined and then synthesized hydrothermally in the liquid phase obtained from the filtration. This method yielded highly crystalline binderless zeolite A and X disks.

This method was then improved by Özcan and Kalıpçılar [21] for the synthesis of zeolite A tubes and bars. The starting hydrogel having a composition of $2.5Na_2O:1Al_2O_3:1.7SiO_2:150H_2O$ was filtrated to separate liquid and solid phases. The wet cake was washed until pH dropped around 8. This process required about 20 L distilled water for 100 g of hydrogel. After washing the wet cake was dried at 80°C for one day, conditioned at 87% relative humidity for one day and then it was grounded into powder form. The amorphous powder was mixed with an organic binder, hydroxy ethyl cellulose (HEC), to obtain a paste. This paste was shaped into bars and tubes using a ram extruder. The extrudates were dried at room temperature for one day and then calcined at 600°C to remove excess water and HEC. The calcined tubes were converted to zeolite A macrobodies hydrothermally in the liquid phase separated from the hydrogel. This method also yielded pure and highly crystalline zeolite A tubes and bars with moderate mechanical strength.

2.3. Preparation of Zeolite Membranes

A membrane is a semi-permeable barrier. It allows passage of some molecules or particles and rejects others, depending on their size and chemical nature (polarity, charge, etc) under the influence of a driving force [37]. Zeolites are recognized as attractive materials to prepare membranes because of their microporous crystalline structures with monodispersed pores. Zeolite membranes are therefore likely to show high performance in the separation of gas and liquid mixtures [37].

Tsikoyiannis et al. [38] synthesized a compact film of ZSM-5-type zeolite crystals on Teflon sheets. The film was then peeled off from the substrate to obtain a self-supported membrane with a thickness of approximately 100 μm and surface area of few square centimeters. The membrane was essentially free of macro- and mesopores and showed an ideal selectivity of 17.2 for 2,2-dimethlybutane over n-hexane, which is slightly higher than the Knudsen selectivity of 1, where Knudsen selectivity takes place in mesoporous materials. Nevertheless the membranes were very fragile and small so that they had no practical use. Therefore self-supported membranes have been barely studied.

Zeolite membranes are generally synthesized as composites of thin zeolitic films on thick macroporous supports. The thin zeolitic film achieves the separation while the support provides mechanical strength [6]. In the preparation of zeolite membranes, different support materials like stainless steel [7], alumina [5, 8, 11, 39, 40, 41], glass [9] and titania [42] with different geometries such as disks or tubes were used. Main concerns that affects the choice of the support is related to the resistance of the support to the flux and the selectivity, adhesion of the zeolite to the support, the chemical changes in the synthesis solution around the support due to leaching of support into the solution and the differences between the thermal expansion coefficients of the support and the zeolite [6].

The pore size of the support may influence the flux, whereas adsorption of the permeating components to the support may effect the selectivity [6]. van de Graff et al.

[43] showed that the separation performance of the composite membrane depends on the resistance of the support to the permeation.

Ceramic supports can be preferred to stainless steel supports since stainless steel may not have sites for zeolite crystals to attach. In such cases, additional pretreatment to create new sites on the support may be needed [6, 13]. But the adventageous features of the metallic supports are that they are more chemically stable and they do not have irregular pore size distribution as ceramics [13].

In addition, the leaching of support due to the highly alkaline synthesis medium may cause a change in the compostion of the crystallization mixture around the support. Geus et al. [14] reported that, using the same synthesis solution, only MFI crystals were synthesized on insoluble zirconia supports, whereas analcime formed on α-Al_2O_3 supports. The leaching of alumina support caused the formation of alumina rich analcime type zeolite. The support leaching may also influence the rates of crystallization and nucleation over the support surface. Therefore, the selection of the support is crucial to obtain a high quality zeolite membrane [6, 10, 12, 13, 44].

Another problem that has often been encountered is the difference in the thermal expansion coefficients of the support and the zeolite layer. The thermal expansion coefficients of Al_2O_3, SiO_2 and stainless steel are 2-7, 11 and 15-19x10^{-6}/°C, respectively. For zeolites, the value may be positive at 10x10^{-6}/°C near room temperature, but change to -10x10^{-6}/°C at higher temperatures [6]. The difference in thermal expansion of support and zeolite may cause stress at the interface and result in cracks on the membrane layer [44]. Therefore, a support with a thermal expansion coefficient similar to the zeolites is desired. Synthesis of zeolite membrane layers on zeolite supports, that is synthesis of asymmetric self-supported membranes, would be useful to eliminate this problem.

Zeolite A is mainly used as detergent builder for water softening by ion exchange [1] and as adsorbent in air separation [45]. Recently zeolite A membranes have been used in dehydration of organic solvents due to hydrophilic character of zeolite A [5, 8, 11, 25,

39, 40, 42]. Zeolite A has also potential in the separation of molecules with small kinetic diameters, such as CO_2 (0.33 nm), CH_4 (0.38), N_2 (0.36 nm) and O_2 (0.35 nm) [39].

Zeolite A membranes are synthesized hydrothermaly from aluminosilicate hydrogels on porous supports [5, 8, 11]. Recently, studies have also been published reporting the synthesis from clear solutions [25, 30]. In the preparation of zeolite A membranes, the support surface is generally coated with seed crystals of zeolite A before synthesis [3, 4]. For hydrothermal synthesis, the support is put in an autoclave filled with synthesis mixture, either the hydrogel or clear solution. The autoclave is then placed in an oven kept at the synthesis temperature. The zeolite A film grows on the support (Table 1).

Andac et al. [7] synthesized zeolite A membranes over stainless steel supports using a composition of $50Na_2O:Al_2O_3:5SiO_2:1000H_2O$. The stainless steel supports were treated with toluene for 30 min and then kept in a mixture of 30 vol% H_2O_2, 25 vol% NH_4OH and finally rinsed with water at 60°C for 15 min. The hydrothermal syntheses was carried out in a conventional oven by changing the synthesis time from 1 to 10 h at 60°C or in an ultrasonic bath at 35 kHz. After a synthesis period of 3h, a continuous zeolite A layer with a thickness of 0.6 μm was obtained with ultrasonic treatment. The membrane thickness was 1.5 μm without ultrasound.

Van den Berg et al. [42] studied the formation of zeolite A membranes on TiO_2 coated stainless steel disks. The TiO_2 coatings had a thickness 10 μm and a mean pore size of 0.12 μm, and the stainless steel support had a a thickness of 180 μm and a pore size of 2-5 μm. Disk shaped supports had a diameter of 25 mm. The TiO_2 coating was exposed to ultraviolet light to improve the hydrophilicity of the support surface. Zeolite A film was synthesized using a crystallization mixture with a composition of $41.9Na_2O:Al_2O_3:4.4SiO_2:833.3H_2O$. Synthesis was carried out at 80°C for 4h. After synthesis, membranes were cooled to room temperature with a cooling rate of 0.5°C/min in order to prevent crack formation. The membranes were made of densely packed and highly intergrown sharp edged cubic crystals. The membrane thickness was about 3.5 μm. The membranes were characterized by pervaporation separation of a 95

wt% EtOH- 5 wt% water solution at 45°C. The selectivities were greater than 10,000 and the flux values were around 0.8 $kgm^{-2}h^{-1}$.

Kita et al. [5, 8, 39] prepared zeolite A membranes on tubular supports with an average pore size of 1 μm and porosity of 40 %. Supports were composed of a mullite, alumina and cristoballite. The tubes had an inside diameter of 9 mm, outside diameter of 12 mm and length of 80 cm. Before the synthesis, the supports were mechanically polished with SiC paper and coated with NaA zeolite A seed crystals in order enhance the formation of the zeolite layer. The synthesis was carried out at 100°C for 3-4 h in a hydrogel with a composition of $2Na_2O:Al_2O_3:2SiO_2:120H_2O$. After synthesis, the membranes were dried at 70°C in reduced pressure. The membranes were completely covered with 2-4 μm sized zeolite A crystals and the layer had the thickness of 10 μm. Pervaporation experiments of the membranes, which were carried out at 120°C with 90 wt% ethanol-10 wt% water mixture, showed a selectivity of 47,000 with a flux of 8.37 $kgm^{-2}h^{-1}$. These membranes were further developed to dehydrate ethanol-water mixtures and were then commercialized by Mitsui Engineering in Japan.

Zah et al. [25] used tubular, 60-mm long, 18.3-mm inner diameter α-alumina supports. A clear synthesis solution with a composition of $49Na_2O:Al_2O_3:5SiO_2:980H_2O$ was used. The synthesis was carried out at 85°C and at autogeneous pressure for 4 h. The autoclave was rotated around the horizontal axis at 25 rpm during synthesis and cooling. The cooling was carried out at a rate of 0.5C°/min, to eliminate the possibility of cracking due to differences in the thermal expansion coefficients for the zeolite A layer and the α-alumina support. A pure zeolite film was formed from highly intergrown sharp-edged cubic crystals and the layer thickness of the membrane was around 3 μm.

The geometry and the material of the support have effect on the performance of zeolite membranes. It can be suggested that, preparation of the asymmetric membrane, instead of composite membrane is a solution to overcome the problems associated with the fact that the incompatibility between the support and the zeolite A top layer. From all, the most important factors that results in the loss in the productivity is leaching and the thermal incompatibility which can be solved by asymmetric membranes.

Table 2.1. Examples from the literature for zeolite membranes synthesized by different conditions

Reference	Support Type	Support geometry	Pretreatment of the support	Synthesis Composition*	Synthesis Temperature (°C)	Time (h)	Membrane Thickness (μm)	Remarks
[7]	Stainless steel	Disk	1) toluene for 30 min 2) - 30 vol% H_2O_2, - 25 vol% NH_4OH } mixture - 45 vol% H_2O at 60°C for 15 min	50N:Al:5S:1000H	60	1- 10	0.6	continuous zeolite layer
[42]	TiO2 coated metalic support	Tubular	UV-photon pretreatment	41.9N:Al:4.4S:833.3H	80	4	3.5	cubic densely packed, intergrown membrane layer formed of sharp edged cubic crystals
[5]	Mullite–alumina-cristobalite	Tubular	Seeding	2N:A:2S:120H	100	3 – 4	10	continuous zeolite layer
[35]	α-Alumina	Tubular	-	49N:A:5S:980H	85	4	3	film was formed from highly intergrown sharp-edged cubic crystals

*where A demonstrates Al_2O_3, S demonstrates SiO_2, H demonstrates H_2O and N demonstrate Na_2O

2.4. Pervaporation separation of liquid mixtures by zeolite A membranes

Pervaporation is a membrane process in which a liquid solution is separated by a membrane (Figure 2.2) In this separation process, the feed or upstream side is kept at atmospheric pressure whereas the permeate or downstream side is evacuated.

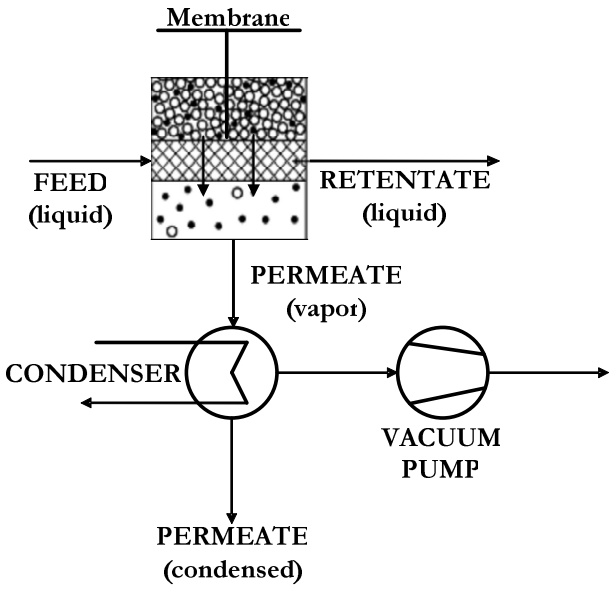

Figure 2.2. Schematic drawing of a general pervaporation process

The membrane acts as a barrier layer between the liquid and vapor phase implying that a phase transition occurs during the passage form feed to the permeate. The low pressure existing on the permeate side determines the phase transformation of the liquid phase into vapor. The vapor in the permeate side is then usually condensed and removed as a liquid. The low pressure can be achieved by means of a vacuum pump. The differences in the adsorption coverage and diffusivity of permeating molecules determine the performance of membrane in pervaporation process [44].

Pervaporation offers significant energy saving since it only requires the energy needed to vaporize the liquid passing through the membrane. Also, lower temperatures can be applied for the separation of solutions that are difficult by more conventional techniques [3, 4, 44, 45, 46]. In particular, a great deal of studies have been devoted to the preparation of hydrophilic zeolite membranes for dehydrating azeotropic and close-boiling liquid mixtures by pervaporation [4].

Zeolites can withstand severe conditions in terms of pH and temperature [1]. In addition, they can also behave as molecular sieves since their pores are approximately of the same size as small molecules which enable them to carry out separations with high selectivities. Zeolites are also attracted in adsorption based separations, like pervaporation, because of their hydrophilic or hydrophobic character [4]. Therefore, the separation performance of zeolite membranes by pervaporation relies on a molecular sieving effect and on the differences between the adsorption and diffusion properties of the components to be separated.

Zeolite membranes are applied for pervaporation processes such as separation of mixtures forming azeotropes (e.g. NaA – Ethanol/Water [5]), removal of organics from water (e.g. Ge-ZSM-5 – Ethanol/Water [47]), removal of water from organics -also known as dehydration- (e.g. Mordenite – Propanol/Water [48]) and removal of organics from organics (e.g. NaY – Ethanol/Water [41]).

Zeolite A, with its hydropilicity, is mostly employed for the pervaporation separation of alcohol-water mixtures [8, 25, 44, 48]. The first large-scale pervaporation plant has been settled by Mitsui Engineering and Shipbuilding Co. in Japan using tubular ceramic supported zeolite A type membranes [5]. The unit processes alcohols up to 530 L/h with separation factors as high as 10,000 bringing the 10 wt% water containing feed solution to 0.2 wt% water.

CHAPTER 3

EXPERIMENTAL

3.1. Materials for Synthesis of Zeolite A Macrobodies

Throughout this study alumino silicate hydrogels were prepared by using water glass (extra pure, Merck, $0.287Na_2O:SiO_2:8.036H_2O$), sodium hydroxide pellets (pure, Carlo Erba, NaOH), aluminum hydroxide powder (pure, $Al(OH)_3$, Merck) and distilled water. For the preparation of the macrobodies, 2-Hydroxy-Ethyl Cellulose (HEC) was used as nonionic organic binder [49]. The average molecular weight of HEC is 72,000 g/mol and the viscosity of 2 wt% aqueous solution is 4,500,000-6,500,000 cps at 25°C (Aldrich).

3.2. Preparation of Alumino Silicate Hydrogel

The hydrogel that has a composition of $2.5Na_2O:1Al_2O_3:1.7SiO_2.150H_2O$ was prepared by mixing sodium silicate and sodium aluminate solutions. Sodium silicate solution was prepared by diluting water glass with distilled water (Figure 3.1.a). The respective weights of water glass and distilled water necessary to prepare 100 g of hydrogel were also shown in Figure 3.1.a. For the preparation of sodium aluminate solution (Figure 3.1.b), sodium hydroxide pellets were dissolved in small amount of water, and aluminum hydroxide was added to this solution. The resulting slurry was stirred vigorously and heated until a clear solution was obtained. This solution was left for 5 to 10 minutes for cooling down to the room temperature. Lastly, the remaining water was added to obtain

the sodium aluminate solution. The weight of each component in sodium aluminate solution necessary to prepare 100 g of hydrogel was shown in Figure 3.1.b as well.

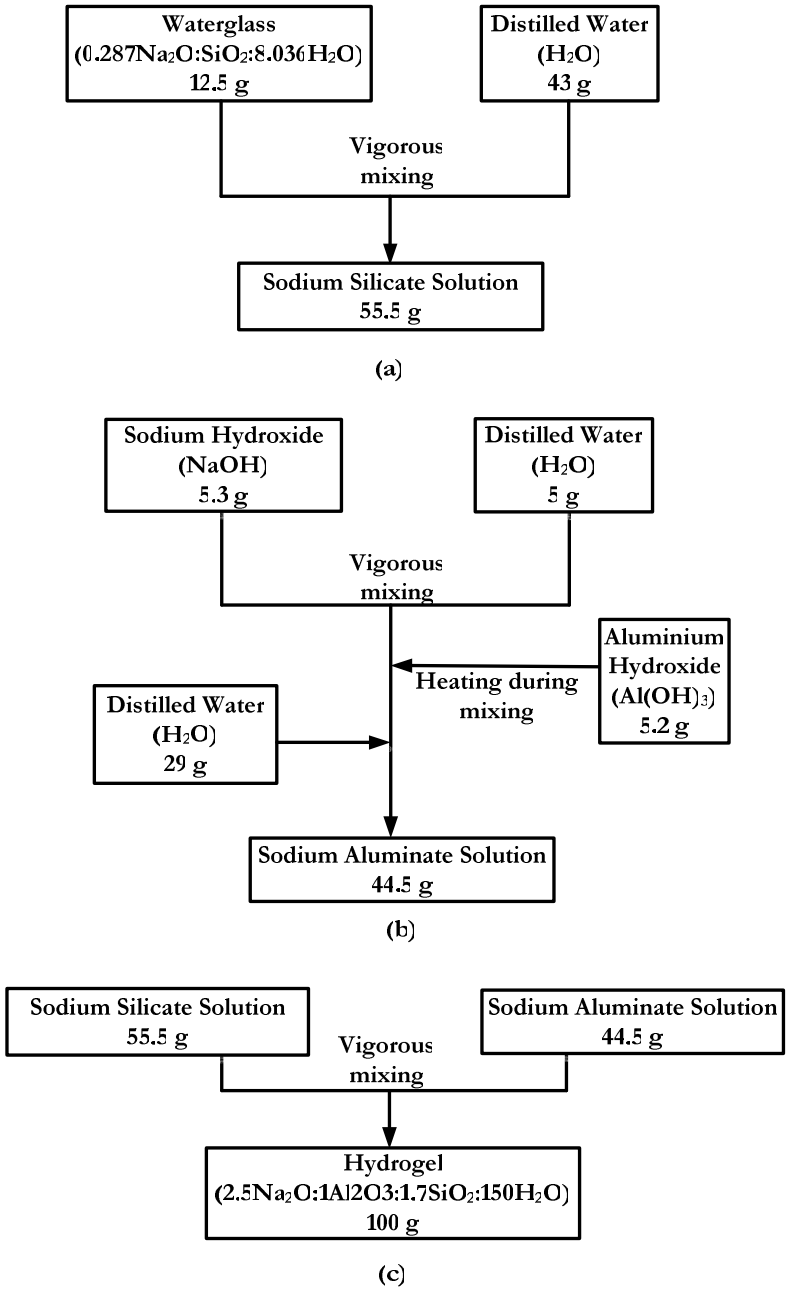

Figure 3.1. Preparation of (a) the sodium silicate solution, (b) the sodium aluminate solution and (c) the hydrogel

In order to obtain the hydrogel, the sodium aluminate solution is added onto the sodium silicate solution and it is mixed vigorously at least for an hour to homogenize it (Figure 3.1.c). Evetually, 100 g of hydrogel was composed of 12.5 g of water glass, 5.3 g of NaOH, 5.2 g of $Al(OH)_3$ and 77 g of distilled water. A sample calculation for this batch composition is shown in Appendix A.

3.3. Synthesis of zeolite A bars and tubes from amorphous alumino silicate extrudates

Synthesis of zeolite A bars and tubes consisted of four main steps, which are preparation of hydrogel, preparation of paste, shaping into tubes or bars and hydrothermal conversion. Figure 3.2 summarizes the entire procedure of making zeolite A macrobodies.

The hydrogel was filtered to separate the solid and liquid phases. Filtration was carried out by a Buchner funnel and Whatman No:41 filter paper (9-cm in diameter). Approximately 45 g wet cake was obtained from 100 g of hydrogel.

The wet cake was washed with distilled water and then dried at 80°C for one day. The dried solid was kept in a desicattor with 86% relative humidity until extrusion. The solid saturated with water weighted approximately 8 g. The solid was pounded in a porcelain mortar for an hour to obtain fine powder of amorphous alumino silicate.

The amorphous powder (7 g) was mixed with 8.6 g 4 wt% HEC solution in a porcelain mortar until a homogeneous paste was obtained. The 4 wt% HEC solution, which is pseudoplastic, was prepared by dissolving 4 g of hydroxyethyl cellulose powder in 96 g of distilled water in a beaker for 2 days on a magnetic stirrer at room temperature. The paste had a composition of 44.9 wt% amorphous powder, 52.9 wt% distilled water and 2.2 wt% of HEC.

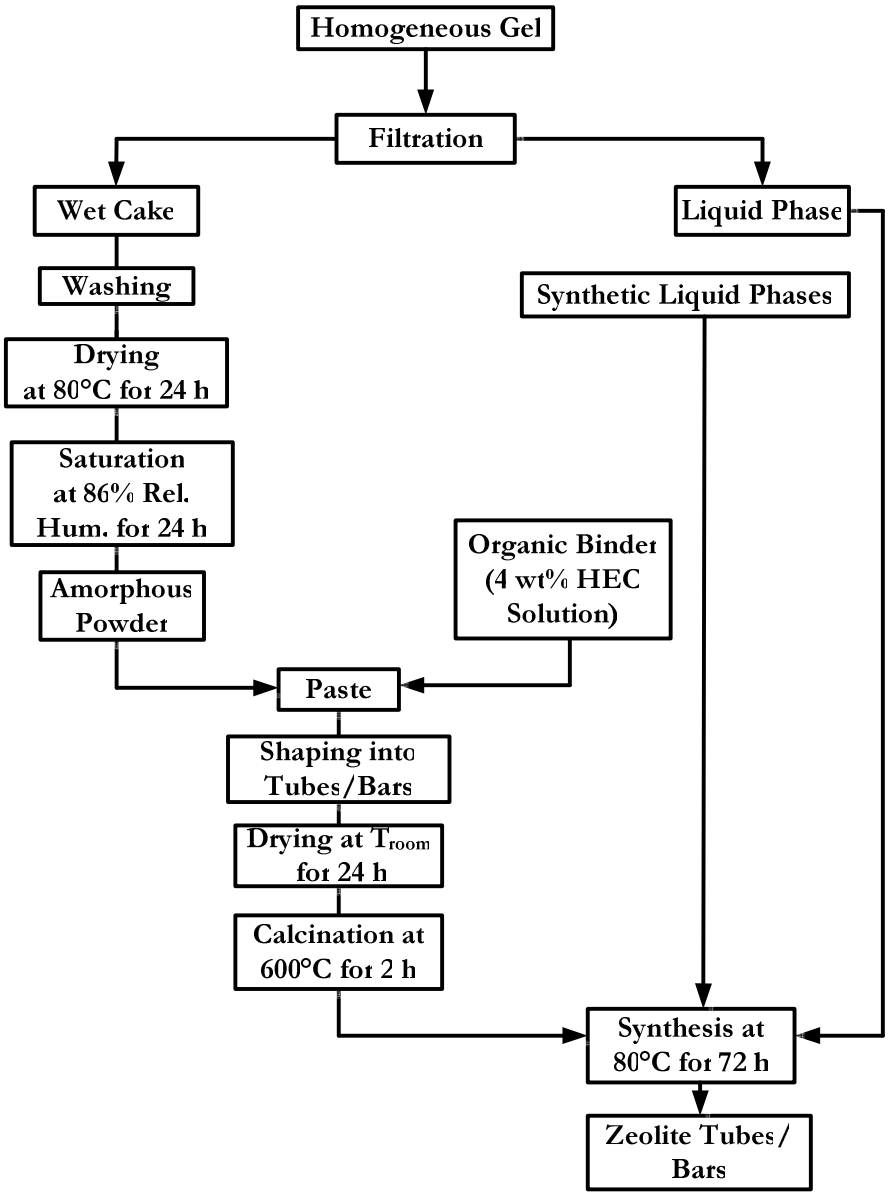

Figure 3.2. Synthesis procedure of zeolite A tubes and bars

The paste was shaped into bars and tubes using a homemade ram extruder (Figure 3.3.a). All parts of the extruder were stainless steel. It was assembled a barrel as a feeder of the paste, a piston to push the paste and a die to obtain the macrobody with desired shape. Tubes were extruded when a central spacer stick was installed, and bars were made without the central stick.

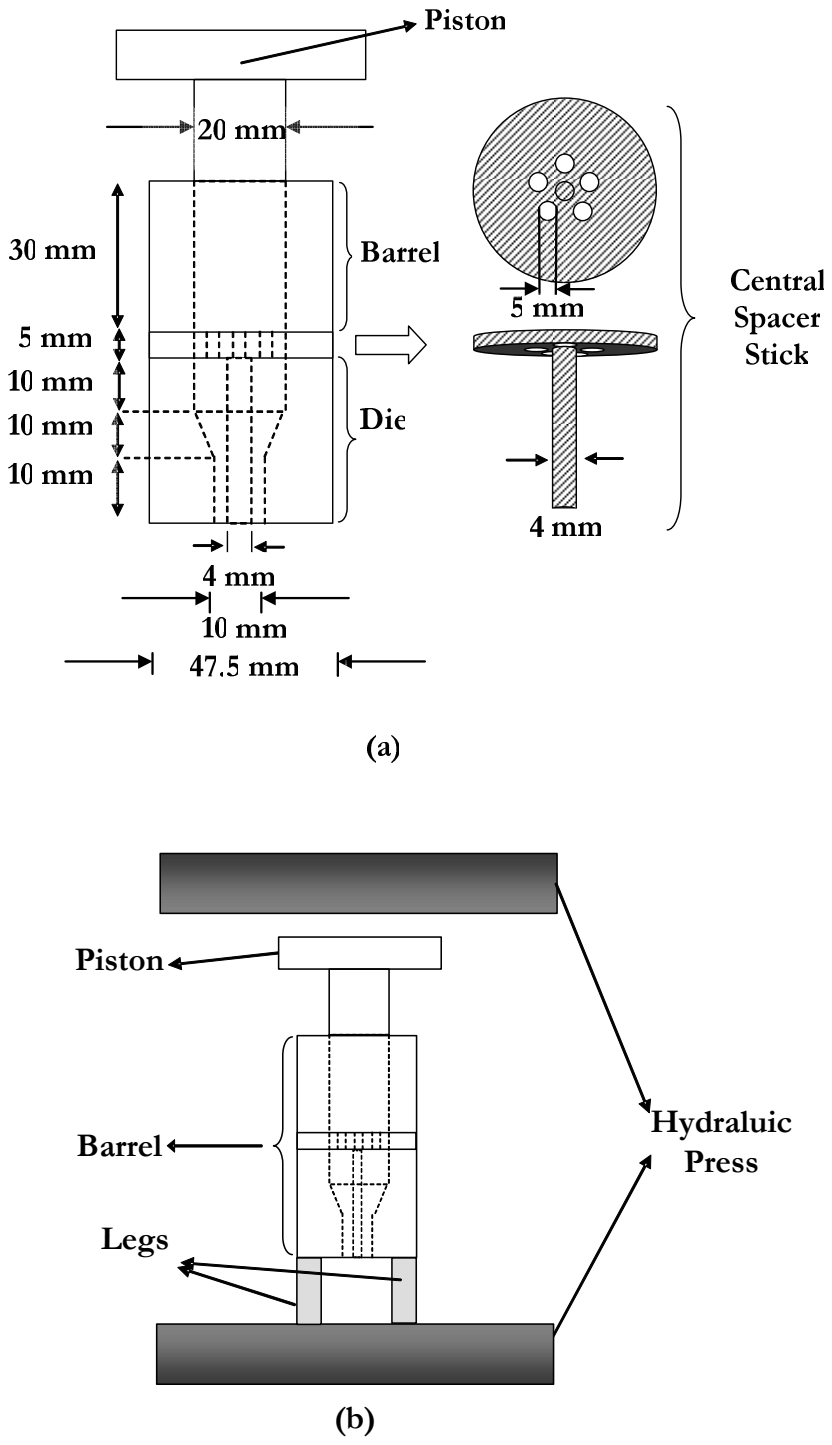

Figure 3.3. (a) Schematic presentation of stainless steel ram extruder, which can be used to extrudate bars with central spacer stick and tubes without central spacer stick filler (b) Schematic representation of the extrusion process

For extrusion, the ram extruder is placed on 7.5 cm-long legs to provide a space for the extrudate to come out of the die. The entire set-up was then put on a hydraulic press vertically and the piston of the extruder was slowly and continuously pushed down by the hydraulic press (Figure 3.3.b). During the extrusion, pressure increases until the paste comes out. After that point, the pressure stays constant. The tubular extrudates had an outer diameter of 9 mm and inner diameter of 3.5 mm.

In the case of the disk preparation, the amorphous alumino silicate powder was pressed into disks under a pressure of 0.5 MPa without addition of the HEC. The diameter and thickness of disks were 20 mm and 1 mm, respectively.

The amorphous extrudates and disks were dried at room temperature overnight and were calcined in air at 600°C for 2 hours in a muffle furnace. The heating rate was 2°C/min.

For the hydrothermal conversion of amorphous extrudates into zeolite A, either the liquid phase separated from the hydrogel by filtration or a reactive solution prepared with a molar composition similar to the liquid phase was used. The filtered liquid phase, kept in plastic cups with tightly closed lids, was transparent and stable for nearly 3 weeks, then precipitation occurred although no turbidity was observed. The preparation of reactive solution was described in Section 3.4.2 in detail.

The hydrothermal treatment was carried out PTFE cups of 15 ml and 30 ml capacity 80°C. PTFE tape was wrapped around the mouth of the PTFE cup to prevent leakage and the tap was closed tightly. The weight of liquid solution to the solid extrudate solution was typically 14. After synthesis, bars and tubes were washed with distilled water and dried at room temperature. The synthesis was generally carried out for 72 h, yet the synthesis time was changed between 0 to 72 h for some batches in order to monitor the course of crystallization of the macrobodies. Sample codes starting with CG represents the all synthesized tubes, bars and disk as binderless macrobodies and all are given in Appendix B with numerical order according to their synthesis conditions and XRD and SEM characterization results.

3.4. Parameters investigated in the crystallization of tubes

3.4.1. Effect of gel washing

The solid phase separated from the hydrogel was washed with distilled water to obtain the powder for the preparation of amorphous alumino silicate extrudates. The washing was carried out using four methods (Figure 3.4).

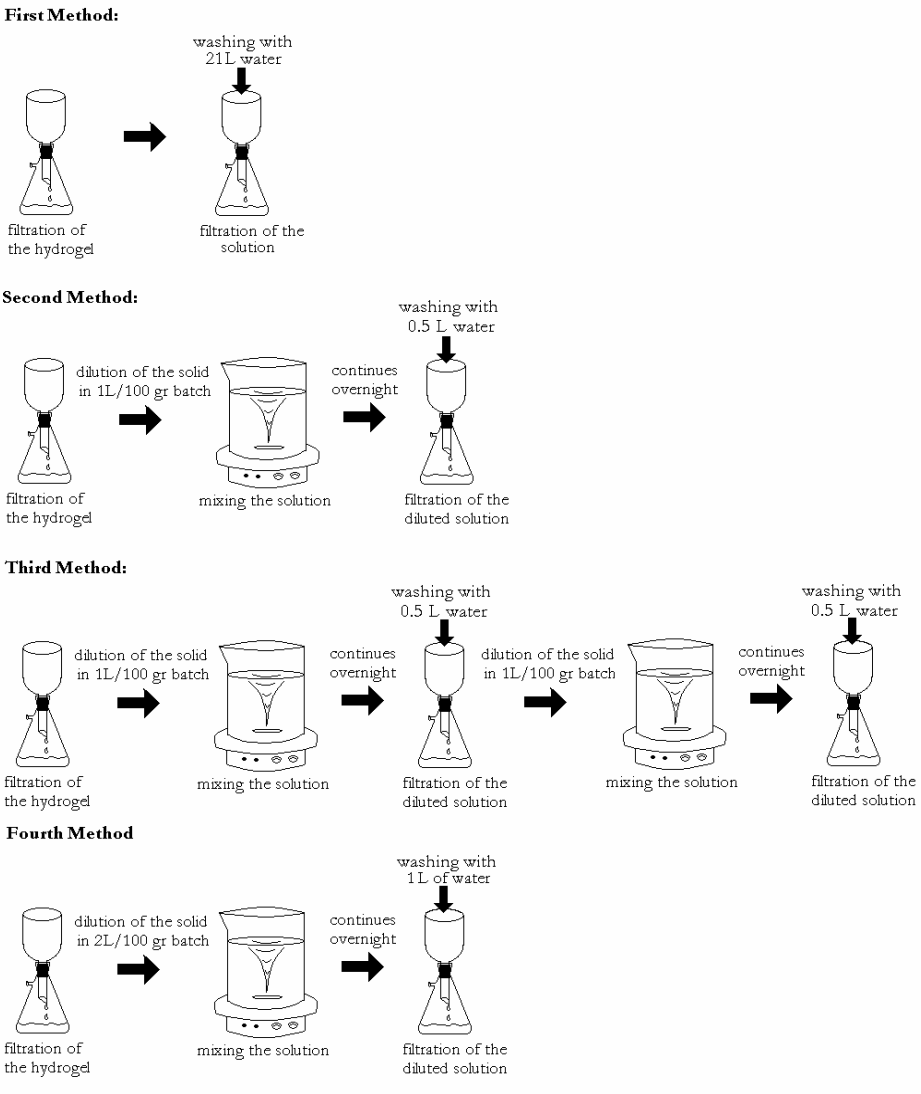

Figure 3.4. Schematic presentations of the four washing methods.

In the first method, wet cake is washed with approximately 21 L distilled water for 100 g of hydrogel as described by Özcan [21]. In the washing process, distilled water is flown over the solid deposited onto the filter paper. In Methods 2 and 3, the solid phase obtained from 100 g hydrogel is dispersed in 1 and 2 L distilled water, respectively, and stirred overnight. The mixtures were then filtered using a Buchner funnel to recover the solid phase again. The cake deposited on the filter paper was finally washed with 0.5 L distilled water in Method 2 and with 1 L distilled water in Method 3. In Method 4, the procedure followed in the Method 2 was repeated so that the cake was again dispersed in 1 L distilled water, filtered and finally washed with 0.5 L distilled water. These methods are also summarized in Table 3.1.

Table 3.1. Washing methods

	Dispersion and washing amounts		**Times of dispersion and washing**	
Method	Dispersion (L)	Washing (L)	Dispersion (L)	Washing (L)
1	-	21	-	Once
2	1	0.5	Once	Once
3	1	0.5	Twice	Twice
4	2	1	Once	Once

3.4.2. Effect of synthesis liquid

Syntheses of the extrudates are carried out by using the liquid composition that is separated from the hydrogel or a reactive solution as already mentioned in Section 3.3. The reactive solutions are prepared according to the same method that has been explained in Section 3.2. The compositions of the reactive solutions have the same main formula $N_xS_yA_1H_z$ which is prepared by changing $0 \leq x \leq 8.5$, $0 \leq y \leq 5.88$. The water in the reactive solution was set to 95% by mol of the total so that z changes between 0 and 990. Compositions of the all the reactive solutions that are used are given in Appendix B.

3.4.3. Effect of synthesis liquid to solid extrudate weight ratio

The conversion of amorphous alumino silicate extrudates to zeolite A was carried out in PTFE cups filled with the liquid synthesis solution as described in Section 3.3. The ratio of weight of liquid to the weight of solid was typically 14 in each PTFE cup (hereafter it will be shortly cited as liquid/solid ratio). The effect of liquid/solid ratio on the crystallinity and morphology of tubes was investigated in a set of experiments. For this purpose, synthesis was carried out at liquid/solid ratios of 3.5, 7, 14, 21, 35, 42, 56 and 105 with two different synthesis solutions by following the procedures described in Section 3.4.2. The compositions of synthesis solutions were $N_{4.8}A_1S_{0.07}H_{400}$ and $N_{2.33}S_1H_{330}$, where N is Na_2O, A is Al_2O_3, S is SiO_2 and H is H_2O.

3.5. Characterization of the macrobodies

3.5.1. Phase identification and determination of crystallinity by XRD

Philips PW 1729 X-ray Diffractometer (XRD) was used for phase identification of macrobodies. For analysis, macrobodies were crashed into powder in an agate mortar. The analyses were made using Ni filtered Cu Kα radiation. The other conditions were 30 kV voltage, 24 mA amperes, 0.1° 2θ/s scan speed, 10000 counts/s range, 1.0 s of time constant and 0.2 mm of slit.

For phase identification, the XRD pattern of a sample was compared with the XRD pattern of zeolite A given in ICDD (PDF No: 39-0223) and with the XRD pattern of commercial zeolite A powder (Merck Lot No: 5251610, Art: 6103). XRD patterns were also used for semi-quantitative determination of crystallinity by intensity summation method using Equation 3.1.

$$\% \text{ Crystallinity} = \frac{\sum I}{\sum I_0} \times 100 \qquad (3.1)$$

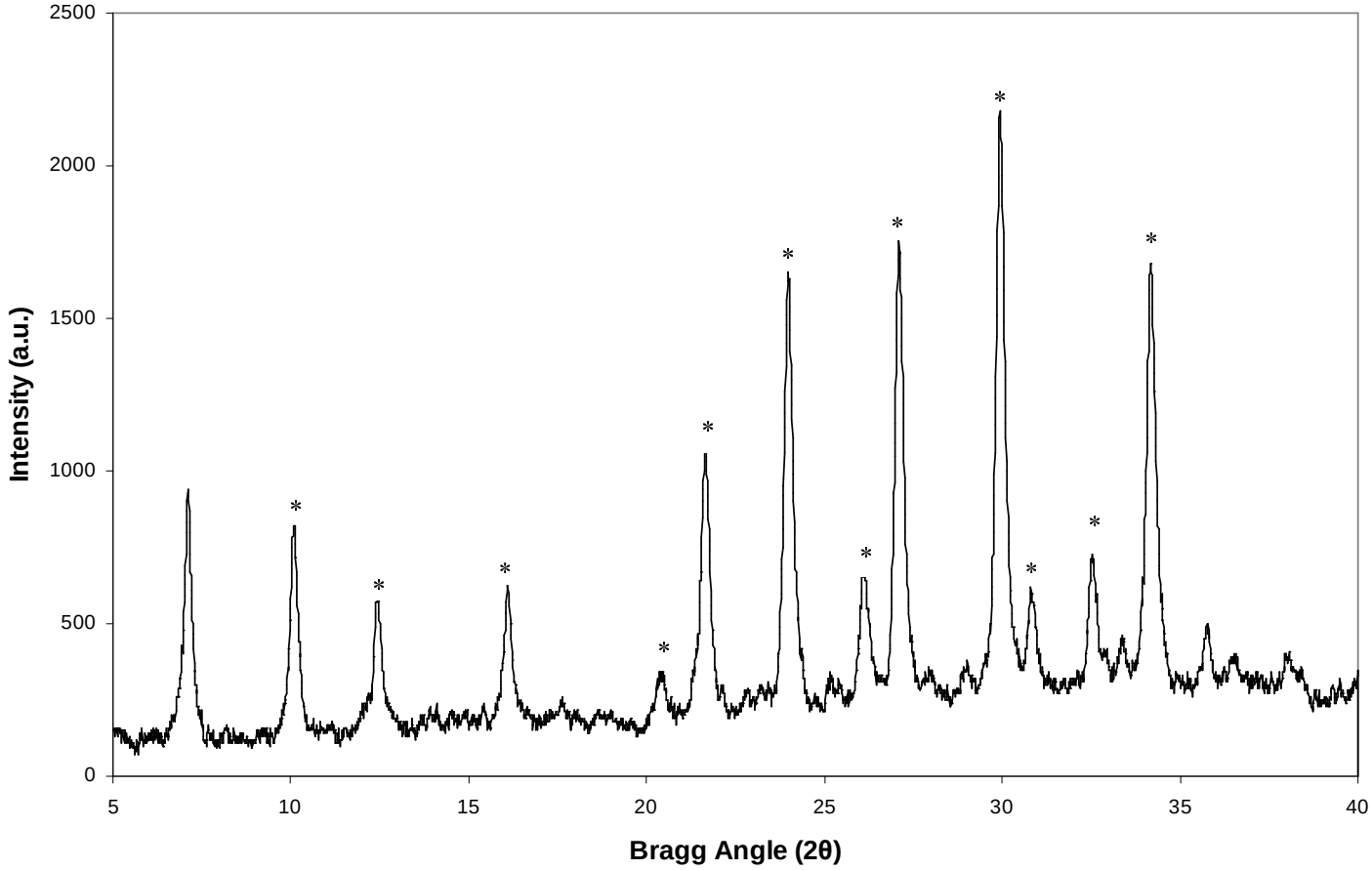

Figure 3.5. XRD pattern of commercial zeolite A powder. The peaks marked with asterisk (*) were used for crystallinity calculation

For this purpose, commericial zeolite A powder, assuming it is 100 % crystalline, was used as the reference. The intensities of 12 peaks on the XRD pattern of commercial zeolite A (Figure 3.5) were summed after purging background radiation. Similarly total intensity for the sample was calculated using the peaks at the same angles. The ratio of total intensities was defined as the relative percent crystallinity.

3.5.2. Determination of morphology by SEM

The scanning electron microscopy (SEM) images were taken by FEI QUANTA 400F Field Emission SEM at Central Laboratory and by JEOL JSM6400 Scanning Microscope at the Department of Metallurgical and Materials Engineering at METU. Experiments were done at 20 kV or 30 kV accelerating voltage. Samples were put on brass sample stubs and coated with gold and platinum. The micrographs were taken at magnifications of 400X, 500X, 1000X, 1500X, 2000X, 3000X, 5000X, 10000X and 50000X.

3.5.3. Determination of weight loss by TGA

Thermal gravimetric analysis (TGA) experiments were performed using Perkin Elmer Pyris 1 TGA at Central Laboratory in METU. The samples were heated in air with a heating rate of 10°C/min. The temperature was increased from room temperature to 900°C. For each analysis, approximately 15 mg of sample was used.

3.5.4. Characterization of pore structure by mercury porosimetry and nitrogen adsorption

The macropore and mesopore structure of samples which are dried at 80°C are determined using Quantochrome Corporation, Poremaster 60 mercury porosimeter at the Central Laboratory in METU. Analyses were carried out at high pressure range of 20-50000 psi at room temperature.

rnThe BET surface areas of the macrobodies were determined by nitrogen adsorption at 77 K using Quantochrome Corporation, Autosorb-1-C/MS at 77 K. Prior to analysis, samples were converted from as-synthesized Na-form to Ca-form by ion exchange. For ion exchange, 1 g of zeolite A was put into 150 ml of 1M Ca^{2+} solution in a constant temperature bath for a week. The temperature was kept constant at 25 ^{o}C, and the Ca^{2+} solution was refreshed daily. The Ca^{2+} solution was prepared either using $Ca(NO_3).10H_2O$ (pure, Merck) or $CaCl_2$. Ion exchanged samples were then dried at room temperature and then dried further at 300°C for 3 hours before testing.

3.5.5. Elemental analysis by EDX and ICP

The elemental analysis (Na, Si and Al) of the solid samples were performed using Perkin-Elmer model DRC II inductively coupled plasma-mass spectroscopy (ICP-MS). For this purpose, the samples were dissolved in HF by microwave digestion. The elemental analysis on some of the samples were performed by energy dispersive X-ray (EDX), which is an attachment to the SEM.

3.6. Synthesis of membrane layer on tubes and disks

Zeolite A films were synthesized over zeolite A bars, tubes and disks for use as membrane. The hydrothermal synthesis of zeolite A films was carried out using three different gel compositions extracted from the literature. Those compositions are known to yield highly crystalline zeolite A membranes over alumina tubes, which works well in pervaporation and gas separation applications. The selected compositions are $N_2A_1S_2H_{120}$ [9], $N_2A_1S_2H_{150}$ [11] and $N_{49}A_1S_5H_{980}$ [25], where N is Na_2O, A is Al_2O_3, S is SiO_2 and H is H_2O. These compositions will be referred to MC1, MC2 and MC3, respectively. The procedure described in Section 3.2. is also followed to prepare the synthesis solution of the membranes.

Zeolite A support was put in a PTFE container and the container was filled with synthesis solution up to 28 ml for stainless steel autoclaves and 24 for the PTFE

autoclaves. During synthesis of the zeolite supports, two methods are followed. In dry-support method, the zeolite support to be synthesized in the membrane synthesis compositions (MC) are directly put within the autoclave and then the MC is added over it. However, in wet-support method, the zeolite support to be synthesized is first saturated with water, then it is put into the autoclave and the MC is added over it. When the tubular zeolite A macrobodies are used as support, the lumen of the tube is carefully filled with the synthesis solution. The typical tube length used for the membrane synthesis is 2 cm. Synthesis temperature was 80°C for the composition MC3, while it was 100°C for the others. Synthesis time is changed between 5 and 20 h.

Sample codes starting with CGM represents the all synthesized tubes, bars and disk shaped membranes and all are given in Appendix F with numerical order according to their synthesis conditions.

3.7. Construction of pervaporation set-up

The central spacer stick may not be located precisely at the center of the extruder die because of the problems related with the design and construction of homemade extruder, which causes uneven flow area for the paste. Therefore the velocity of paste in the die will be slightly different at each point at a constant flow rate of paste. As a result of this problem, the zeolite A tubes were not straight, but they were usually bent. In addition since piston of the extuder is pressed manually with a stepwise increase of pressure of the hydraulic press, this discontinuous pressing may also cause bending of the tubes. Therefore the membrane module used in the pervaporation system should provide sufficient elasticity to be able install membranes without breaking. The module was also desired to access mounting of membranes with geometries other than tube such as bars and disks. Therefore, the system was decided to be as small, simple and flexible as possible.

Figure 3.6 shows the schematic presentation of the pervaporation system. The system was composed of three main parts, namely, feed side, permeate side and vacuum side. The permeate side consisted of two collectors placed in liquid nitrogen traps. The

collector closed to the feed side was to accumulate the sample, and the other one was to capture the permeating vapor escaped from the first collector. The permeate side was at nearly 3 mmHg, achieved by Edwards RV70 model vacuum pump.

All piping in the feed side is and the permeate side is stainless steel. The feed side consists of the feed tank, membrane, thermocouple, heater/stirrer and circulation bath. The permeate side consists of a pressure gauge and two liquid nitrogen traps and the vacuum side contains the vacuum pump and the vacuum trap. Glass containers are connected to each other by stainless steel ultra-torr Cajon fittings which are resistant to high vacuum.

The membranes were glued at two pieces of glass tubes, one has a dead end and the other connects the membrane to the vacuum line as shown in Figure 3.7. For this purpose, Varian-Torr Seal adhesive, which is applicable in high vacuum applications, was used. Since the membrane is not assembled to the system from both ends as opposed to the many conventional pervaporation systems [11, 50, 51], no stress develops on the membranes so that the module is likely to minimize the probability of membrane break down. Besides it is possible to mount membranes with different geometries and diameters to the system only by changing the dimensions of glass pieces.

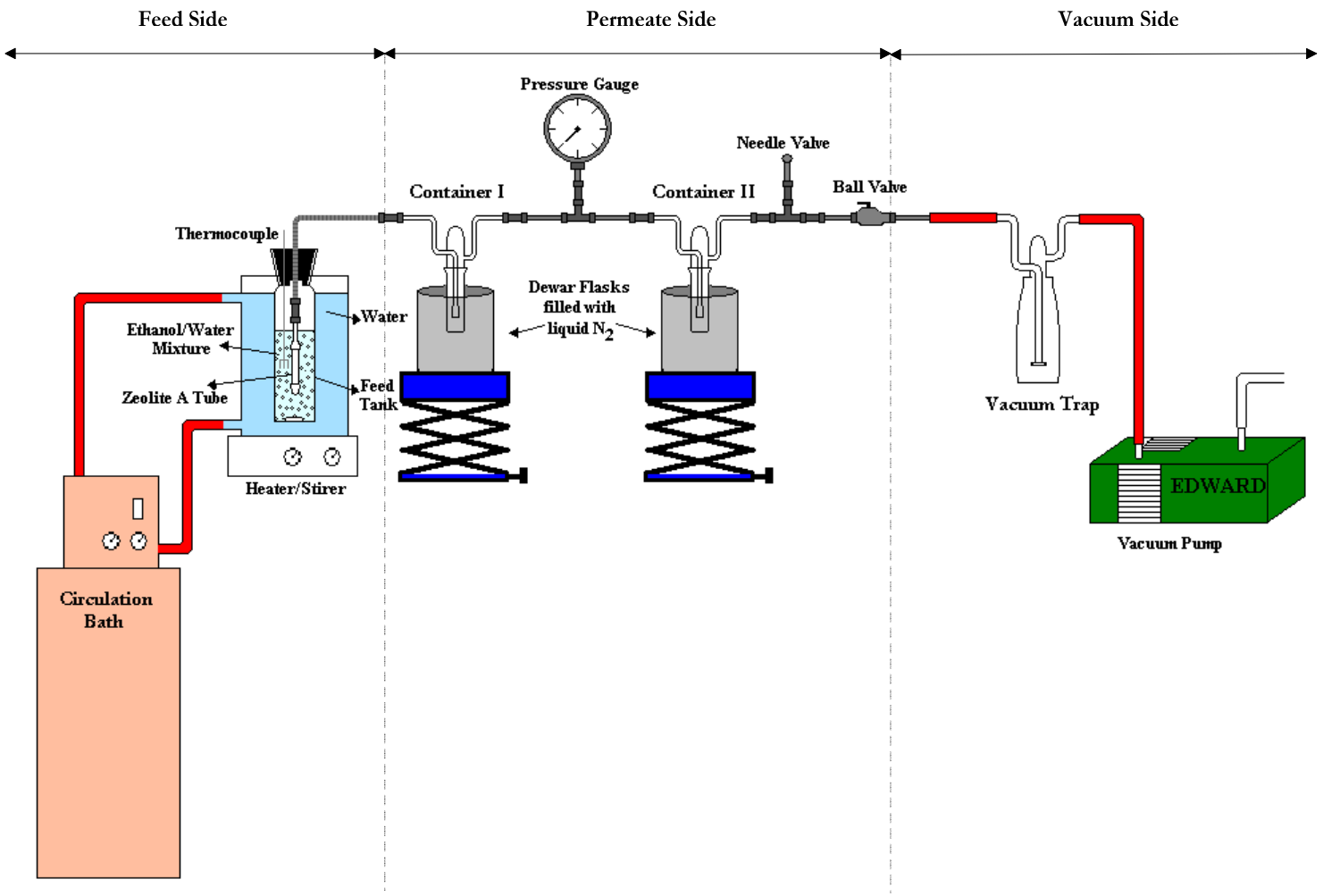

Figure 3.6. Schematical drawing of the pervaporation set-up

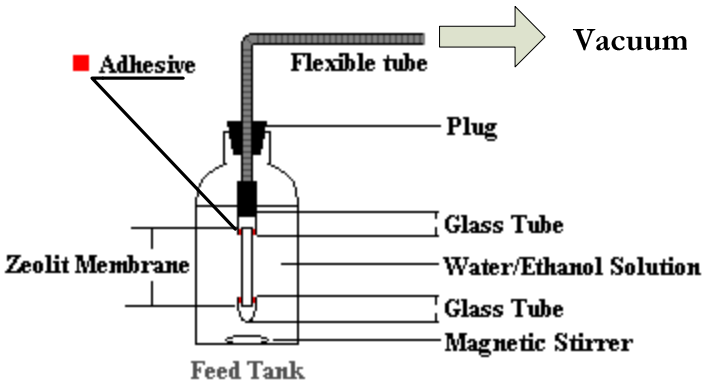

Figure 3.7. Feed tank and placement of the membrane in the tank

The membrane was then put into a glass container with a volume of 600 ml and a diameter of 3.5 cm, which was filled with the feed solution. The feed container was kept at constant temperature with a jacket filled with water recirculating between the system and a constant temperature reservoir. The feed container was also placed on a magnetic stirrer to keep the properties of feed solution uniform and to reduce the concentration gradients in the container.

CHAPTER 4

RESULTS AND DISCUSSION

4.1. Characterization of Binderless Zeolite 4A Bars, Tubes and Disks

The objective of this study is to synthesize self-supported zeolite A membranes. In order to prepare zeolite A membranes, firstly binderless zeolite A macrobodies are prepared as explained in Chapter 3. The macrobodies were then characterized.

This section shows the characterization results of binderless zeolite A tubes, bar or disks. These macrobodies were prepared as follows: the starting hydrogel is filtered to obtain a wet solid cake and a liquid solution. The wet cake is then washed according to the second washing method as described in Part 3.2. The amorphous powder is then shaped into either disks or mixed with HEC to obtain a paste. The paste is then used to prepare bars or tubes. These macrobodies are converted into zeolite A in the liquid solution that has been obtained from the filtration of the hydrogel.

Figure 4.1 shows the XRD patterns of the green (a), calcined (b) and synthesized (c) tubes in comparison with the commercial zeolite A powder (d). The green and calcined tubes are completely amorphous. A hump centered at 28° Bragg angle is characteristic to the amorphous aluminosilicates [52, 53]. The hump is more apparent in the pattern of green tube than in the pattern of calcined tube.

The positions of all peaks on the pattern of synthesized tube (Figure 4.1.c) matches with those of commercial zeolite A powder (Figure 4.1.d), indicating that zeolite A is the only crystalline phase existing in the tubes. The crystallinities of the macrobodies were

calculated by intensity summation method as described in Part 3.2. Accordingly, the synthesized tube, CG16F, has a crystallinity of 95% with respect to the commercial zeolite 4A powder. In this study, the average crystallinity of 10 tubes was 88 %, indicating that it is possible to synthesize binderless zeolite A tube with very high purity by the method described in this work.

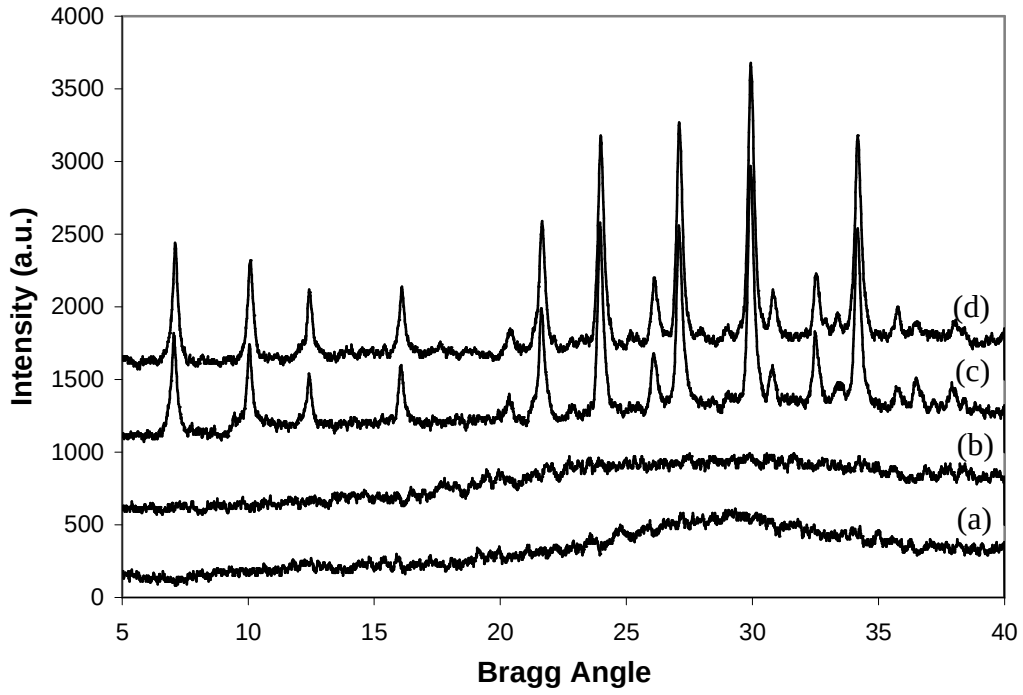

Figure 4.1. XRD patterns of (a) Green tube/CG21 – dried at room temperature for 24h, (b) Calcined tube/CG32 – calcined at 600°C for 2 h, (c) Synthesized tube/CG16F – hydrothermally converted into zeolite A at 80°C for 72 h (d) Reference/TZ4A – the XRD pattern of the commercial zeolite 4A powder.

Figure 4.2 shows the photographs of a binderless zeolite A tube, bar and disk synthesized in this study. The figure also shows the photograph of zeolite A powder,

synthesized directly from the hydrogel at 80°C for 24 h. The tubes and bars had very smooth surface and usually free of large cracks and flaws. However, some thin and short cracks were often observed on the surfaces of tubes and bars after extrusion or after calcination. The possible reasons of thin cracks are:

1. The aluminosilicate powder and the paste were ground on a mortar for at least one hour to obtain fine powder and to remove air bubbles, respectively. Non-uniform particle size and the air trapped in the paste may cause cracks on the green tubes.
2. The barrel of the home-made extruder has small capacity for paste. Therefore the paste in the mortar dries a little and may lose its plasticity. Cracks may form on the tubes prepared from a paste with low plasticity.
3. The wheel of the hydraulic press cannot be turned constantly. Therefore the extruder ram apply force on the paste intermittently, which may also trigger some cracks on the green tubes.

The annulus for paste flow in the tube extruder may not be eccentric but non-eccentric. Uneven paste velocity causes bending of the tubes and originates cracks. Therefore tubes with a length of 2-3 cm were extruded.

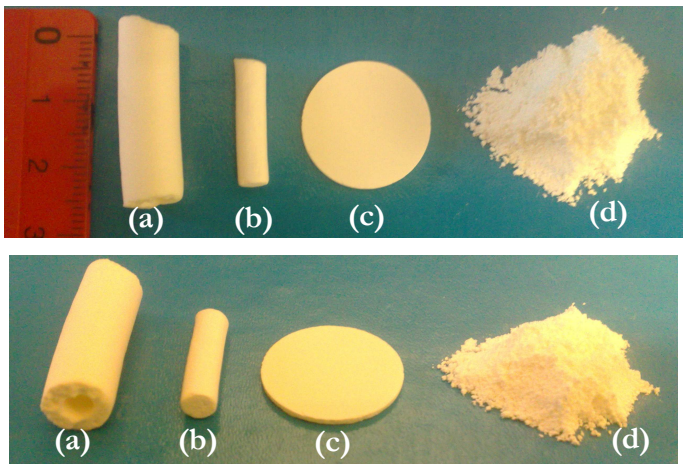

Figure 4.2. Photographs of a zeolite A tube (a), bar (b), disk (c) and zeolite A powder (d)

The dimensions and weights of the green, calcined and synthesized macrobodies are given in Table 4.1. The dimensions stated here are the average of 6 tubes, 10 disks and 7 bars.

The weight of the green bars and tubes decreased on calcination because of the removal HEC and water during calcination. The macrobodies also slightly shrink during calcination. On the other hand, the weight increase with the conversion into zeolite A can mainly be attributed to the water adsorption since zeolite A is a very hydrophilic material.

Table 4.1. Average weight and dimensions of the green, calcined and synthesized macrobodies

Macrobody	**Form**	**Dimensions**			
		Weight (g)	**Length (cm)**	**Inner Diameter (cm)**	**Outer Diameter (cm)**
Tube	Green	2.13	3.03	0.35	0.99
	Calcined	1.09	2.90	0.36	0.90
	Synthesized	1.93	2.93	0.36	0.90
		Weight (g)	**Length (cm)**	**Diameter (cm)**	
Bar	Green	0.27	2.12	0.52	
	Calcined	0.23	2.11	0.45	
	Synthesized	0.26	2.12	0.46	
		Weight (g)	**Thickness (mm)**	**Diameter (cm)**	
Disk	Green	0.48	1.28	1.99	
	Calcined	0.47	1.22	1.95	
	Synthesized	0.64	1.30	1.98	

Figure 4.3 shows the Thermal Gravimetric Analysis (TGA) results of the tubes. TGA analyses were carried out in air atmosphere, from room temperature to 900°C at a heating rate of 10°C/min. The weight of green tube decreases by 21.9 % up to 500°C. The weight loss is essentially due to the removal of the HEC and water from the structure. Note that HEC decomposes at 210°C in air [54], yet complete removal of HEC from a porous structure may require higher temperatures.

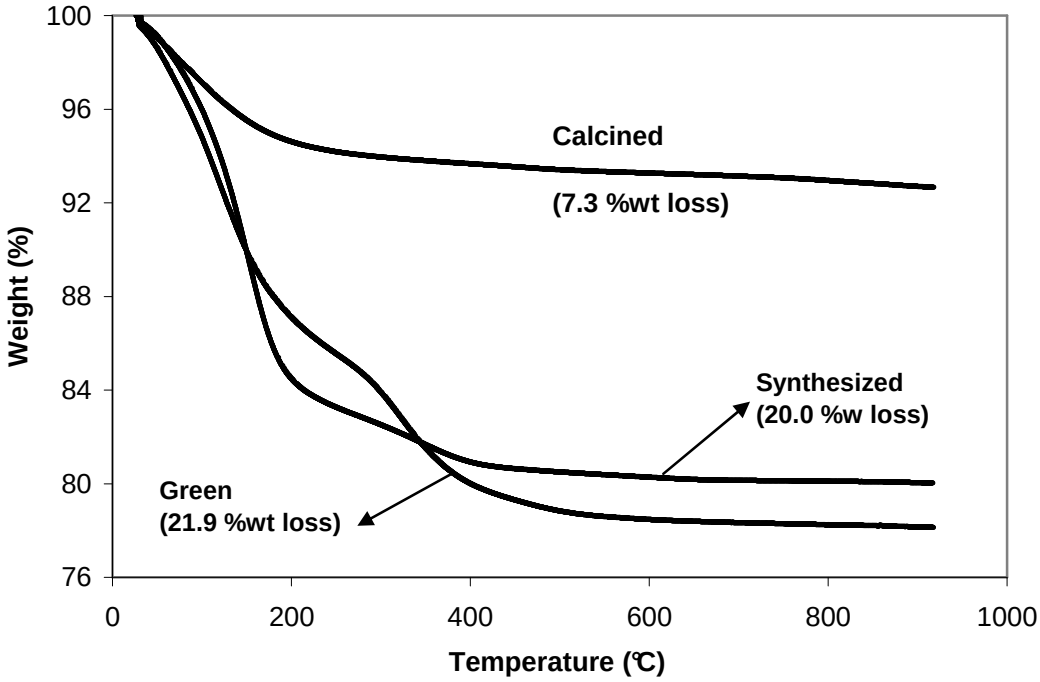

Figure 4.3. TGA analysis of the green (CG16G), calcined (CG16C) and synthesized (CG16F) tubes.

TGA of the calcined tube shows a 7.33 % weight loss up to 300°C, and then the weight of the tube nearly stays constant. The weight loss is due to the water content of the tubes, which is possible considering that they have being stored in zipped bags during

the period of time between calcination and TGA analysis. Synthesized tube also shows a weight loss of 20.0 %, which can again be attributed to water since zeolite A is a very hydrophilic zeolite. The pseudo unit cell of zeolite A has the oxide formula of $Na_{12}[(AlO_2)_{12}(SiO_2)_{12}].27H_2O$, which shows that the water content of a zeolite crystal is 22.2 wt% [1]. This is consistent with the water content of zeolite A tubes, suggesting that the tubes are highly pure zeolite A.

Figure 4.5 shows the SEM images taken from different sections of a zeolite A tube. By what is meant by different cross sections is shown by an image in Figure 4.4. SEM images at lower magnifications, thus showing a larger area, are inserted in Appendix C. All sections of the tube exhibited a similar structure. The tube is composed of highly intergrown zeolite A crystals, among which large cavities and pores formed. Intergrowth of crystals is essential to have a firm structure with macropores. The crystals are cubic that is the characteristic shape of zeolite A crystals. The average crystal size was 3.5 μm, and exhibited relatively wide size distribution as shown in Figure B.1 in Appendix B.

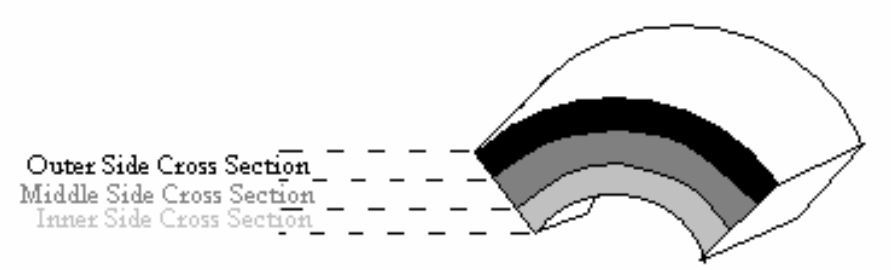

Figure 4.4. Schematic representation of the differentiation of the cross section parts for a tube from where the SEM images taken.

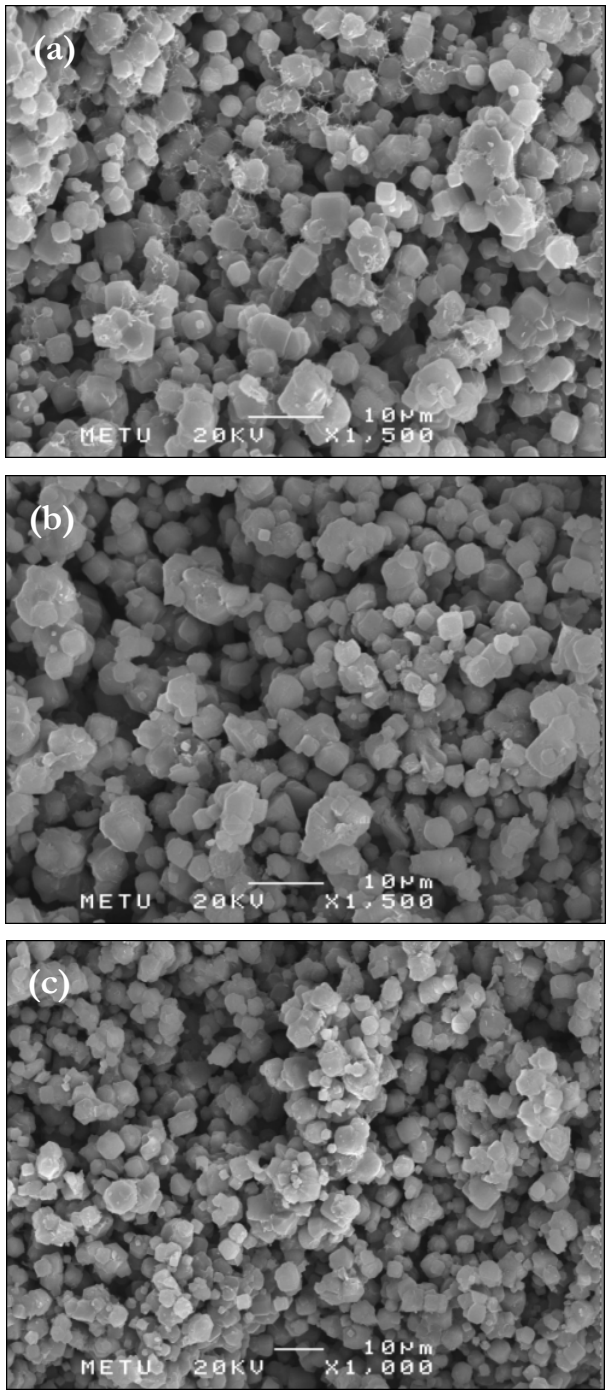

Figure 4.5. SEM pictures taken from **(a)** outer **(b)** middle **(c)** inner sides of the cross section of the CG16F.

4.2. Simplifying the synthesis procedure by changing washing procedure

The alkalinity of the wet cake is usually around 13 for sodium aluminosilicate gels [55], and it mainly arises from the sodium hydroxide used to prepare the gel. The excess sodium ions may deposit as sodium hydroxide again after drying of wet cake to obtain the aluminosilicate powder. Thus there exists sodium hydroxide in the extrusion paste and consequently in the green macrobodies. Excess sodium hydroxide may change the water content of paste during extrusion because of its hygroscopic structure, and may initiate the formation of undesired crystalline or glassy phases during calcination.

In the literature there is no standard pH value that the aluminosilicate gels should have after washing and a specific amount of water necessary for washing of 100 g of gel. For example, Krznaric et al. [55] that deals with the microstructure of amorphous aluminisilicate gel, decreases the pH of the wet cake to 9 by washing. In another study carried out by Morsli et al. [56], the filtered solid phase was washed with a deionised water, whose amount is just the twice the amount of synthesis batch.

The procedure proposed by Özcan [21] to make zeolite A bars involves the washing of the wet cake to decrease the pH around 8. For this step of process, the wet cake obtained from 100 g of hydrogel was washed with approximately 20 L of distilled water. The wet cake was on a Whatman No: 42 filter paper in a Buchner funnel with an active area of 95 cm^2. The wash-water was drawn from the cake by strong vacuum, which was generated by a rotary vacuum pump. The washing process under these conditions took about 8 h. Apparently, the washing step consumes remarkably high quantity of distilled water and takes long time so that it is likely to be replaced with a more efficient washing procedure.

In this study, the washing step and its possible effects on the synthesized tubes have been investigated by means of four methods. The first method is the method originally used by Özcan [21], and the washing is continued until the pH of the wet cake dropped to 8. In the other methods the wet cake was dispersed in a specific amount of distilled

water and stirred for one day and then filtered to recover the solid. The solid was finally washed with 0.5 L distilled water. The characterization of zeolite A tubes prepared by different washing methods were characterized by mainly XRD and SEM. Reproducibility of the results were also investigated.

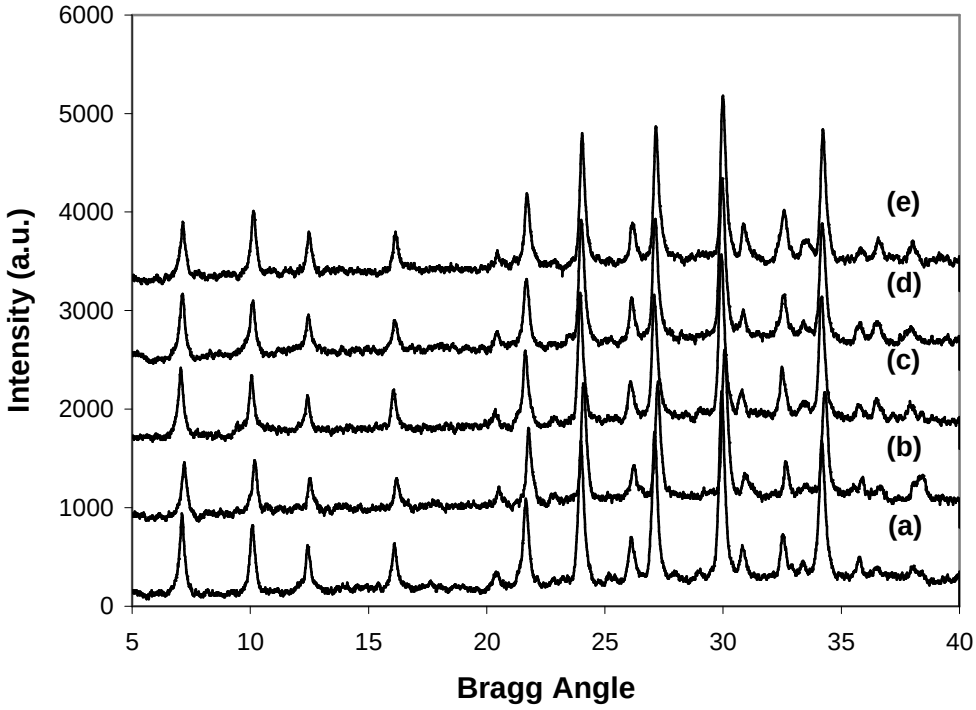

Figure 4.6. XRD patterns of the synthesized tubes according to the varying washing method in comparison to commercial zeolite 4A powder **(a)** first method (CG6A) **(b)** second method (CG16F) **(c)** third method (CG14F1) **(d)** fourth method (CG15F) **(e)** commercial zeolite 4A powder. The syntheses of tubes were performed in the original liquid solution at 80°C for 72 h.

Figure 4.6 shows the XRD patterns of the synthesized tubes with respect to their washing method and the pattern of the commercial zeolite A powder. The percent crystallinities calculated by intensity summation method are shown in Table 4.2.

Regardless of the washing method all tubes were zeolite A without any impurities present as determined from XRD patterns. The intensities of the characteristic zeolite A peaks of the synthesized tubes are slightly lower than those of commercial zeolite A powder. The disorder on the crystal planes because of twinning or intergrowth of crystals may cause a decrease in the XRD peak intensities. Therefore the zeolite A bars may seem to have lower crystallinity than the powder zeolite A. The crystallinities change between 81 and 97%, however, there is no clear correlation between the washing method and the crystallinity. Apparently, washing method has no significant effect on the crystallinity of zeolite A tubes. The average crystallinity of tubes is 88, suggesting that highly pure zeolite A tubes can be prepared regardless of washing method.

Table 4.2. Crystallinity values of the tubes synthesized by using differing washing methods. The syntheses of tubes were performed in the original liquid solution at 80°C for 72 h.

Washing Method	**Dilution amount (L)**	**Times of dilution**	**Sample Code**	**Crystallinity %**
Method 1	21	Once	CG6A	81
			AÖ129H	86
Method 2	1	Once	CG13F1	84
			CG16F	94
Method 3	1	Twice	CG14F1	86
			CG17F	93
Method 4	2	Twice	CG15F	82
			CG18F	97

Since the washing procedure has no influence on the crystallinity of tubes, only tubes prepared by Method 1 and 2 were further characterized. Method 1 had also been used

by Özcan [21] and Method 2 is the simplest procedure among all. The further characterizations were performed by ICP, SEM, mercury intrusion porosimetry, N_2 adsorption and BET surface area analysis, and TGA.

The ICP analysis and calculations for their dry compositions based on the analysis of the amorphous aluminosilicate powders obtained by by Method 1 and Method 2 are given in Appendix E. Accordingly, the amorphous aluminosilicate powder prepared by Method 1 has a composition of $1.09Na_2O:Al_2O_3:2.94SiO_2$, whereas the washing Method 2 has the composition of $1.07Na_2O:Al_2O_3:2.66SiO_2$. The compositions indicate the closeness of the amorphous aluminosilicate powders that is used for the preparation of the solid extrudates

Figure 4.7 shows the SEM images of tubes synthesized by Methods 1 and 2. Both tubes have very similar structure, they consist of highly intergrown cubic zeolite A crystals with an average size of 3.6 μm. The crystals have chamfered edges. The porous structure of the tubes can also be noticed from the images.

Figure 4.8 shows the pore size distribution of tubes, which were obtained by mercury intrusion porosimeter operating in 2-50000 psi pressure range. The tube synthesized with Method 1 has wider pore size distribution that the tube synthesized with Method 2. The average pore sizes are nearly the same, 3.6 and 3.1 for the washing methods 1 and 2, respectively. The porosity of the synthesized tube using the washing Method 1 was 39 % with an intraparticle volume of 0.489 cm^3/g, and the tubes obtained by Method 2 has a porosity of 35% and intraparticile volume of 0.310 cm^3/g.

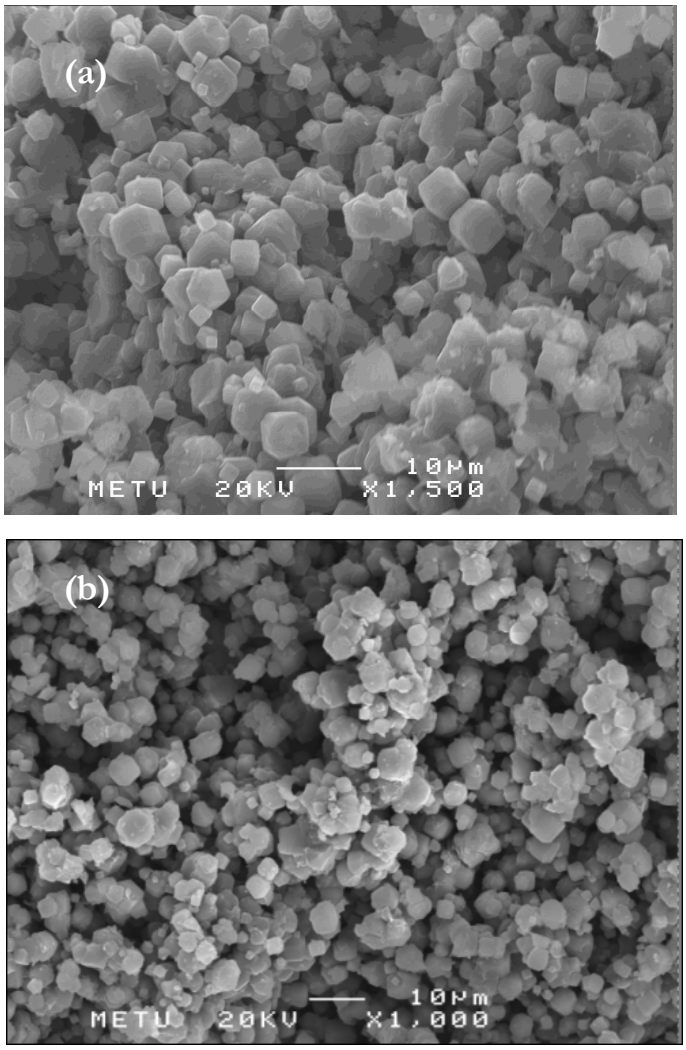

Figure 4.7. SEM images taken from the middle cross section of the zeolite A tubes that are prepared by (a) Method 1 (AÖ129H) (b) Method 2 (CG13F1). The synthesis was carried out in the liquid solution with a molar composition of $4.8Na_2O:Al_2O_3:0.07SiO_2:400H_2O$ at 80°C for 72 h.

.

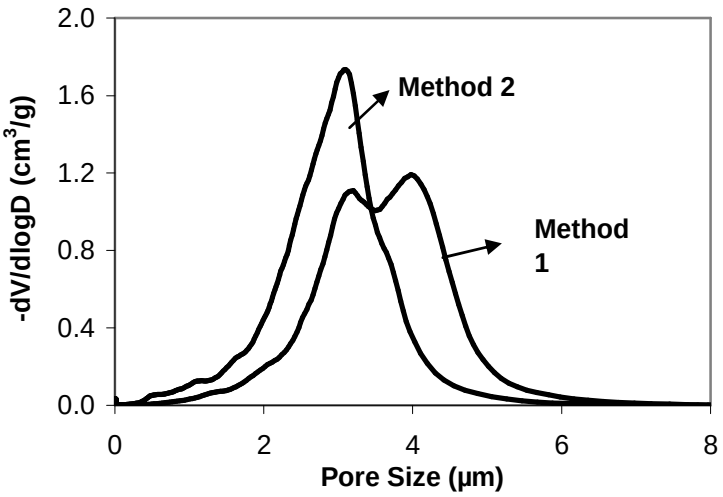

Figure 4.8. Pore size distrubition by mercury porosimetry of the synthesized tubes using washing Methods 1 (AÖ35T) and 2 (CG13F1).

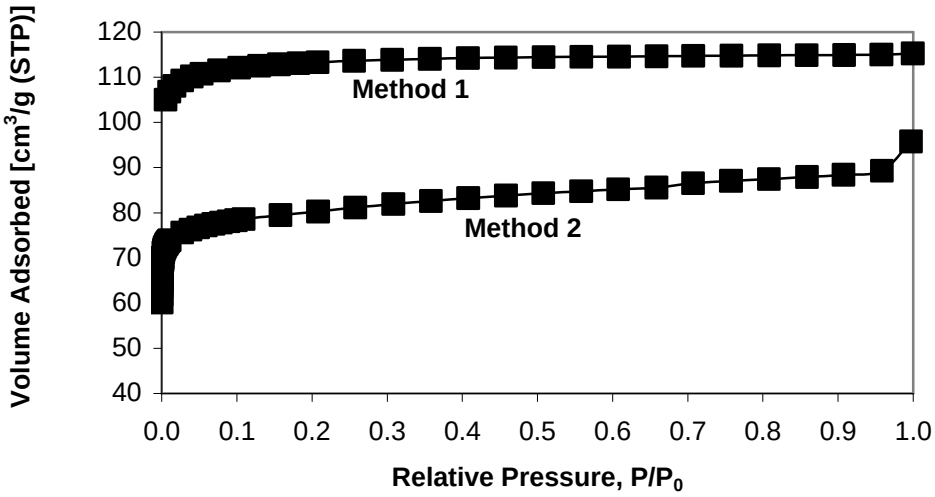

Figure 4.9. BET isotherms of the zeolite A tubes prepared using Method 1 (AÖ120) and Method 2 (CG13F1).

The BET isotherms for the tubes obtained by using these two methods can be seen in Figure 4.9. Prior to N_2 adsorption, the zeolite A forming the tubes were converted from sodium form to calcium form by ion exchange since N_2 cannot penetrate into the 0.42-nm pores of zeolite Na-A at the saturation temperature of N_2 [1]. The tube produced Method 1 exhibited a Type-1 isotherm, which is typical to microporous materials and also to zeolites [57]. On the other hand, the tube produced by Method 2 has a Type-II isotherm, which is characteristic to mesoporous materials. However the Type I isotherm was also expected for the tube obtained by washing method 2, considering high crystallinity determined by XRD and high morphological resemblance observed by SEM. The Type II isotherm for the sample prepared with Method 2 is therefore attributed to the poor ion exchange procedure.

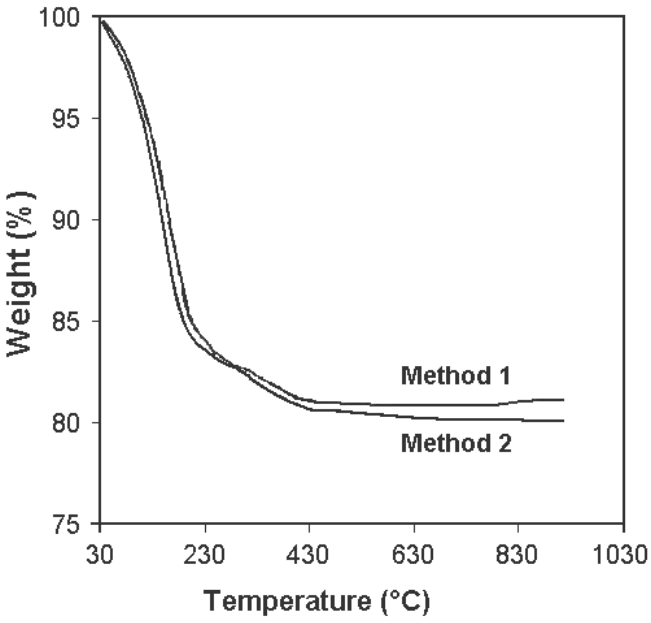

Figure 4.10. TGA results obtained for the synthesized zeolite A tubes using different washing methods. Sample codes AÖ60H for Method 1 and CG16F for Method 2.

The results obtained by TGA, given in Figure 4.10, also indicates the resemblance of the two synthesized zeolite A tubes, prepared by two different washing methods. The weight loss is nearly 20% for the two tubes, indicating the purity and same hydrophilictiy of the structure.

Table 4.3 summarizes the results of different characterization techniques. It can be concluded that regardless of the washing method, the synthesized zeolite A tubes are highly crystalline and have very similar physical properties. They are composed of cubic chamfered edge crystals with an average crystal size of 3.5 um. They have also very similar microstructure with a porosity of nearly 35.

Table 4.3. Summary of the results obtained for the zeolite A tubes prepared by washing method 1 and 2.

Washing Method	**Crystallinty %**	**Crystal size d_{ave} (μm)**	**Total Porosity %**	**BET surface area**	**Weight loss %**
1	86	3.6	39	439	19
2	85	3.5	35	304	20

4.3. Simplifying the synthesis procedure by using synthetic liquid solutions

Another drawback of the method proposed by Özcan [21] was that the conversion of amorphous macrobodies should be carried out in the liquid solution separated from the hydrogel. The water content of the hydrogel is 88 wt%. However, only nearly half of the liquid can be recovered during filtration, depending on the power of the vacuum and the time of filtration. On the other hand, the maximum amount of amorphous solid

powder that can be obtained is 8 wt% of the hydrogel (see Chapter 3.3.). The typical amount of liquid over the amount of extrudate ratio was 14 in the synthesis medium, thus the original liquid was insufficient to synthesize all the amorphous solid powder obtained.

In addition, the original liquid stays transparent and stable about 8 days. After this time, some precipitation occurs and a more opaque solution is observed. Özcan [21] also reported that zeolite Y and P may form when the synthesis is carried out in solutions aged for a long time. Preparation of a zeolite A tube takes typically 4 days from filtration of hydrogel to the beginning of hydrothermal synthesis, indicating that aging of synthesis solution is a limiting factor to be considered. Instead of using synthesis solutions filtered from hydrogel, using liquid solutions that can be prepared separately also simplifies the synthesis procedure significantly.

The oxide formula of the original liquid solution was 4.8 Na_2O: 1 Al_2O_3: 0.07 SiO_2: 400 H_2O, which was analyzed by ICP [21]. This formula was then simplified by dropping one of the components in the formula each time until only water remained left (Table 4.4). All the reactive solutions were separately prepared according to the methods described in Part 3.2 using sodium silicate solution, $Al(OH)_3$, NaOH and distilled water. The amorphous tubes were prepared by first washing method.

Table 4.4. Tubes used for the synthesis of the reactive solutions prepared to imitate the original liquid solution

Case	Sample Code	Reactive Solution
A	CG6E	Deionized Water
B	CG27A1	$2.4Na_2O{:}400H_2O$
C	CG31C5	$4.8Na_2O{:}400H_2O$
D	CG31D3	$4.8Na_2O{:}Al_2O_3{:}400H_2O$
E	CG31E1	$4.8Na_2O{:}Al_2O_3{:}0.07SiO_2{:}400H_2O$
F	CG16F	Original Liquid Solution

Figure 4.11 shows the XRD patterns of the tubes synthesized in the solutions with the compositions given in Table 4.2. The crystallinities of the tubes are given in Table 4.5. In deionized water, which is the simplest solution possible, the tube remained amorphous. Similarly, the synthesis in solution B, which is a dilute sodium hydroxide solution and free of alumina and silica, resulted in an amorphous tube. On the other hand, synthesis in concentrated sodium hydroxide, solution C, yielded a mixture of zeolite A (25%) and zeolite X (64%) although there were no alumina and silica in the initial liquid. Zeolite A and X are zeolites with SiO_2/Al_2O_3 ratio of 2 and 2.5-5, respectively [58, 59]. Therefore zeolite X can be viewed as a zeolite rich in silica with respect to zeolite A.

By introducing alumina into the synthesis solution, pure zeolite A tube with a crsytallinity of 94% was obtained. The addition of very small quantity of silica to the synthesis solution had no significant effect on the type of resultant crystals, the tube was again zeolite A with a crystallinity of 95%.

.

The crystallization of zeolites is proposed to follow solution-mediated transport [60]. According to this mechanism, the amorphous gel is dissolved, and the dissolved precursor species form the zeolite crystals, which finally precipitate. The conversion of amorphous tubes may follow a similar mechanism. However rate of dissolution should be slower that the rate of crystallization to preserve the structural integrity of the tube. During the synthesis in concentrated sodium hydroxide, Solution C, sufficiently high rate of dissolution may initiate the zeolitization process. However, Figure 4.11.c also indicates increase of the sodium hydroxide concentration without addition of alumina and silica into the synthesis solution also results in other crystal phases on the tube synthesized.

It can be said that it is possible to use a reactive solution instead of the liquid filtered from the hydrogel. These synthetic solutions can be prepared at desired quantities and at any time necessary for hydrothermal synthesis. Thus it introduces remarkable flexibility to the procedure to make binderless zeolite A bodies and significantly simplifies the procedure.

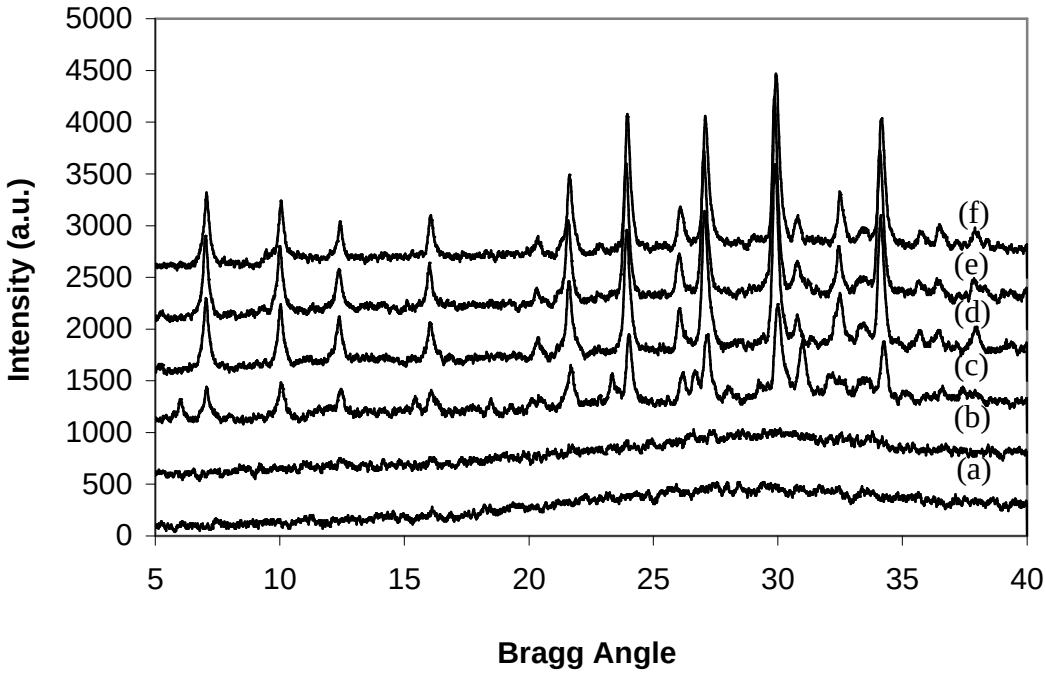

Figure 4.11. XRD patterns of the synthesized tubes using the imitated solution (a) Solutions A, (b) B, (c) C, (d) D, (e) E, (f) F. The oxide formulas of solutions are given in Table 4.4.

Table 4.5. The percent crystallinities of the tubes synthesized using different reactive solutions, in comparison to the original liquid.

Case	Reactive Solution	Crystallinity %
A	Deionized Water	0
B	$2.4Na_2O:400H_2O$	0
C	$4.8Na_2O:400H_2O$	25 (A) – 64 (X)
D	$4.8Na_2O:Al_2O_3:400H_2O$	94
E	$4.8Na_2O:Al_2O_3:0.07SiO_2:400H_2O$	95
F	Original Liquid Solution	94

4.4. Crystallization field of zeolite A macrobodies

The crystallization field of zeolite A macrobodies was determined by synthesis of zeolite A bars in synthesis solutions with different compositions. The liquid solutions were prepared as described in Part 3.2. The crystallization was carried out at 80°C for 72 h irrespective of the composition of liquid solution. The crystallization field of zeolite A macrobodies was compared with the crystallization field of zeolite A powder reported by Breck [1], who synthesized zeolite A from hydrogels containing 90 to 98 mole% water at 100°C.

It should be noted that the zeolite A tubes were prepared from amorphous aluminosilicate powders prepared at different times by following the same procedure (washing method 2). Therefore, the chemical composition of the amorphous solid extrudates and their structural properties were presumed to be the same throughout the study. The oxide formula of solid extrudates was $1.07Na_2O:Al_2O_3:2.66SiO_2$ in dry basis.

The major difference between the synthesis of zeolite macrobodies and zeolite powder is that zeolite powder is synthesized from homogeneous hydrogels while the zeolite macrobodies are obtained by hydrothermal conversion of preshaped amorphous zeolite macrostructures. Therefore the synthesis medium is not uniform as opposed to the powder synthesis. For this reason, it is possible to construct a phase diagram either using only the composition of liquid solutions regardless of the composition and amount of solid in the autoclave or using the overall composition in the autoclave, in which the composition of solid phase and the relative amounts of solid and liquid phases are taken into account. In this thesis, both types of phase diagrams are reported.

Figure 4.12 shows the phase diagram prepared considering only the composition of liquid synthesis solution. The diagram was prepared using 32 different solutions. The compositions of these solutions are inserted in Appendix F, along with their coordinates on the ternary diagram. The water content of the reactive solutions were 98 mole% or higher. The existing phases in the macrobodies after hydrothermal treatment are shown

by red markers as shown in Figure 4.12. The figure also shows the crystallization field of powder zeolite A and other zeolite types by bold solid lines.

Zeolite A was the only crystalline phase obtained from 22 of 32 solutions, 2 of them yielded a mixture of zeolite A and zeolite X phases. The solid macrobody remained amorphous after synthesis in 8 of them. Accordingly the border of the field for crystallization of zeolite A was established on the ternary diagram as shown in Figure 4.12.

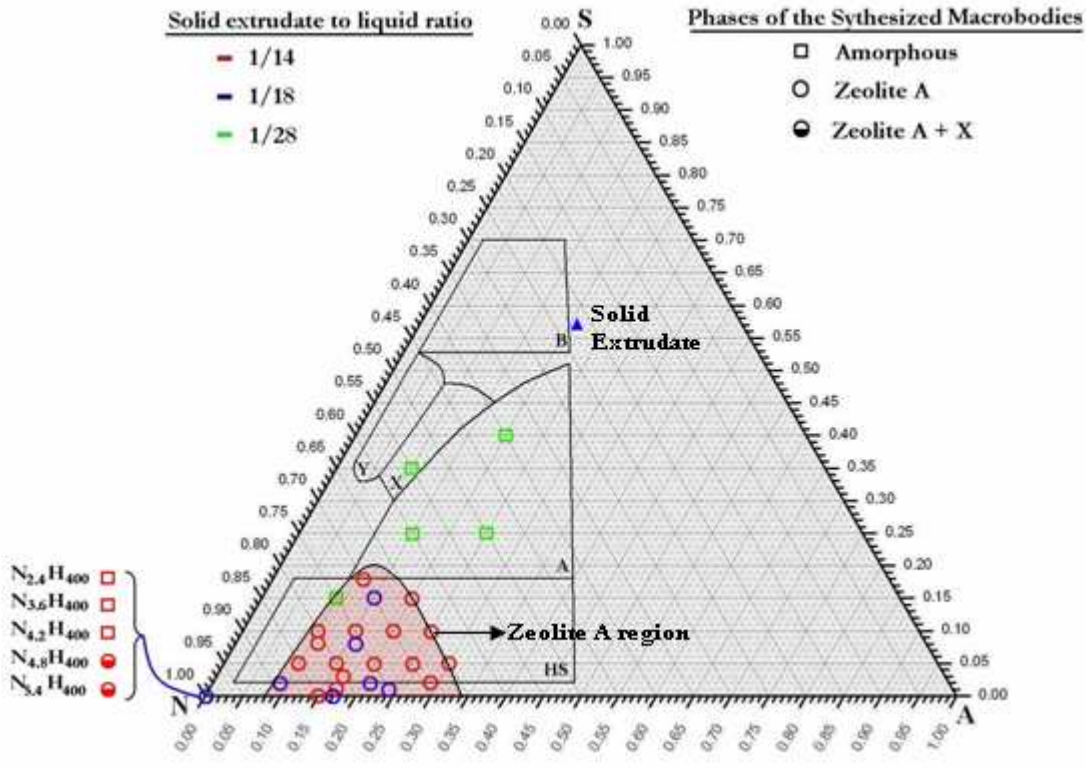

Figure 4.12. Ternary phase diagram based on the liquid solution composition in the autoclave for the syntheses of binderless macrobodies at 80°C for 72 h. The H_2O content of the liquid compositions are greater than 97 mole %. Bounded Areas [1]: Projection of N-A-S-H system for the hydrogels synthesized at 100°C. H_2O content of the gel is 90-98 mole %. The affirmations represent the zeolite A, X, Y, B (P) and hydroxy sodalite (HS). Corners: N represents the Na_2O, A represents the Al_2O_3, S represents the SiO_2.

Figure 4.13 shows the phase diagram prepared using the overall composition of the synthesis medium. Using the solid extrudate composition $1.07Na_2O:Al_2O_3:2.66SiO_2$ and the liquid compositions shown in Figure 4.12 and Appendix F, the overall composition is calculated for each solid extrudate to reactive solution within the reactive medium. The calculations to determine the overall composition in the reactor is given in Appendix G. Although the same liquid compositions are used as in Figure 4.12, due to the change of relative amounts of solid extrudate to reactive solution within the synthesis medium more data points is observed on the ternary diagram for the overall composition. The region yielding zeolite A exactly matches with the crystallization field of zeolite A proposed by Breck [1], suggesting that overall composition of the autoclave governs the conversion of amorphous macrobodies into zeolite A.

The ratio of weight of solid extrudate to the weight of liquid solution was changed in a set of experiments to determine the effect of the liquid and the overall compositions on the crystallization of the binderless zeolite A macrobodies (Figure 4.14). Thus the overall composition in the autoclave was changed although the individual compositions of liquid and solid phases remained the same. For this purpose the solid extrudate (S) to reactive solution (R) ratio (S/R) in the autoclave was changed from 1/3.5 to 1/105.

Two different compositions were selected for the liquid solution; $4.8Na_2O:Al_2O_3:0.07SiO_2:400H_2O$ and $2.33Na_2O:SiO_2:330H_2O$ as reactive solution 1 and reactive solution 2, respectively. According to Figure 4.12, phase diagram based on the composition of liquid solutions, the reactive solution 1 is expected to yield pure zeolite A tubes. On the other hand, the amorphous tubes are likely to remain amorphous after crystallization in reactive solution 2 based on Figure 4.12.

Figure 4.14 shows the tubes synthesized from reactive solution 1 turned to zeolite A at all S/R ratios, although the overall composition in the autoclave was out of the region for synthesis of zeolite A at some S/R ratios. Likely the tubes synthesized from reactive solution 2 remained amorphous at all S/R ratios. Those results suggest that the crystallization into zeolite A mainly governed by the composition of liquid solution. However, it should be noted that the local composition of the synthesis medium can be

falling into the field proposed by Breck at the vicinity of solid-liquid interface because of dissolution of the amorphous tubes. Ural and Çulfaz [24] synthesized different number of disks in an autoclave while keeping the liquid amount constant, and found that all disks were zeolite A no matter how many disks were put into the autoclave. They also concluded that the local composition governs the synthesis rather than the overall composition in the autoclave.

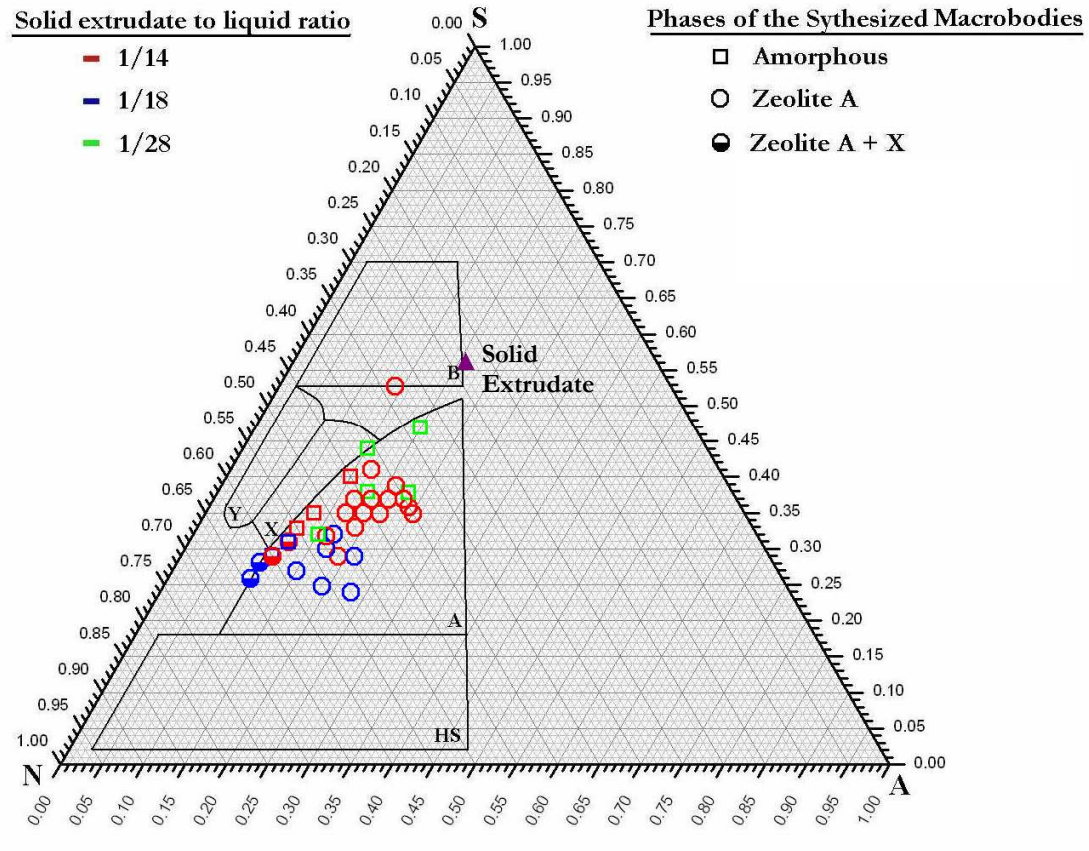

Figure 4.13. Ternary phase diagram based on the overall composition in the autoclave for the syntheses of binderless macrobodies at 80°C for 72 h. The H_2O content of the overall compositions are greater than 96 mole %. Bounded Areas [1]: Projection of N-A-S-H system for the hydrogels synthesized at 100°C. H_2O content of the gel is 90-98 mole %. The affirmations represent the zeolite A, X, Y, B (P) and hydroxy sodalite (HS). Corners: N represents the Na_2O, A represents the Al_2O_3, S represents the SiO_2.

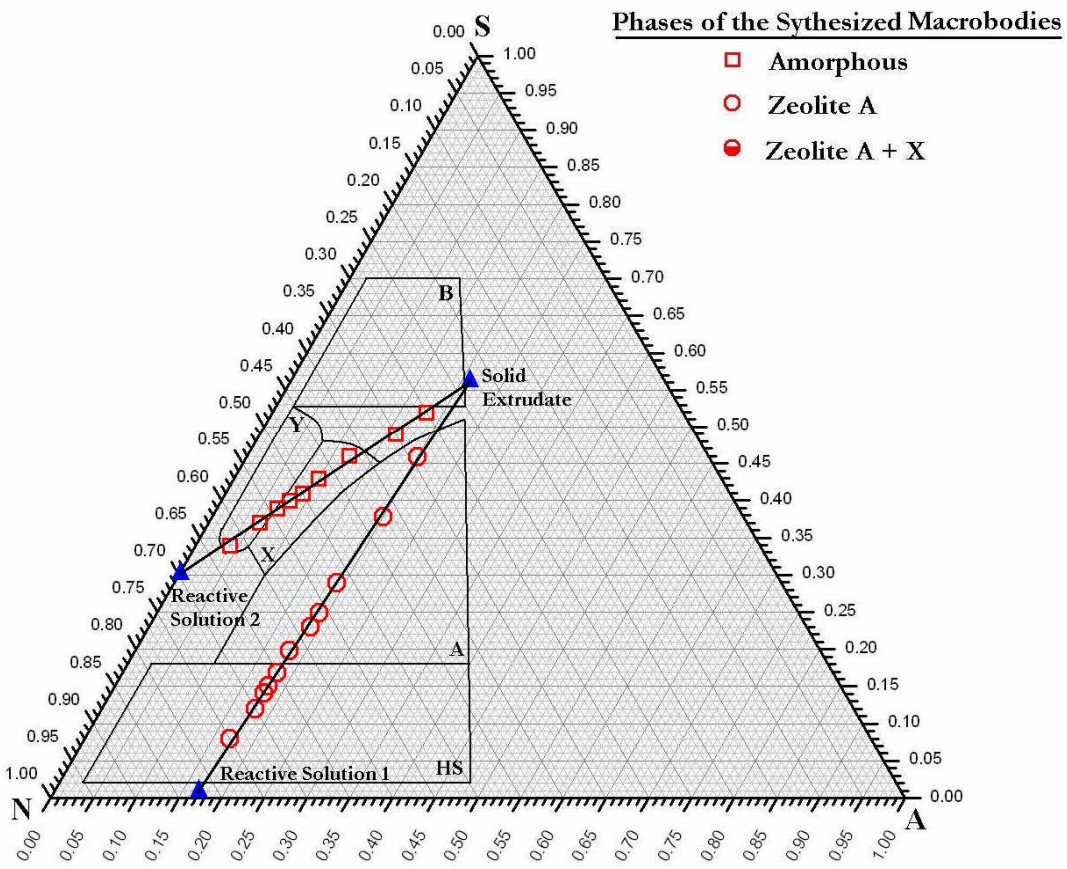

Figure 4.14. Ternary phase diagram based on the overall composition determined by changing the solid extrudate to reactive liquid composition ratio in the autoclave for the syntheses of binderless macrobodies at 80°C for 72 h. The reactive solutions used are $4.8Na_2O:Al_2O_3:0.07SiO_2:400H_2O$ and $2.33Na_2O:SiO_2:330H_2O$ as reactive solution 1 and reactive solution 2, respectively. The H_2O content of the overall compositions are greater than 92 mole %. Bounded Areas [1]: Projection of N-A-S-H system for the hydrogels synthesized at 100°C. H_2O content of the gel is 90-98 mole %. The affirmations represent the zeolite A, X, Y, B (P) and hydroxy sodalite (HS). Corners: N represents the Na_2O, A represents the Al_2O_3, S represents the SiO_2.

.

4.5. The course of crystallization

The morphology of binderless zeolite bars was monitored to establish a better understanding of crystallization period. There are many studies in the literature dealing

with the crystallization period of the zeolite powder from aluminosilicate hydrogels [55, 56, 60, 61, 62, 63]. However, the course of the crystallization is expected to be indifferent for the binderless zeolite macrobodies prepared in this study.

The change of crystallinity of the zeolites with time follows an S shaped curve as shown in Figure 4.15. The nucleation time is defined as the point on the crystallization curve where conversion to the crystalline phase is just starting. A crystallization period follows the nucleation time.

The bars, which were prepared by washing Method 2, were synthesized in a solution with a molar composition of $4.8Na_2O:Al_2O_3:0.07SiO_2:400H_2O$. The powder zeolite A was synthesized from a hydrogel with a molar composition of $2.5Na_2O:Al_2O_3:1.7SiO_2:150H_2O$.

Figure 4.15 shows the crystallization curve of the binderless zeolite bars and the zeolite powder that is obtained by using the same aluminosilicate hydrogel. The nucleation period was nearly 3 and 5 h for powder and bars, respectively. The crystallinity rises sharply during the powder synthesis although the crsytallinity of bars increased slowly. The rate of crystallization is defined as the rate of conversion at 50% of the maximum conversion level in terms of percent crystallinity per hour [64]. The crystallization rate of the powder and the bar are determined as approximately 0.165 %/h and 16 %/h, respectively. Both the nucleation time and crystallization rate for the bars are significantly slower that those for the powder. The bars are likely to convert into zeolite A by solution-mediated transport mechanism, which requires the leaching of bars before crystallization so that crystallization of bars is expected to be slower than the crystallization of hydrogel.

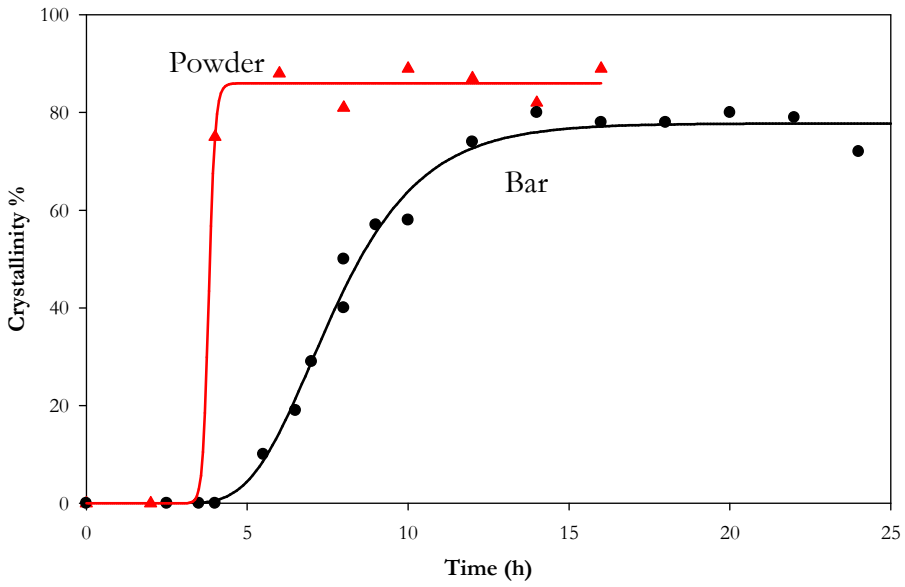

Figure 4.15. Crystallization curves of binderless bars and powder.

Figure 4.16 to 4.18 shows the change of morphology of bars with synthesis time. The SEM images of all samples at smaller magnifications can be seen in Appendix D. All images illustrated in Figure 4.16 to 4.18 were taken from the center of bars.

In Figure 4.16.a, the SEM image of the tube synthesized for 4 h is given. There are no crystals or crystalline products present within the structure, as also suggested by XRD. As the synthesis time is increased to 5.5h, see Figure 4.16.b, bright spots were seen in the amorphous structure. These spots were interpreted as the view of early stages of a crystal or an aggregate of crystals. Valtchev et al. observed similar structures by transmission electron microscopy during the crystallization of zeolite A type zeolite and defined them as negative crystals. After 6 and 7 hours of crystallization, the number of these spots increased and became more visible as shown in Figure 4.16.c and Figure 4.17.a. The crystallinity of the tube increased to 30% with respect to XRD after 7 hours of crystallization. In addition, the porosity seemed to increase with increasing size of spots. The density difference between the amorphous solid and the bright spots may create porosity in the bar. Thus new pore appeared when the amorphous solid was consumed. After 8 and 9 hours of crystallization, the XRD crystallinity increased to 60%

and the size and number of bright spots increased significantly, suggesting that these spots have a crystalline structure (Figure 4.17.b and Figure 4.17.c). After 12 hours of crystallization, twinned crystals with cubic shape can be more clearly seen as shown in Figure 4.18.a. After 18 hour of synthesis, Figure 4.18.b, the chamfered edge cubic shape of zeolite A crystals can easily been distinguished from the amorphous solid. The XRD crystallinity is about 70 % in this bar. Figure 4.18.c shows the SEM image of a bar synthesized for 72 hours, the bar is completely composed of cubic zeolite A crystals, which are highly intergrown. The XRD crystallinity increases to about 90%. Indeed no amorphous solid can be seen on SEM images.

Figure 4.19 shows the change of chemical composition of bars with time, which was determined by EDX. The molar SiO_2/Al_2O_3 ratio of the bar was initially 3.6 and dropped to 2.5 after 18 hours of crystallization. The molar SiO_2/Al_2O_3 ratio was 2 after 72 h of crystallization (not shown in the figure). This is expected because the molar Si/Al ratio of a pure zeolite A crystal should be one, and the bars were highly crystalline zeolite A after 72 h of synthesis.

Figure 4.20 shows the change of morphology across the cross-section of a bar. The period of synthesis was 9 hours. Although the XRD crystallinity was about 60%, SEM images showed that the core of the bar was completely amorphous although the surface was composed of cube-like particles. Those particles are expected to be partly crystalline zeolite A. XRD shows the average crystallinity through the bar; however, SEM results suggest that the crystallization process starts from the outer surface proceed toward the core of the bar probably because of limited penetration of liquid solution into the core. With the formation of new pores because of density difference between zeolite A and amorphous solid, liquid solution can flow deeply and increases the rate of crystallization.

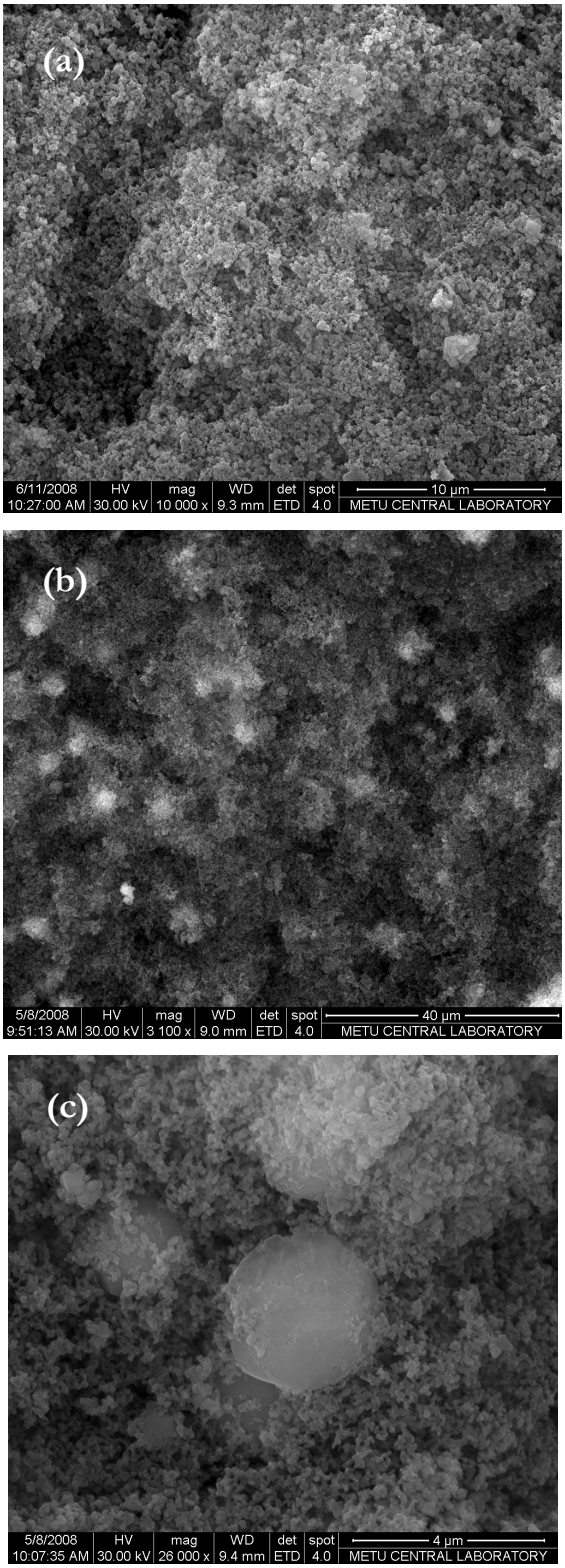

Figure 4.16. Change of crystallization with respect to time according to the SEM pictures of the binderless zeolite bars (a) 4 h (b)5.5 h (c) 6.5 h

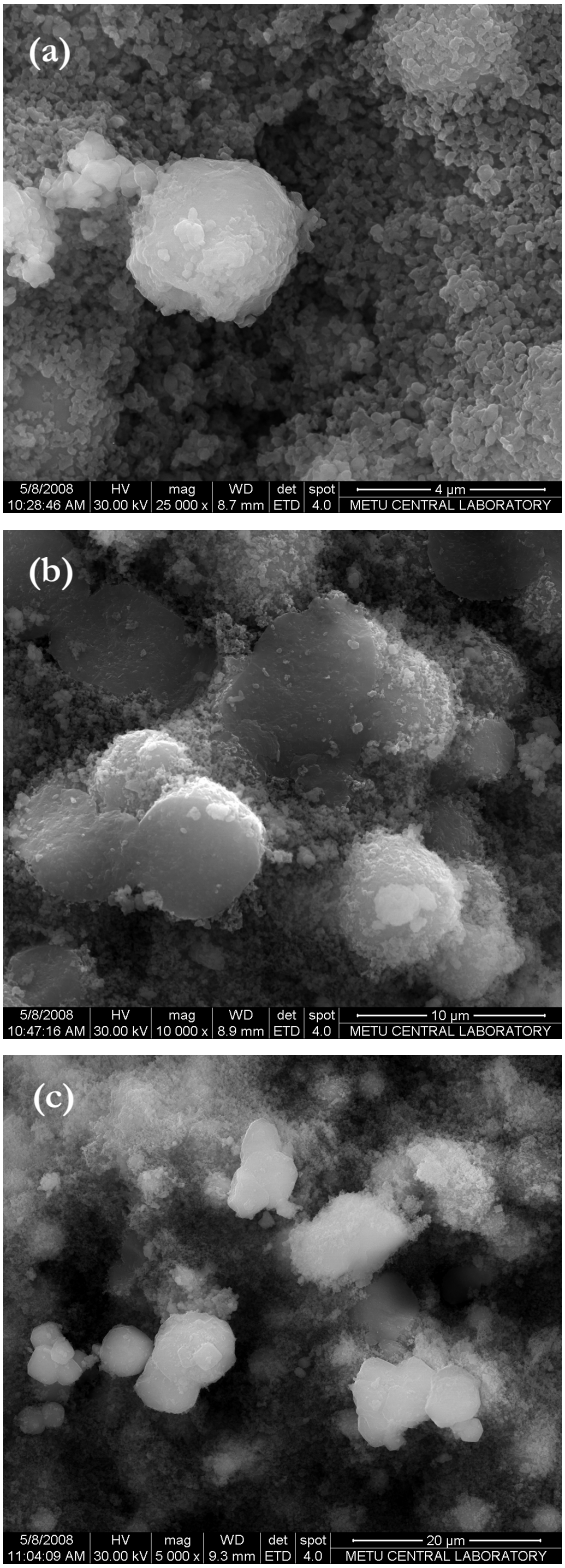

Figure 4.17. Change of crystallization with respect to time according to the SEM pictures of the binderless zeolite bars (a) 7 h (b) 8 h (c) 9 h

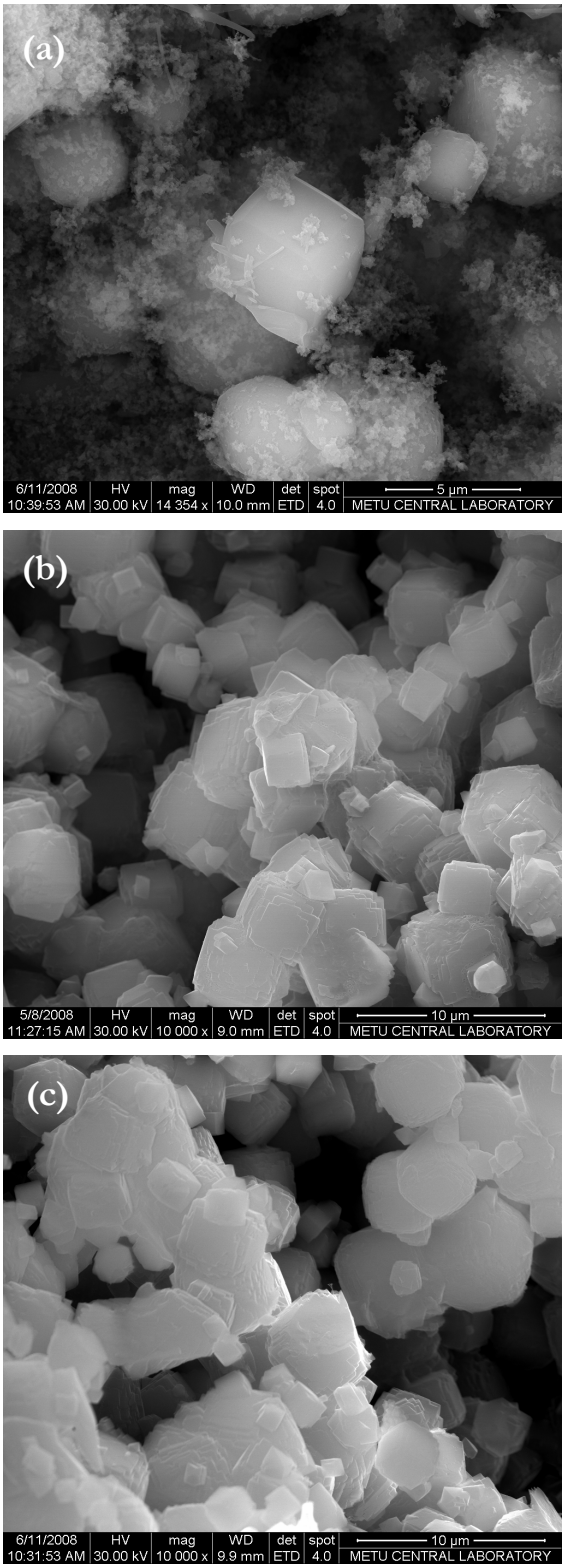

Figure 4.18. Change of crystallization with respect to time according to the SEM pictures of the binderless zeolite bars (a) 12 h (b) 48 h (c) 72 h

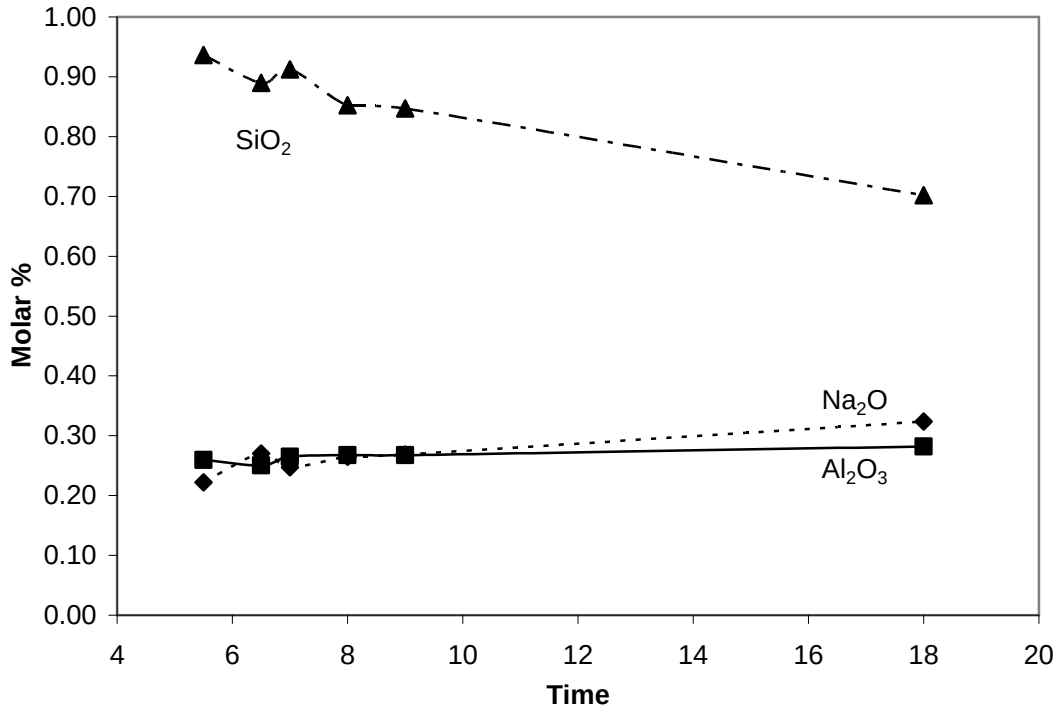

Figure 4.19. Molar % change of the Na_2O, SiO_2 and Al_2O_3 during synthesis with time.

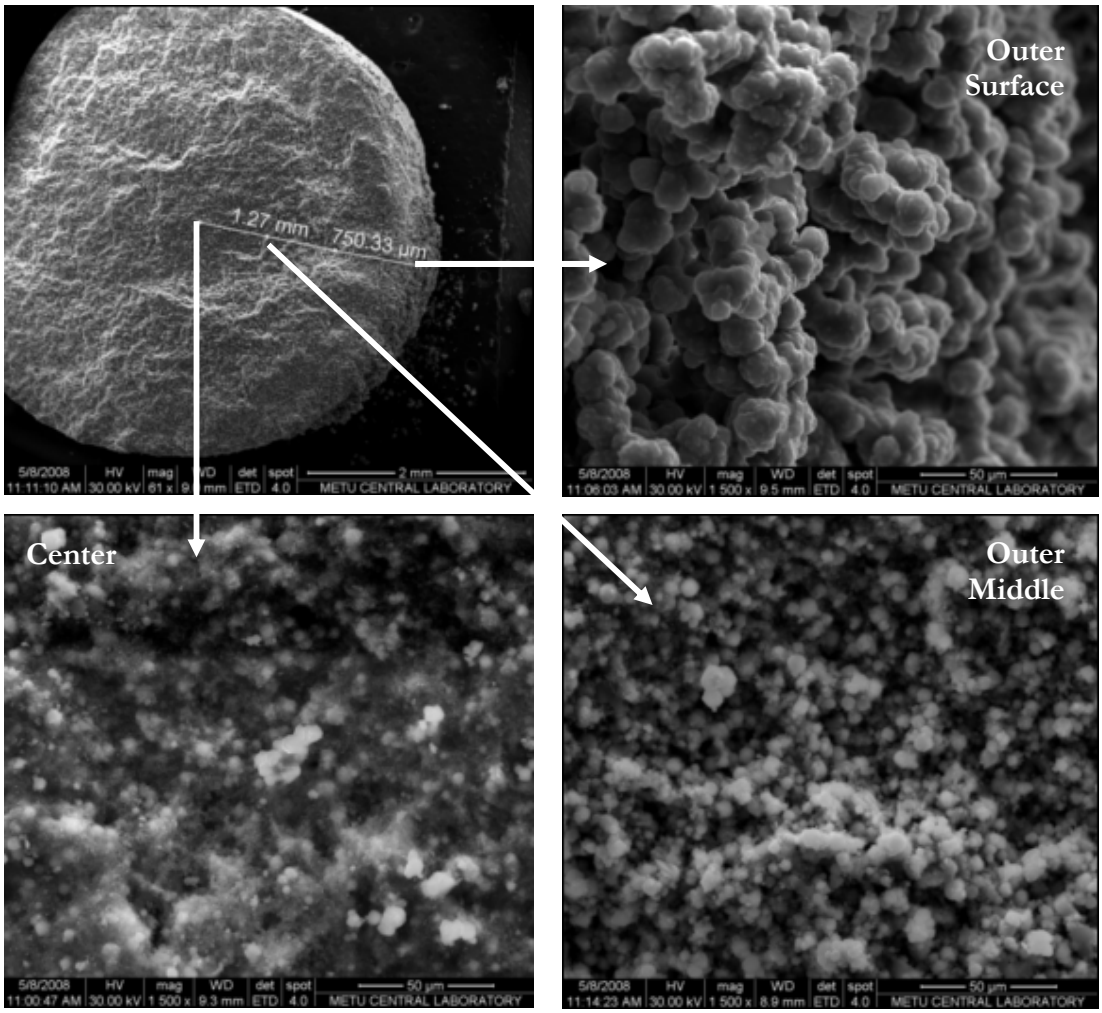

Figure 4.20. Change of crystallization of bars according to the cross section for 9 h of synthesis.

4.6. Syntheses of Self-Supported Zeolite 4A Disk and Tube Membranes

One of the objectives of this study was to synthesize a thin and continuous zeolite A layer over the zeolite A macrobodies for use as membrane. For the syntheses of zeolite membranes, the support material is immersed into a hydrogel, and subjected to thermal treatment for a predetermined period of time at the desired temperature. A similar

strategy was followed in this study. Binderless zeolite A disks and tubes were used as membrane support. During the study, when the binderless zeolite A disk/tube has been treated with the membrane synthesis composition is directly named as membrane, whether a thin layer formation is observed or not. A group of membranes was synthesized on dry zeolite A tubes, and another group was synthesized on zeolite A tubes saturated with water.

The membrane layers were mostly synthesized from a hydrogel with a molar composition of $2Na_2O:1Al_2O_3:2SiO_2:120H_2O$ at 100°C for 4 h, and a few membranes on disk supports were synthesized from a clear synthesis solution with a molar composition of $49Na_2O:1Al_2O_3:5SiO_2:980H_2O$ at 80°C for 8 h. The support tubes and disks were prepared from amorphous tubes prepared by washing Method 2 in the synthesis solution with a molar composition of $4.8Na_2O:Al_2O_3:0.07SiO_2:400H_2O$ or in the filtered liquid solution at 80°C for 72 h. The details of membrane preparation were given Part 3.6. Binderless zeolite A disks are put on to a Teflon holder to keep them straight within the autoclave, and then the synthesis solution is inserted. The syntheses of the disks have been made in the PTFE autoclaves and thus the volume of the membrane synthesis composition in the autoclave was always kept to be 24 ml. The syntheses of the disks are all made using the dry-suport method. All the synthesis conditions and the characterization results of the membranes are given in Appendix H.

Figure 4.21 shows the XRD patterns of the disk shaped binderless zeolite A support and of the zeolite A membrane after the synthesis on this support. The membrane layer was very thin and it was formed on a zeolite A disk, therefore the reflections from the membrane layer and the support cannot be distinguished from each other. Since no crystalline phase other than zeolite A was observed in the membrane (Figure 4.21b), it can be assumed that the membrane layer is also pure zeolite A.

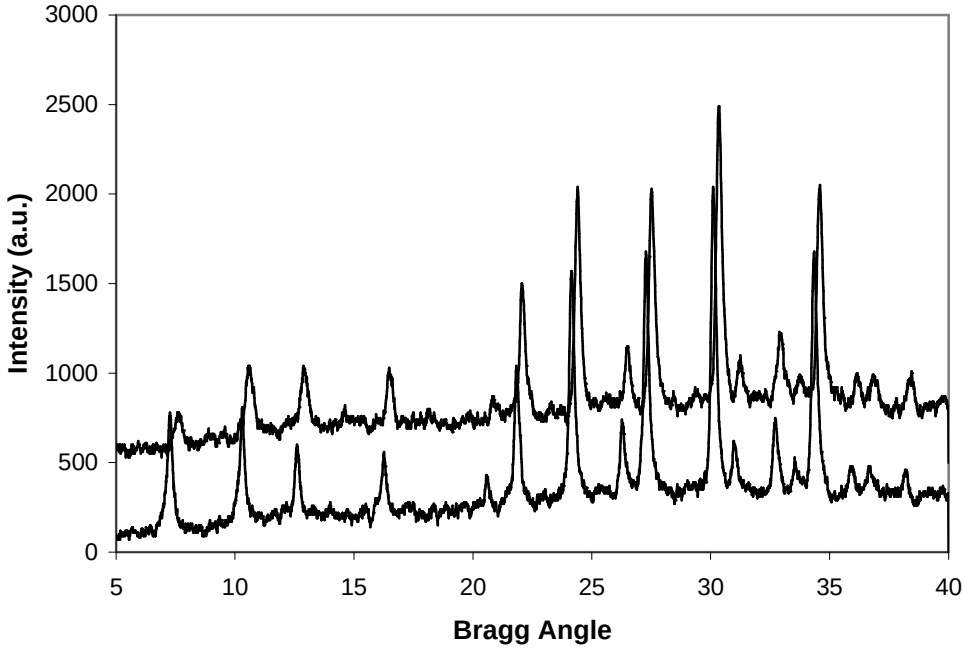

Figure 4.21. XRD patterns of (a) the disk shaped zeolite A support (sample code: CG25D5) and (b) the membrane after synthesis of the thin zeolite A layer (sample code: CGM5; synthesized in solution with a composition of $49Na_2O:1Al_2O_3:5SiO_2:980H_2O$ at 80°C for 8h).

Figure 4.22 shows the SEM images of the cross-section and the surface of disk shaped support. There is a zeolite A film on the surface with a nonuniform thickness. The disks were prepared by applying force perpendicular to the surface, which may cause a more compact amorphous structure than that can be obtained in tube extrusion. The more compact amorphous structure may result in the formation of denser zeolite A layer after hydrothermal treatment.

Following the second synthesis, a more uniform and compact zeolite A layer was obtained on the disk surface as shown in Figure 4.23. The membrane CGM5 was synthesized from the synthesis solution with a molar composition of $4.8Na_2O:Al_2O_3:0.07SiO_2:400H_2O$ at 80°C for 72 h and has a thickness of 5.7 μm. CGM7 was synthesized from a hydrogel with a molar composition of

$2Na_2O:1Al_2O_3:2SiO_2:120H_2O$ at 100°C for 4 h and has a thickness of 6 μm. Although there was zeolite A film on the disk shaped support, it was only partly continuous. The second synthesis resulted a continuous zeolite A film. As the support is also zeolite A, it may behave like a seed layer favoring the formation of a continuous zeolite A film. In literature, zeolite A membranes on ceramic supports can only be synthesized after coating the support surface with seed crystals [5]. Therefore seeding is essential for the preparation of continuous zeolite A membranes. Using zeolite A supports in the shape of disk or tube may therefore be an alternative for the zeolite membrane secondary synthesis techniques since the support itself is also a seed film.

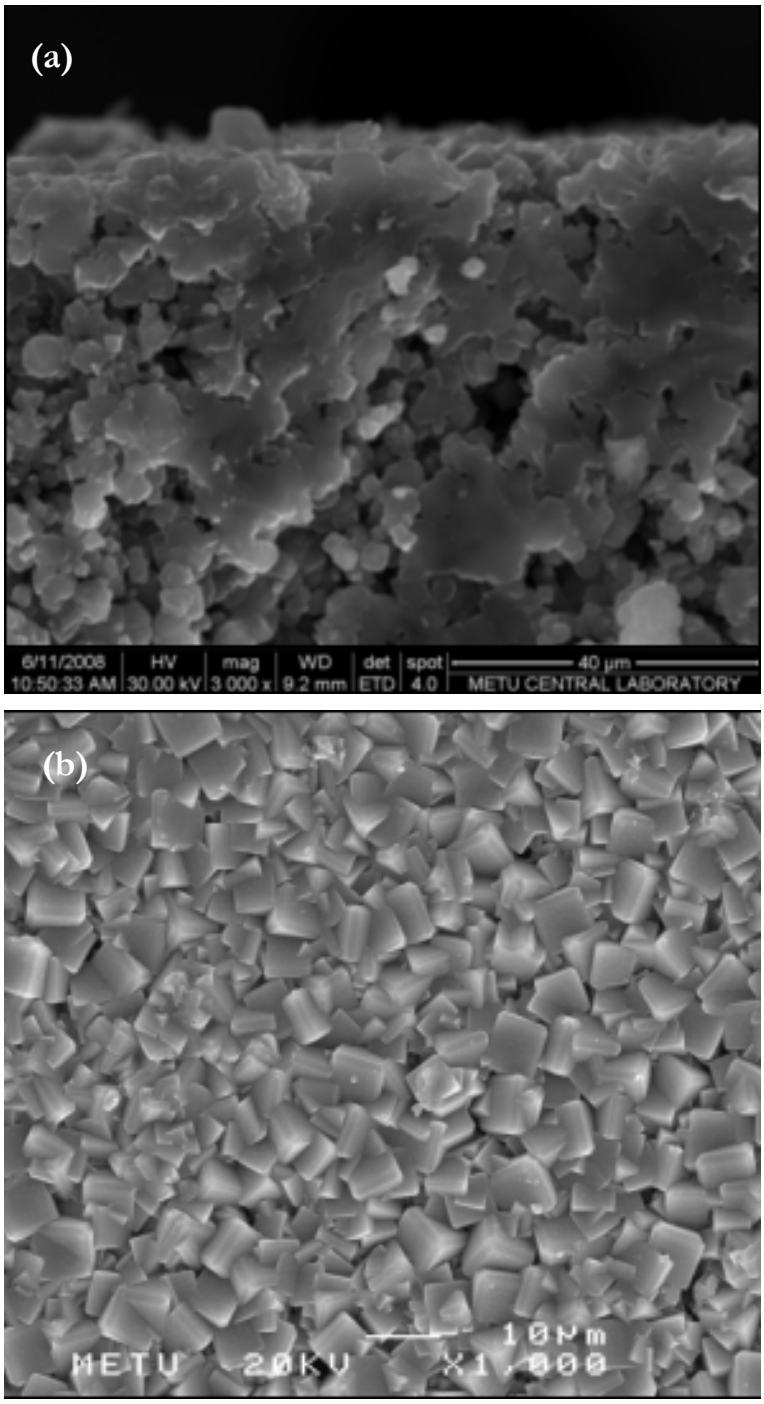

Figure 4.22. SEM pictures of the disk shaped supports (a) cross-section (sample code: CG25D5) and (b) surface (sample code: CG20D6)

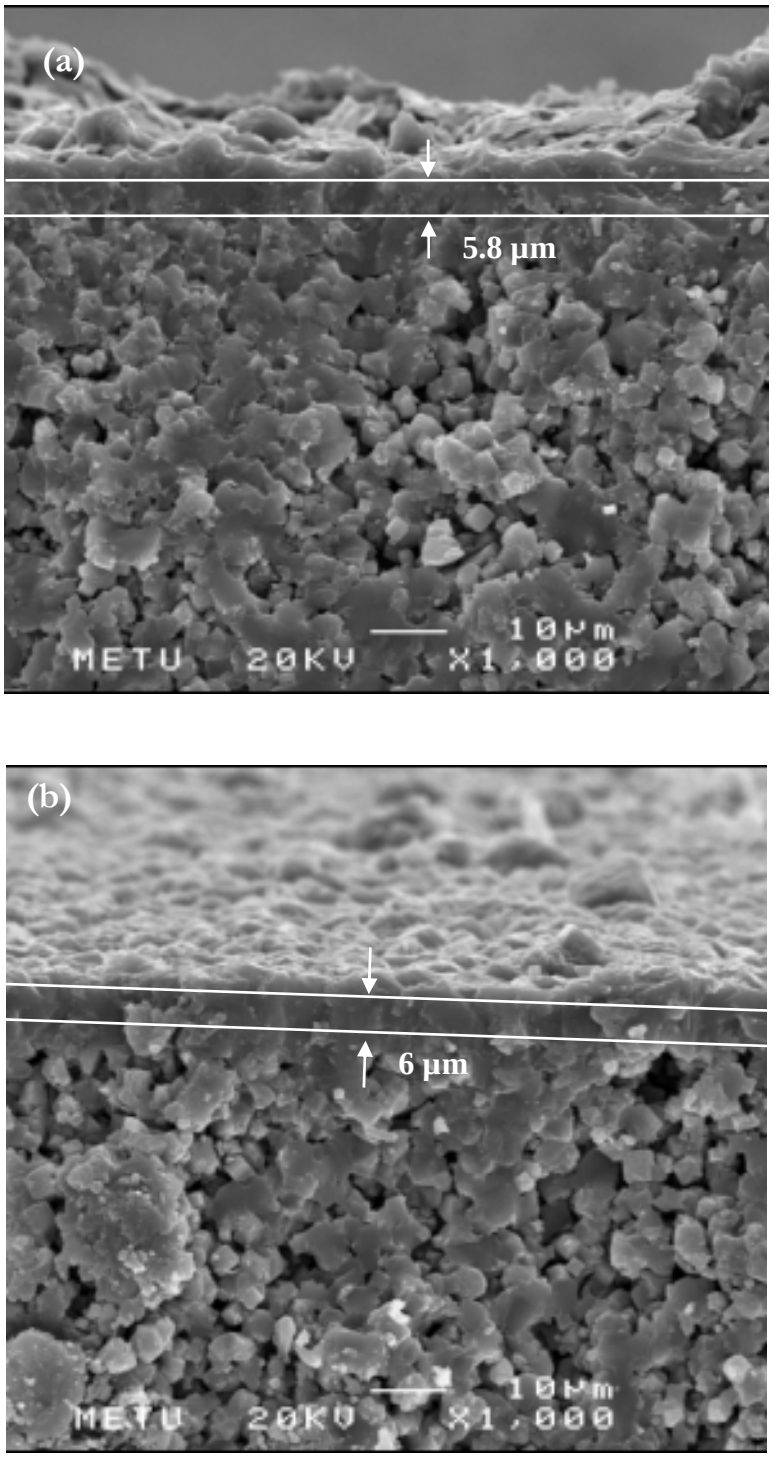

Figure 4.23. SEM pictures of the zeolite A films formed on disk shaped supports (a) cross-section (sample code: CGM5) and (b) surface (sample code: CGM7). The molar composition of synthesis solution and synthesis conditions for CGM5 is $4.8Na_2O:Al_2O_3:0.07SiO_2:400H_2O$ and 80°C for 72 h. The molar composition of synthesis solution and synthesis conditions for CGM7 is $2Na_2O:1Al_2O_3:2SiO_2:120H_2O$ and 100°C for 4 h.

Figure 4.24 shows the cross-sectional SEM images of tubular zeolite A membranes formed on a dry-support. The second synthesis for the preparation of membrane film was performed in a hydrogel with a molar composition of $2Na_2O:1Al_2O_3:2SiO_2:120H_2O$ at 100°C for 4 h. The SEM images were taken from the inner and outer cross-sections. The membrane has no compact zeolite A film over the support surface but a loosely packed layer of crystals can be seen on the surface.

The membrane has zeolite A crystals with two different morphologies: sharp edge cubes and chamfered edge cubes as shown in Figure 4.24.d. The SEM images of the support tubes showed that the tubes has sharp edge cubes, suggesting that the chamfered edge cubes formed during the second synthesis. Besides the second synthesis resulted in formation of loosely packed crystals on the surface rather than a film of highly intergrown zeolite A crystals.

These membranes were synthesized in hydrogels with a molar composition of $2Na_2O:1Al_2O_3:2SiO_2:150H_2O$. This composition is often used by Sato et al [11] and Kita et al [5] to prepare high quality zeolite A membranes on alumina tubes with high reproducibility. Therefore the lack of continuous zeolite A film was ascribed to the hydrophilic character of the support, which is also pure zeolite A. When the support was immersed into the hydrogel for second synthesis, the dry-support absorbed water from hydrogel and yielded a thick and dense gel layer surrounding the support. It is observed that even when the support is taken out of the autoclave, the gel surrounding gel was strongly attached to the support. The residual gel particles from this gel can be seen in Figure 4.25. The crystallization conditions on the support were likely to be different from the bulk hydrogel and this gel layer hindered the formation of membrane film.

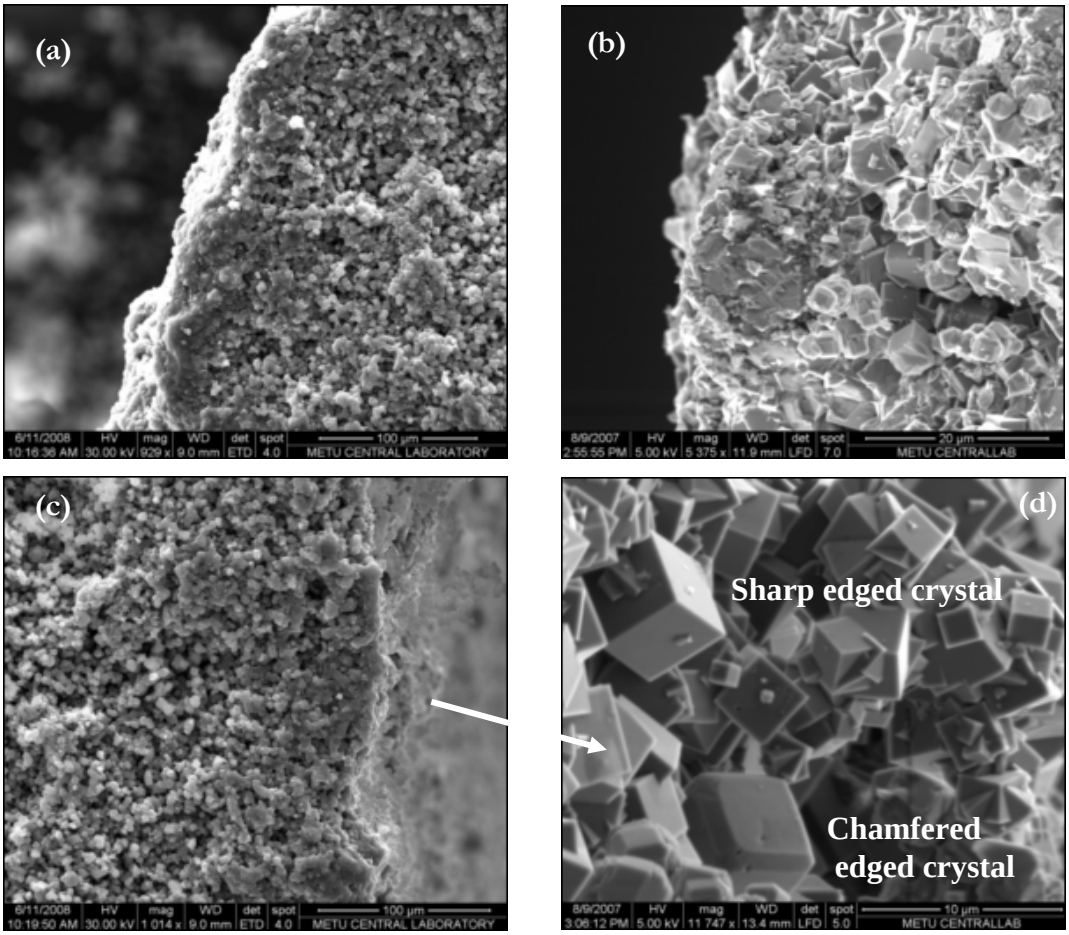

Figure 4.24. SEM pictures of tubular zeolite A membrane prepared on dry-support sample code: CGM8), (a) outer cross section (b) magnified view of the outer cross section (c) inner cross section (d) crystals seen over the inner cross section. The molar composition of synthesis solution and synthesis conditions for CGM8 is $2Na_2O:1Al_2O_3:2SiO_2:120H_2O$ and 100°C for 4 h.

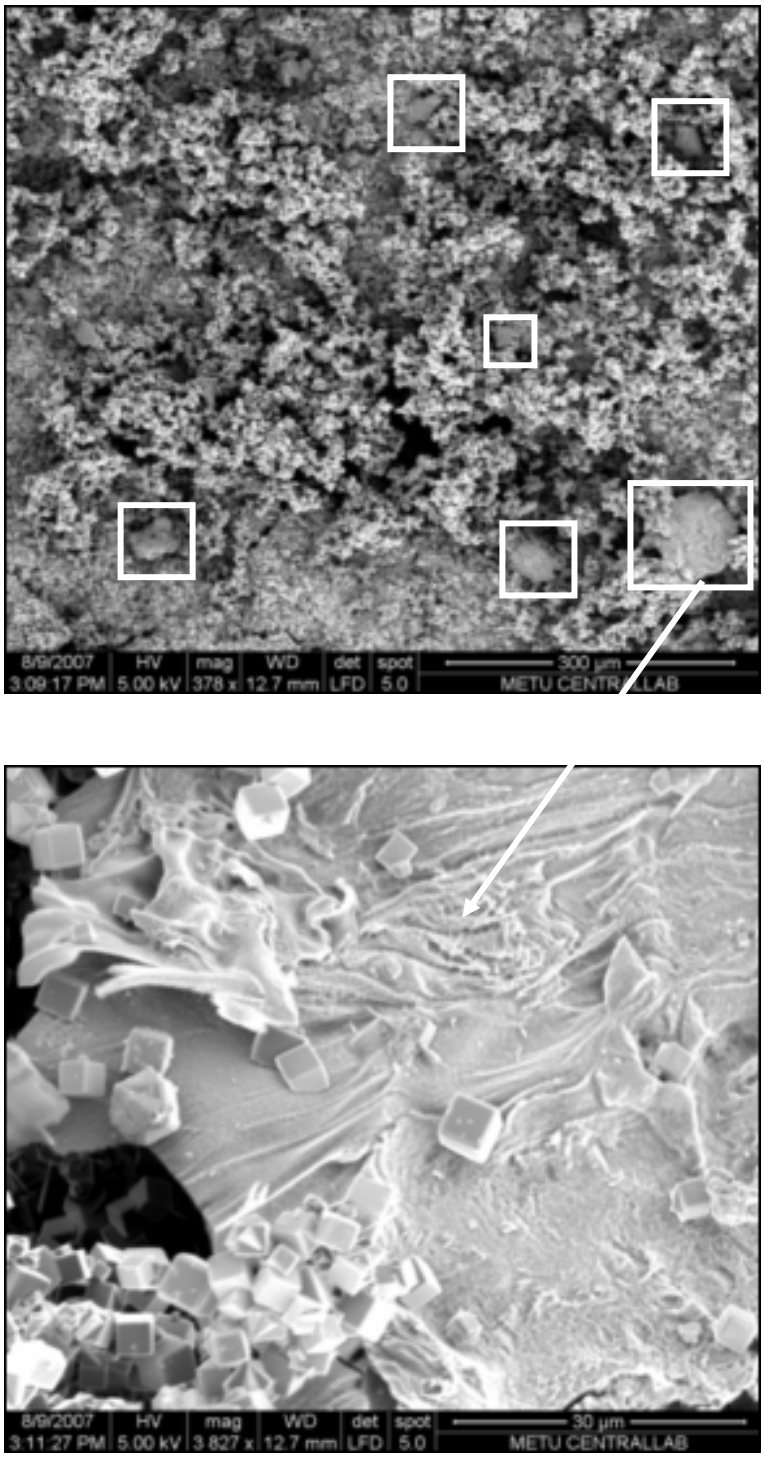

Figure 4.25. SEM pictures of CGM8, taken from (a) inner surface (b) amorphous particle on the inner surface. The molar composition of synthesis solution and synthesis conditions for CGM8 is $2Na_2O:1Al_2O_3:2SiO_2:120H_2O$ and 100°C for 4 h.

A set of membranes were therefore synthesized on zeolite A tubes saturated with water prior to the synthesis of membrane layer. By this way, it is thought that the probable formation of the gelous layer at the interface is provided. Figure 4.26 shows the surface SEM images of membranes synthesized on wet-supports from the synthesis solution with a molar composition of $2Na_2O:1Al_2O_3:2SiO_2:120H_2O$ and 100°C for 4 h. The surface is completely covered with highly intergrown zeolite A crystals without any pinholes or defects. The crystals forming the zeolite A films had similar crystal shape; all were chamfered edged cubes.

The cross-section images of the membrane showed that both inner and outer sides of the tube had continuous zeolite A layer with no detectable interzeolitic pores (Figure 4.27). The film has a very uniform thickness at both sides. The thickness of layer was around 8.4 and 12 μm at inside and outside, respectively. Figure 4.28 shows the inner cross-sectional SEM image of another sample prepared under similar conditions. As seen from the figure, the film thickness over the cross section is about 11.8 μm.

In literature, continuous zeolite A films over ceramic supports usually obtained after two or three successive crystallizations [66], however, synthesis of zeolite A films over zeolite A supports can be accomplished only after single synthesis step. The SEM images also showed that the zeolite A support should be saturated for the formation of a continuous zeolite A film.

These prepared zeolite tubes have also been tested at the pervaporation set-up, of which the details have been given in Part 3.7, during the study. The trials ended unsuccessfully because of the microcracks on the tubes due to bending. As already mentioned in Part 4.1, bending is caused uneven paste velocity. This problem may be eliminated by improving the extruder design to be confident of eccentric annulus flow of paste through extruder.

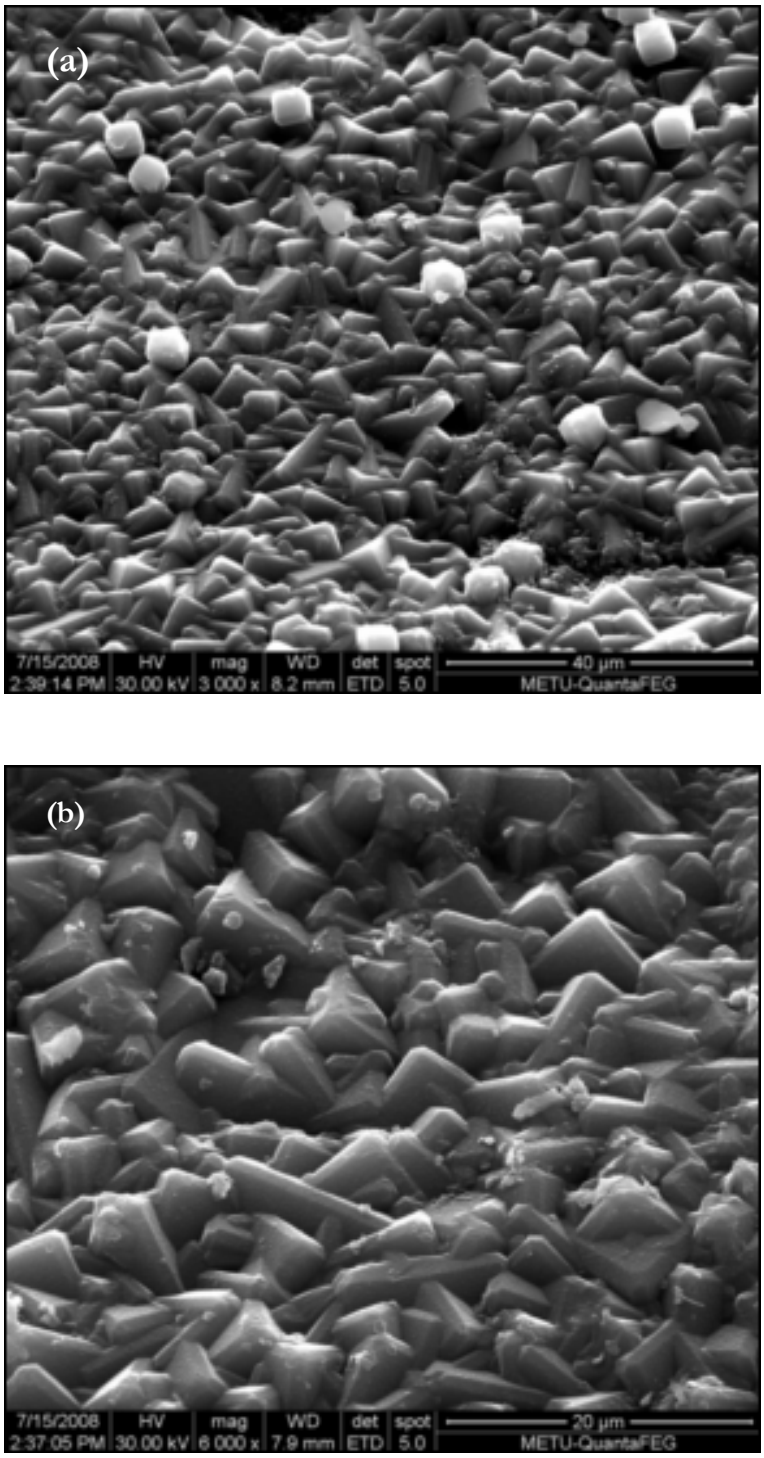

Figure 4.26. The surface SEM images of a tubular zeolite A membrane prepared on wet-support (sample code: CGM26). (a) outer surface, (b) closer view of the outer surface given in (a). The molar composition of synthesis solution and synthesis conditions is $2Na_2O:1Al_2O_3:2SiO_2:120H_2O$ and 100°C for 4 h.

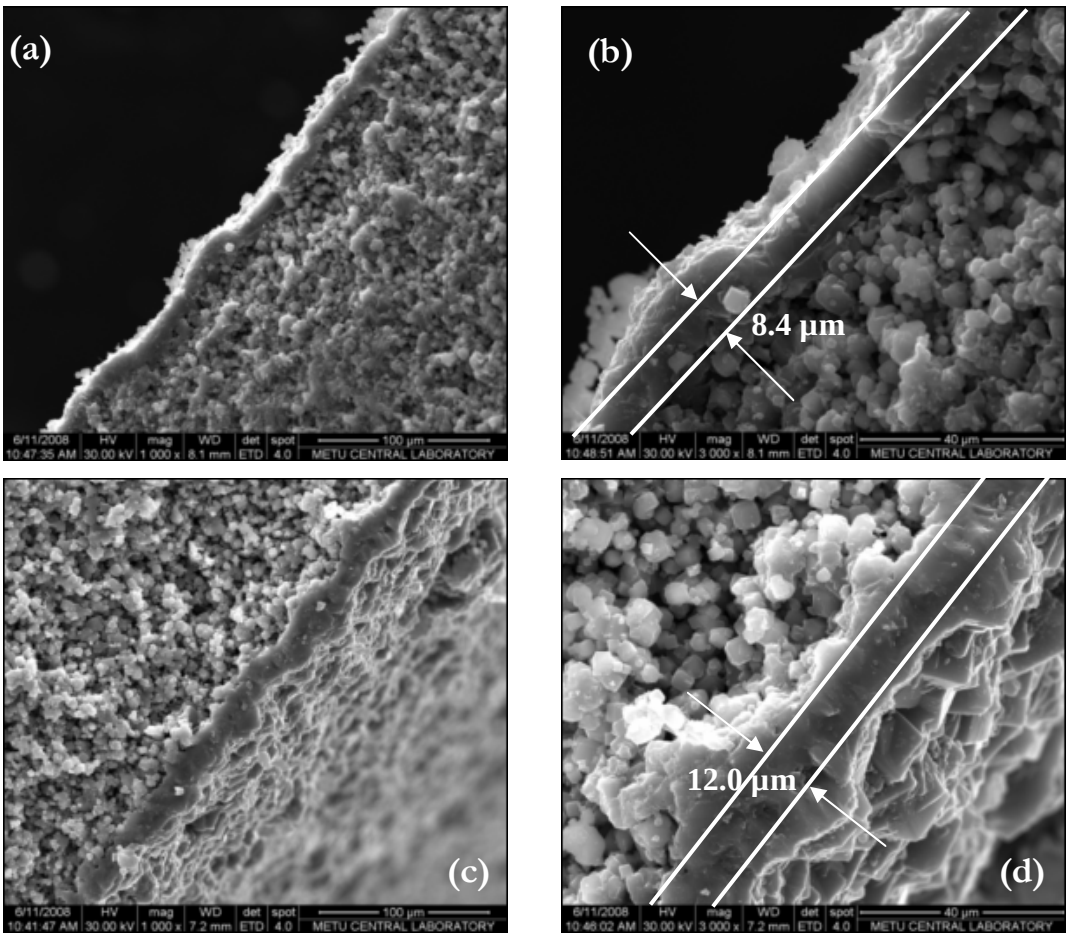

Figure 4.27. The cross-sectional SEM images of a tubular zeolite A membrane prepared on wet-support (sample code: CGM26). (a) inner cross section (b) closer view of the inner cross section given in (a), (b) inner cross section (c) closer view of the inner cross section given in (b). The molar composition of synthesis solution and synthesis conditions is $2Na_2O:1Al_2O_3:2SiO_2:120H_2O$ and 100°C for 4 h.

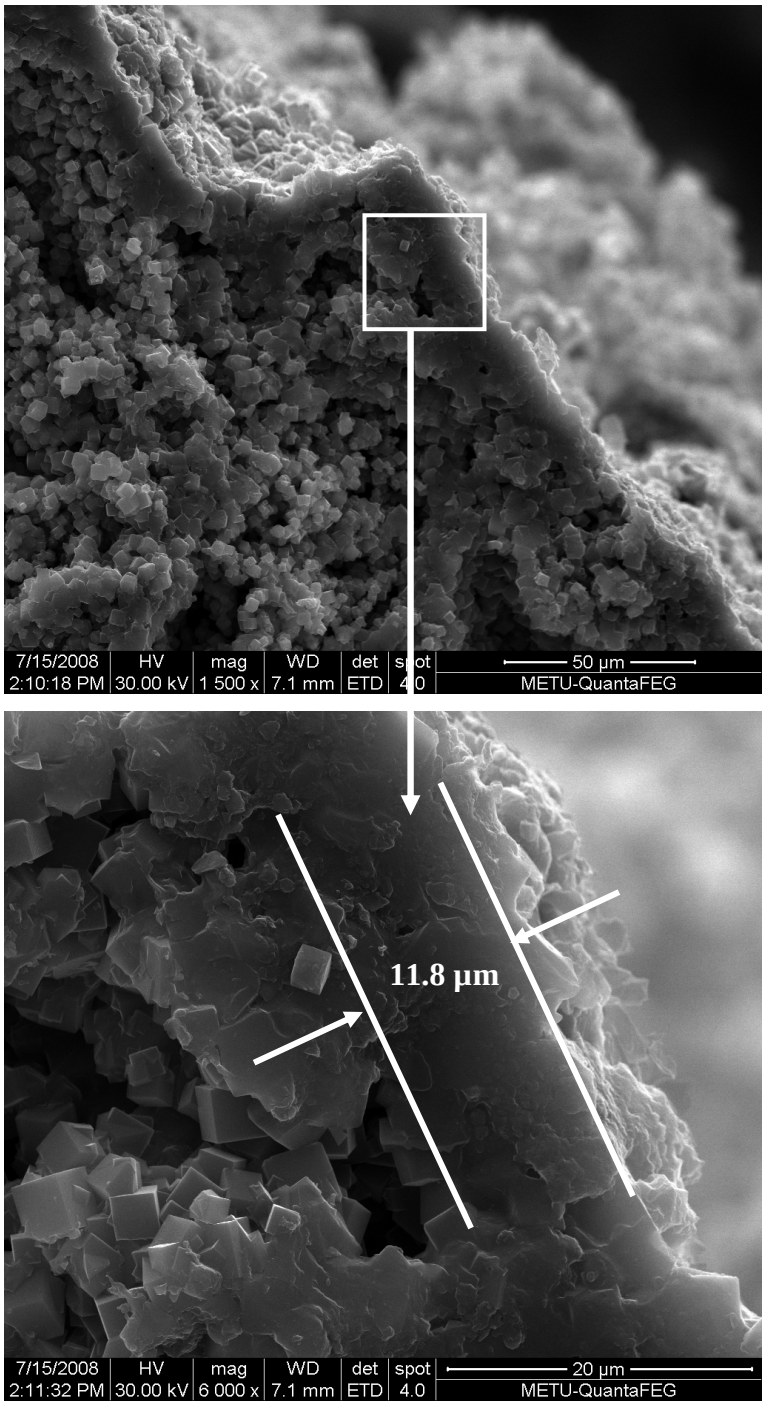

Figure 4.28. The cross-sectional SEM images of a tubular zeolite A membrane prepared on wet-support (sample code: CGM30). (a) inner cross section (b) closer view of the inner cross section given in (a). The molar composition of synthesis solution and synthesis conditions is $2Na_2O:1Al_2O_3:2SiO_2:120H_2O$ and 100°C for 4 h.

CHAPTER 5

CONCLUSIONS

This study aimed to synthesize thin zeolite A layer over a zeolite A support. The first phase of the study was to synthesize the zeolite supports and second phase was to prepare zeolite A membranes. The conclusions arrived at the end of the study can be summarized as:

1. Self-standing, pure and porous zeolite A bodies with disk, bar and tube shapes have been prepared.
2. A crystallization field by using binderless extrudates has been established on phase diagram. Formation of the binderless zeolite macrobodies is dependent upon the local composition of the liquid solution rather than the overall composition.
3. Compact zeolite A layer with a thickness of approximately 12 μm on the outer surface and approximately 8 μm on the inner surface were synthesized over the tubular macrobodies that are saturated with water. No continuous film was observed from the synthesis made on dry tubular macrobodies.

RECOMMENDATIONS

1. Procedure developed for the synthesis of the binderless macrobodies can be applied for the high silica zeolites, such as ZSM-5 and Zeolite X
2. Asymetric zeolite bead/fibers can be prepared by using the technique used in this study.
3. For longer zeolite supports and membranes with no bending and cracks, the design of the home made extruder should be improved.
4. Synthesis of the thin zeolite layer over the zeolite A support can be formed by using a less viscous synthesis solutions, in order to overcome the problems associated with the hydrophilicty of the supports and film formation.

REFERENCES

1. Breck, D. W. *Zeolites, Molecular Sieve Structure, Chemistry and Use*; John Wiley: New York, 1974.

2. Sircar, S., *Basic research needs for design of adsorptive gas separation processes,* Industrial and Engineering Chemistry Research, Vol. 45, 2006, pp. 5435 – 5448.

3. Coronas, J. and Santamaria, J., *Separations Using Zeolite Membranes*, Separation and Purification Methods, Vol. 28, 1999, p.127.

4. Bowen, T. F., Noble, R. D., Falconer, J.L., *Fundamentals and applications of pervaporation through zeolite membranes*, Journal of Membrane Science, Vol. 245, 2004, pp. 1-33.

5. Morigami, Y., Kondo, M., Abe, J, Kita, H., Okamoto, K., *The first large-scale pervaporation plant using tubular-type module with zeolite NaA membrane*, Separation and Purification Technology, Vol. 25, 2001, pp.251-260.

6. Chiang, A.S.T. and K.-j. Chao, *Membranes and films of zeolite and zeolite-like materials.* Journal of Physics and Chemistry of Solids, Vol. 62, 2001, pp. 1899- 1910.

7. Andac, O., et al., *Effects of ultrasound on the preparation of zeolite A coatings.* Microporous and Mesoporous Materials, Vol. 88, 2006, pp. 72-76.

8. Kondo, M., Komori, M., Kita, H., Okamoto, K., *Tubular-type pervaporation module with zeolite NaA membrane*, Journal of Membrane Science, Vol. 133, 1997, pp. 133-141.

9. Dong W.Y., Long, Y.C., *Preparation and characterization of preferentially oriented continuous MFI-type zeolite membranes from porous glass*, Microporous and Mesoporous Materials, Vol. 76, 2004, pp. 9-15.

10. Tosheva, L., Valtchev, V. P., *Supported and self-bonded molecular sieve structures*, C.R. Chimie 8, Vol. 8, 2005, pp. 475 – 484.

11. Sato, K., Sugimoto, K., Nakane, T., *A highly reproducible fabrication method for industrial production of high flux NaA zeolite membrane*, Journal of Membrane Science, Vol. 301, 2007, pp.151-161.

12. Mcleary, E.E., Jansen, J.C., Kapteijn, F., *Zeolite based films, membranes and membrane reactors: Progress and prospects,* Microporous and Mesoporous Materials, Vol. 90, 2006, pp. 198 – 220.

13. Bonaccorsi, L., Proverbio, E., *Synthesis of thick zeolite 4A coatings on stainless steel,* Microporous and Mesoporous Materials, Vol. 74, 2004, pp. 221-229.

14. Geus, E.R., den Exter, M.J., van Bekkum, H., *Synthesis and Characterization of Zeolite (MFI) Membranes on Porous Ceramic Supports*, Journal of Chemical Society Faraday Transactions, Vol. 88, 1992, p.3101

15. Lei, Q., Zhao, T., Li, F., Wang, Y. F., Hou, *Zeolite Beta monoliths with hierarchical porosity of bimodal pore silica gel*, Journal of Porous Materials, 2007.

16. Michalko, E., *Method for Preparing Spherically Shaped Crystalline Zeolite Particles,* U.S. Patent No: 3, 1968, 386, 802.

17. Heinze, G., Reiss, G., Schwochow, F., Ulisch, G., *Zeolite Adsorbents*, U.S. Patent No: 3, 1973, 773, 690.

18. E. Michalko, *Method for Producing Molecular Sieve Zeolite Particles,* 1967, US Patent No: 3,356,451.

19. Tosheva, L., Valtchev, V., Sterte, J., *Silicalite -1 containing microspheres prepared using shape-directing macro-templates*, Microporous Mesoporous Materials, Vol. 35-36, 2000, pp. 621-629.

20. Naydenov, V., Tosheva, L., Sterte, J., *Vanadium modified AlPO-5 spheres through resin macrotemplating*, Microporous Mesoporous Materials, Vol. 66, 2003, pp. 321-329.

21. Özcan, A., Kalıpçılar H., *Preparation of Zeolite A Tubes from Amorphous Aluminosilicate Extrudates*, Industrial and Engineering Chemistry Research, Vol. 45, 2006, pp. 4977-4984.

22. Zhang, B., Davis, S. A., Mann, S., *Starch gel templating of spongelike macroporous silicate monoliths and mesoporous films*, Chemistry of Materials, Vol. 14, 2002, pp. 1369 – 1375.

23. J. L. Williams, *Monolith structures, materials, properties and uses*, Catalysis Today, Vol. 69, 2001, pp. 3-9.

24. Ural, A.T., *Zeolite membranes for gas separations: Synthesis and Transport properties*, Ph.D. Thesis in Chemical Engineering, METU, Ankara 1999

25. Zah, J., Henning M. K., Breyentenbach, J.C., *Layer development and growth history of polycrystalline zeolite A membranes synthesized from a clear solution*, Microporous Mesoporous Materials, Vol. 93, 2006, p. 141.

26. Zeolyst International, *http://www.zeolyst.com/html/faq.asp#eleven*, last accessible 22 August 2008.

27. Zeolite Molecular Sieve, http://www.molecularsieve.org/Zeolite_Molecular_Sieve.htm, last accessible 11 August 2008.

28. Howell, P. A., Acara, N. A., *Process for Producing Molecular Sieve Bodies*, U.S. Patent No: 3, 1964, 119, 660.

29. C.D.Madhusoodana, Y.Kameshima, A.Yasumori, K.Okada, *Preparation of fiber-reinforced binderless zeolite disks in solid state*, Journal of Materials Science Letters, Vol. 22, 2003, 553-556.

30. Y.Y.Li, S.P.Perera, B.D.Crittenden, J.Bridgwater *The effect of the binder on the manufacture of a 5A zeolite monolith*, Powder Technology, Vol. 116, 2001, 85-86

31. B. Zhang, S. A. Davis and S. Mann, *Starch gel templating of spongelike macroporous silicalite monoliths and mesoporous films*, Chemical Materials, Vol. 14, 2002, pp. 1369-1375

32. Schmizu, S., Hamada, H., *Direct conversion of bulk materials into MFI zeolites by a bulk material dissolution technique*, Advanced Materials Communications, Vol. 12, 2000, pp. 1332 – 1335.

33. G. Heinze, *Process for the Production of Molecular Sieve Granules,* 1964, US Patent, 3,356,450

34. W. L. Haden, F. J. Dzierzanowski, *Method for Producing Synthetic Crystalline Zeolite Aggregates,* 1960, US Patent No: 3,100,684

35. Jung, K.T., Shul, Y.G., *A new method for the synthesis of TS-1 monolithic zeolite*, Microporous Mesoporous Materials, Vol. 21, 1998, pp. 281-288

36. Jung , K. T., Hyun, J. H., Shul, Y. G., Koo, K.-K., *Nanoparticle synthesis of titanium silicalite for fiber, film, and monolith formation*, Ceramics Processing, Vol. 43, 1997, pp. 2802 – 2808.

37. Tavolaro, A., Drioli, E., *Zeolite Membranes*, Advanced Materials, Vol. 11, 975-996, 1999

38. Tsikoyiamis, J. G., Haog, W.O., *Synthesis & characterization of a pure zeolitic membrane*, Zeolites, Vol. 12, 1992, p.126

39. Kita, H., et al., *Synthesis of a zeolite NaA membrane for pervaporation of water/organic liquid mixtures* Journal of Materials Science Letters, Vol. 14, 1995, pp. 206-208

40. Pina, M.P., et al., *A semi-continuous method for the synthesis of NaA zeolite membranes on tubular supports*. Journal of Membrane Science, Vol. 244, 2004, pp. 141-150.

41. Sato, K., Sugimoto, K., Nakane, T., *Synthesis of industrial scale NaY zeolite membranes and ethanol permeating performance in pevaporation and vapor permeation up to 130°C and 570 kPa*, Journal of Membrane Science., Vol. 310, 2008, pp. 161-173

42. van den Berg, A.W.C., et al., *Zeolite A membranes synthesized on a UV irradiated TiO2 coated metal support: the high pervaporation performance.* Journal of Membrane Science, Vol. 224, 2003, pp. 29-37.

43. van de Graaf, J. M., van der Bijl, E., Stol, A., Kapteijn, F., Moulijn, J. A., *Effect of operating conditions and membrane quality on the separation performance of composite silicate-1 membranes*, Ind. Eng. Chem. Res., Vol. 37, pp. 4071 – 4083, 1998.

44. Murcia, A.B., Martinez, J.G., Amoros, D. C., Salono, A.L., Fuertes, A.B., *Silicalite-1 membranes supported on porous carbon discs,* Microporous and Mesoporous Materials, Vol. 59, 2003, pp. 147 – 159.

45. Li, Y.Y., Perera, S.P., Crittenden, B.D., *Zeolite Monoliths for Air Separation Part:1 Manufacture and Characterization.*, Chemical Engineering Research and Design, Vol. 76, 1998, p. 921.

46. Boudreau, L.C., J.A. Kuck, and M. Tsapatsis, *Deposition of oriented zeolite A films: in situ and secondary growth.* Journal of Membrane Science, Vol. 152, 1999, pp. 41-59.

47. Li, S., Tuan, V. A., Falconer, J. L., Noble, R. D., *Properties and separation performance of Ge-ZSM-5 membranes*, Microporous and Mesoporous Materials, Vol. 58, 2003, pp. 137-154.

48. Salomon, M. A., Coronas, J., Menendes, M., Santamaria, J., *Synthesis of a mordenite/ZSM-5/chabazite hydrophilic membrane on a tubular support. Application to the separation of a water–propanol mixture,* Studies in Surface Science and Catalysis, Vol. 125, 1999, pp.189-196.

49. R. Moreno, *The role of Slip Additives in tape casting technology Part II – Binders and Plasticizers*, American Chemical Society Bulletin, Vol. 71, 1992, pp. 1647-1657.

50. Huang, A., W. Yang, and J. Liu, *Synthesis and pervaporation properties of NaA zeolite membranes prepared with vacuum-assisted method,*. Separation and Purification Technology, Vol. 6, 2007, p. 158-167.

51. Zah, J., H.M. Krieg, and J.C. Breytenbach, *Pervaporation and related properties of time-dependent growth layers of zeolite NaA on structured ceramic supports.* Journal of Membrane Science, Vol. 284, 2006, pp. 276-290.

52. Franklin, K. R., Lowe, B.M., *Preparation and properties of gel particle silicalite*, Zeolites 7, Vol. 7, 1987, pp.135-142.

53. Akolekar D., Chaffee A., Howe R.F. *The transformation of kaolin to low silica X zeolite*, Zeolites, Vol.19, 1997, pp. 359-365

54. Great Vista Chemicals, *http://www.greatvistachemicals.com/industrial_and_specialty_chemicals/hydroxyethyl_cellulose.html,* last accessible, August 2008

55. Krznaric, I., Antonic, T., Subotic, B., *Physical chemistry of aluminosilicate gels. Part 1: Influence of batch concentration on chemical composition of the gels*, Zeolites, Vol. 19, 1997, pp. 29-40.

56. Morsli, A., Driole, M. F., Cacciaguerra, T., Arletti, R., Chiche, B., Hamidi, F., Benguedach, A., Quignard, F., Di Renzo, F., *Microporosity of the amorphous aluminosilicate precursors of zeolites: The case of the gel of synthesis of mordenite*, Microporous and Mesoporous Materials, Vol. 104, 2007, pp. 209-216.

57. Thomas, J. W., Crittenden, B., *Adsorption technology and design*, Chapter 3, 1988, pp. 31-65.

58. International Zeolite Association, *http://izasc.ethz.ch/fmi/xsl/IZASC/mat_xrd.xsl?db=crystal_data&lay=web&STC=LTA&-find,* last accessible 7 August 2008.

59. International Zeolite Association, *http://izasc.ethz.ch/fmi/xsl/IZASC/mat_xrd.xsl?db=crystal_data&lay=web&STC=FAU&-find,* last accessible 15 August 2008.

60. Cundy, C. S., Cox, P. A., The hydrothermal synthesis of zeolites: Precursors, intermediates and reaction mechanism, Microporous Mesoporous Materials, Vol. 82, 205, pp. 1-28.

61. Feijen, E. J. P., Martens, J. A., Jacobs, P. A., *Zeolite and Their Structural Mechanism of synthesis*, Studies in Surface Science and Catalysis, Vol. 84, 1994, pp. 3-19.

62. Kosanovic C, Bosnar, S., Subotic, B., Svetlicic, V., Misic, T., Drazic, G., Havancsak, K., *Study of the microstructure of amorphous aluminosilicate gel before and after its hydrothermal treatment*, Microporous Mesoporous Materials, 2008, pp. 177-185.

63. Jelic, T. A., Bronic, J., Hadzija, M., Subotic, B., Maric, I., *Influence of the freeze-drying of hydrogel on the critical processes occurring during crystallization of zeolite A – A new evidence of the gel "memory" effect*, Microporous and Mesoporous Materials, Vol. 05, 2007, pp. 65-74.

64. Kalıpçılar, H., M.S., *Modification of Morphology of Zeolite A for Use as Phosphate Replacement in Detergents*, M.S. Thesis in Chemical Engineering, METU, Ankara, 1995

65. Valtchev, V. P., Bozhilov, K. N., Evidences for zeolite nucleation at the solid-liquid interfaces of gel cavities, J. Am. Chem. Soc., Vol. 127, 2005, pp. 16171-16177.

66. Jansen, K., Mashmeyer, T., *Progress in zeolitic membranes*, Topics in Catalysis, Vol. 9, 1999, pp. 113-122.

APPENDIX A

SAMPLE CALCULATION FOR A BATCH COMPOSITION

Table A.1. Composition of raw materials used in the synthesis experiments

Reactants	**Na_2O (mole)**	**Al_2O_3 (mole)**	**SiO_2 (mole)**	**H_2O (mole)**
Water Glass	0.287	-	1	8.036
$Al(OH)_3$	-	0.5	-	1.5
NaOH	0.5	-	-	0.5

Table A.2. Formula weight of raw materials

Reactants	**Formula Weight (g/mol)**
Water glass	222.44
$Al(OH)_3$	78
NaOH	40
H_2O	18

Table A.3. Molecular weights of reactants

Reactant	Molecular Weight (g/mol)
Na_2O	62
Al_2O_3	102
SiO_2	60
H_2O	18

Molar composition of the batch: $2.5Na_2O{:}1Al_2O_3{:}1.7SiO_2{:}150H_2O$ ($N_{2.5}{:}A_1{:}S_{1.7}{:}H_{150}$)

Formula weight of the batch: $2.5\times62 + 1\times102 + 1.7\times60 + 150\times18 = 3059$ g

Silica source: Water glass (sodium silicate solution)

$N_{0.287}S_1H_{8.036}$

Aluminum Source: $Al(OH)_3$

$Al_2O_3 + 3\ H_2O \rightarrow 2\ Al(OH)_3$

Sodium source: NaOH

$Na_2O + H_2O \rightarrow 2\ NaOH$

Basis: 100g batch

Calculation of amounts of raw materials required to prepare the batch:

- Water glass (Sodium Silicate Solution):

$$100\text{ g batch}\times\frac{1\text{ mol batch}}{3059\text{ g batch}}\times\frac{1.7\text{ mol }SiO_2}{1\text{ mol batch}}\times\frac{1\text{ mol water glass}}{1\text{ mol }SiO_2}$$

$$\times\frac{222.44\text{ g water glass}}{1\text{ mol water glass}} = 12.36\text{ g water glass}$$

- $Al(OH)_3$:

$$100\text{ g batch}\times\frac{1\text{ mol batch}}{3059\text{ g batch}}\times\frac{1\text{mol }Al_2O_3}{1\text{ mol batch}}\times\frac{2\text{ mol }Al(OH)_3}{1\text{ mol }Al_2O_3}\times\frac{78\text{ g }Al(OH)_3}{1\text{ mol }Al(OH)_3}$$

$$= 5.1\text{ g }Al(OH)_3$$

- NaOH:

$$100\text{ g batch}\times\frac{1\text{ mol batch}}{3059\text{ g batch}}\times\frac{2.5\text{ mol }Na_2O}{1\text{ mol batch}}\times\frac{2\text{ mol NaOH}}{1\text{ mol }Na_2O}\times\frac{40\text{ g NaOH}}{1\text{ mol NaOH}}$$

$$= 6.54\text{ g NaOH}$$

$$100\text{ g batch}\times\frac{1\text{ mol batch}}{3059\text{ g batch}}\times\frac{1.7\text{ mol }SiO_2}{1\text{ mol batch}}\times\frac{1\text{ mol water glass}}{1\text{ mol }SiO_2}\times\frac{0.287\text{ mol }Na_2O}{1\text{ mol water glass}}$$

$$\times\frac{2\text{ mol NaOH}}{1\text{ mol }Na_2O}\times\frac{40\text{ g NaOH}}{1\text{ mol NaOH}} = 1.27\text{ g NaOH (from waterglass)}$$

$$m_{\text{NaOH, needed}} = 6.54\text{ g} - 1.27\text{ g} = 5.27\text{ g} \cong 5.3\text{ g NaOH}$$

- H_2O:

$$100\text{ g batch}\times\frac{1\text{ mol batch}}{3059\text{ g batch}}\times\frac{1.7\text{ mol }SiO_2}{1\text{ mol batch}}\times\frac{1\text{ mol water glass}}{1\text{ mol }SiO_2}\times\frac{8.036\text{ mol }H_2O}{1\text{ mol water glass}}$$

$$\times\frac{18\text{ g }H_2O}{1\text{ mol }H_2O} = 8.04\text{ g }H_2O\text{ (from silica source)}$$

$$100\text{ g batch}\times\frac{1\text{ mol batch}}{3059\text{ g batch}}\times\frac{1\text{ mol }Al_2O_3}{1\text{ mol batch}}\times\frac{2\text{ mol A(OH)}_3}{1\text{ mol }Al_2O_3}\times\frac{3\text{ mol }H_2O}{2\text{ mol }Al(OH)_3}$$

$$\times\frac{18\text{ g }H_2O}{1\text{ mol }H_2O} = 1.77\text{ g }H_2O\text{ (from aluminum source)}$$

$$100\text{ g batch} \times \frac{1\text{ mol batch}}{3059\text{ g batch}} \times \frac{2.5\text{ mol } Na_2O}{1\text{ mol batch}} \times \frac{2\text{ mol NaOH}}{1\text{ mol } Na_2O} \times \frac{1\text{ mol } H_2O}{2\text{ mol NaOH}}$$

$$\times \frac{18\text{ g } H_2O}{1\text{ mol } H_2O} = 1.47\text{ g } H_2O \text{ (from sodium source)}$$

$$100\text{ g batch} \times \frac{1\text{ mol batch}}{3059\text{ g batch}} \times \frac{150\text{ mol } H_2O}{1\text{ mol batch}} \times \frac{18\text{ g } H_2O}{1\text{ mol } H_2O} = 88.26\text{ g } H_2O \text{ (theoretically)}$$

$$m_{H_2O,needed} = 88.26\text{ g} - (8.04\text{ g} + 1.77\text{ g} + 1.47\text{ g}) = 76.98\text{ g} \cong 77\text{ g } H_2O$$

APPENDIX B

SYNTHESIS CONDITIONS OF THE BINDERLESS MACROBODIES AND THEIR CHARACTERIZATION RESULTS BASED ON XRD AND SEM

For all the samples inserted here,

- The starting hydrogel composition, $2.5Na_2O:1Al_2O_3:1.7SiO_2:150H_2O$
- The conditioning conditions, at 87% relative humidity
- The drying conditions, at room temperature for 1 day
- The calcination conditions, 600°C for 2h and
- The synthesis conditions 80°C for 72h (except for the ones prepared for the crystallination curve analysis of the binderless bodies)

are kept constant. Apart from these, the preparation conditions and the characterization results of these macrobodies based on XRD and SEM analysis are given in Table B1.

Table B.1. Experimental conditions for the macrobodies and their characterization based on XRD and SEM

Sample Code	Washing Method	Geometry	Support Synthesis Liquid Composition	Synthesis Ratio (S/L)	Zeolite type	Crystallinity %	SEM micrographs (overall)	Ave. Crystal Size (SEM)	Remarks
CG6A	1	Tube	Filtrated liquid	1/14	Zeolite A	81	2-10 μm	-	Hard to break
CG6B	1	Tube	$N_{4.8}A_{1}S_{0.77}H_{400}$	1/14	Zeolite A	76	3-7 μm	-	Hard to break
CG6C	1	Tube	$N_{4.8}H_{400}$	1/14	Zeolite A + Zeolite X	53 (A) – 27 (X)	3-12 μm	5.19 μm	Easy to break
CG6D	1	Tube	$N_{2.4}H_{400}$	1/14	Amorphous	0	-	-	Hard to break
CG6E	1	Tube	Deionized W	1/14	Amorphous	0	-	-	Hard to break
CG6F	1	Tube	$N_{7.4}A_{1}S_{0.7}H_{624}$	1/14	Zeolite A	52	-	-	Hard to break
CG6G	1	Tube	Centrifuged form of CG6F	1/14	Zeolite A	86	-	-	Hard to break
CG6H	1	Tube	$N_{4.8}A_{1}S_{0.77}H_{400}$	1/14	Zeolite A	86	-	-	Hard to break
CG6B2	1	Tube	$N_{4.8}A_{1}S_{0.77}H_{400}$	1/14	Zeolite A	92	-	-	Hard to break
CG13F1	2	Tube	Filtrated liquid	1/14	Zeolite A	84	-	-	Hard to break
CG13F2	2	Tube	Filtrated liquid	1/14	Zeolite A	86	-	-	Hard to break
CG13L1	2	Tube	$N_{4.8}A_{1}S_{0.77}H_{400}$	1/14	Zeolite A	83	-	-	Hard to break
CG13L2	2	Tube	$N_{4.8}A_{1}S_{0.77}H_{400}$	1/14	Zeolite A	104	-	-	Hard to break
CG14F1	3	Tube	Filtrated liquid	1/14	Zeolite A	92	1-8 μm	2.72 μm	Hard to break
CG14F2	3	Tube	Filtrated liquid	1/14	Zeolite A	93	-	-	Hard to break
CG14L1	3	Tube	$N_{4.8}A_{1}S_{0.77}H_{400}$	1/14	Zeolite A	87	-	-	Hard to break
CG14L2	3	Tube	$N_{4.8}A_{1}S_{0.77}H_{400}$	1/14	Zeolite A	92	-	-	Hard to break
CG15F	4	Tube	Filtrated liquid	1/14	Zeolite A	82	2-6 μm	2.76 μm	Hard to break

Table B.1. cont'd

Sample Code	Washing Method	Geometry	Support Synthesis Liquid Composition	Synthesis Ratio (S/L)	Zeolite type	Crystallinity %	SEM micrographs (overall)	Ave. Crystal Size (SEM)	Remarks
CG15L	4	Tube	$N_{4.8}A_1S_{0.77}H_{400}$	1/14	Zeolite A	89	-	-	Hard to break
CG16F	2	Tube	Filtrated liquid	1/14	Zeolite A	94	2-7 μm	3.47 μm	Hard to break
CG16L	2	Tube	$N_{4.8}A_1S_{0.77}H_{400}$	1/14	Zeolite A	90	-	-	Hard to break
CG17F	3	Tube	Filtrated liquid	1/14	Zeolite A	93	-	-	Hard to break
CG17L	3	Tube	$N_{4.8}A_1S_{0.77}H_{400}$	1/14	Zeolite A	96	-	-	Hard to break
CG18F	4	Tube	Filtrated liquid	1/14	Zeolite A	97	-	-	Hard to break
CG18L	4	Tube	$N_{4.8}A_1S_{0.77}H_{400}$	1/14	Zeolite A	81	-	-	Hard to break
CG20D1-D25	2	Disk	$N_{4.8}A_1S_{0.77}H_{400}$	1/14	Zeolite A	NA	-	-	Hard to break
CG21T1-T2	2	Tube	$N_{4.8}A_1S_{0.77}H_{400}$	1/14	Zeolite A	≈ 90 (avg)	-	-	-
CG25D1-D11	2	Disk	$N_{4.8}A_1S_{0.77}H_{400}$	1/14	Zeolite A	≈ 88 (avg)	-	-	-
CG27A1	2	Tube	$N_{2.4}H_{400}$	1/14	Amorphous	0	-	-	Hard to break
CG27B1	2	Tube	$N_{3.6}H_{400}$	1/14	Amorphous	0	-	-	Hard to break
CG27B2	2	Tube	$N_{3.6}H_{400}$	1/14	Amorphous	0	-	-	Hard to break
CG27C1	2	Tube	$N_{4.8}H_{400}$	1/14	Zeolite A	65	-	-	Deformation on the surface
CG27C2	2	Tube	$N_{4.8}H_{400}$	1/14	Zeolite A	46	-	-	Deformation on the surface
CG27G1	2	Tube	$N_{4.2}H_{400}$	1/14	Amorphous	0	-	-	Hard to break
CG29C3	2	Tube	$N_{4.8}H_{400}$	1/14	Zeolite A (possible X)	68	-	-	Easy to break
CG29C4	2	Tube	$N_{4.8}H_{400}$	1/18	Zeolite A (possible X)	79	-	-	Deformation on the surface
CG29G2	2	Tube	$N_{4.2}H_{400}$	1/18	Amorphous	0	-	-	Deformation on the surface
CG29H1	2	Tube	$N_{5.4}H_{400}$	1/14	NA	NA	-	-	Hard to break
CG29H2	2	Tube	$N_{5.4}H_{400}$	1/18	Zeolite X (possible A)	81	-	-	Hard to break

Table B.1. cont't

Sample Code	Washing Method	Geometry	Support Synthesis Liquid Composition	Synthesis Ratio (S/L)	Zeolite type	Crystallinity %	SEM micrographs (overall)	Ave. Crystal Size (SEM)	Remarks
CG29D1	2	Tube	$N_{4.8}A_1H_{400}$	1/18	NA	NA	-	-	Hard to break
CG29B3	2	Tube	$N_{3.0}H_{400}$	1/18	NA	NA	-	-	Hard to break
CG29D2	2	Tube	$N_{4.8}A_1H_{400}$	1/18	Zeolite A	96	-	-	Hard to break
CG31D3	2	Tube	$N_{4.8}A_1H_{400}$	1/18	Zeolite A	94	-	-	Hard to break
CG31C5	2	Tube	$N_{4.8}H_{400}$	1/18	Zeolite A + Zeolite X	25 (A) – 64 (X)	-	-	Easy to break
CG31B4	2	Tube	$N_{3.0}H_{400}$	1/18	NA	NA	-	-	Hard to break
CG31E1	2	Tube	$N_{4.8}A_1S_{0.07}H_{400}$	1/18	Zeolite A	95	1-5 μm	2.35 μm	Hard to break
CG31K1	2	Tube	$N_{4.8}A_{1.5}S_{0.07}H_{400}$	1/18	Zeolite A	91	0-4 μm	2.09 μm	Hard to break
CG31I1	2	Tube	$N_{4.8}A_1S_{0.5}H_{400}$	1/18	Zeolite A	95	0-5 μm	2.30 μm	Harder to break
CG31J1	2	Tube	$N_{4.8}A_1S_1H_{400}$	1/18	Zeolite A	88	0-5 μm	2.30 μm	Harder to break
CG32F1-F2	2	Tube	Filtrated Liquid	1/18	Zeolite A	NA	-	-	Deformation on the surface
CG33L1	2	Tube	$N_{4.8}A_{0.5}S_{0.07}H_{400}$	1/18	Zeolite A	89	1-4 μm	1.95 μm	Hard to break
CG33M1	2	Tube	$N_{3.0}A_1S_{0.07}H_{400}$	1/18	Zeolite A	95	0-3 μm	1.81 μm	Hard to break
CG33N1	2	Tube	$N_{2.4}A_1S_{0.07}H_{400}$	1/14	Amorphous	0	-	-	Harder to break
CG34P1	2	Bar	$N_{7.5}A_1S_{1.5}H_{990}$	1/28	Amorphous	0	-	-	NA
CG34P2	2	Bar	$N_4A_1S_{1.67}H_{660}$	1/28	Amorphous	0	-	-	NA
CG34P3	2	Bar	$N_2A_1S_2H_{495}$	1/28	Amorphous	0	-	-	NA
CG34P4	2	Bar	$N_{5.5}A_1S_{3.5}H_{990}$	1/28	Amorphous	0	-	-	NA
CG34P5	2	Bar	$N_2A_1S_1H_{396}$	1/28	Amorphous	0	-	-	NA
CG34P6	2	Bar	$N_{3.75}A_1S_{0.25}H_{495}$	1/14	Zeolite A	NA	-	-	NA
CG34P7	2	Bar	$N_{5.33}A_1S_{0.33}H_{660}$	1/14	Zeolite A	NA	-	-	NA
CG34P8	2	Bar	$N_{8.5}A_1S_{0.5}H_{990}$	1/14	Zeolite A	NA	-	-	NA
CG34P9	2	Bar	$N_{5.67}A_1H_{660}$	1/14	Zeolie A	NA	-	-	NA

Table B.1. cont't

Sample Code	Washing Method	Geometry	Support Synthesis Liquid Composition	Synthesis Ratio (S/L)	Zeolite type	Crystallinity %	SEM micrographs (overall)	Ave. Crystal Size (SEM)	Remarks
CG34P10	2	Bar	$N_{3.5}A_1S_{0.5}H_{495}$	1/14	Zeolite A	NA	-	-	NA
CG34P11	2	Bar	$N_5A_1S_{0.67}H_{660}$	1/14	Zeolite A	NA	-	-	NA
CG34P12	2	Bar	$N_8A_1S_1H_{990}$	1/14	Zeolite A	NA	-	-	NA
CG40P13	2	Bar	$N_{4.71}A_1S_{5.88}H_{582.35}$	1/14	Zeolite A	NA	-	-	NA
CG40P14	2	Bar	$N_{3.25}A_1S_{0.75}H_{495}$	1/14	Zeolie A	NA	-	-	NA
CG40P15	2	Bar	$N_{2.17}A_1S_{0.17}H_{330}$	1/14	Zeolite A	NA	-	-	NA
CG40P16	2	Bar	$N_{2.6}A_1S_{0.4}H_{396}$	1/14	Zeolite A	NA	-	-	NA
CG40P17	2	Bar	$N_{5.83}A_1S_{1.5}H_{825}$	1/14	Zeolite A	NA	-	-	NA
CG40L1-CG40L9	2	Bar	$N_{4.8}A_1S_{0.07}H_{400}$	1/3.5 to 1/105	Zeolite A	72-90	-	-	Synthesized for solid extrudate to reactive solution ratio analysis
CG41L1-CG41L6	2	Bar	$N_{4.8}A_1S_{0.07}H_{400}$	1/14	-	-	-	-	-
CG41F1-CG41F6	2	Bar	Filtarted Liquid	1/14	-	-	-	-	-
CG42L 4h-72h	2	Bar	$N_{4.8}A_1S_{0.07}H_{400}$	1/14	Zeolite A	10 - 88			Synthesized for crystallinity curve analysis
CG43X1-9	2	Bar	$N_{2.33}A_1H_{330}$	1/3.5 to 1/105	Amorphous	0	-	-	Synthesized for solid extrudate to reactive solution ratio analysis

APPENDIX C

XRD FIGURES

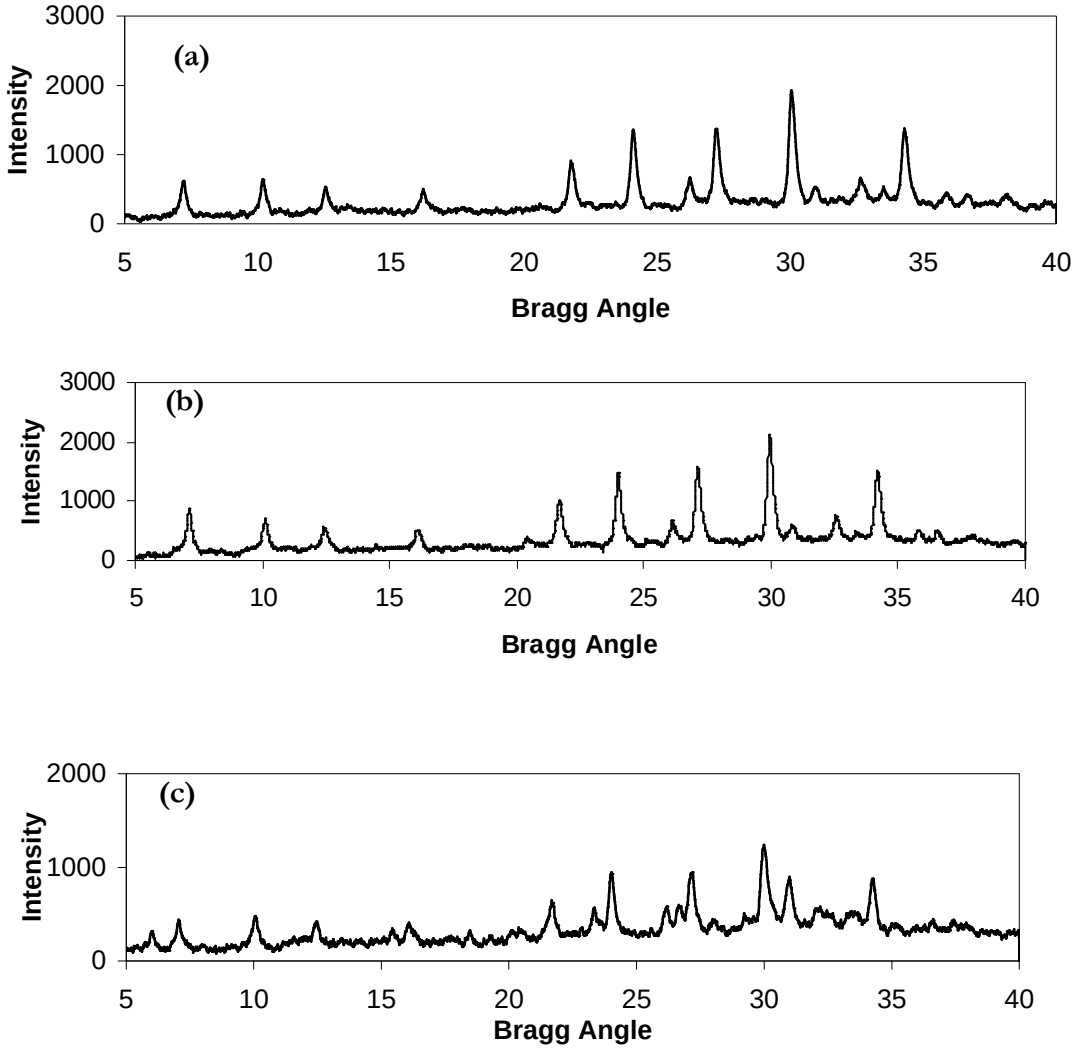

Figure C.1. XRD pattern of (a) CG6A (XRD5972), (b) CG6B (XRD5975) and (c) CG6C (XRD 5976)

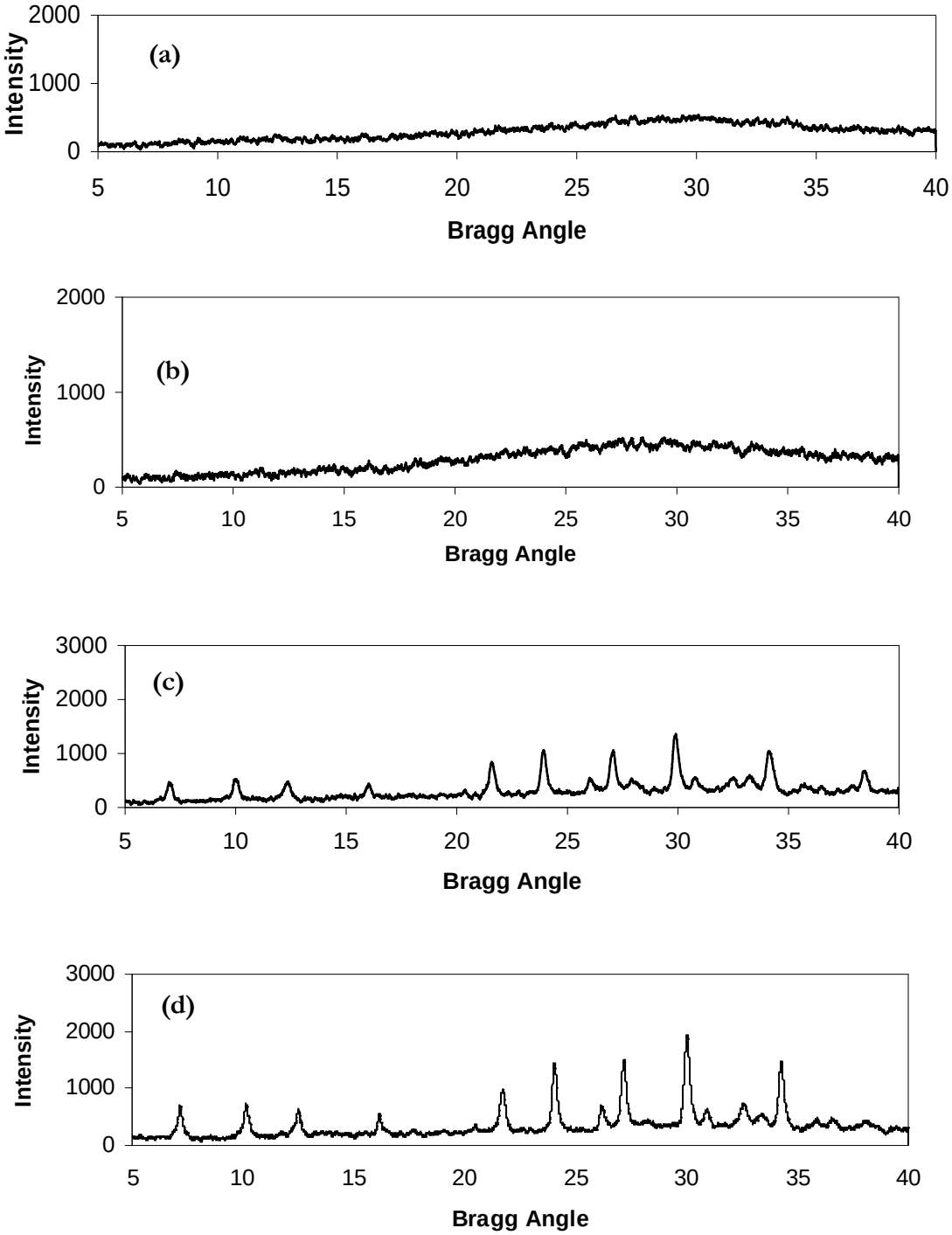

Figure C.2. XRD pattern of (a) CG6D (XRD 5974), (b) CG6E (XRD 5973), (c) CG6F (XRD 5978) and (d) CG6G (XRD 5977)

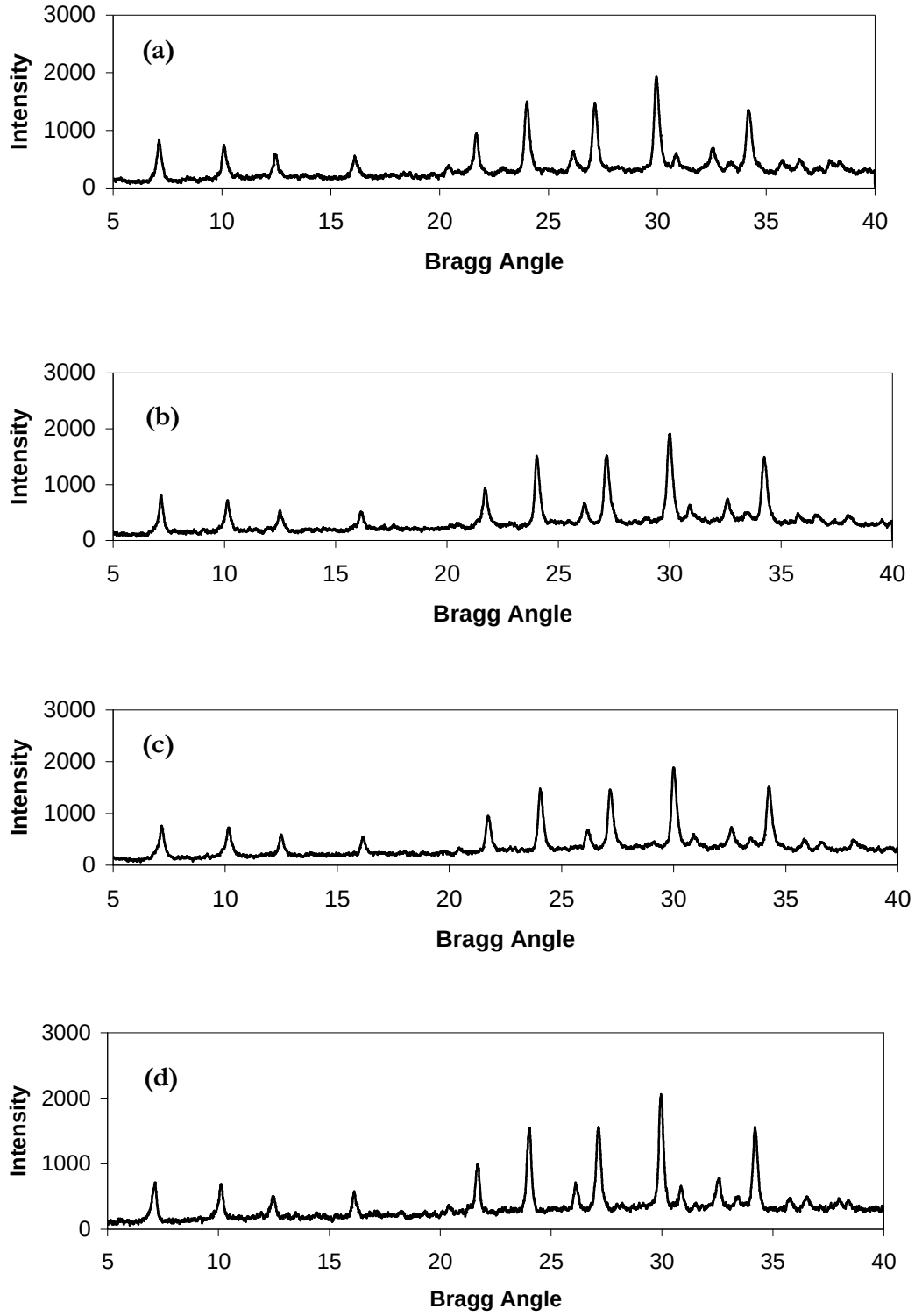

Figure C.3. XRD pattern of (a) CG6H (XRD 5974), (b) CG13F1 (XRD 6225), (c) CG13L1 (XRD 6226) and (d) CG13F2 (XRD 6246)

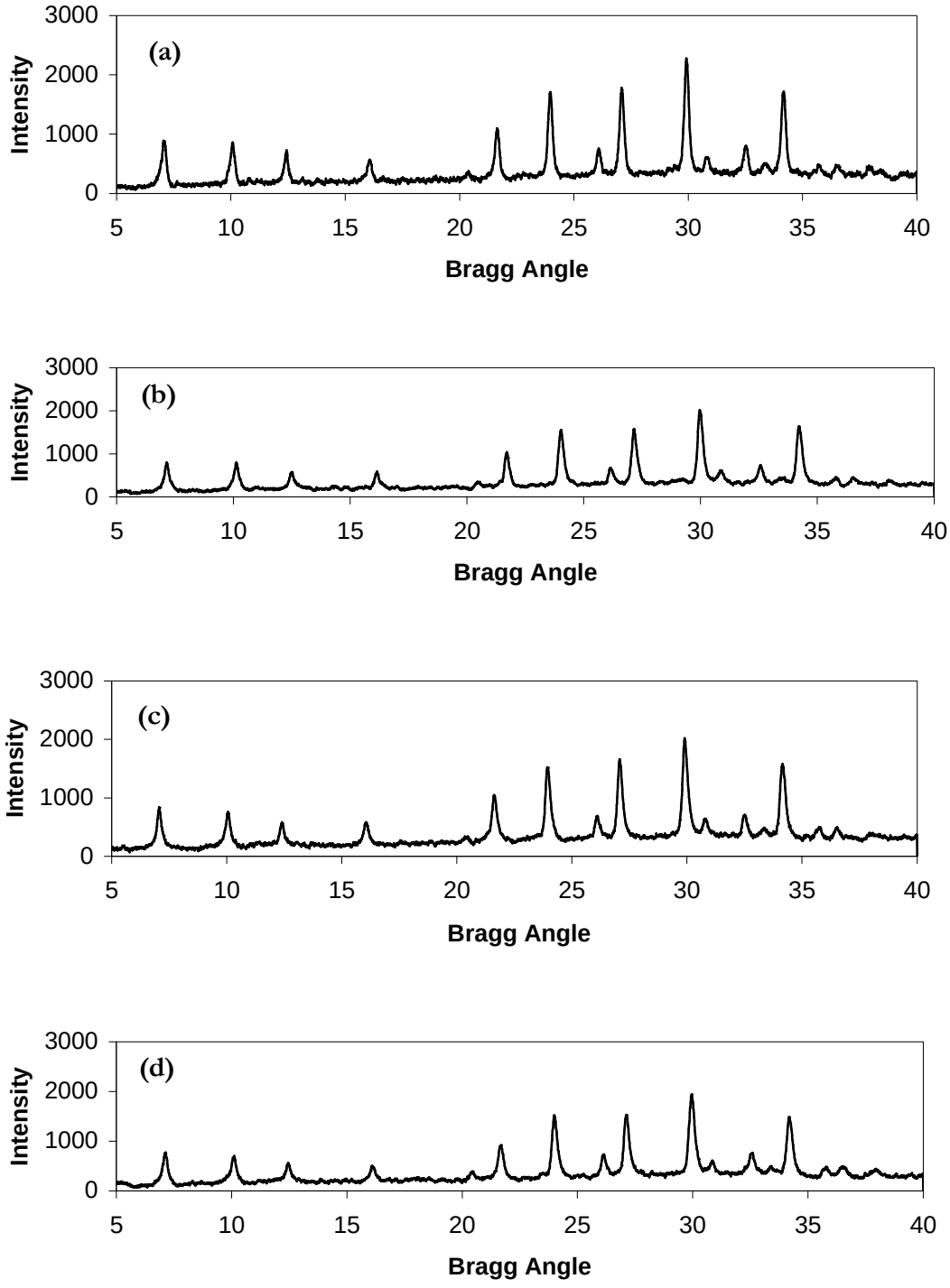

Figure C.4. XRD pattern of (a) CG13L2 (XRD 6248), (b) CG14F1 (XRD 6223), (c) CG14L1 (XRD 6224) and (d) CG14F2 (XRD 6228)

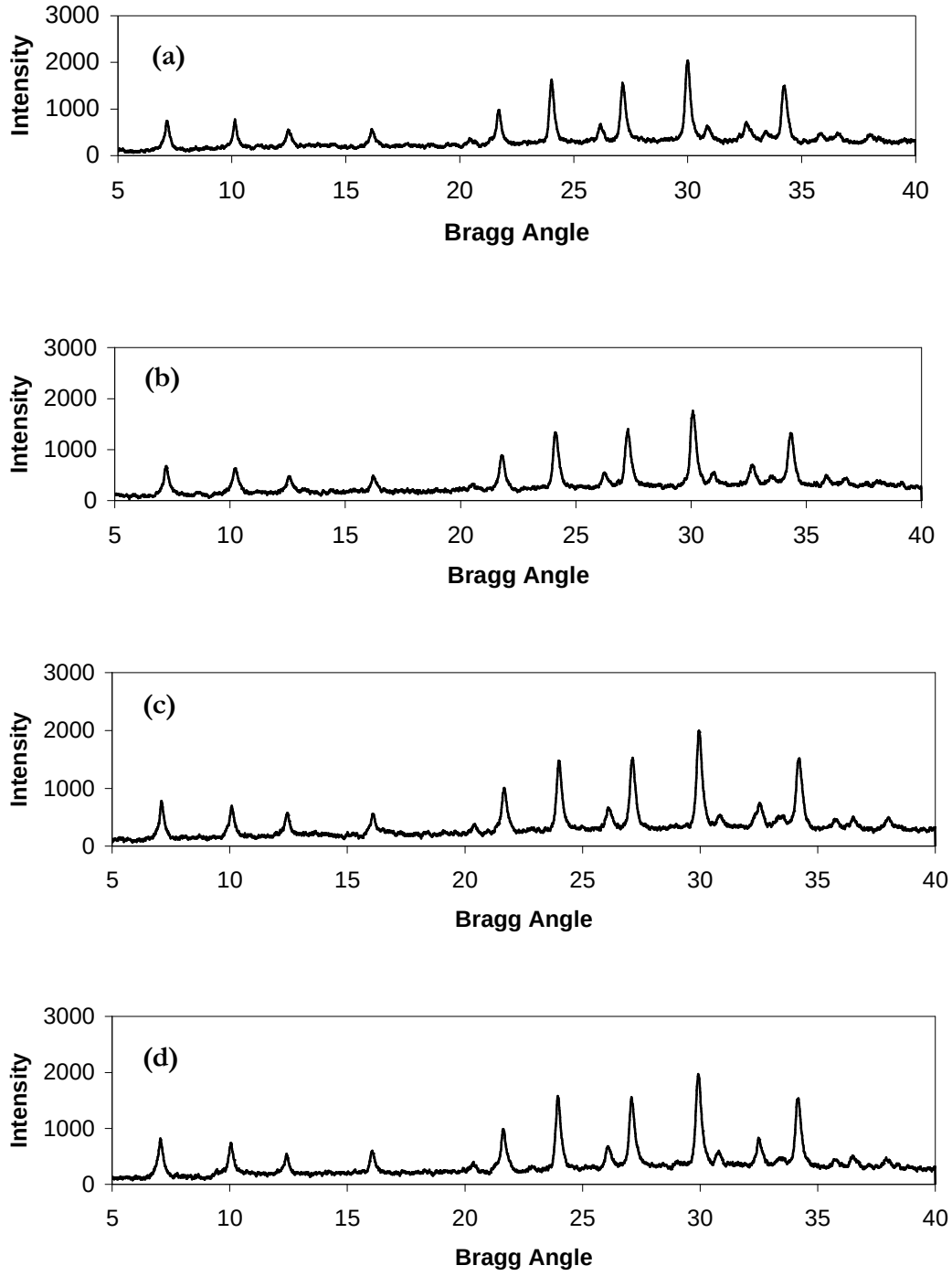

Figure C.5. XRD pattern of (a) CG14L2 (XRD 6241), (b) CG15F (XRD 6287), (c) CG15L (XRD 6286) and (d) CG16F (XRD 6235)

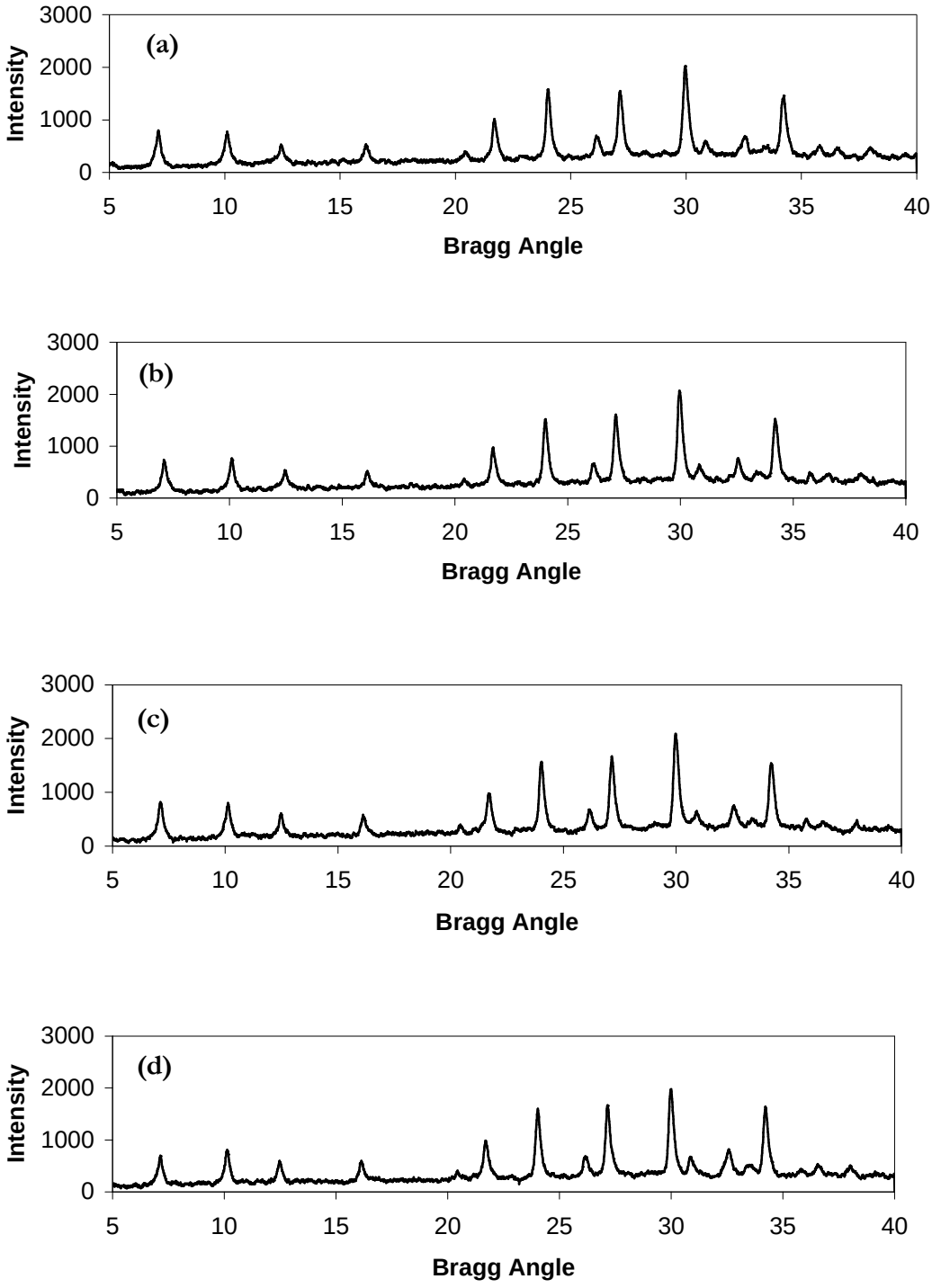

Figure C.6. XRD pattern of (a) CG16L (XRD 6237), (b) CG17F (XRD 6346), (c) CG17L (XRD 6344) and (d) CG18F (XRD 6345)

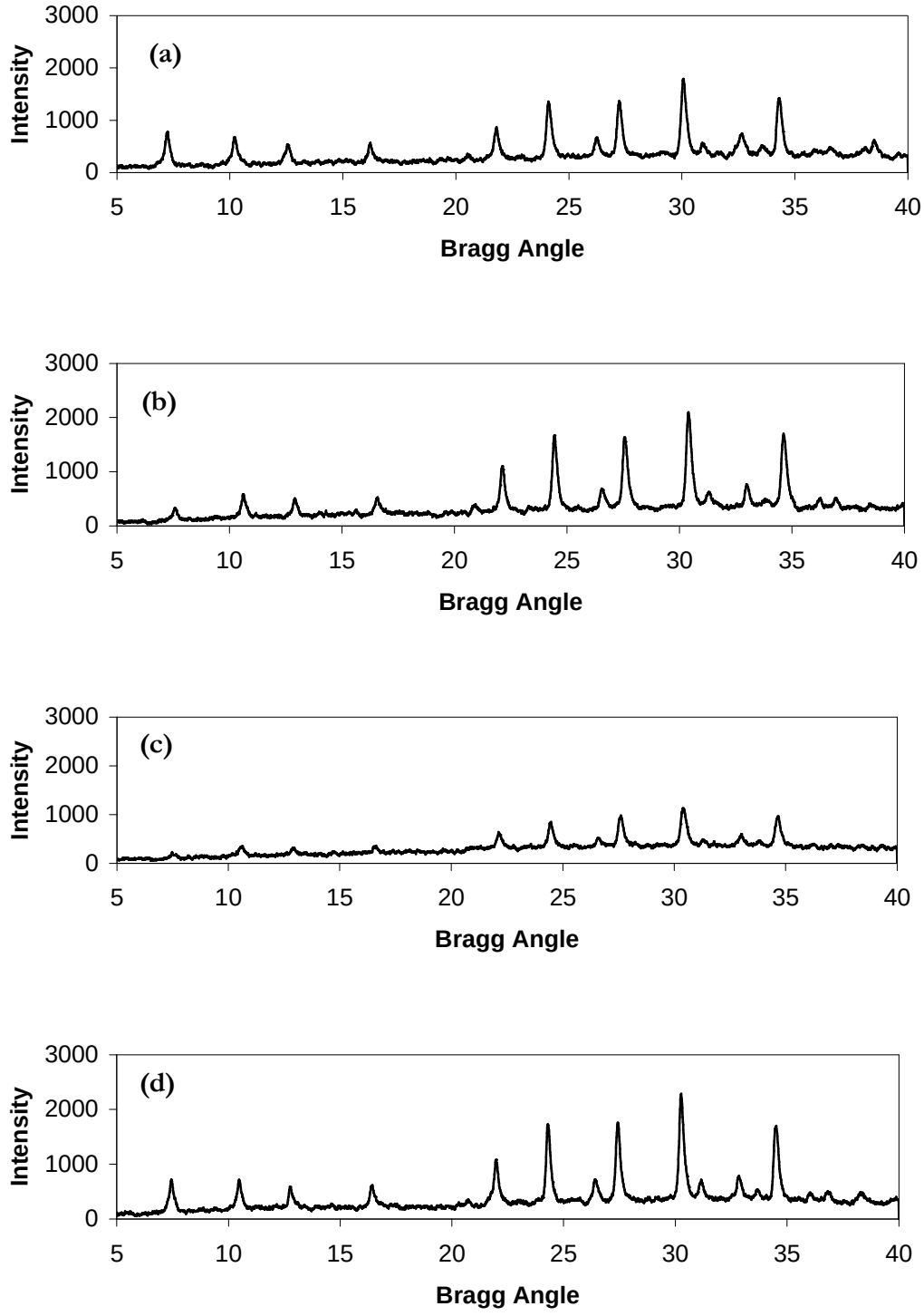

Figure C.7. XRD pattern of (a) CG18L (XRD 6347), (b) CG25D1 (XRD 6442), (c) CG25D1-back (XRD 6444) and (d) CG25D3 (XRD 6451)

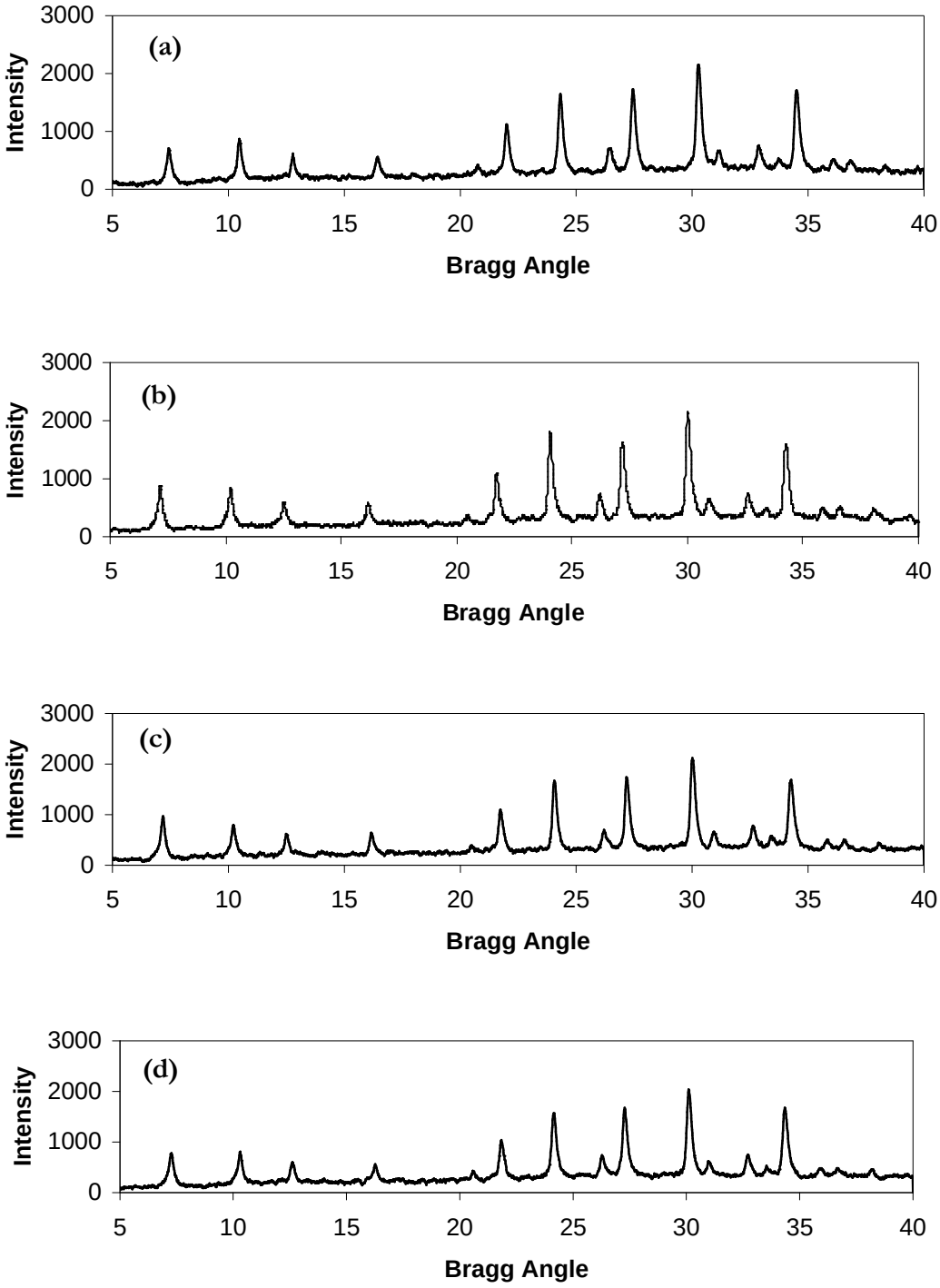

Figure C.8. XRD pattern of (a) CG25D3-back (XRD 6452), (b) CG25D4 (XRD 6453), (c) CG25D4-back (XRD 6454) and (d) CG25D5 (XRD 6445)

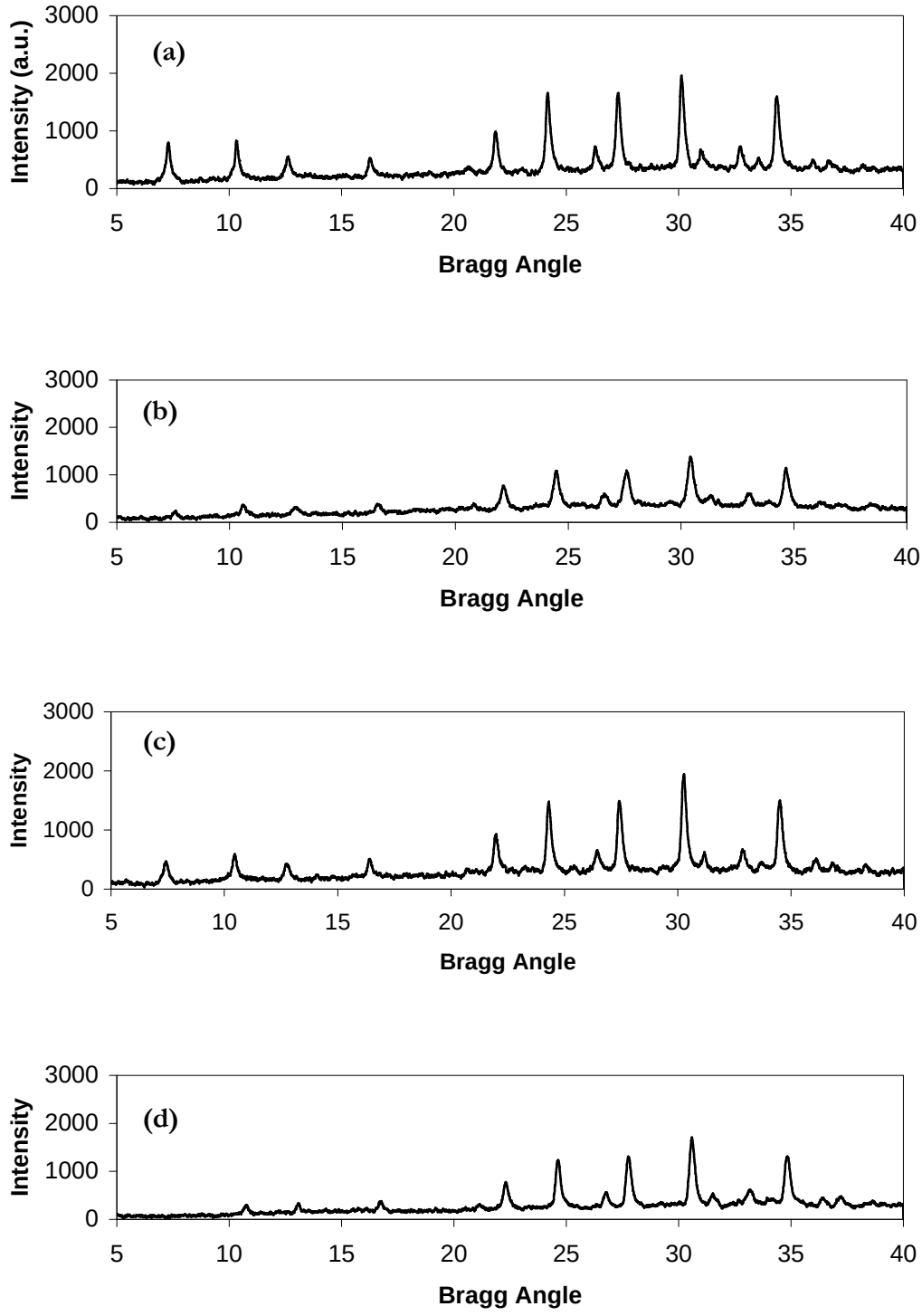

Figure C.9. XRD pattern of (a) CG25D5-back (XRD 6446), (b) CG20D1 (XRD 6397), (c) CG20D21-back (XRD 6398) and (d) CGM1 (XRD 6383)

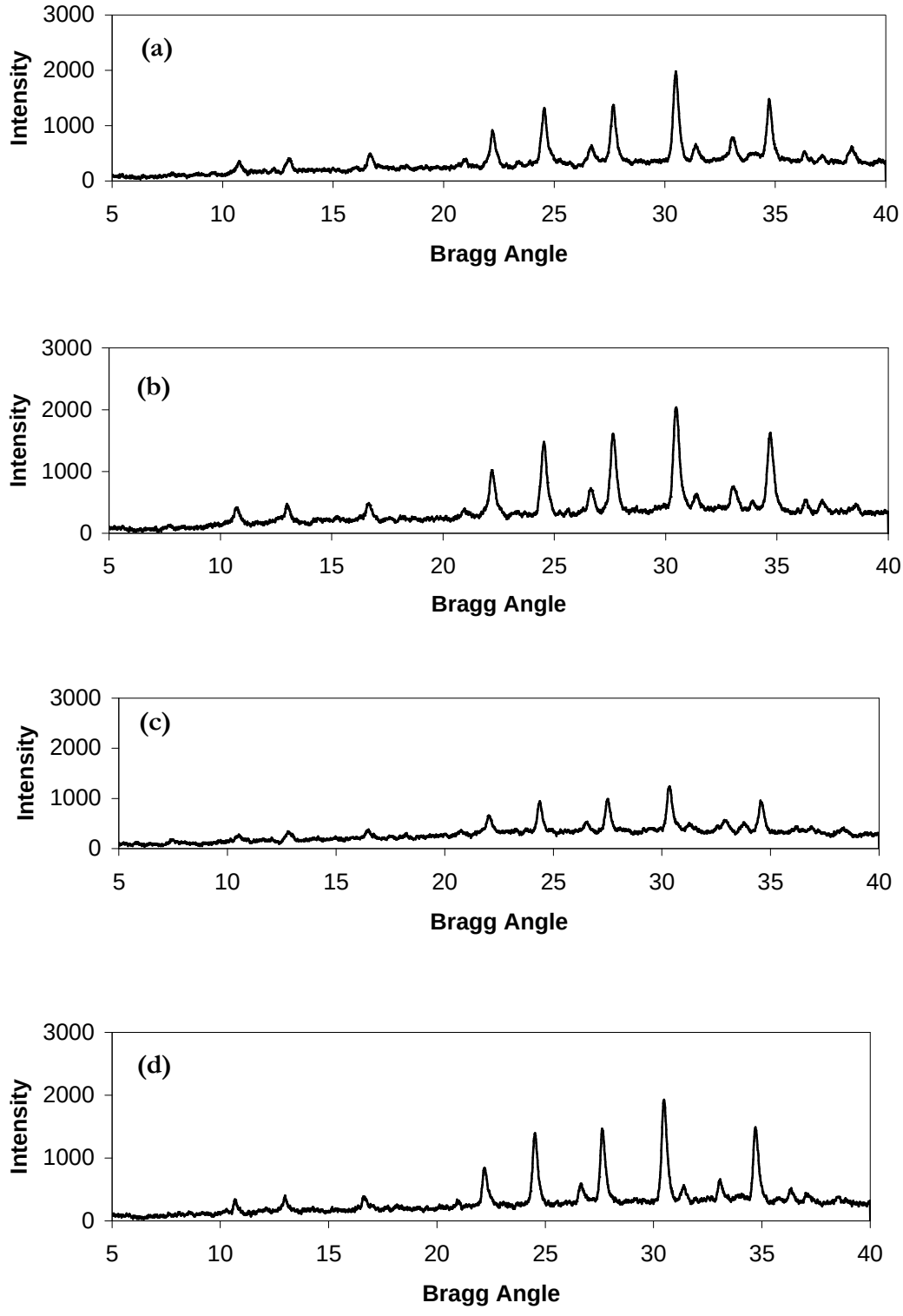

Figure C.10. XRD pattern of (a) CGM1-back (XRD 6377), (b) CGM2 (XRD 6386), (c) CGM2-back (XRD 6378) and (d) CGM3 (XRD 6385)

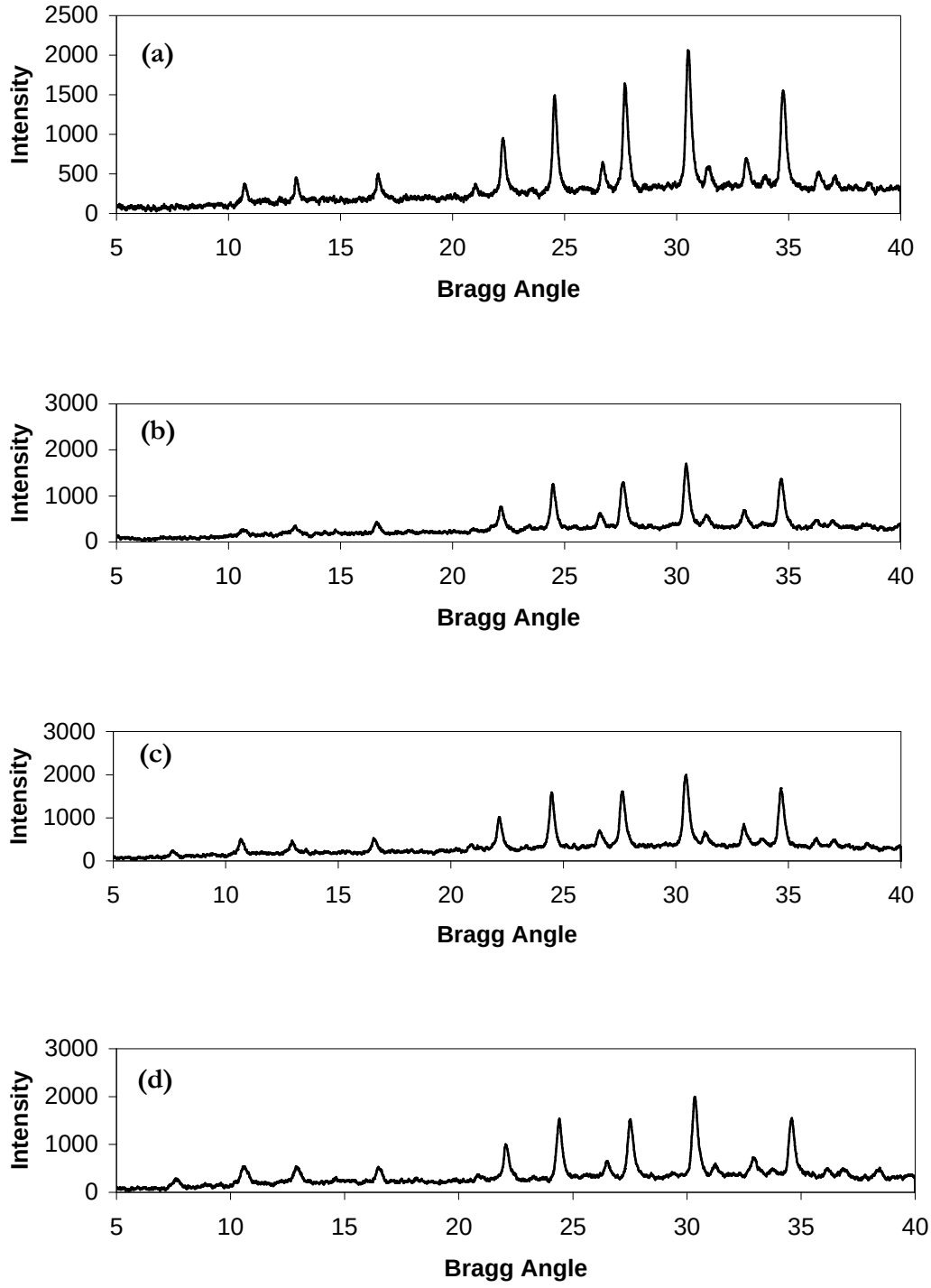

Figure C.11. XRD pattern of (a) CGM3-b (XRD 6380), (b) CGM4 (XRD 6384), (c) CGM4-b (XRD 6379) and (d) CGM5 (XRD 6479)

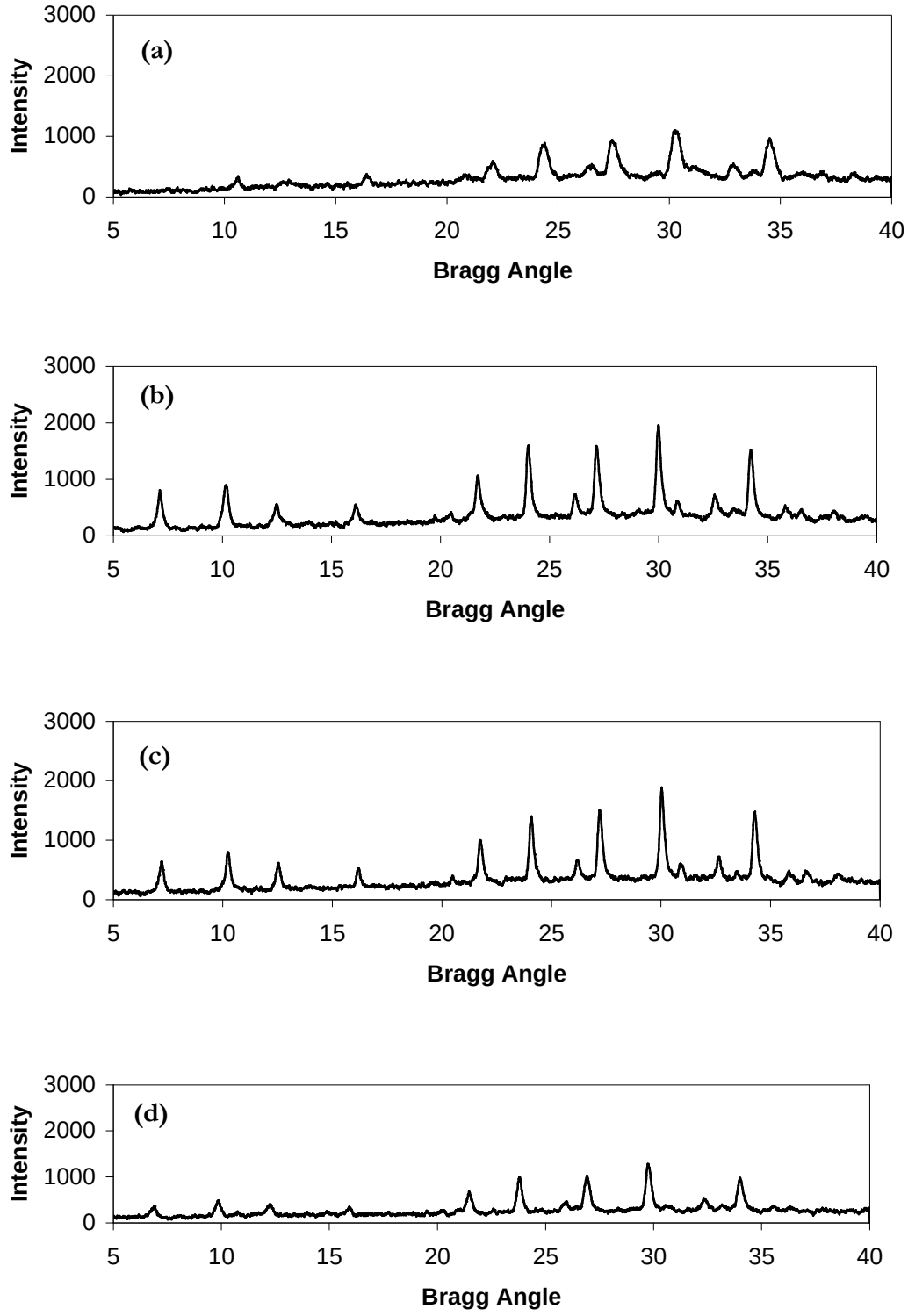

Figure C.12. XRD pattern of (a) CGM6 (XRD 6478), (b) CGM7 (XRD 6480), (c) CGM7-back (XRD 6481) and (d) CGM9 (XRD 6479)

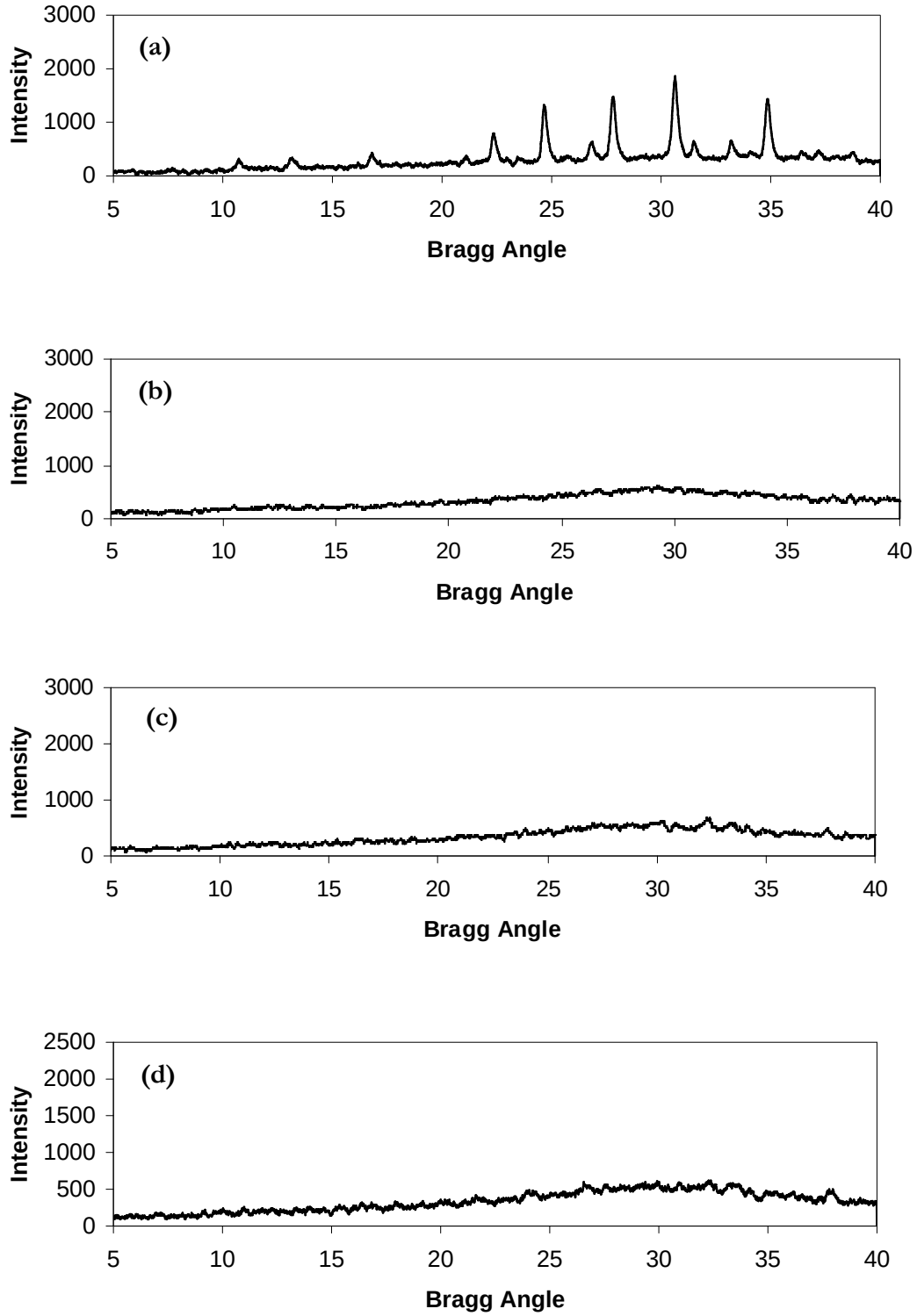

Figure C.13. XRD pattern of (a) CGM10 (XRD 6508), (b) CG27A1 (XRD 6511), (c) CG27B1 (XRD 6512) and (d) CG27B2 (XRD 6510)

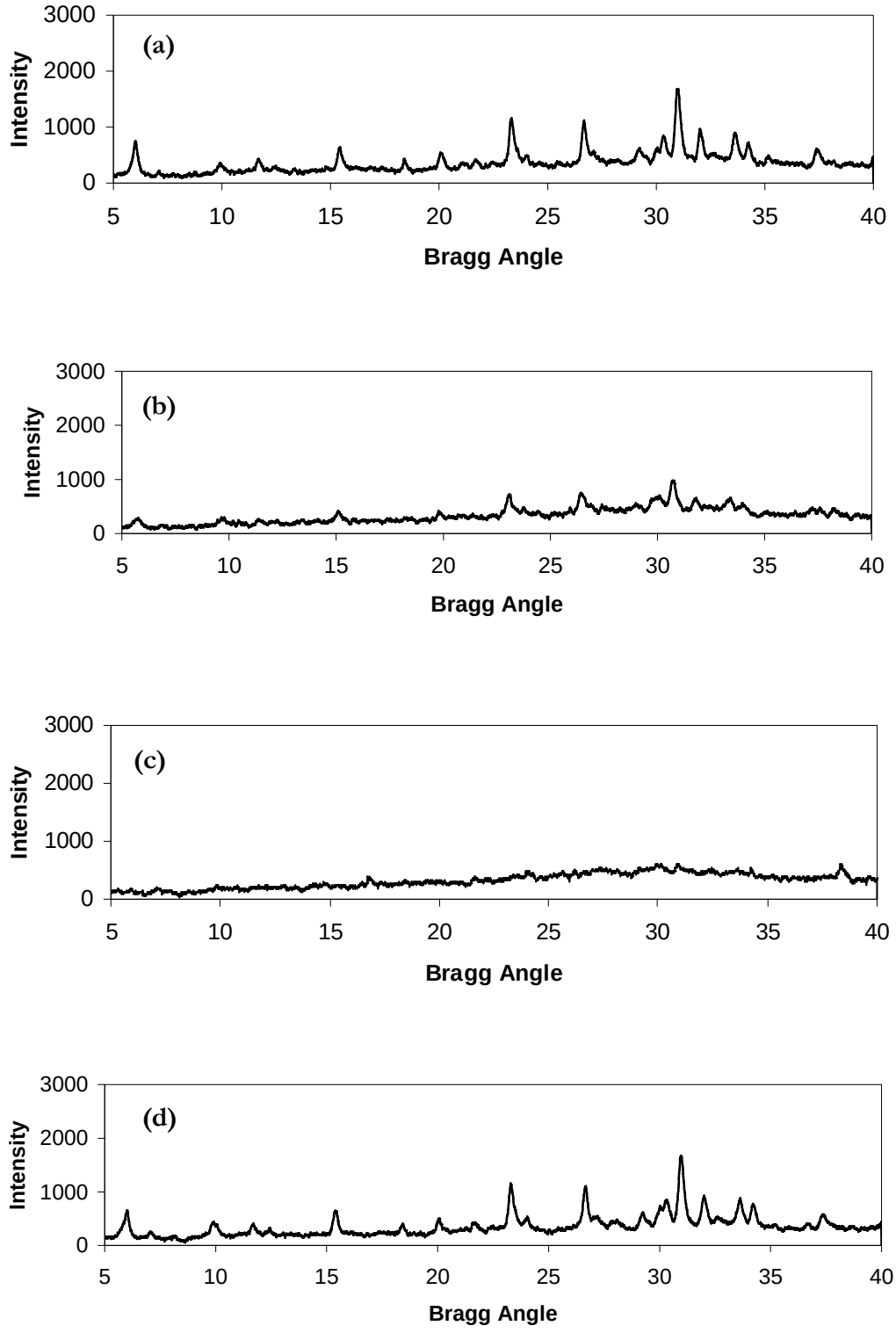

Figure C.14. XRD pattern of (a) CG27C1 (XRD 6529), (b) CG27C2 (XRD 6526), (c) CG27G1 (XRD 6527) and (d) CG27C3 (XRD 6524)

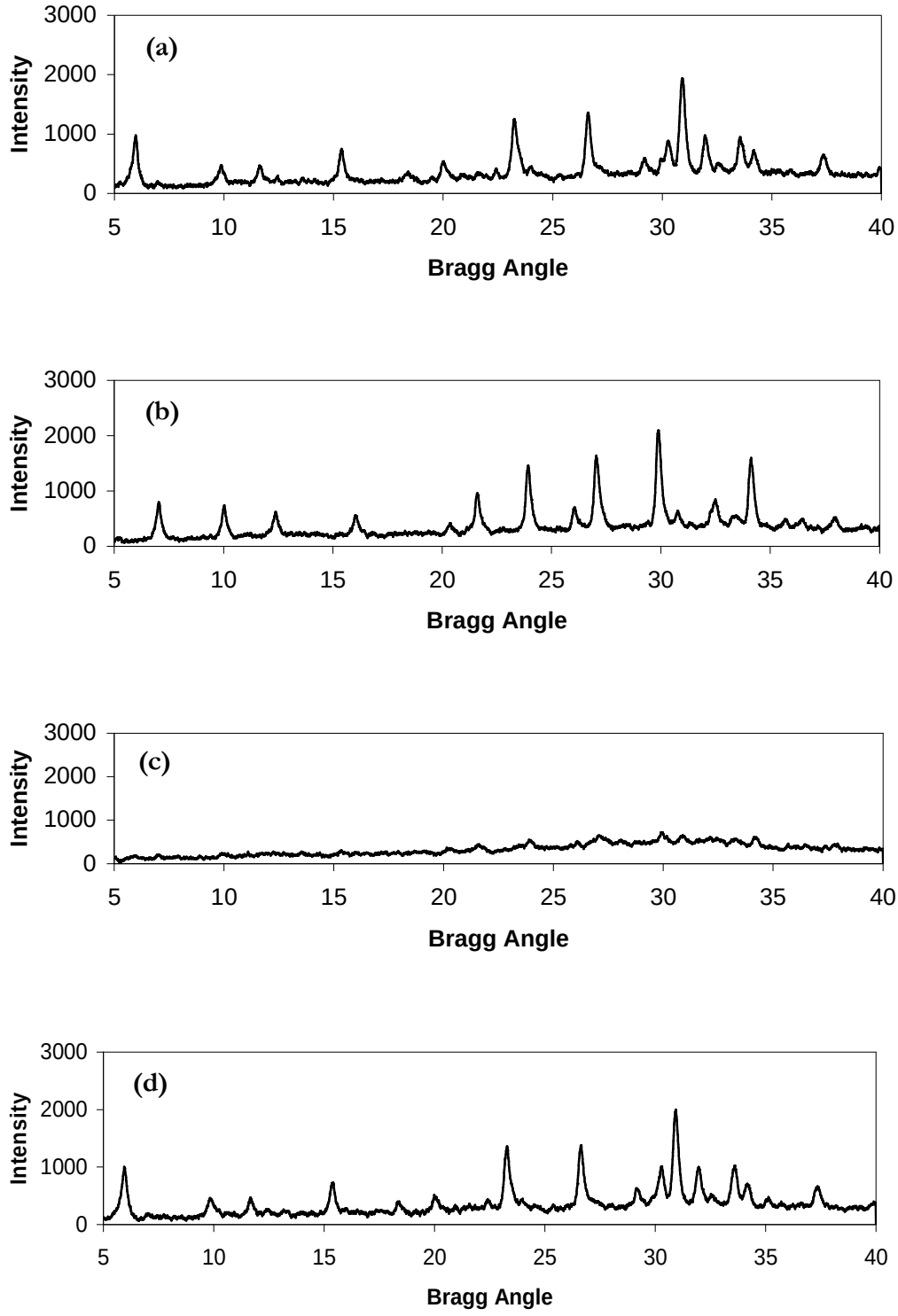

Figure C.15. XRD pattern of (a) CG27C4 (XRD 6535), (b) CG27D2 (XRD 6537), (c) CG29G2 (XRD 6538) and (d) CG27H2 (XRD 6536)

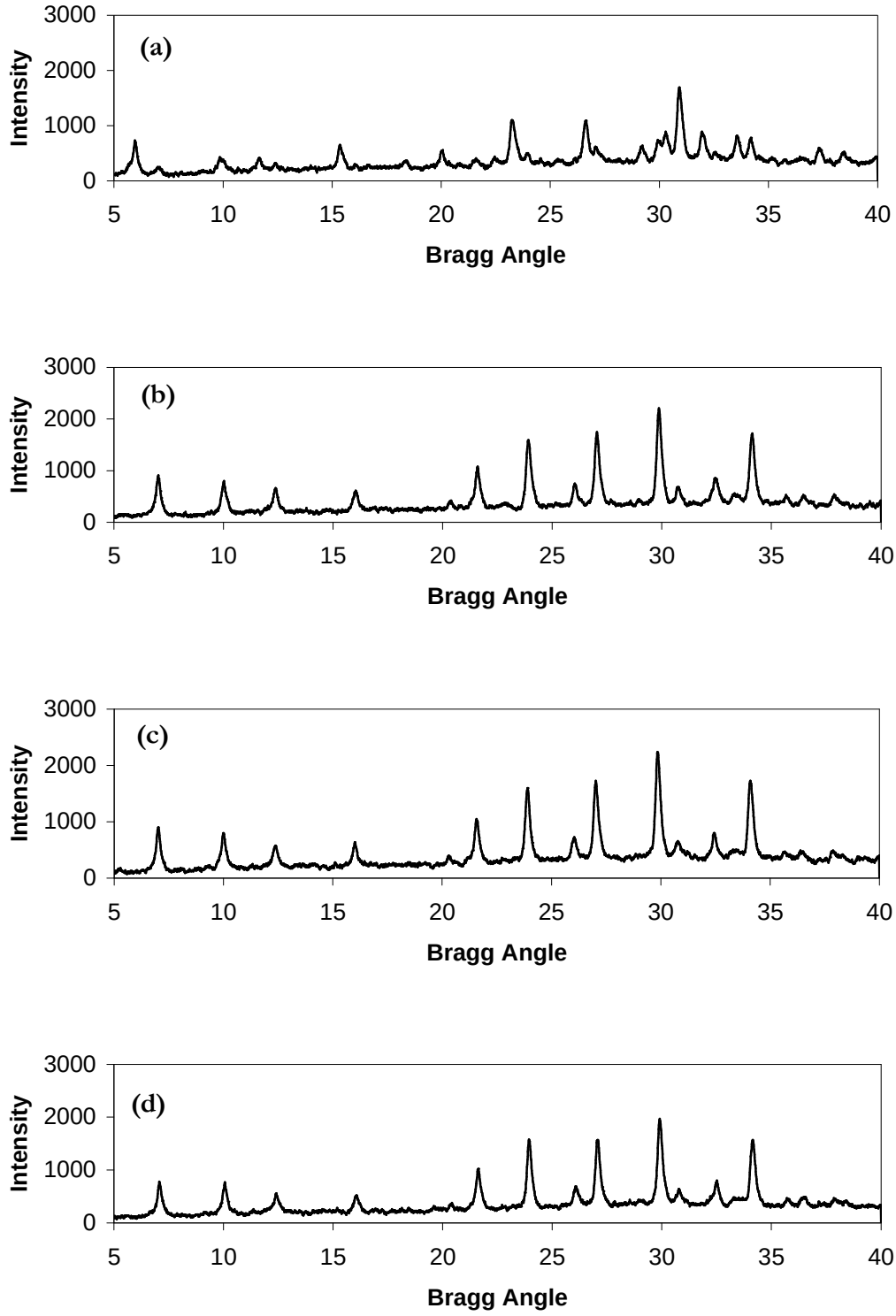

Figure C.16. XRD pattern of (a) CG31C5 (XRD 6558), (b) CG31D3 (XRD 6560), (c) CG31E1 (XRD 6559) and (d) CG33M1 (XRD 6639)

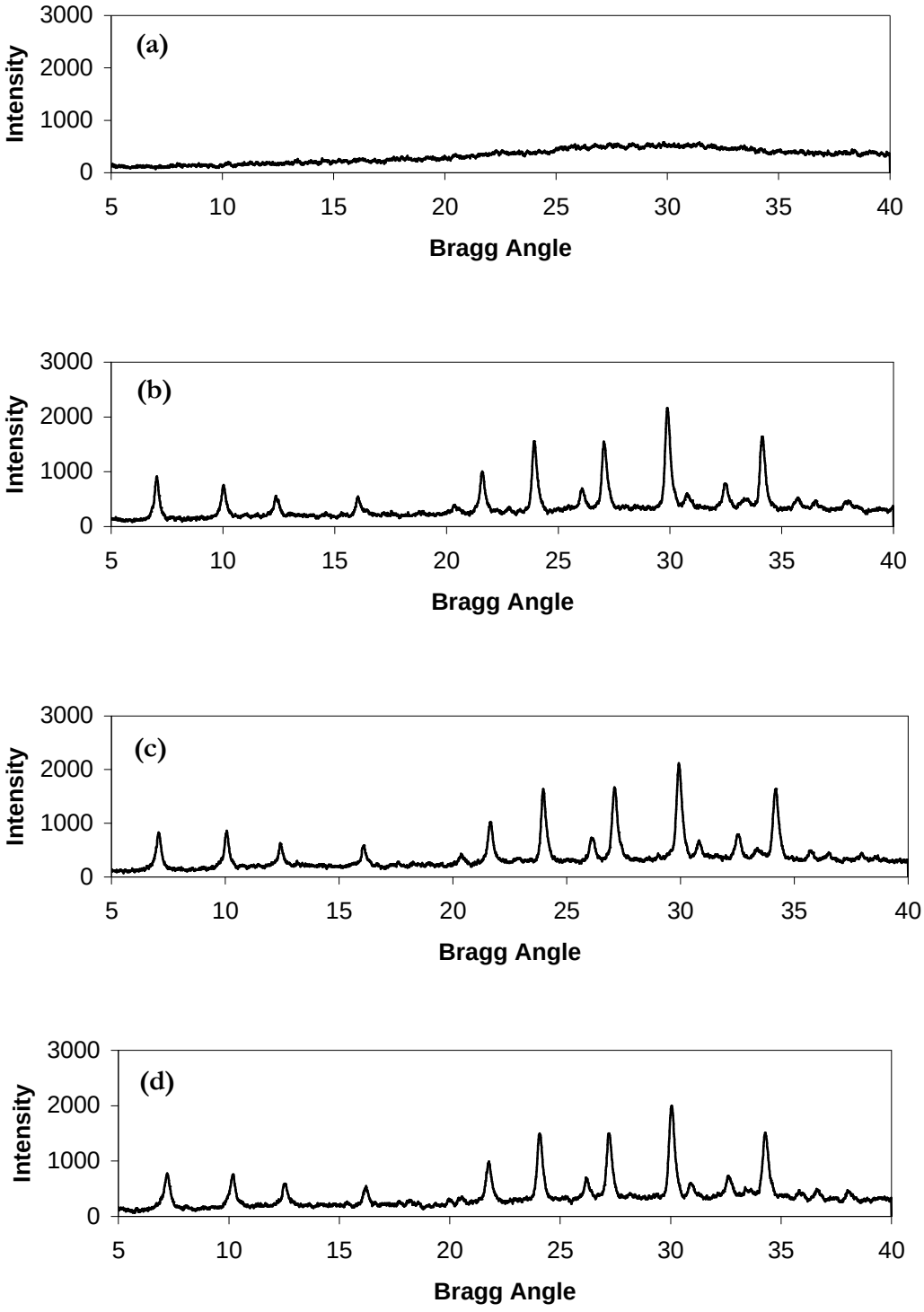

Figure C.17. XRD pattern of (a) CG33N1 (XRD 6640), (b) CG31K1 (XRD 6563), (c) CG31I1 (XRD 6564) and (d) CG33J1 (XRD 6567)

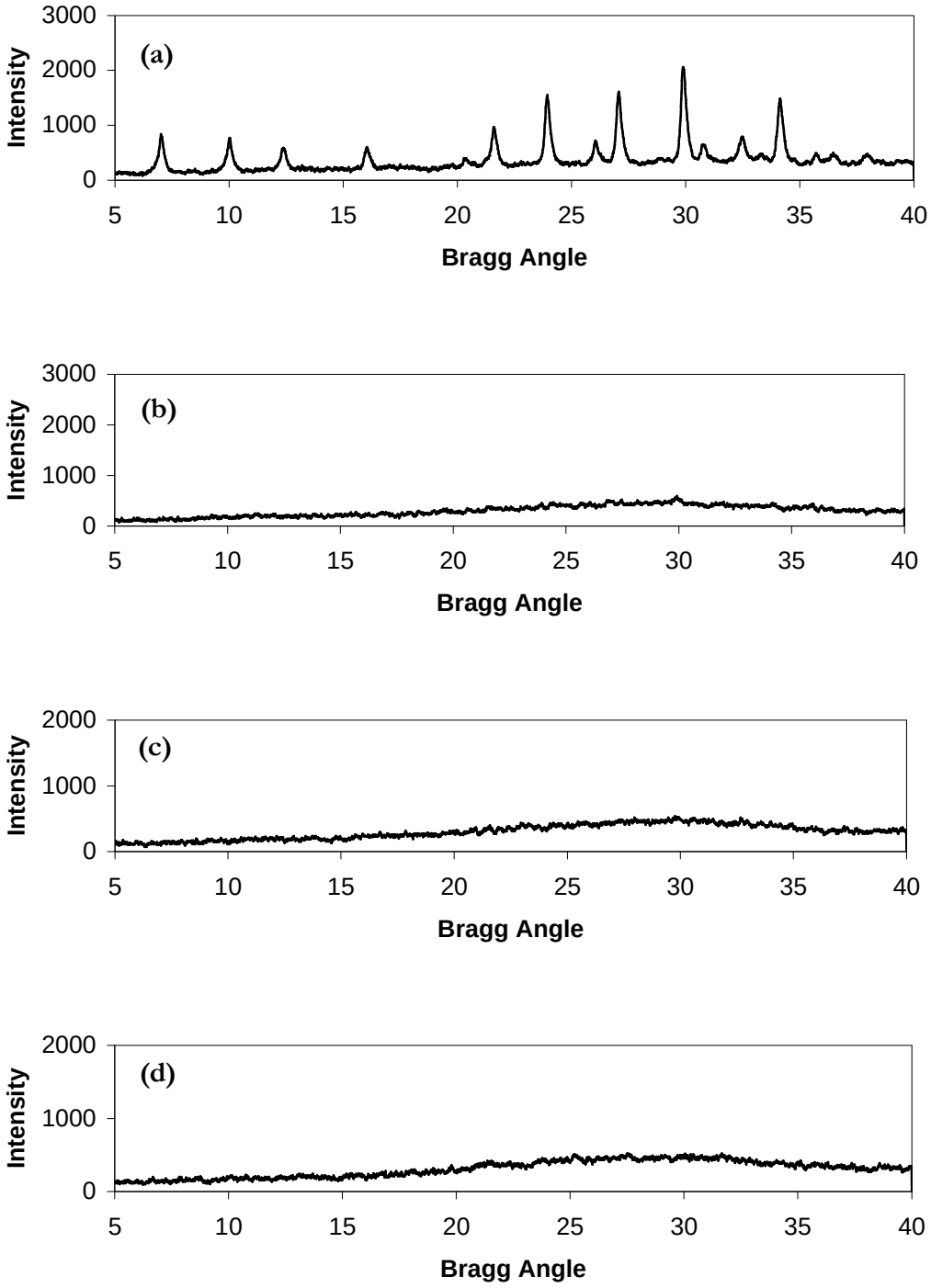

Figure C.18. XRD pattern of (a) CG33L1 (XRD 6568), (b) CG34P1 (XRD 6676), (c) CG34P2 (XRD 6677) and (d) CG34P3 (XRD 6669)

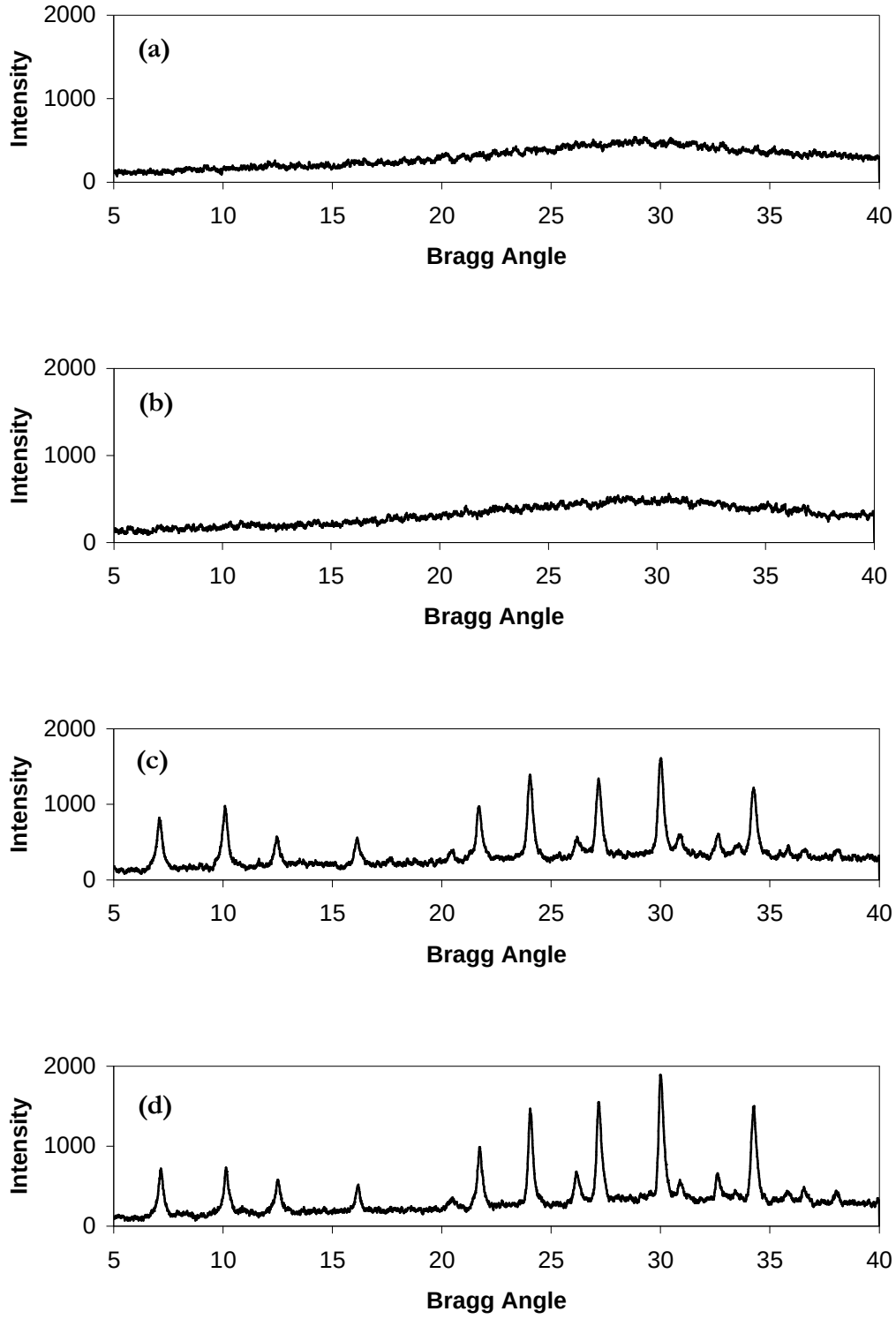

Figure C.19. XRD pattern of (a) CG34P4 (XRD 6666), (b) CG34P5 (XRD 6678), (c) CG34P6 (XRD 6708) and (d) CG34P7 (XRD 6709)

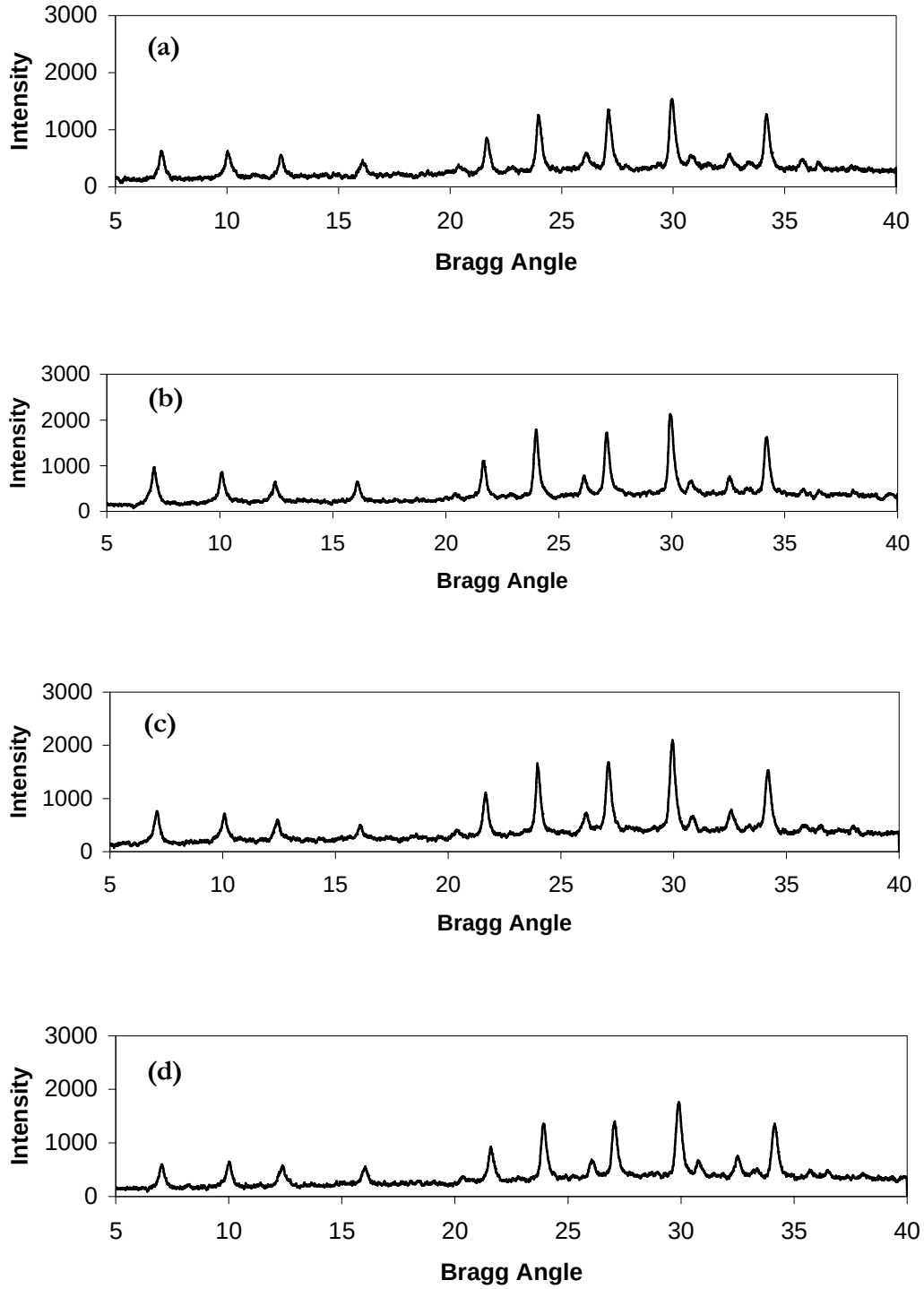

Figure C.20. XRD pattern of (a) CG34P8 (XRD 6710), (b) CG34P9 (XRD 6737), (c) CG34P10 (XRD 6738) and (d) CG34P11 (XRD 6739)

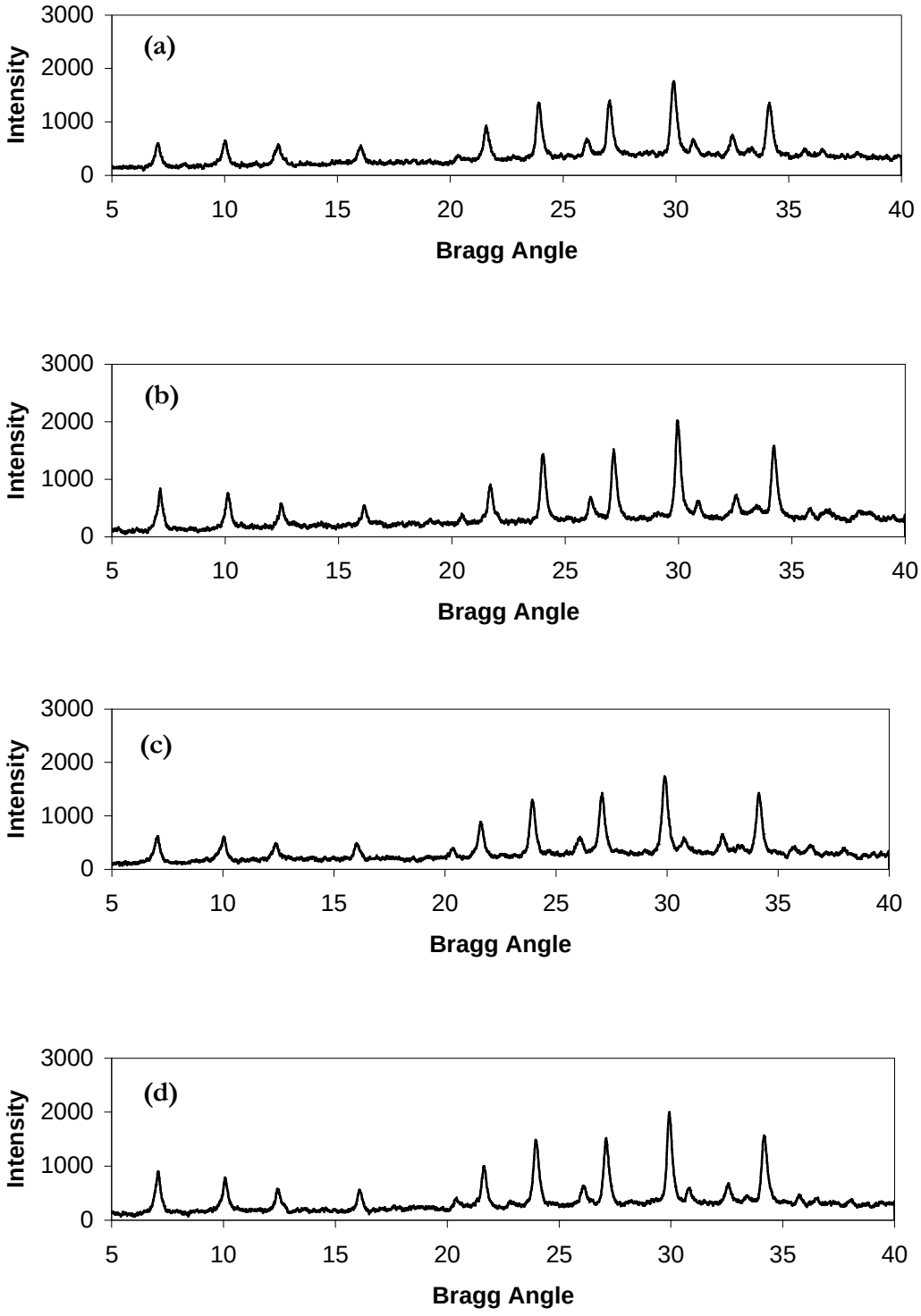

Figure C.21. XRD pattern of (a) CG34P12 (XRD 6740), (b) CG34P13 (XRD 6830), (c) CG34P14 (XRD 6765) and (d) CG34P15 (XRD 6766)

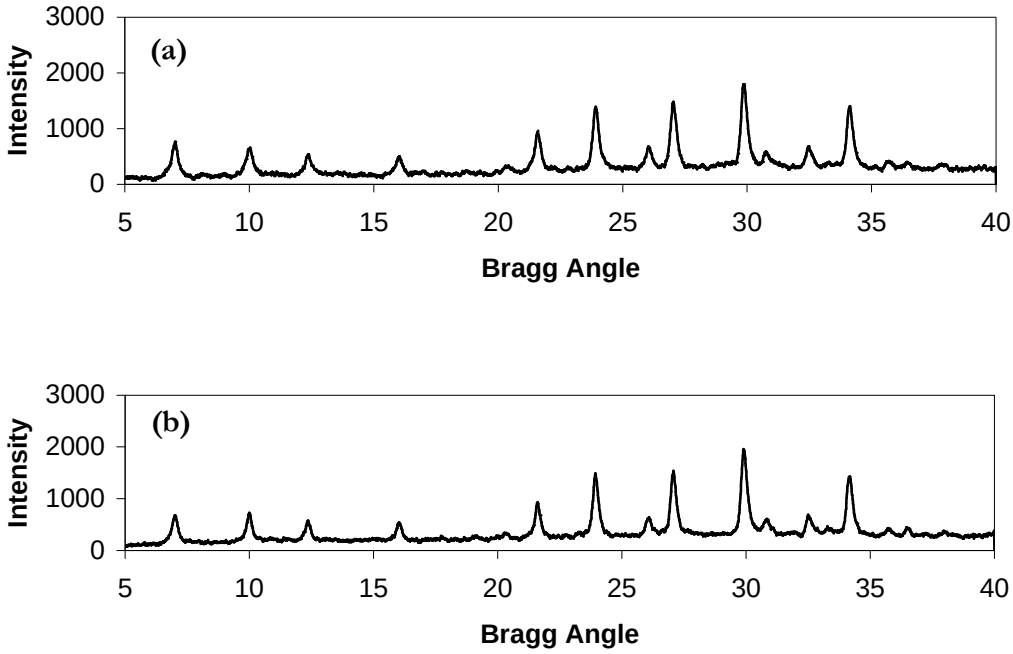

Figure C.22. XRD pattern of (a) CG34P16 (XRD 6767), (b) CG34P17 (XRD 6768)

APPENDIX D

SEM IMAGES

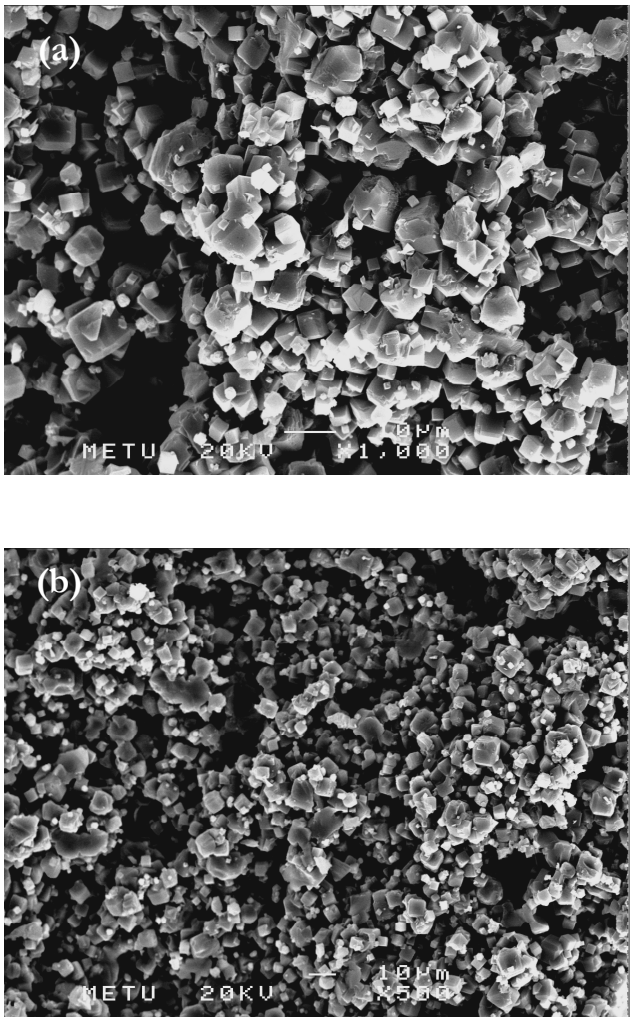

Figure D.1. SEM image of (a) CG6A inner cross section (X1000) and (b) CG6A inner cross section (X500)

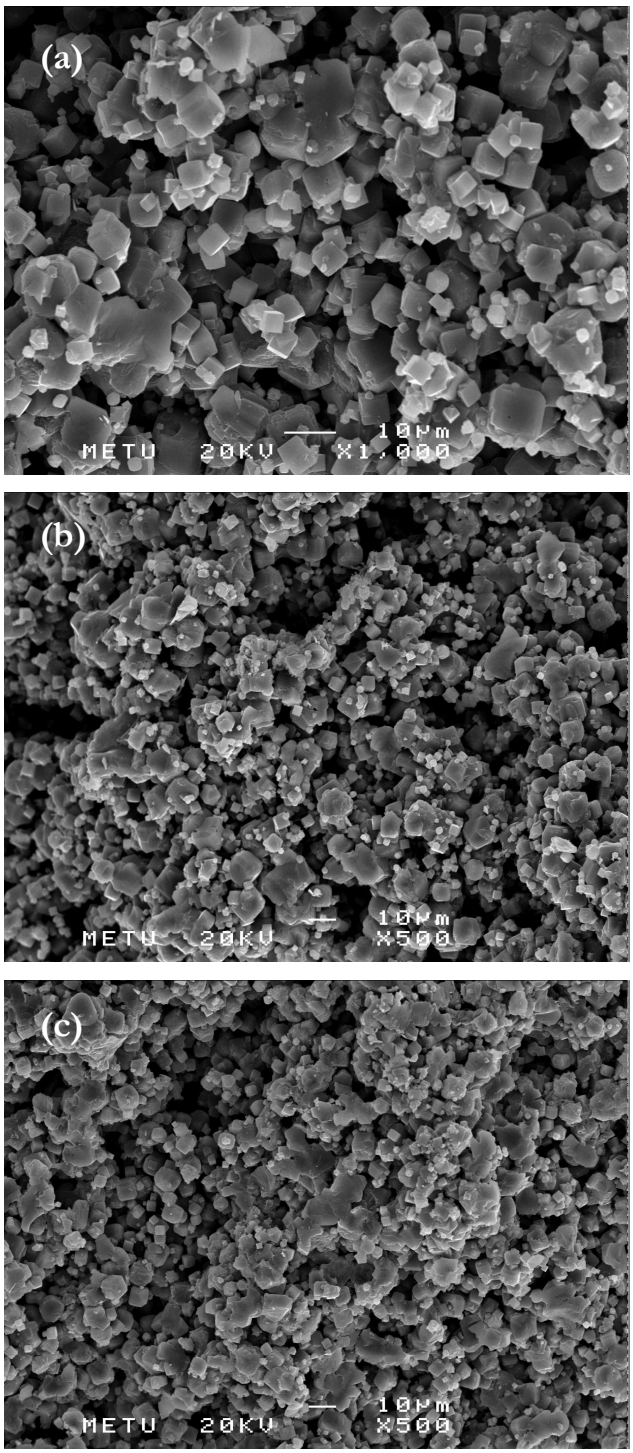

Figure D.2. SEM image of (a) CG6A middle cross section (X 1000), (b) CG6A middle cross section (X 500) and (c) CG6C outer cross section (X 500)

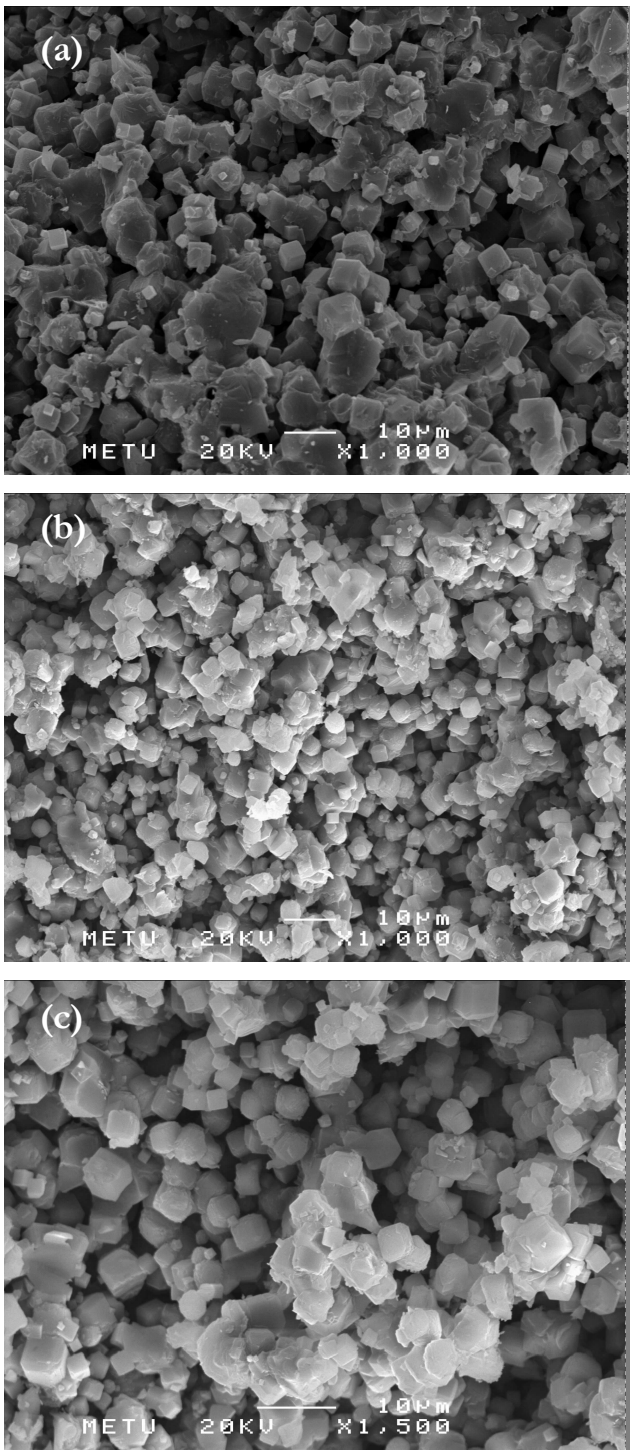

Figure D.3. SEM image of (a)CG6A outer cross section (X 1000), (b) CG14F1 inner cross section (X 1000) and (c) CG614F1 inner cross section (X 1500)

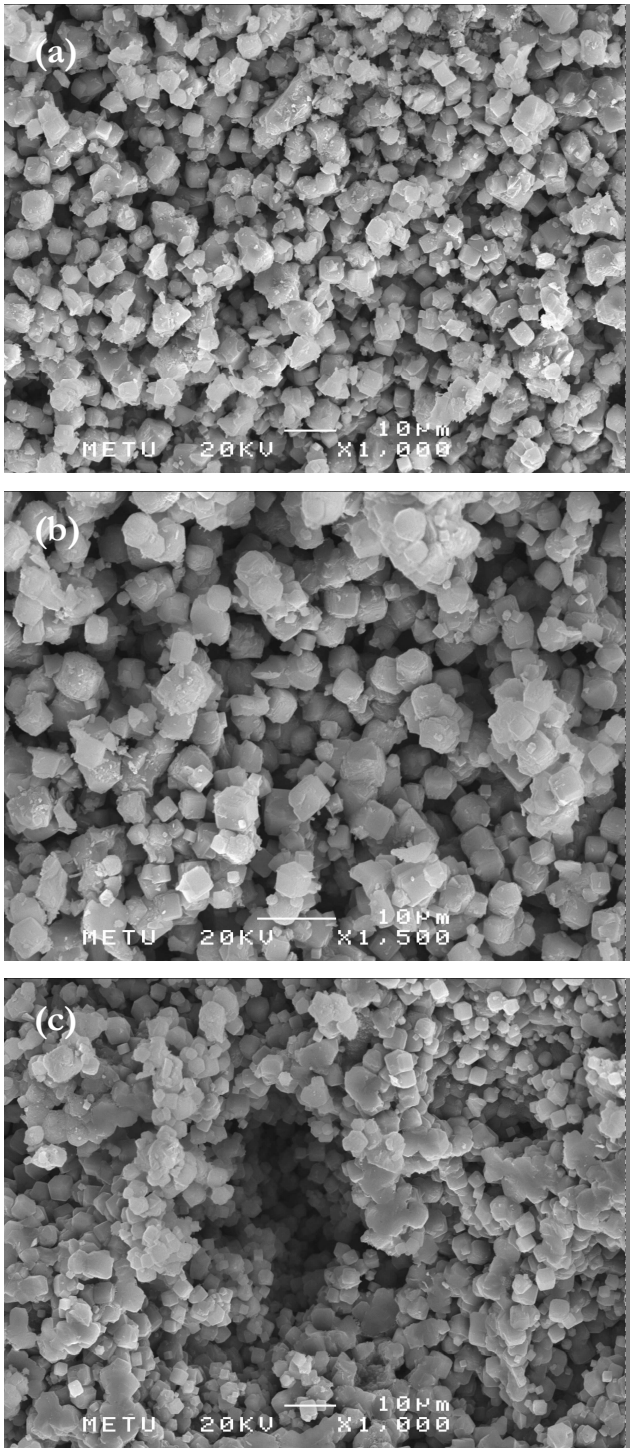

Figure D.4. SEM image of (a) CG14F1 middle cross section (X 51000), (b) CG14F1 middle cross section (X 1500) and (c) CG14F1 outer cross section (X 500)

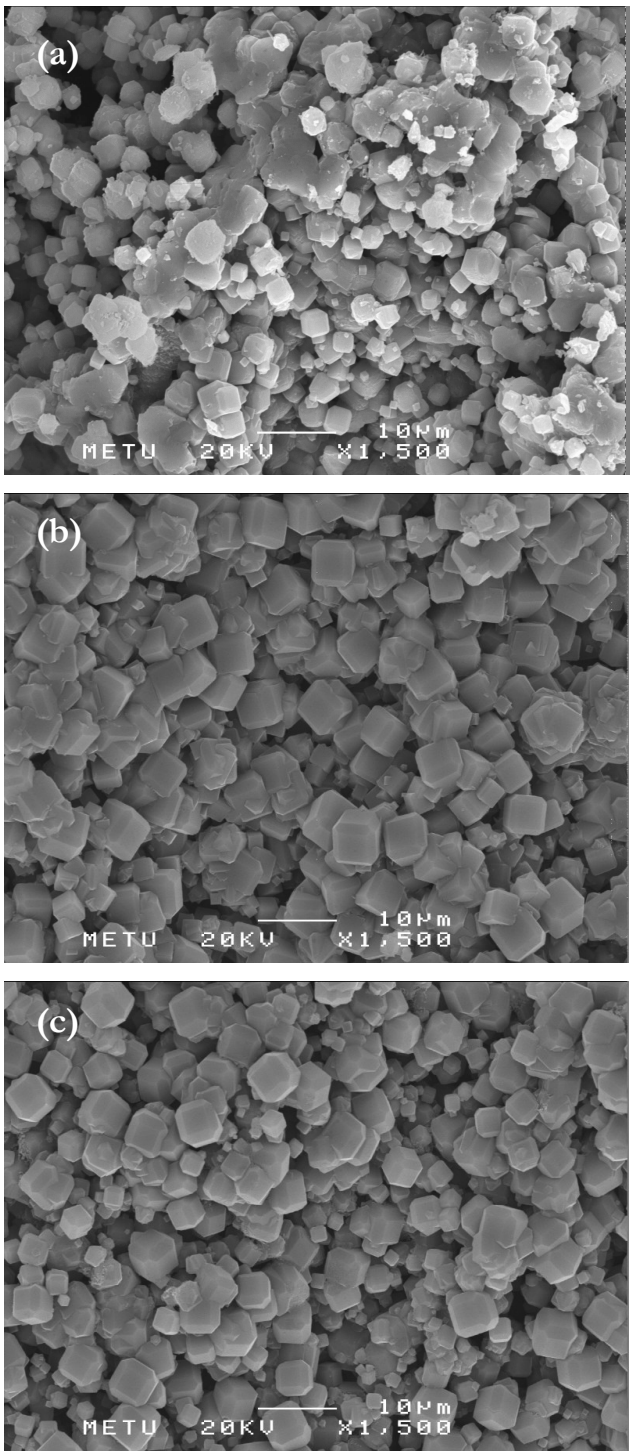

Figure D.5. SEM image of (a) CG14F1 outer cross section (X 1000), (b) CG14F1 inner surface (X 1500) and (c) CG14F1 outer surface – tilted 60° (X 1500)

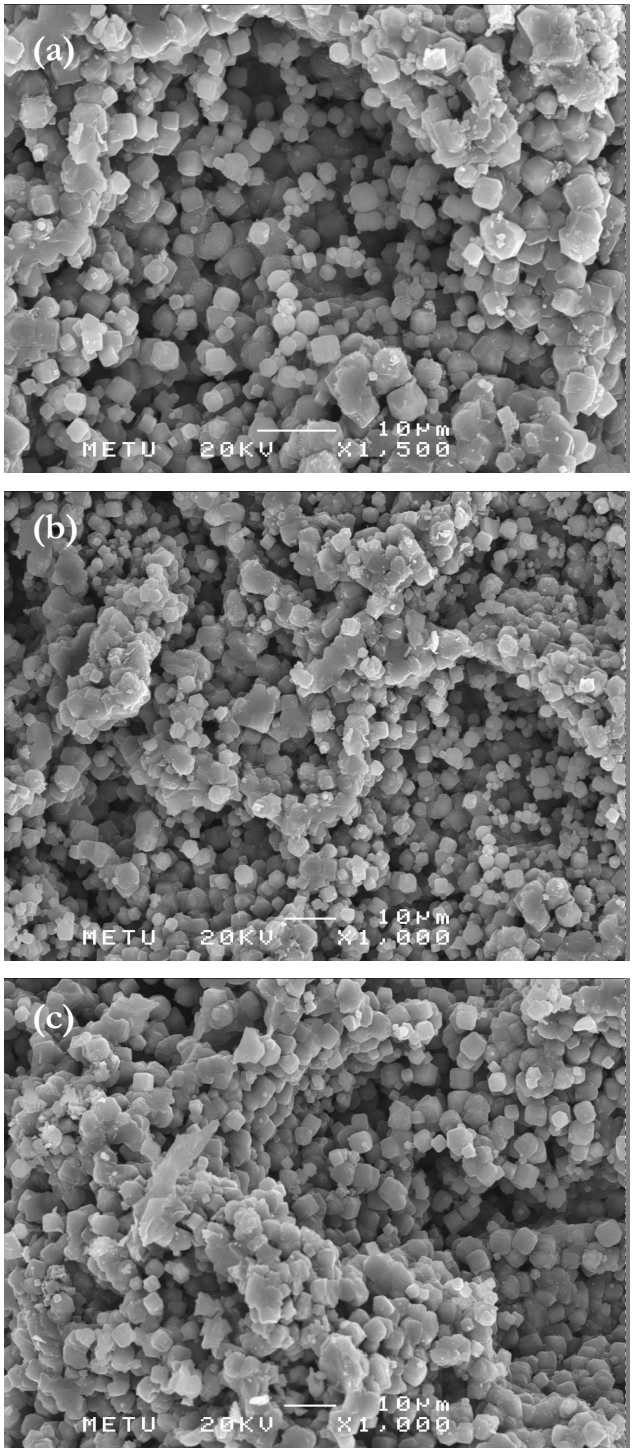

Figure D.6. SEM image of (a) CG15F inner cross section (X 1500), (b) CG15F inner cross section (X 1000) and (c) CG15F middle cross section (X 1000)

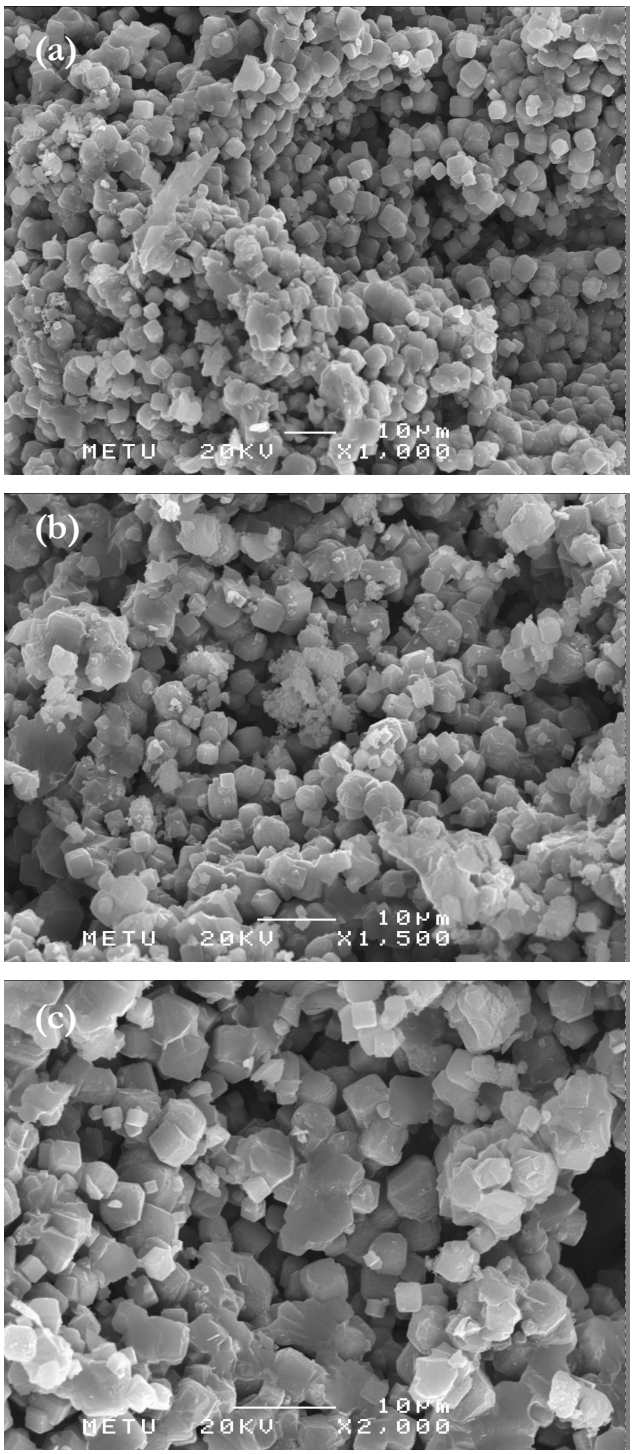

Figure D.7. SEM image of (a) CG15F middle cross section (X 1000), (b) CG15F outer cross section (X 1500) and (c) CG15F outer cross section (X 2000)

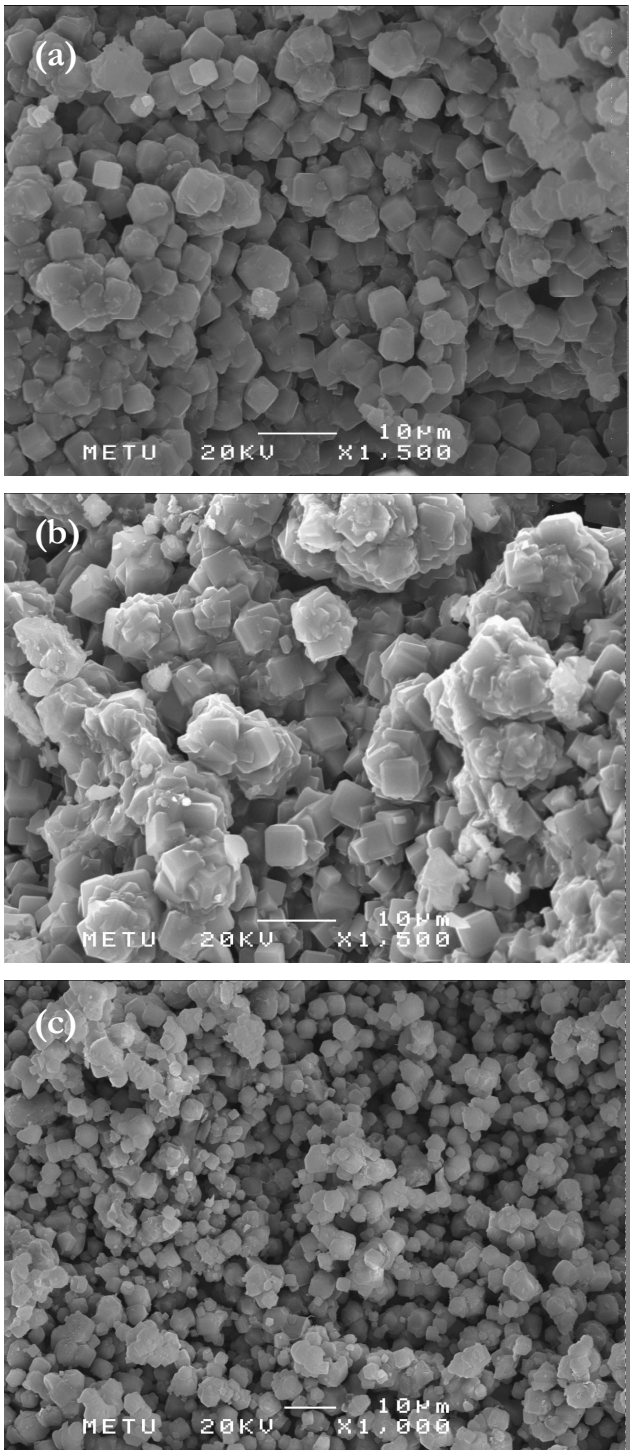

Figure D.8. SEM image of (a) CG15F inner surface (X 1500), (b) CG15F outer surface – tilted 60° (X 1500) and (c) CG16F inner cross section (X 1000)

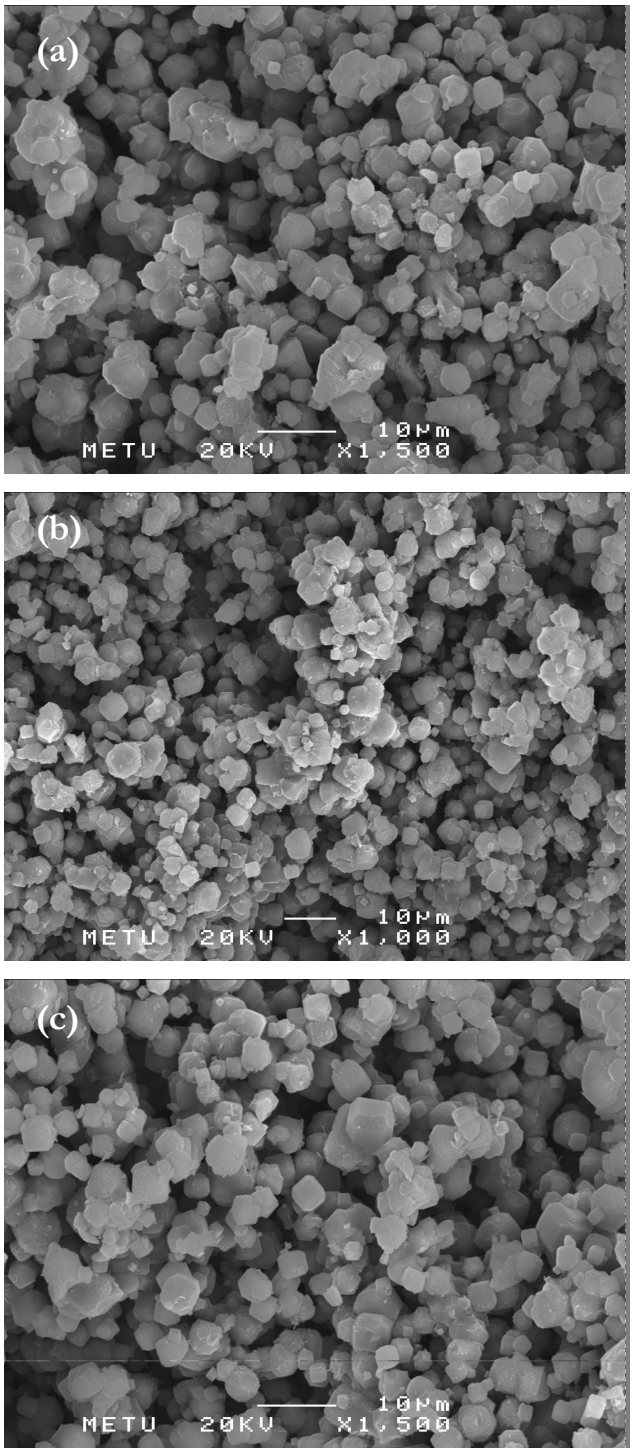

Figure D.9. SEM image of (a) CG16F inner cross section (X 1500), (b) CG16F middle cross section (X 1500) and (c) CG16F middle cross section (X 1000)

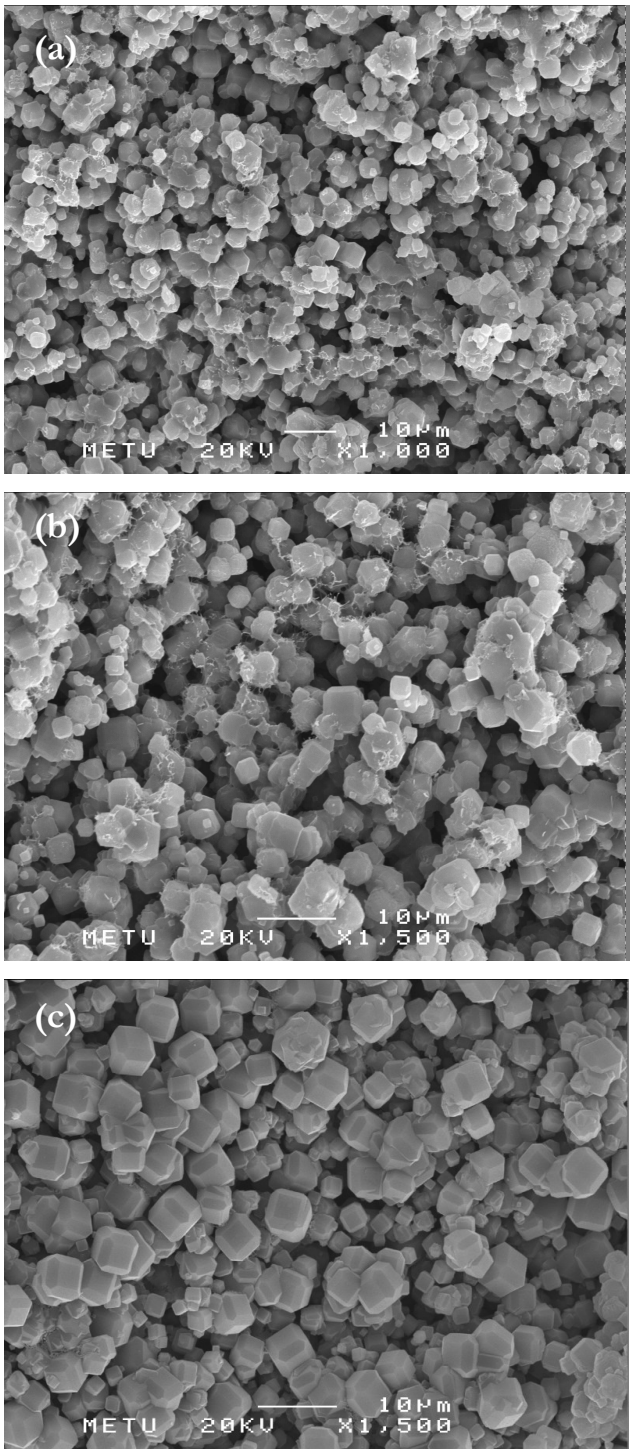

Figure D.10. SEM image of (a) CG16F outer cross section (X 1000), (b) CG16F outer cross section (X 1500) and (c) CG16F inner surface (X 1500)

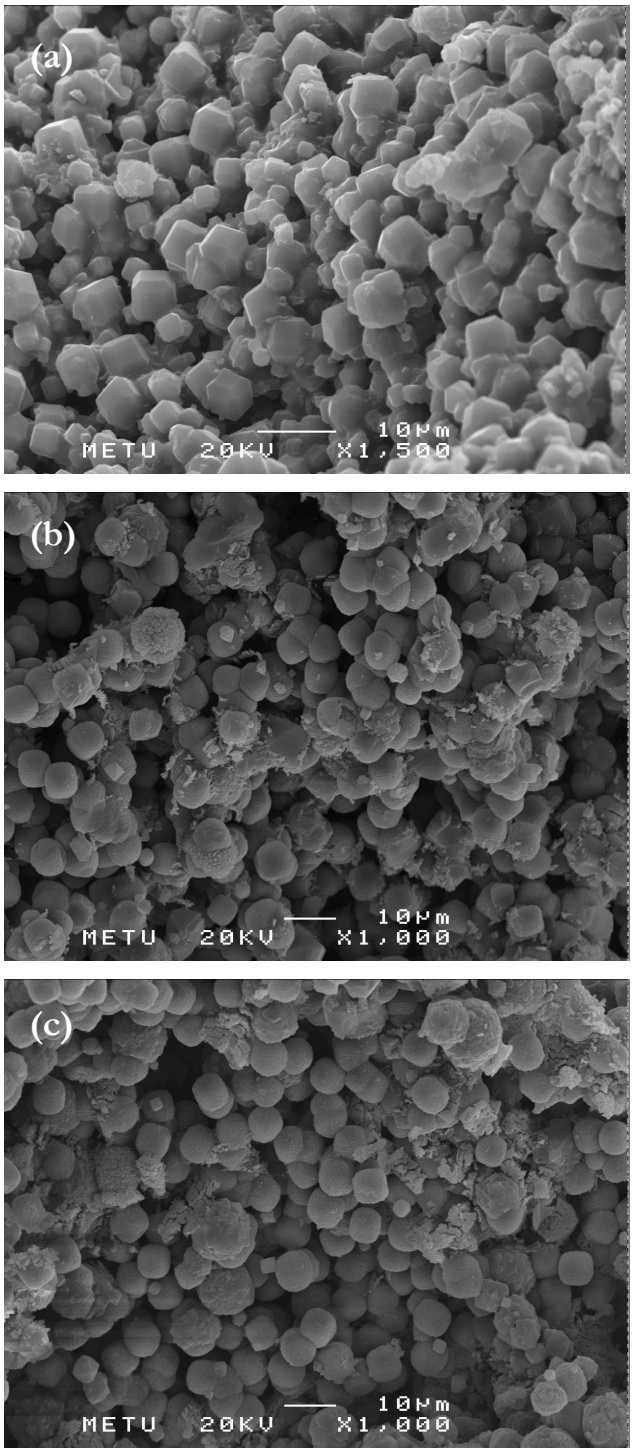

Figure D.11. SEM image of (a) CG16F outer surface – tilted 60° (X 1000), (b) CG6C inner cross section (X 1000) and (c) CG6C middle cross section (X 1000)

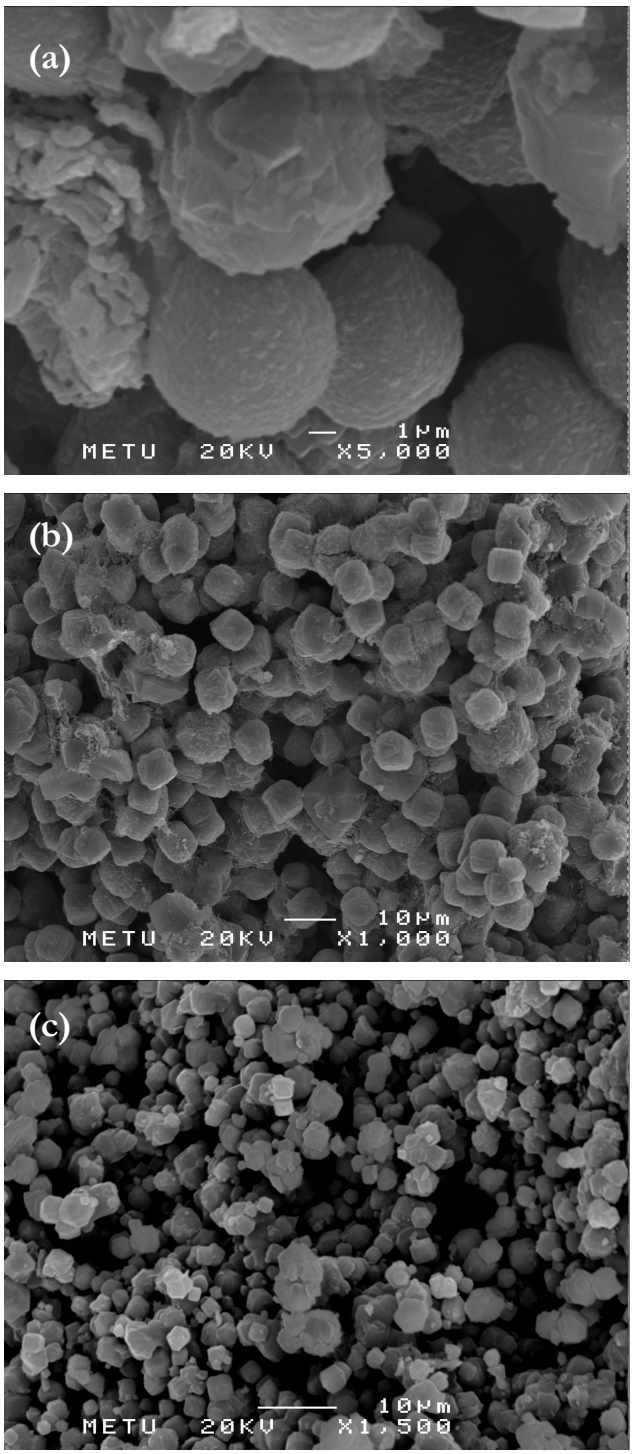

Figure D.12. SEM image of (a) CG6C middle cross section (X 5000), (b) CG6C outer cross section (X 1500) and (c) CG31E1 inner cross section (X 1500)

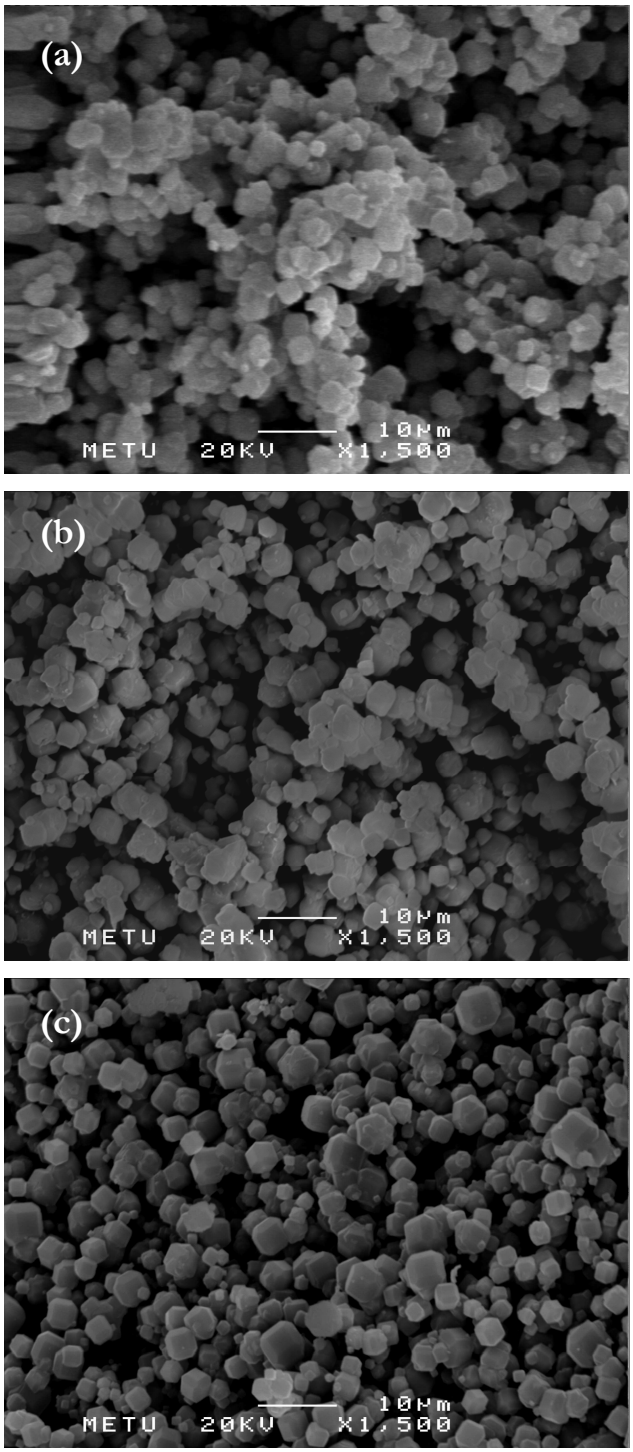

Figure D.13. SEM image of (a) CG31E1 middle cross section (X 1500), (b) CG31E1 outer cross section (X 1500) and (c) CG31E1 inner surface (X 1500)

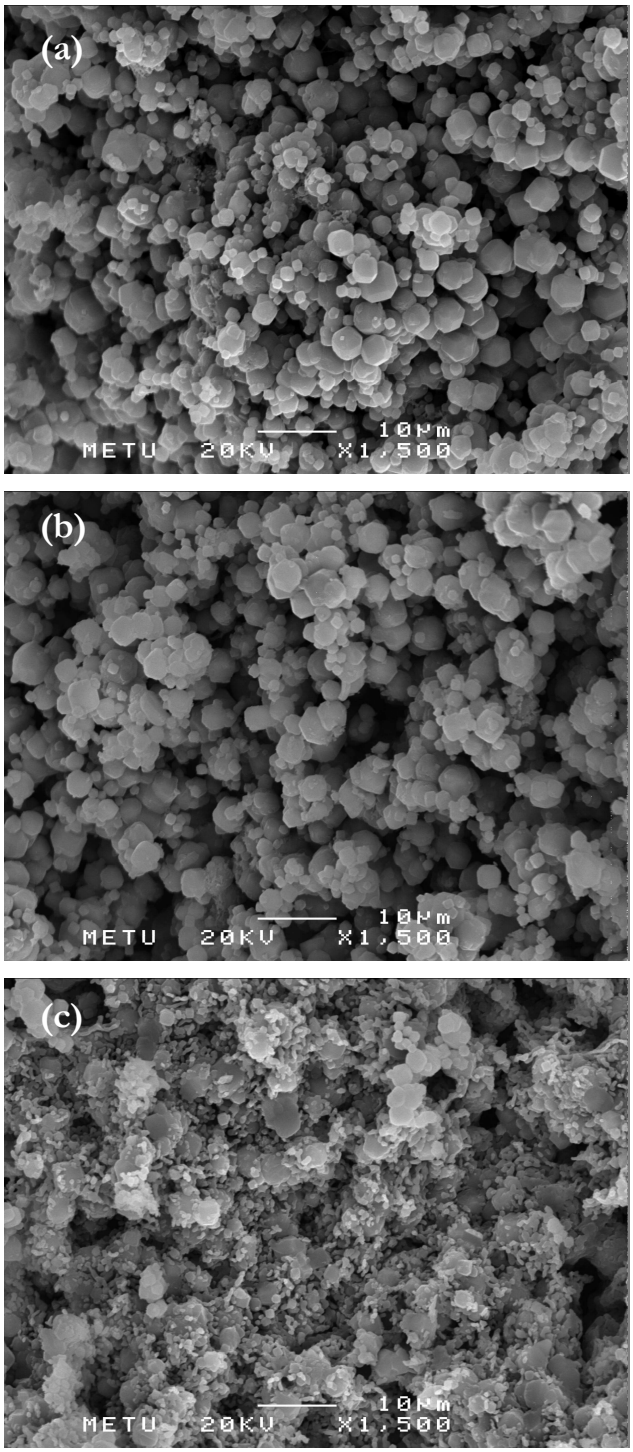

Figure D.14. SEM image of (a) CG33M1 inner cross section (X 1500), (b) CG33M1 middle cross section (X 1500) and (c) CG33M1 outer cross section (X 1500)

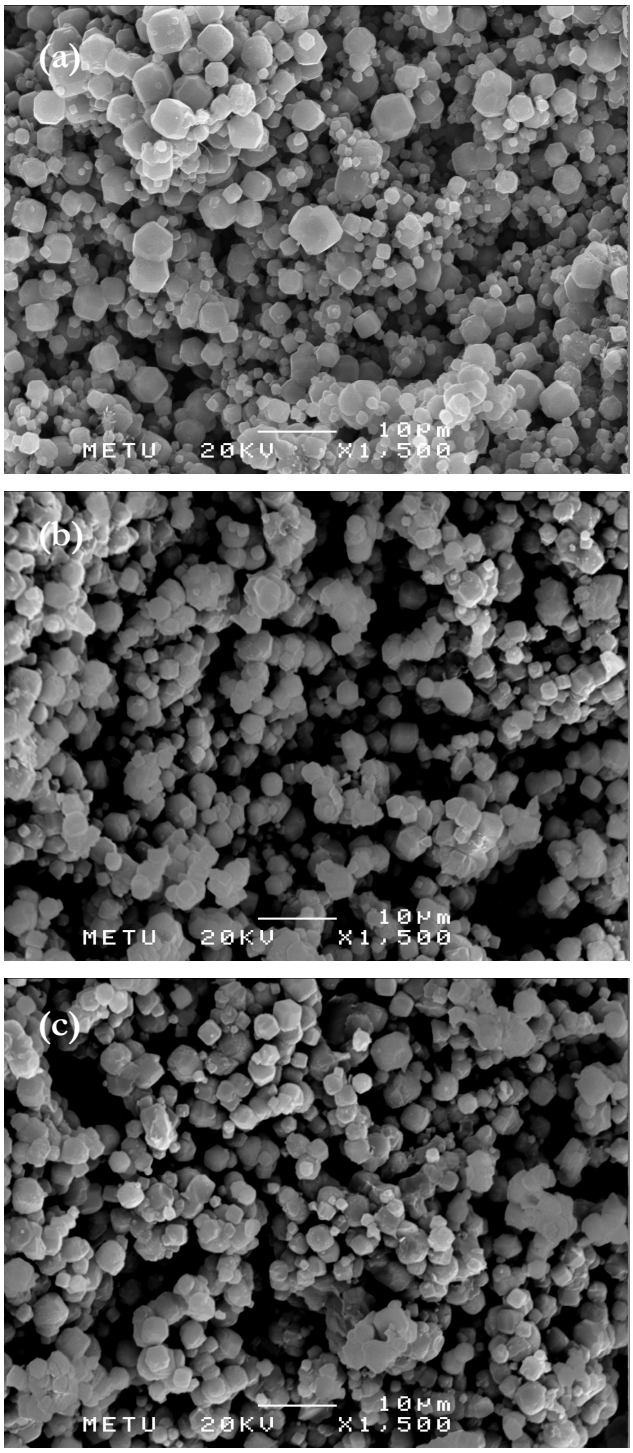

Figure D.15. SEM image of (a) CG33M1 inner surface (X 1500), (b) CG29D1 inner cross section (X 1500) and (c) CG29D1 middle cross section (X 1500)

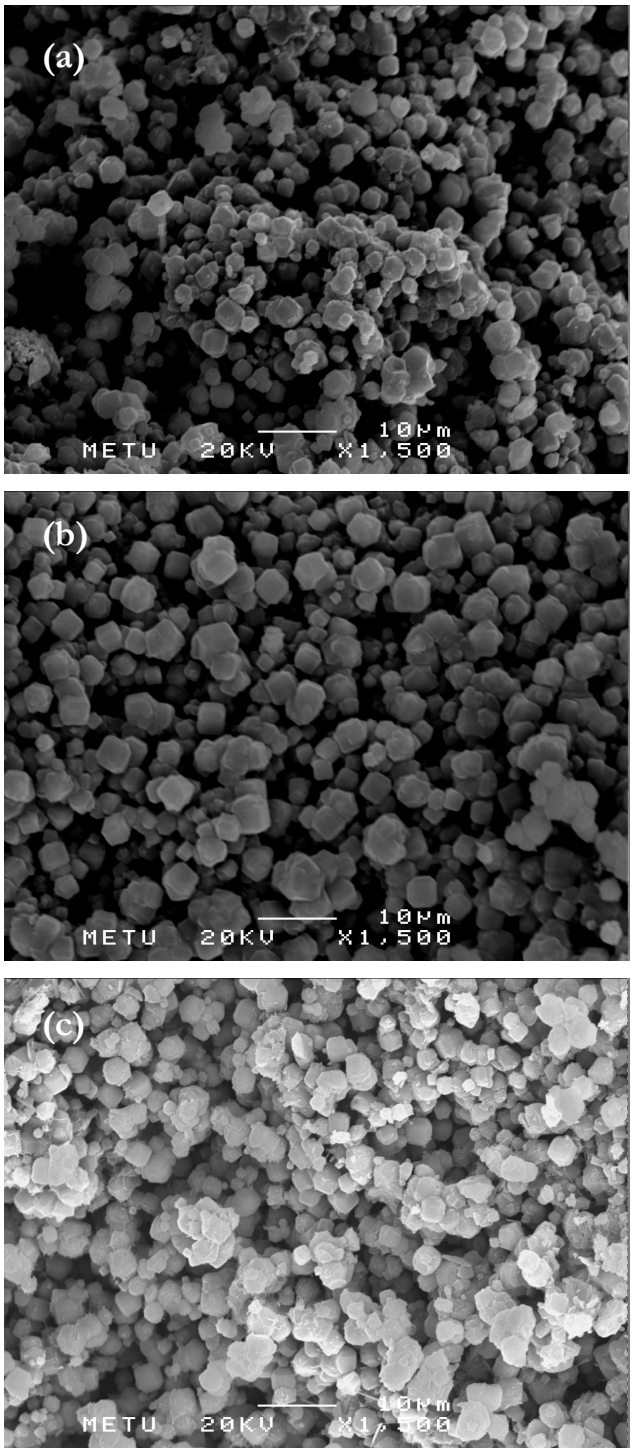

Figure D.16. SEM image of (a) CG29D1 outer surface (X 1500), (b) CG29D1 inner surface (X 1500) and (c) CG31I1 inner cross section (X 1500)

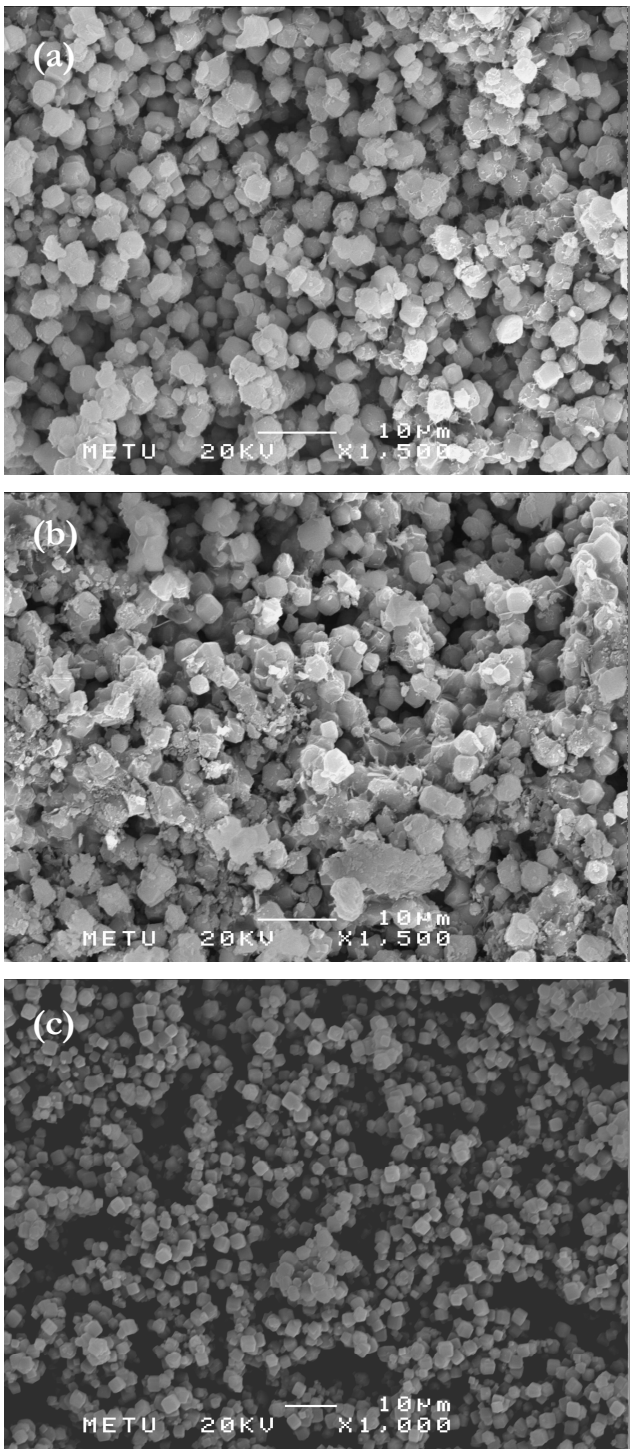

Figure D.17. SEM image of (a) CG31I1 middle cross section (X 1500), (b) CG31I1 outer cross section (X 1500) and (c) CG31I1 inner surface (X 1500)

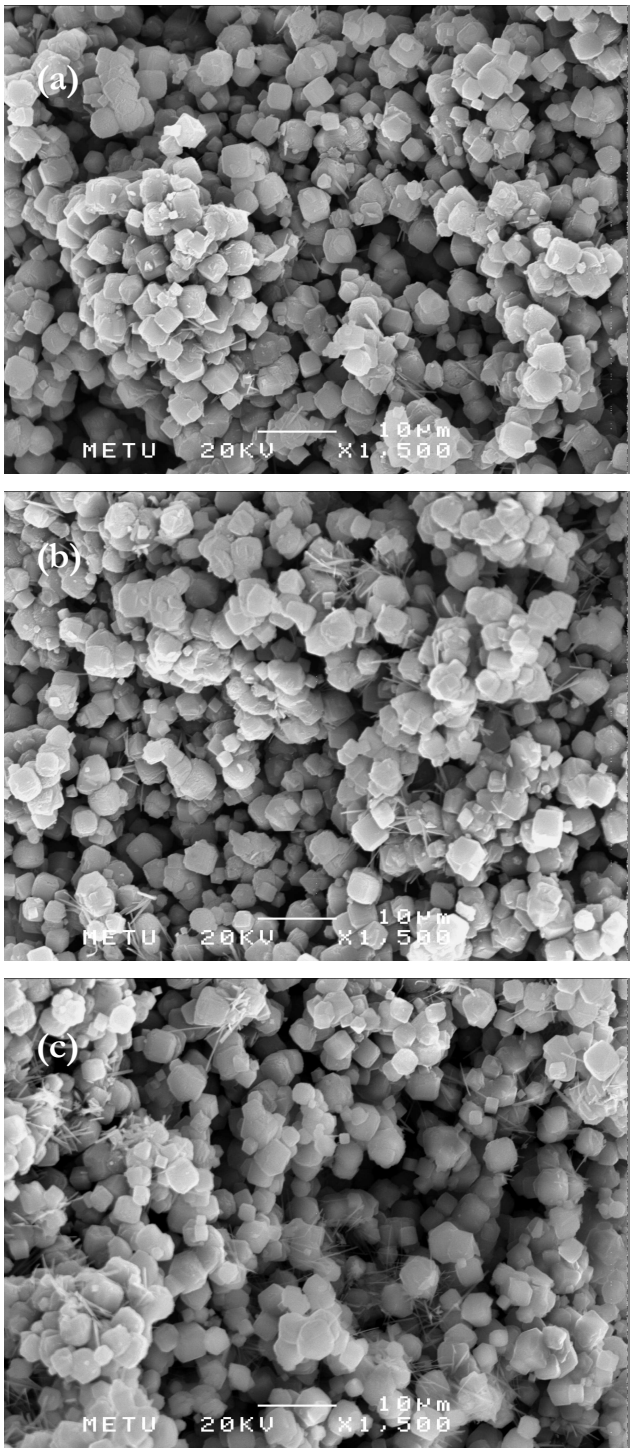

Figure D.18. SEM image of (a) CG31J1 inner cross section (X 1500), (b) CG31J1 middle cross section (X 1500) and (c) CG31J1 outer surface (X 1500)

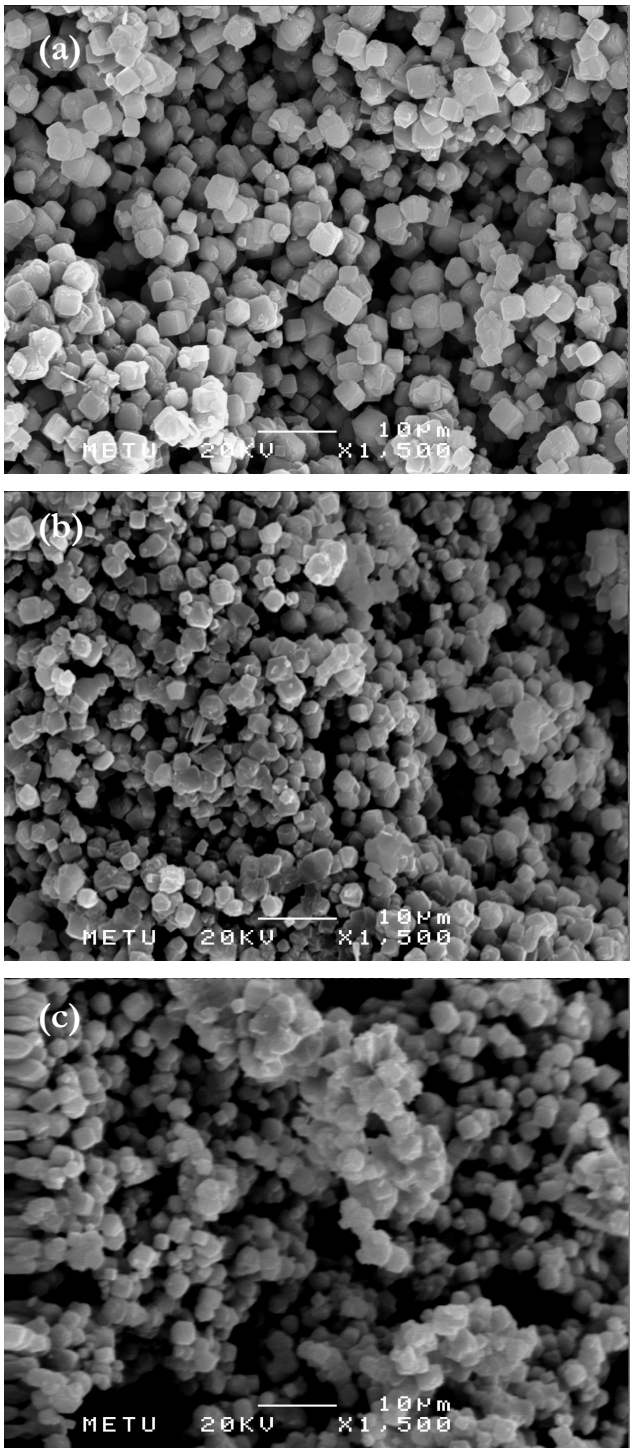

Figure D.19. SEM image of (a) CG31J1 inner surface (X 1500), (b) CG33L1 inner cross section (X 1500) and (c) CG33L1 middle cross section (X 1500)

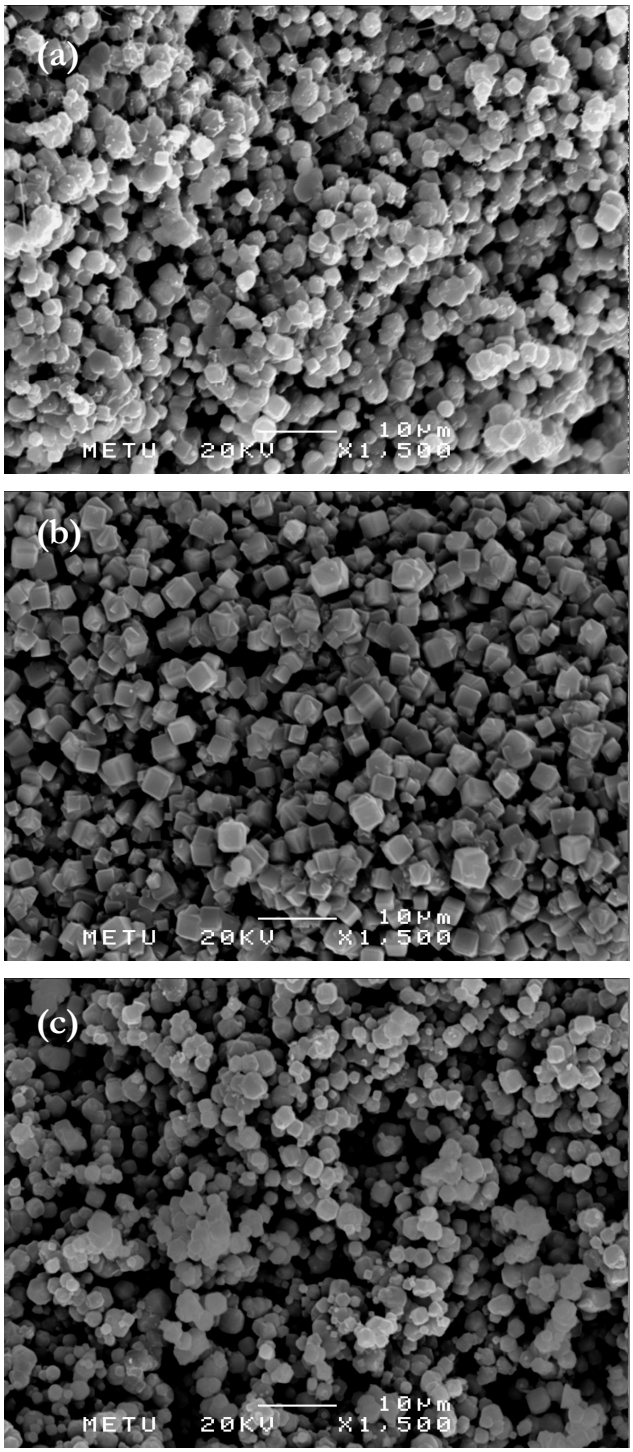

Figure D.20. SEM image of (a) CG33L1 outer cross section (X 1500), (b) CG33L1 inner surface (X 1500) and (c) CG33K1 inner cross section (X 1500)

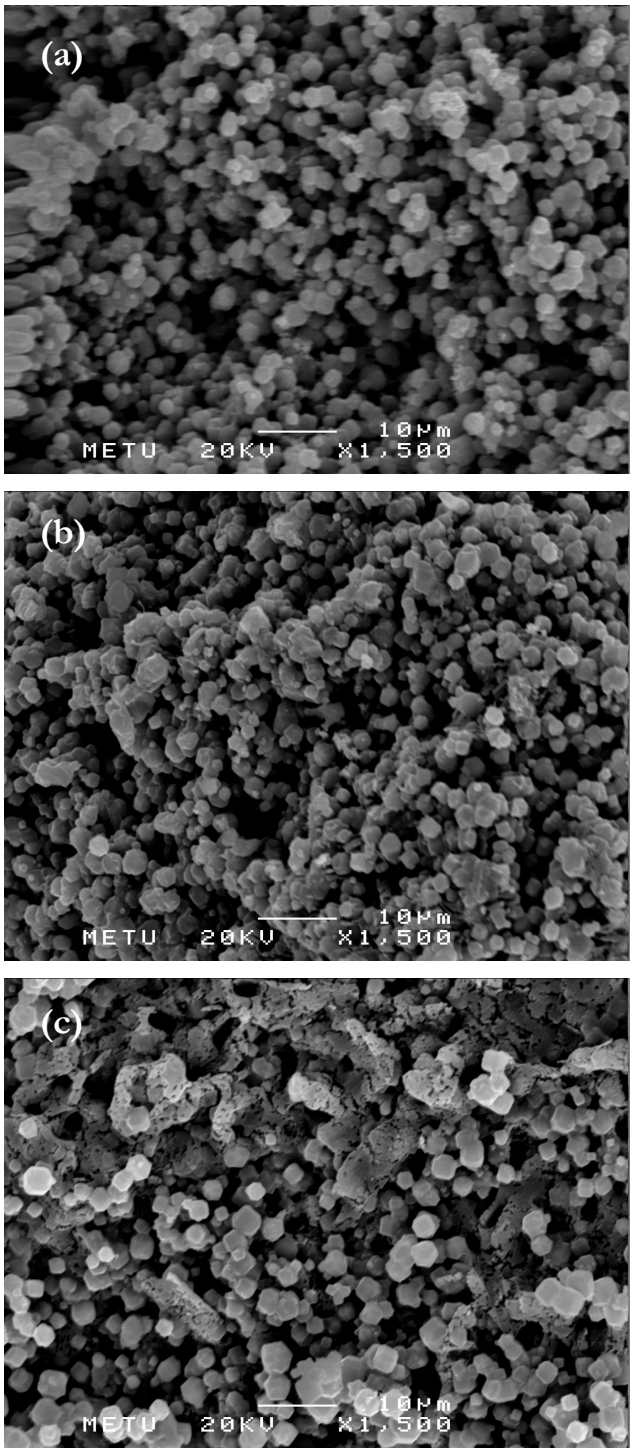

Figure D.21. SEM image of (a) CG33K1 middle cross section (X 1500), (b) CG33K1 outer cross section (X 1500) and (c) CG33K1 inner surface (X 1500)

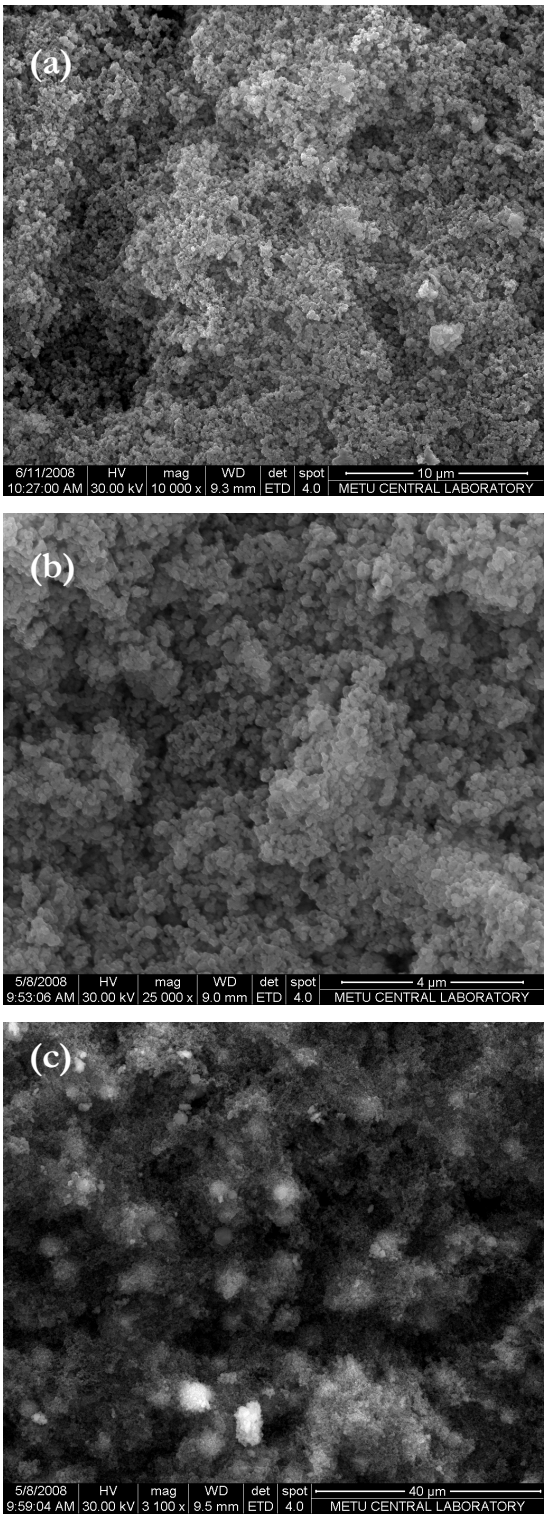

Figure D.22. SEM image of (a) CG42L-4h middle cross section (X 10000), (b) CG42L-5.5h outer cross section (X 25000) and (c) CG42L-6.5h middle cross section (X 3100)

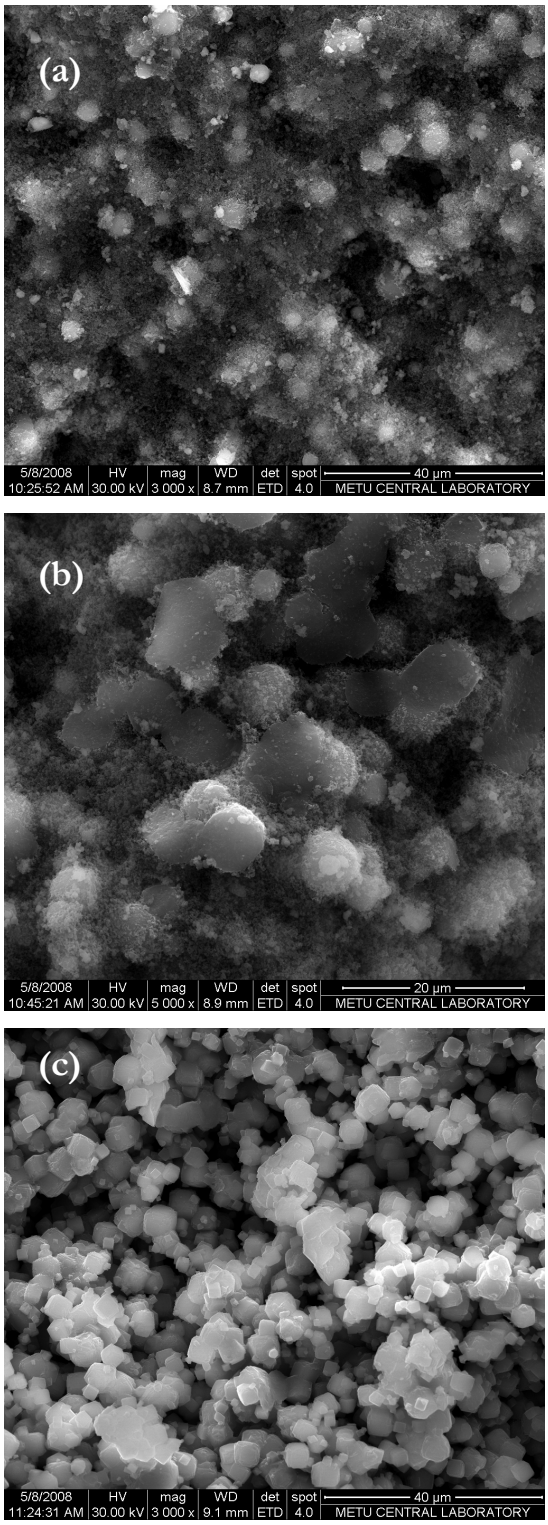

Figure D.23. SEM image of (a) CG42L-7h middle cross section (X 3000), (b) CG42L-8h outer cross section (X 5000) and (c) CG42L-9h middle cross section (X 3000)

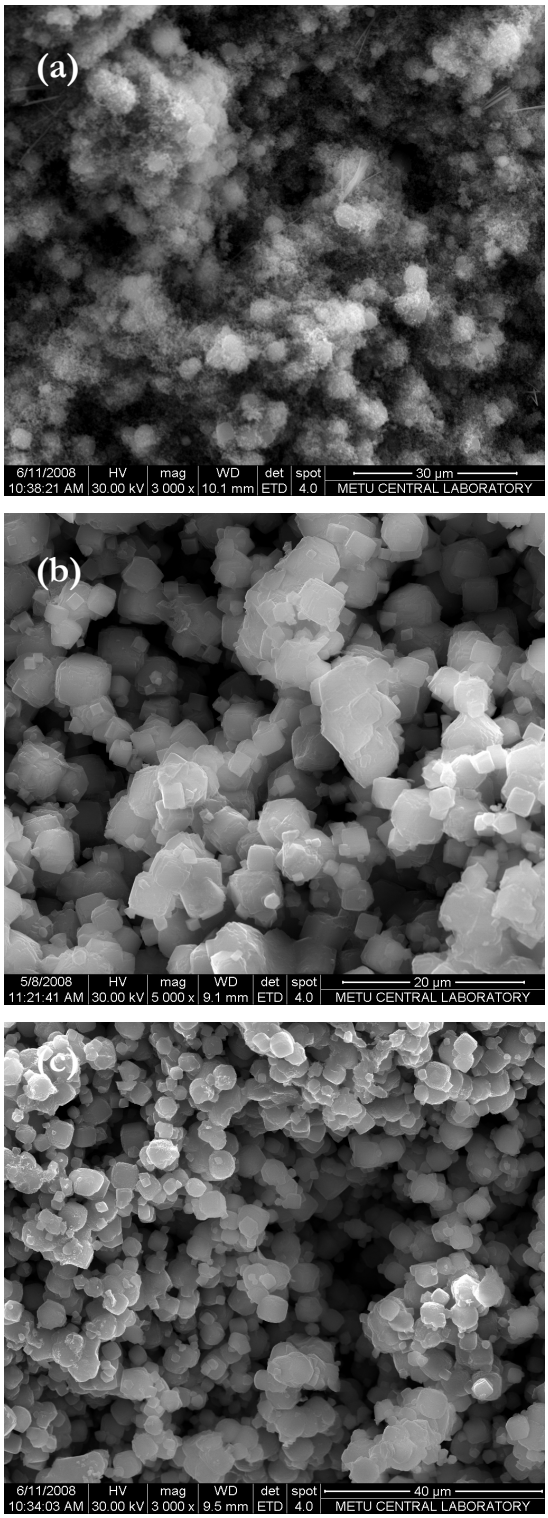

Figure D.24. SEM image of (a) CG42L-12h middle cross section (X 3000), (b) CG42L-48h outer cross section (X 5000) and (c) CG42L-72h middle cross section (X 3000)

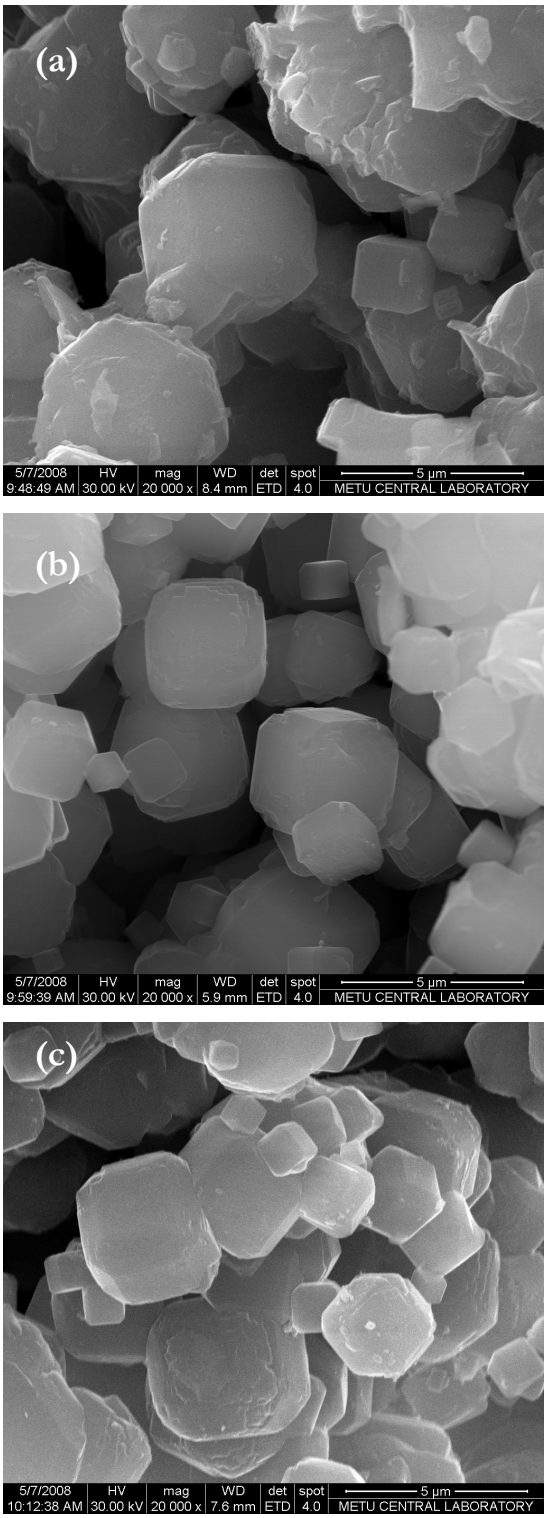

Figure D.25. SEM image of (a) CG40L - 1/3.5 middle cross section (X 20000), (b) CG40L-1/7 middle cross section (X 20000) and (c) CG40L-1/14 middle cross section (X 20000)

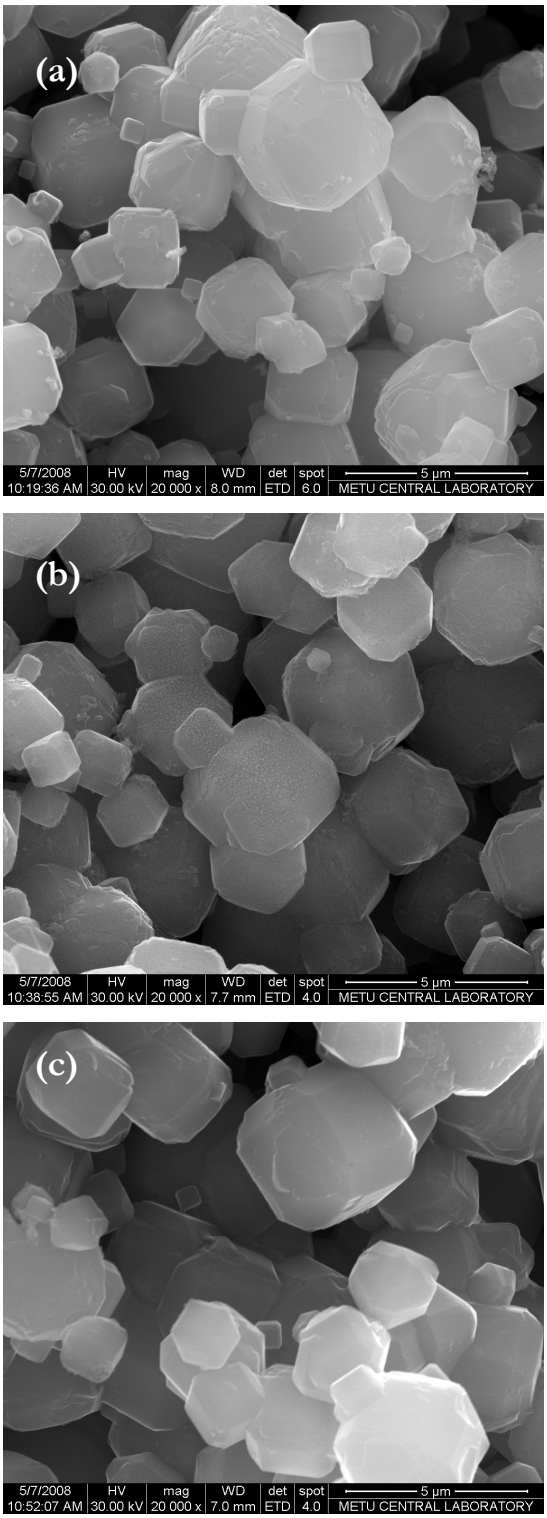

Figure D.26. SEM image of (a) CG40L - 1/28 middle cross section (X 20000), (b) CG40L-1/49 middle cross section (X 20000) and (c) CG40L-1/105 middle cross section (X 20000)

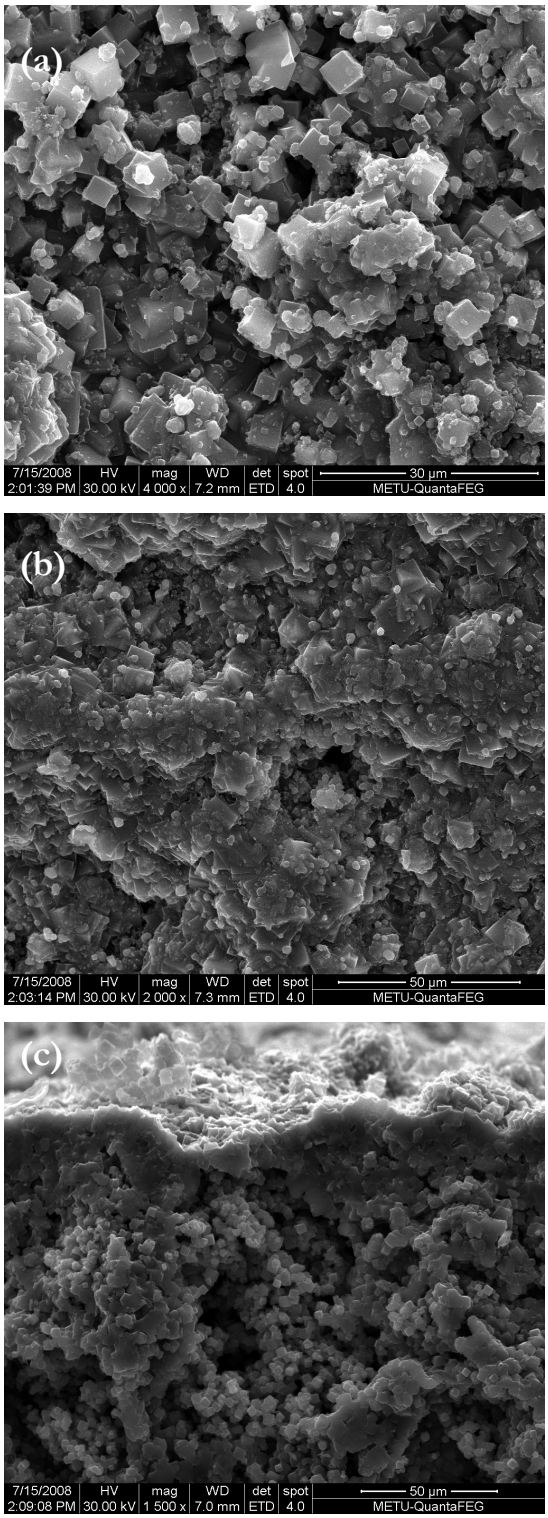

Figure D.27. SEM image of (a) CGM30 outer surface (X 4000), (b) CGM30 outer surface (X 2000) and (c) CGM30 inner cross section (X 1500)

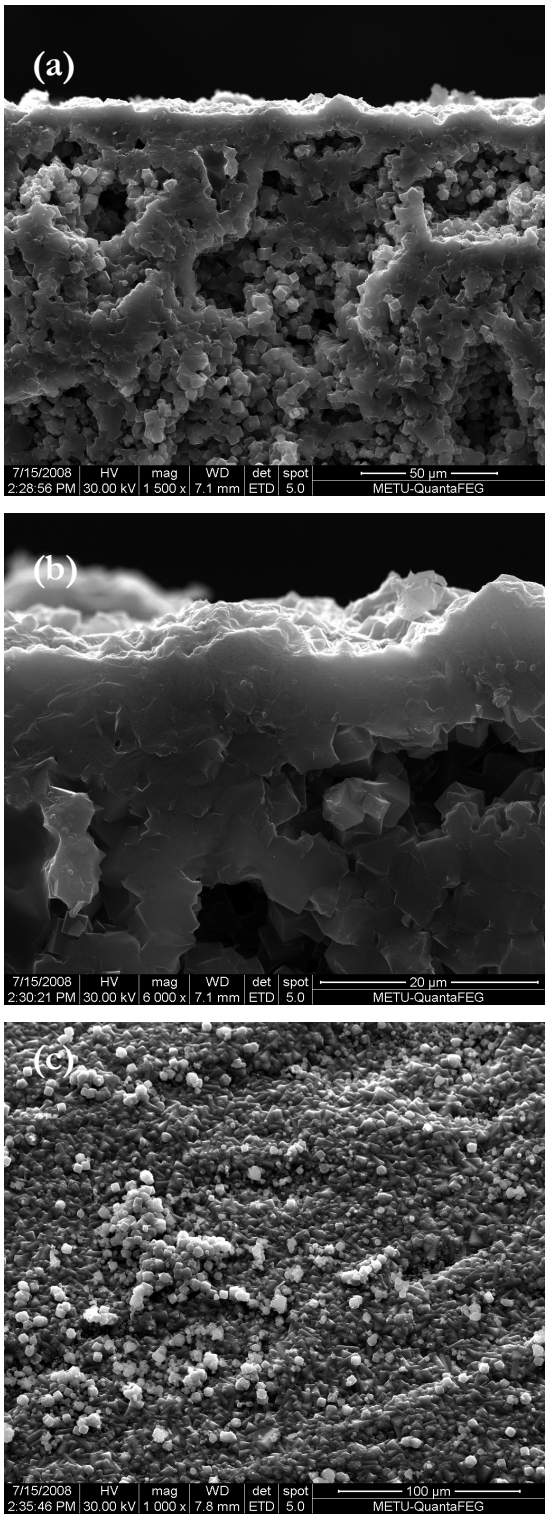

Figure D.28. SEM image of (a) CGM30 outer surface (X 4000), (b) CGM30 outer surface (X 6000) and (c) CGM33 outer surface (X 1000)

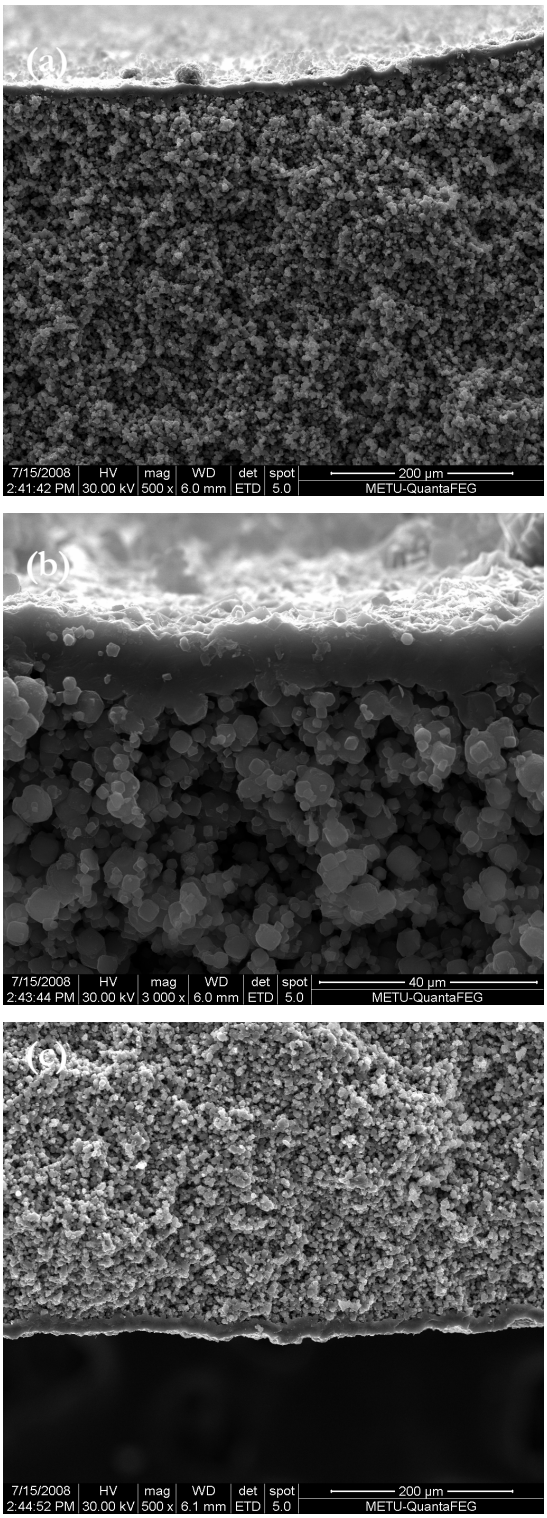

Figure D.29. SEM image of (a) CGM33 inner cross section (X 500), (b) CGM33 inner cross section (X 3000) and (c) CGM33 outer cross section (X 500)

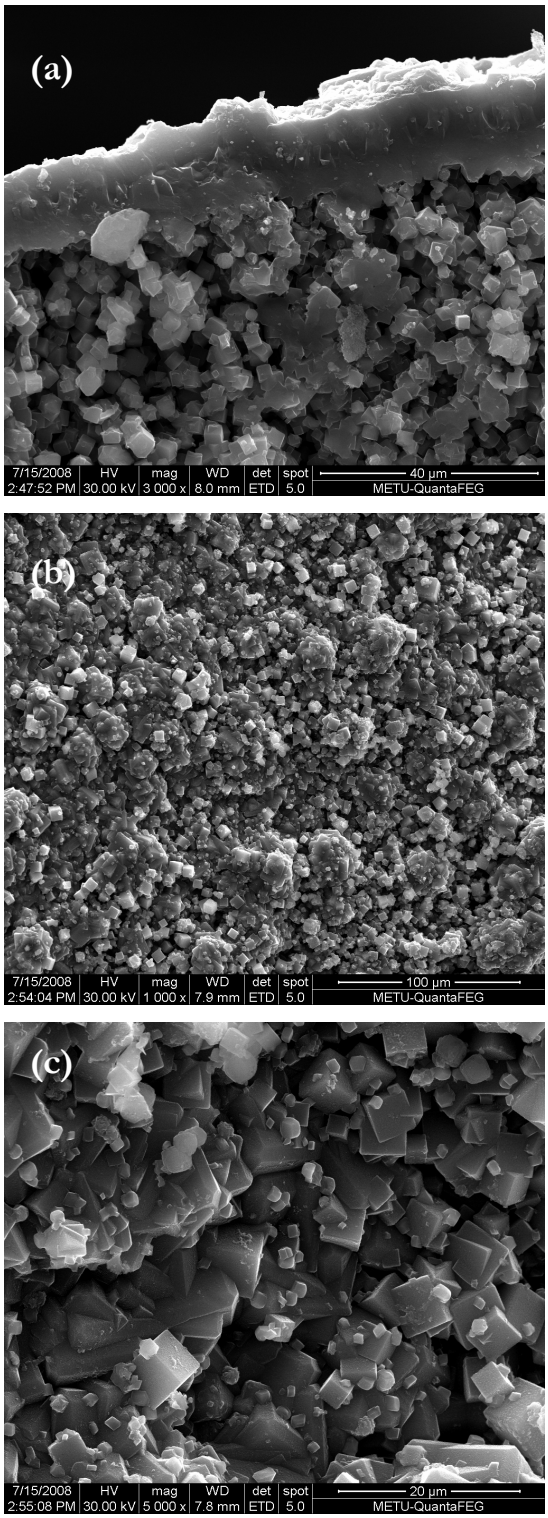

Figure D.30. SEM image of (a) CGM33 outer cross section (X 3000), (b) CGM33 outer surface (X 1000) and (c) CGM33 outer surface (X 5000)

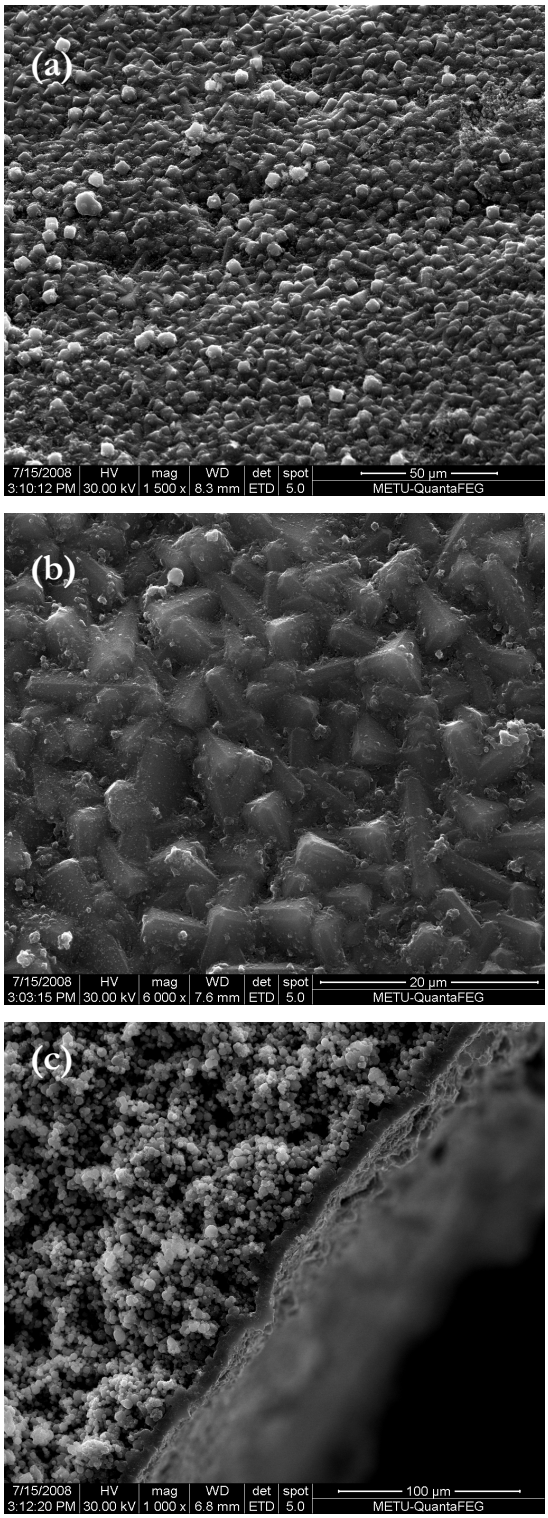

Figure D.31. SEM image of (a) CGM28 outer surface (X 1500), (b) CGM28 outer surface (X 6000) and (c) CGM28 inner cross section (X 5000)

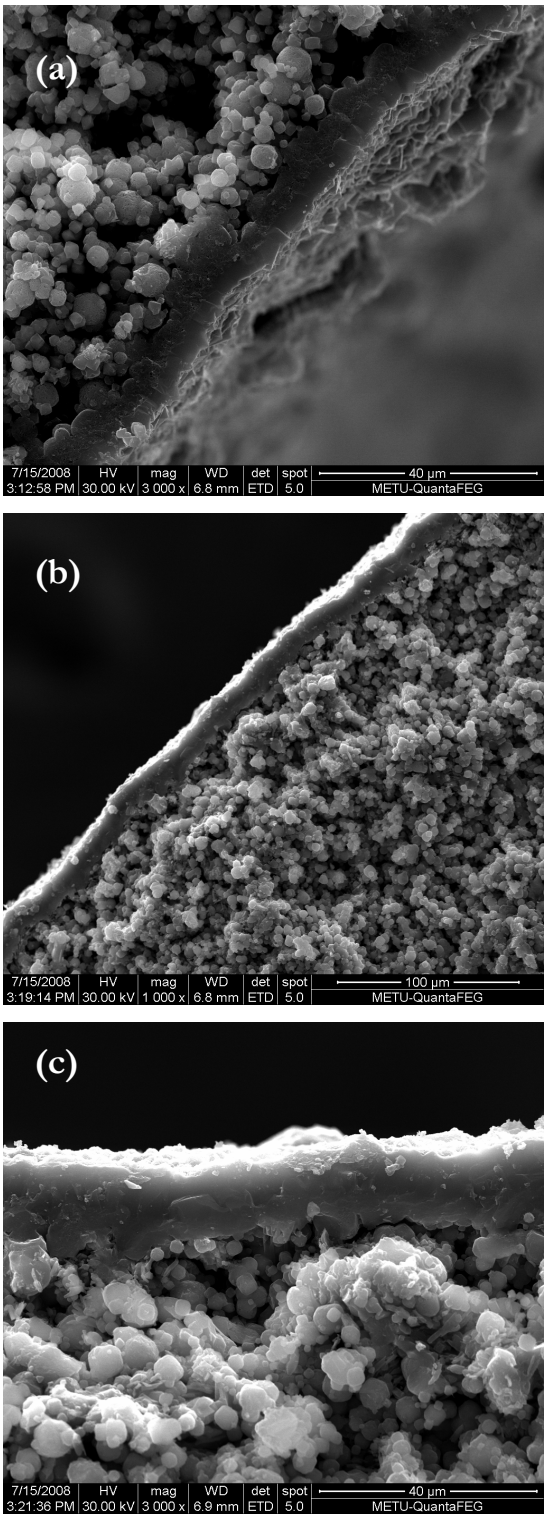

Figure D.32. SEM image of (a) CGM28 outer surface (X 3000), (b) CGM28 outer cross section (X 1000) and (c) CGM28 outer cross section (X 5000)

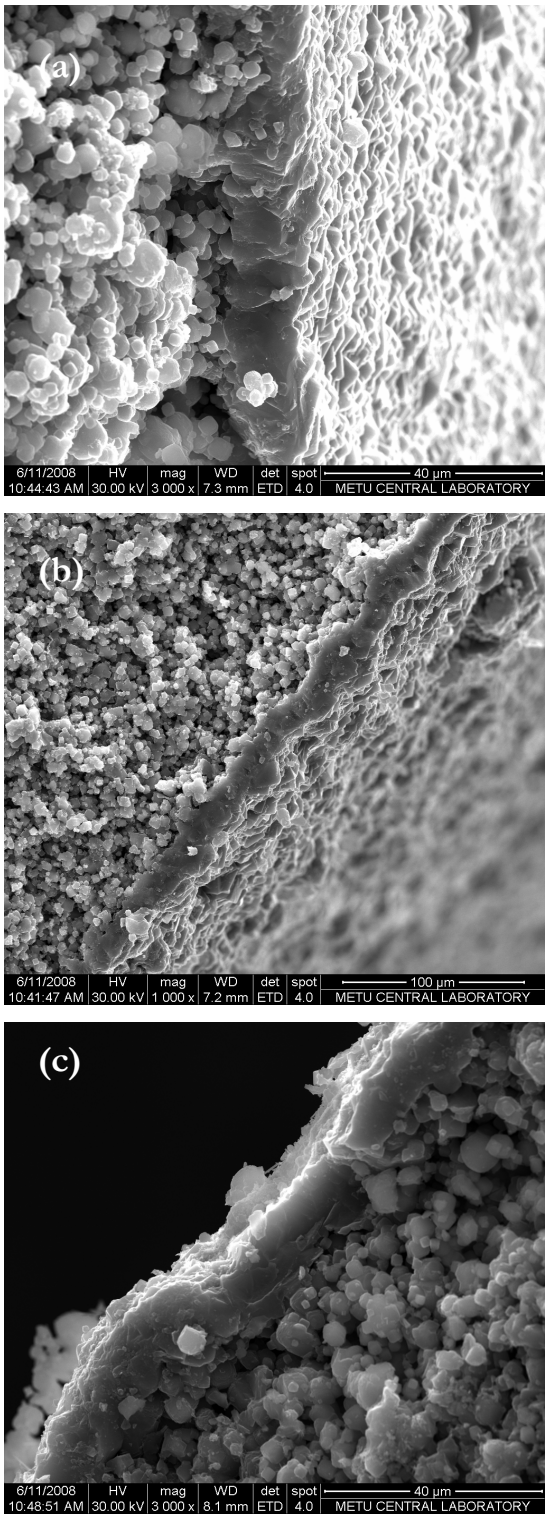

Figure D.33. SEM image of (a) CGM26 inner cross section (X 3000), (b) CGM26 inner cross section (X 1000) and (c) CGM26 outer cross section (X 3000)

APPENDIX E

CALCULATION OF THE SOLID COMPOSITION FROM THE ICP RESULTS

Table E.1. ICP analysis of the solid composition for the batch CG6 and CG16

Sample	Na (%)	Si (%)	Al (%)
CG6 – a	10.53	17.33	11.34
CG6 – b	10.42	17.35	11.24
Average	10.48	17.34	11.27
CG16 – a	11.36	17.18	12.62
CG16 – b	11.53	17.66	12.59
Average	11.45	17.42	12.61

Calculation for the CG6 – a:

For 100 g of sample, m_{Na}= 10.53, m_{Si}= 17.33 and m_{Al}= 11.34

$$n_{Na} = \frac{10.53g}{23g/mol} = 0.458mol \Rightarrow n_{Na_2O} = 0.229mol$$

$$\Rightarrow n_{O,Na_2O} = 0.229mol \searrow$$

$$n_{Si} = \frac{17.33g}{28.1g/mol} = 0.617mol \Rightarrow n_{SiO_2} = 0.617mol$$

$$\Rightarrow n_{O,SiO_2} = 1.233mol \rightarrow$$

$$n_{Al} = \frac{11.34g}{27g/mol} = 0.420mol \Rightarrow n_{Al_2O_3} = 0.210mol$$

$$\Rightarrow n_{O,Al_2O_3} = 0.630mol \nearrow$$

$$n_{O,dry} = 2.092mol$$

Then composition of the solid in dry basis can be found as:

$$\left.\begin{aligned} n_{Al_2O_3} &= \frac{0.210\text{mol}}{0.210\text{mol}} = 1 \\ n_{SiO_2} &= \frac{0.617\text{mol}}{0.210\text{mol}} = 2.94 \\ n_{Na_2O} &= \frac{0.229\text{mol}}{0.210\text{mol}} = 1.09 \end{aligned}\right\} \text{In dry basis: } \boxed{N_{1.09}A_1S_{2.94}}$$

where N demonstrates Na_2O, A demonstrates Al_2O_3 and S demonstrates SiO_2

Using the calculation for the amount of oxygen within the Al_2O_3, SiO_2 and Na_2O; we can determine the amount of the H_2O within the structure

$$\begin{aligned} m_{O,dry} &= n_{O,dry} \times MW_O = 2.092\text{mol} \times 16\text{g/mol} = 33.47\text{g} \\ m_{total,dry} &= m_{Si} + m_{Al} + m_{Na} + m_{O,dry} \\ &= 10.53\text{g} + 17.33\text{g} + 11.34\text{g} + 33.47\text{g} \\ &= 72.67\text{g} \\ m_{H_2O} &= m_{total} - m_{total,dry} \\ &= 100\text{g} - 72.67\text{g} \\ &= 27.33\text{g} \\ n_{H_2O} &= \frac{m_{H_2O}}{MW_{H_2O}} = \frac{27.33\text{g}}{18\text{g/mol}} = 1.518\text{mol} \end{aligned}$$

Then in wet basis;

$$\left.\begin{aligned} n_{Al_2O_3} &= \frac{0.210\text{mol}}{0.210\text{mol}} = 1 \\ n_{SiO_2} &= \frac{0.617\text{mol}}{0.210\text{mol}} = 2.94 \\ n_{Na_2O} &= \frac{0.229\text{mol}}{0.210\text{mol}} = 1.09 \\ n_{H_2O} &= \frac{1.518\text{mol}}{0.210\text{mol}} = 7.23 \end{aligned}\right\} \text{In wet basis: } \boxed{N_{1.09}A_1S_{2.94}H_{7.23}}$$

where N demonstrates Na_2O, A demonstrates Al_2O_3 and S demonstrates SiO_2

In the same way according to the calculations for the rest of the ICP analysis, following values are determined:

Table E.2. Solid Composition for batch CG6 determined according to the ICP analysis

Sample	**Solid Composition**	
	Dry Basis	**Wet Basis**
CG6 – a	$N_{1.09}A_1S_{2.94}$	$N_{1.09}A_1S_{2.94}H_{7.23}$
CG6 – b	$N_{1.09}A_1S_{2.97}$	$N_{1.09}A_1S_{2.97}H_{7.38}$
Average	$N_{1.09}A_1S_{2.95}$	$N_{1.09}A_1S_{2.95}H_{7.31}$
CG16 – a	$N_{1.06}A_1S_{2.61}$	$N_{1.06}A_1S_{2.61}H_{5.73}$
CG16 – b	$N_{1.08}A_1S_{2.70}$	$N_{1.08}A_1S_{2.70}H_{5.46}$
Average	$N_{1.07}A_1S_{2.66}$	$N_{1.07}A_1S_{2.66}H_{5.60}$

APPENDIX F

TERNARY DIAGRAM DATA OF THE LIQUID AND THE OVERALL COMPOSITION

Calculations of the ternary diagram locations are based on the dry bases on the compositions. The location of the soda concentration, for example, found by dividing the mole of soda to the total dry mol of the alumino, silica and soda present in the dry composition. The molar amount of the water present within the composition is also presented on the ternary diagram by means of an interval.

The liquid and overall compositions of the reactive solutions along with their ternary diagram data are given in Figure F.1., and the liquid and overall compositions in case of different solid extrudate to reactive liquid composition is given in Figure F.2 and F.3, for reactive solution 1 and reactive solution 2, respectively.

Table F.1. Ternary diagram data of liquid and overall compositions

Liquid Composition	# N	# A	# S	H_2O mole %	Synthesis Ratio (S/R)	Overall Composition	# N	# A	# S	H_2O mole %	Zeolite Type
$N_{4.8}A_1S_{0.07}H_{400}$	0.82	0.17	0.01	99	1/14	$N_{2.72}A_1S_{1.52}H_{180}$	0.52	0.19	0.29	97	Zeolite A
					1/18	$N_{2.95}A_1S_{1.36}H_{204}$	0.56	0.19	0.25	97	
$N_{4.8}A_1H_{400}$	0.83	0.17	-	99	1/18	$N_{2.95}A_1S_{1.32}H_{204}$	0.56	0.19	0.25	97	Zeolite A
$N_{4.8}H_{400}$	1	-	-	99	1/14	$N_{4.91}A_1S_{2.66}H_{326}$	0.57	0.12	0.31	97	Zeolite A + X
					1/18	$N_{6.01}A_1S_{2.66}H_{417}$	0.62	0.10	0.28	98	
$N_{4.2}H_{400}$	1	-	-	99	1/14	$N_{4.45}A_1S_{2.66}H_{327}$	0.55	0.12	0.33	98	Amorphous
					1/18	$N_{5.41}A_1S_{2.66}H_{419}$	0.60	0.11	0.29	98	
$N_{3.6}H_{400}$	1	-	-	99	1/14	$N_{3.98}A_1S_{2.66}H_{329}$	0.52	0.13	0.35	98	Amorphous
					1/18	$N_{4.81}A_1S_{2.66}H_{421}$	0.57	0.12	0.31	98	
$N_{5.4}H_{400}$	1	-	-	99	1/14	$N_{5.37}A_1S_{2.66}H_{324}$	0.60	0.11	0.29	97	Zeolite A + X
					1/18	$N_{6.60}A_1S_{2.66}H_{415}$	0.64	0.10	0.26	98	
$N_{2.4}H_{400}$	1	-	-	99	1/14	$N_{3.03}A_1S_{2.66}H_{332}$	0.45	0.15	0.40	98	Amorph
$N_{4.8}A_1S_{0.5}H_{400}$	0.76	0.16	0.08	98	1/18	$N_{2.95}A_1S_{1.57}H_{204}$	0.53	0.18	0.29	97	Zeolite A
$N_{4.8}A_1S_1H_{400}$	0.70	0.15	0.15	98	1/18	$N_{2.94}A_1S_{1.83}H_{204}$	0.51	0.17	0.32	97	Zeolite A
$N_{4.8}A_{0.5}S_{0.07}H_{400}$	0.89	0.09	0.02	99	1/18	$N_{3.95}A_1S_{1.81}H_{274}$	0.58	0.15	0.27	98	Zeolite A
$N_{4.8}A_{1.5}S_{0.07}H_{400}$	0.75	0.24	0.01	98	1/18	$N_{2.35}A_1S_{1.09}H_{163}$	0.53	0.23	0.24	97	Zeolite A
$N_{3.6}A_1S_{0.07}H_{400}$	0.77	0.21	0.02	99	1/18	$N_{2.35}A_1S_{1.35}H_{205}$	0.50	0.21	0.29	98	Zeolite A
$N_{2.4}A_1S_{0.07}H_{400}$	0.69	0.29	0.02	99	1/14	$N_{1.66}A_1S_{1.50}H_{182}$	0.40	0.24	0.36	98	Zeolite A
$N_{7.4}A_1S_{0.7}H_{624}$	0.81	0.11	0.08	99	1/14	$N_{3.20}A_1S_{2.00}H_{214}$	0.52	0.16	0.32	97	Zeolite A
$N_{7.5}A_1S_{1.5}H_{990}$	0.75	0.10	0.15	99	1/28	$N_{3.60}A_1S_{2.20}H_{393}$	0.53	0.15	0.32	98	Amorphous
$N_4A_1S_{1.67}H_{660}$	0.60	0.15	0.25	99	1/28	$N_{2.52}A_1S_{2.17}H_{328}$	0.44	0.18	0.38	98	Amorphous

Table F.1. cont'd

Liquid Composition	# N	# A	# S	H_2O mole %	Synthesis Ratio (S/R)	Overall Composition	# N	# A	# S	H_2O mole %	Zeolite Type
$N_2A_1S_2H_{495}$	0.40	0.20	0.40	99	1/28	$N_{1.60}A_1S_{2.29}H_{282}$	0.33	0.20	0.47	98	Amorphous
$N_{5.5}A_1S_{3.5}H_{990}$	0.55	0.10	0.35	99	1/28	$N_{2.81}A_1S_{2.99}H_{393}$	0.41	0.15	0.44	98	Amorphous
$N_2A_1S_1H_{396}$	0.50	0.25	0.25	99	1/28	$N_{1.64}A_1S_{1.63}H_{247}$	0.39	0.23	0.38	98	Amorphous
$N_{3.75}A_1S_{0.25}H_{495}$	0.75	0.20	0.05	99	1/14	$N_{2.12}A_1S_{1.71}H_{198}$	0.44	0.21	0.35	98	Zeolite A
$N_{5.33}A_1S_{0.33}H_{660}$	0.80	0.15	0.05	99	1/14	$N_{2.46}A_1S_{1.90}H_{220}$	0.46	0.19	0.35	98	Zeolite A
$N_{8.5}A_1S_{0.5}H_{990}$	0.85	0.10	0.05	99	1/14	$N_{2.89}A_1S_{2.13}H_{247}$	0.48	0.17	0.35	98	Zeolite A
$N_{5.67}A_1H_{660}$	0.85	0.15	0.00	99	1/14	$N_{2.58}A_1S_{1.79}H_{220}$	0.48	0.19	0.33	98	Zeolite A
$N_{3.5}A_1S_{0.5}H_{495}$	0.70	0.20	0.10	99	1/14	$N_{2.03}A_1S_{1.81}H_{198}$	0.42	0.21	0.37	98	Zeolite A
$N_5A_1S_{0.67}H_{660}$	0.75	0.15	0.10	99	1/14	$N_{2.36}A_1S_{2.01}H_{220}$	0.44	0.19	0.37	98	Zeolite A
$N_8A_1S_{1.00}H_{990}$	0.80	0.10	0.10	99	1/14	$N_{2.77}A_1S_{2.25}H_{247}$	0.46	0.17	0.37	98	Zeolite A
$N_{4.71}A_1S_{5.88}H_{582}$	0.80	0.17	0.03	99	1/14	$N_{2.34}A_1S_{3.78}H_{207}$	0.33	0.14	0.53	97	Zeolite A
$N_{3.25}A_1S_{0.75}H_{495}$	0.65	0.2	0.15	99	1/14	$N_{1.93}A_1S_{1.91}H_{198}$	0.40	0.21	0.39	98	Zeolite A
$N_{2.17}A_1S_{0.17}H_{330}$	0.65	0.30	0.05	99	1/14	$N_{1.61}A_1S_{1.43}H_{165}$	0.40	0.25	0.35	98	Zeolite A
$N_{2.6}A_1S_{0.4}H_{396}$	0.65	0.25	0.10	99	1/14	$N_{1.75}A_1S_{1.65}H_{180}$	0.40	0.23	0.37	98	Zeolite A
$N_{5.83}A_1S_{1.5}H_{825}$	0.70	0.12	0.18	99	1/14	$N_{2.40}A_1S_{2.33}H_{235}$	0.42	0.17	0.41	98	Zeolite A

Table F.2. Ternary diagram data for the overall compositions results from different solid extrudate to reactive liquid composition, $4.8Na_2O:Al_2O_3:0.07SiO_2:400H_2O$

Liquid Composition	# N	# A	# S	H_2O mole %	Synthesis Ratio (S/L)	Overall Composition	# N	# A	# S	H_2O mole %	Zeolite Type
$N_{4.8}A_1S_{0.07}H_{400}$	0.82	0.17	0.01	99	1/3.5	$N_{1.68}A_1S_{2.23}H_{70.6}$	0.34	0.20	0.45	93	Zeolite A
$N_{4.8}A_1S_{0.07}H_{400}$	0.82	0.17	0.01	99	1/7	$N_{2.13}A_1S_{1.93}H_{197}$	0.42	0.20	0.38	96	Zeolite A
$N_{4.8}A_1S_{0.07}H_{400}$	0.82	0.17	0.01	99	1/14	$N_{2.72}A_1S_{1.52}H_{180}$	0.52	0.19	0.29	97	Zeolite A
$N_{4.8}A_1S_{0.07}H_{400}$	0.82	0.17	0.01	99	1/18	$N_{2.95}A_1S_{1.36}H_{204}$	0.56	0.19	0.25	97	Zeolite A
$N_{4.8}A_1S_{0.07}H_{400}$	0.82	0.17	0.01	99	1/21	$N_{3.09}A_1S_{1.26}H_{219}$	0.58	0.19	0.23	98	Zeolite A
$N_{4.8}A_1S_{0.07}H_{400}$	0.82	0.17	0.01	99	1/28	$N_{3.35}A_1S_{1.07}H_{247}$	0.62	0.18	0.20	98	Zeolite A
$N_{4.8}A_1S_{0.07}H_{400}$	0.82	0.17	0.01	99	1/35	$N_{3.55}A_1S_{0.94}H_{267}$	0.65	0.18	0.17	98	Zeolite A
$N_{4.8}A_1S_{0.07}H_{400}$	0.82	0.17	0.01	99	1/42	$N_{3.69}A_1S_{0.84}H_{283}$	0.67	0.18	0.15	98	Zeolite A
$N_{4.8}A_1S_{0.07}H_{400}$	0.82	0.17	0.01	99	1/49	$N_{3.81}A_1S_{0.76}H_{295}$	0.68	0.18	0.14	98	Zeolite A
$N_{4.8}A_1S_{0.07}H_{400}$	0.82	0.17	0.01	99	1/56	$N_{3.90}A_1S_{0.69}H_{305}$	0.70	0.18	0.12	98	Zeolite A
$N_{4.8}A_1S_{0.07}H_{400}$	0.82	0.17	0.01	99	1/105	$N_{4.26}A_1S_{0.44}H_{343}$	0.75	0.17	0.08	98	Zeolite A

Table F.3. Ternary diagram data for the overall compositions results from different solid extrudate to reactive liquid composition, $2.33Na_2O:SiO_2:330H_2O$

Liquid Composition	# N	# A	# S	H_2O mole %	Synthesis Ratio (S/R)	Overall Composition	# N	# A	# S	H_2O mole %	Zeolite Type
$N_{2.33}S_{1.00}H_{330}$	0.70	0	0.30	99	1/3.5	$N_{1.64}A_1S_{2.90}H_{86.2}$	0.30	0.18	0.52	94	Amorphous
$N_{2.33}S_{1.00}H_{330}$	0.70	0	0.30	99	1/7	$N_{2.21}A_1S_{3.15}H_{167}$	0.35	0.16	0.49	96	Amorphous
$N_{2.33}S_{1.00}H_{330}$	0.70	0	0.30	99	1/14	$N_{3.35}A_1S_{3.64}H_{328}$	0.42	0.12	0.46	98	Amorphous
$N_{2.33}S_{1.00}H_{330}$	0.70	0	0.30	99	1/21	$N_{4.48}A_1S_{4.13}H_{489}$	0.47	0.10	0.43	98	Amorphous
$N_{2.33}S_{1.00}H_{330}$	0.70	0	0.30	99	1/28	$N_{5.62}A_1S_{4.61}H_{650}$	0.50	0.09	0.41	98	Amorphous
$N_{2.33}S_{1.00}H_{330}$	0.70	0	0.30	99	1/35	$N_{6.76}A_1S_{5.10}H_{812}$	0.52	0.08	0.42	98	Amorphous
$N_{2.33}S_{1.00}H_{330}$	0.70	0	0.30	99	1/42	$N_{7.90}A_1S_{5.59}H_{973}$	0.54	0.07	0.39	99	Amorphous
$N_{2.33}S_{1.00}H_{330}$	0.70	0	0.30	99	1/56	$N_{10.2}A_1S_{6.57}H_{1295}$	0.57	0.06	0.37	99	Amorphous
$N_{2.33}S_{1.00}H_{330}$	0.70	0	0.30	99	1/105	$N_{18.1}A_1S_{9.99}H_{2423}$	0.62	0.04	0.34	99	Amorphous

APPENDIX G

SAMPLE CALCULATION OF THE OVERALL COMPOSITION IN THE REACTIVE MEDIUM

Composition of the solid extrudate is $1.07Na_2O:1Al_2O_3:2.66SiO_2:5.60H_2O$ according to the ICP analysis. The reactive solution composition selected as $4.8Na_2O:1Al_2O_3:0.07SiO_2:400H_2O$ for the calculation. The solid extrudate (S) to reactive solution (R) within the autoclave is chosen to be 14.

Table G.1. ICP analysis of the solid composition for the batch CG6 and CG16

Reactant	**Molecular Weight (g/mol)**
Na_2O	62
Al_2O_3	102
SiO_2	60
H_2O	18

Formula weight of R: 4.8×62 + 1×102 + 0.07×60 + 400×18 = 7603.8 g

For 14 g of R,

$$n_R = \frac{14\ g}{7603.8\ g/mole} = 0.0018\ mole$$

$$n_{Na_2O} = n_R x 4.8 = 0.0088\ mole$$
$$n_{Al_2O_3} = n_R x 1 \quad = 0.0018\ mole$$
$$n_{SiO_2} = n_R x 0.07 = 0.0001\ mole$$
$$n_{H_2O} = n_R x 400 = 0.7365\ mole$$

Formula weight of S: 1.07×62 + 1×102 + 2.66×60 + 5.60×18 = 428.74 g

For 1 g of S,

$$n_S = \frac{1\ g}{428.74\ g/mole} = 0.0023\ mole$$

$$n_{Na_2O} = n_S x 1.07 = 0.0025\ mole$$
$$n_{Al_2O_3} = n_S x 1 \quad = 0.0023\ mole$$
$$n_{SiO_2} = n_S x 2.66 = 0.0062\ mole$$
$$n_{H_2O} = n_S x 5.60 = 0.0131\ mole$$

Calculating total moles of Na_2O, Al_2O_3, SiO_2 and H_2O within the synthesis medium:

$$n_{Na_2O,total} = (n_{Na_2O})_R + (n_{Na_2O})_S \quad = 0.0113\ mole$$
$$n_{Al_2O_3,total} = (n_{Al_2O_3})_R + (n_{Al_2O_3})_S = 0.0042\ mole$$
$$n_{SiO_2,total} \quad = (n_{SiO_2})_R + (n_{SiO_2})_S \quad = 0.0063\ mole$$
$$n_{H_2O,total} \quad = (n_{H_2O})_R + (n_{H_2O})_S \quad = 0.7495\ mole$$

Then the overall composition, for 1 mole of Al_2O_3 is:

$$\left.\begin{aligned} n_{Al_2O_3} &= \frac{0.0042\ mole}{0.042\ mole} = 1 \\ n_{SiO_2} &= \frac{0.0063\ mole}{0.0042\ mole} = 1.52 \\ n_{Na_2O} &= \frac{0.0113\ mole}{0.0042\ mole} = 2.72 \\ n_{H_2O} &= \frac{0.7495\ mole}{0.0042\ mole} = 180 \end{aligned}\right\} \boxed{2.72Na_2O{:}Al_2O_3{:}1.52SiO_2{:}180H_2O}$$

APPENDIX H

MEMBRANE SYNTHESIS CONDITIONS AND CHARACTERIZATION RESULTS BASED ON XRD AND SEM

Table H.1. Membrane synthesis conditions and characterization results based on XRD and SEM

Membrane	Support	Membrane Synthesis Composition	Synthesis Conditions	Crystallinity %	Film Thickness
CGM1	CG20D23	$49Na_2O:1Al_2O_3:5SiO_2:980H_2O$	80°C for 24h	79	-
CGM2	CG20D21	$49Na_2O:1Al_2O_3:5SiO_2:980H_2O$	80°C for 8h	84	-
CGM3	CG20D24	$49Na_2O:1Al_2O_3:5SiO_2:980H_2O$	80°C for 8h	88	-
CGM4	CG20D22	$49Na_2O:1Al_2O_3:5SiO_2:980H_2O$	80°C for 8h	93	-
CGM5	CG25D5	$49Na_2O:1Al_2O_3:5SiO_2:980H_2O$	80°C for 8h	88	5. 67 μm
CGM6	CG25D1	$49Na_2O:1Al_2O_3:5SiO_2:980H_2O$	80°C for 8h	45	3.48 μm
CGM7	CG25D2	$2Na_2O:1Al_2O_3:2SiO_2:120H_2O$	100°C for 4h	95	5.97 μm
CGM8	CG21T1	$2Na_2O:1Al_2O_3:2SiO_2:120H_2O$	100°C for 4h	NA	No Film
CGM9	CG25D10	$2Na_2O:1Al_2O_3:2SiO_2:120H_2O$	80°C for 8h	NA	-
CGM10	CG25D11	$49Na_2O:1Al_2O_3:5SiO_2:980H_2O$	100°C for 4h	NA	-
CGM11	CG33T1	$2Na_2O:1Al_2O_3:2SiO_2:150H_2O$	100°C for 4h	NA	-
CGM12	CG33T2	$2Na_2O:1Al_2O_3:2SiO_2:150H_2O$	100°C for 4h	NA	-
CGM13	Alumina Tube	$2Na_2O:1Al_2O_3:2SiO_2:150H_2O$	100°C for 4h	NA	-
CGM14	Alumina Tube	$2Na_2O:1Al_2O_3:2SiO_2:150H_2O$	100°C for 4h	NA	-
CGM15	CG32F1	$2Na_2O:1Al_2O_3:2SiO_2:150H_2O$	100°C for 4h	NA	-
CGM16	CG41L1	$2Na_2O:1Al_2O_3:2SiO_2:150H_2O$	100°C for 4h	NA	-
CGM17	CG41F4	$2Na_2O:1Al_2O_3:2SiO_2:150H_2O$	100°C for 4h	NA	-

Table H.1. cont'd

Membrane	Support	Membrane Synthesis Composition	Synthesis Conditions	Crystallinity %	Film Thickness
CGM18	CG41L2	$2Na_2O:1Al_2O_3:2SiO_2:150H_2O$	100°C for 4h	NA	-
CGM19	CG41F1	$2Na_2O:1Al_2O_3:2SiO_2:150H_2O$	100°C for 4h	NA	-
CGM20	CG41F3	$2Na_2O:1Al_2O_3:2SiO_2:150H_2O$	100°C for 4h	NA	-
CGM21	CG41F2	$2Na_2O:1Al_2O_3:2SiO_2:150H_2O$	100°C for 4h	NA	-
CGM22	CG41L6	$2Na_2O:1Al_2O_3:2SiO_2:150H_2O$	100°C for 4h	NA	-
CGM23	CG41L3	$2Na_2O:1Al_2O_3:2SiO_2:150H_2O$	100°C for 4h	NA	-
CGM24	CG41L4	$2Na_2O:1Al_2O_3:2SiO_2:150H_2O$	100°C for 4h	NA	-
CGM25	CG41L5	$2Na_2O:1Al_2O_3:2SiO_2:150H_2O$	100°C for 4h	NA	-
CGM26	AÖ119H-2	$2Na_2O:1Al_2O_3:2SiO_2:150H_2O$	100°C for 4h	NA	12 μm
CGM27	CG32F2	$2Na_2O:1Al_2O_3:2SiO_2:150H_2O$	100°C for 4h	NA	-
CGM28	AÖ119H-1	$2Na_2O:1Al_2O_3:2SiO_2:150H_2O$	100°C for 4h	NA	9.2 μm
CGM29	AÖ100L-4	$2Na_2O:1Al_2O_3:2SiO_2:150H_2O$	100°C for 4h	NA	-
CGM30	CG15F	$2Na_2O:1Al_2O_3:2SiO_2:150H_2O$	100°C for 4h	NA	11.8 μm
CGM31	CG40L-3	$2Na_2O:1Al_2O_3:2SiO_2:150H_2O$	100°C for 4h	NA	-
CGM32	AÖ100L-5	$2Na_2O:1Al_2O_3:2SiO_2:150H_2O$	100°C for 4h	NA	-
CGM33	AÖ100L-5	$2Na_2O:1Al_2O_3:2SiO_2:150H_2O$	100°C for 4h	NA	11.2 μm

APPENDIX I

EDX ANALYSIS

Table I.1. EDX analysis of the bars prepared for the crystallinity curve

Sample Code	Time	Weight %				Molar %			Composition in dry bases (balance is H_2O)
		Na	Al	Si	O	Na_2O	Al_2O_3	SiO_2	
CG42L - 5.5h	5.5	10.21	14.01	26.22	49.56	0.22	0.26	0.94	$0.86Na_2O:Al_2O_3:3.61SiO_2$
CG42L - 6.5h	6.5	12.44	13.53	24.92	49.10	0.27	0.25	0.89	$1.08Na_2O:Al_2O_3:3.55SiO_2$
CG42L - 7h	7	1137	14.3	25.55	48.78	0.25	0.26	0.91	$0.93Na_2O:Al_2O_3:3.45SiO_2$
CG42L - 8h	8	12.19	14.45	23.86	49.49	0.27	0.27	0.85	$0.99Na_2O:Al_2O_3:3.18SiO_2$
CG42L - 9h	9	12.36	14.45	23.71	49.48	0.27	0.27	0.85	$1.00Na_2O:Al_2O_3:3.16SiO_2$
CG42L - 18h	18	14.89	15.29	19.66	50.23	0.32	0.28	0.70	$1.15\ Na_2O:Al_2O_3:2.49SiO_2$

Table I.2. EDX analysis of the bars prepared for the determination of the effect of the solid extrudate to reactive solution ratio

Sample Code	Solid Extrudate/ Reactive Solution	Weight %				Molar %			Composition in dry bases
		Na	Al	Si	O	Na_2O	Al_2O_3	SiO_2	(balance is H_2O)
CG40L1	1/3.5	10.21	14.01	26.22	49.56	0.36	0.28	0.64	$1.29Na_2O:Al_2O_3:2.36SiO_2$
CG40L2	1/7	12.44	13.53	24.92	49.10	0.32	0.31	0.67	$1.03Na_2O:Al_2O_3:2.17SiO_2$
CG40L3	1/14	1137	14.3	25.55	48.78	0.32	0.32	0.66	$1.00Na_2O:Al_2O_3:2.07SiO_2$
CG40L5	1/28	12.19	14.45	23.86	49.49	0.32	0.32	0.65	$1.02Na_2O:Al_2O_3:2.05SiO_2$
CG40L7	1/49	12.36	14.45	23.71	49.48	0.32	0.32	0.66	$1.00Na_2O:Al_2O_3:2.07SiO_2$
CG40L9	1/105	14.89	15.29	19.66	50.23	0.33	0.31	0.64	$1.08\ Na_2O:Al_2O_3:2.08SiO_2$